178p

~~CONFIDENTIAL~~

X63-11648

# *Space Programs Summary No. 37-19, Volume I*

*for the period November 1, 1962 to December 31, 1962*

## *The Lunar Program*

(Title Unclassified)

CLASSIFICATION CHANGE

TO - UNCLASSIFIED ~~CONFIDENTIAL~~

By authority of ~~AEC~~ No. E.O. 11652

Changed by L. SHIRLEY Date 5-23-73


JET PROPULSION LABORATORY
CALIFORNIA INSTITUTE OF TECHNOLOGY
PASADENA, CALIFORNIA



January 31, 1963



(NASA-CR-138390) SPACE PROGRAMS SUMMARY NO. 37-19, VOLUME 1 FOR THE PERIOD 1 NOVEMBER - 31 DECEMBER 1962. THE LUNAR PROGRAM (Jet Propulsion Lab.) 178 p

N74-73954

Unclas

00/99 36735



an unauthorized person is prohibited by law.


~~CONFIDENTIAL~~

Code - 2

Single copy only

CASE FILE COPY

CONFIDENTIAL

NATIONAL AERONAUTICS AND SPACE ADMINISTRATION
CONTRACT NO. NAS 7-100

# *Space Programs Summary No. 37-19, Volume I*

*for the period November 1, 1962 to December 31, 1962*

## *The Lunar Program*

(Title Unclassified)

Copy No. 0452

JET PROPULSION LABORATORY
CALIFORNIA INSTITUTE OF TECHNOLOGY
PASADENA, CALIFORNIA

January 31, 1963

CONFIDENTIAL

GROUP 4 Downgraded at 3 year intervals; declassified after 12 years.

# Preface

The *Space Programs Summary* is a six volume, bimonthly publication designed to report on JPL space exploration programs, and related supporting research and advanced development projects. These activities are conducted under the sponsorship of the National Aeronautics and Space Administration.

All information formerly documented in the JPL *Research Summary,* together with reports on advanced development projects, is reported in Volumes IV and V. The subtitles of all volumes of the *Space Programs Summary* are:

| | |
|---|---|
| Vol. I. | The Lunar Program (Confidential) |
| Vol. II. | The Planetary–Interplanetary Program (Confidential) |
| Vol. III. | The Deep Space Instrumentation Facility (Unclassified) |
| Vol. IV. | Supporting Research and Advanced Development (Unclassified) |
| Vol. V. | Supporting Research and Advanced Development (Confidential) |
| Vol. VI. | Space Exploration Programs and Space Sciences (Unclassified) |

The *Space Programs Summary,* Volume VI is an unclassified digest of appropriate material from Volumes I through V, plus the space science instrumentation studies of the JPL Space Sciences Division.

W. H. Pickering

W. H. Pickering, *Director*
*Jet Propulsion Laboratory*

This document contains information affecting the national defense of the United States, within the meaning of the Espionage Laws, Title 18, U.S.C., Sections 793 and 794, the transmission or revelation of which in any manner to an unauthorized person is prohibited by law.

Space Programs Summary No. 37-19
Volume I

Copyright © 1963
Jet Propulsion Laboratory
California Institute of Technology

# Contents

I. Program Objectives . . . . . 1

II. *Ranger* Project . . . . . 2
A. Systems . . . . . 2
B. Guidance and Control . . . . . 8
C. Telecommunications . . . . . 29
D. Space Sciences . . . . . 31
E. Propulsion . . . . . 39
F. Supporting Activities and Engineering Facilities . . . . . 40

III. *Ranger* TV Subsystem . . . . . 41
A. Structure . . . . . 42
B. Electrical Integration . . . . . 42
C. Environmental Testing . . . . . 43
D. Electronics . . . . . 43
E. Thermal Control . . . . . 51
F. Ground Support Equipment . . . . . 51

IV. *Surveyor* Project . . . . . 53
A. Introduction . . . . . 53
B. Scientific Instruments . . . . . 53

V. *Surveyor* Spacecraft System . . . . . 57
A. System Engineering Summary . . . . . 59
B. Scientific Payload . . . . . 67
C. System Analysis . . . . . 83
D. Flight Control . . . . . 98
E. Electronics . . . . . 112
F. Electrical Power Supply . . . . . 124
G. Thermal Control . . . . . 129
H. Engineering Mechanics . . . . . 147
I. Propulsion . . . . . 152
J. Spacecraft Vehicle and Mechanisms for Basic Bus . . . . . 155
K. Reliability and System Test . . . . . 160
L. Mission Operations . . . . . 167

# I. Program Objectives

The JPL Lunar Program consists of two major projects: *Ranger* and *Surveyor*. The *Ranger* Project has entered the flight stage; *Surveyor* is in hardware development.

The objective of the *Ranger* Project is to exploit present technology in support of the U.S. manned lunar flight program. Fourteen *Ranger* launchings, using *Atlas–Agena B* rockets, are now planned; five of these flights have been made.

*Rangers 1* and *2* were engineering evaluation flights to test the basic system to be employed in later lunar and planetary vehicles. Several scientific experiments were carried, but on a noninterference basis. The *Ranger 3, 4,* and *5* spacecraft carried a gamma-ray instrument, a radar reflection experiment, a TV camera, and a rough-landing seismometer capsule. All three of these flights failed. As a result, the objectives of future flights are currently under review.

The objective of the *Surveyor* Project is to take the next step in advancing lunar technology by making soft landings on the Moon. Seven flights using *Centaur* launch vehicles are now planned. *Surveyor* spacecraft, being designed and built by the Hughes Aircraft Company under JPL subcontract, will carry a variety of instruments, including TV cameras, radiation environment monitors, and geophysical equipment for determining characteristics of the lunar surface.

# II. *Ranger* Project

Following the *Ranger 5* failure, an extensive review has been made of all operations associated with the spacecraft, and the flight of *Ranger 6* has been indefinitely postponed. Analysis of the failure is continuing, and it is now known that excessive heat was generated in the power switching and logic module which handles the raw dc power from the solar panels and battery. Circuit analysis and tests have, however, not yet revealed any single failure mode which convincingly accounts for all of the observed anomalies, and therefore, the analysis is proceeding into the investigation of multiple or serial failure modes.

Increased probability of success for future *Ranger* flights is being sought through three measures:

(1) Simplification of mission objectives.

(2) Review and improvement of spacecraft subsystem and system design.

(3) Imposition of quality assurance measures for flight and ground hardware.

At the time this *SPS* was prepared, not all of the program implications of these measures were known; hence, the text that follows refers mainly to events preceding the major program revision. Progress in the reoriented project will be reported at a later date.

## A. Systems

### 1. Ranger 5 *Flight Performance Summary*

The *Ranger 5* spacecraft was launched from Cape Canaveral on October 18, 1962, at 16:59 GMT after a smooth countdown, in spite of high surface winds. The performance of the *Atlas–Agena B* launch vehicle was near nominal, and the spacecraft was injected over the Indian Ocean 2,139 sec after launch. The injection conditions were well within the nominal guidance dispersion region, so that approximately 40% of the spacecraft's midcourse correction capability would have been required to obtain a lunar impact in the target area if the spacecraft had performed properly. Since the attempted midcourse maneuver was not successful, the spacecraft's trajectory carried it past the west or trailing edge of the Moon at 8 deg below the lunar equator with a closest approach altitude of 452 miles at 70.9 hr after liftoff.

Most of the spacecraft subsystems performed within their design limits as long as regulated power was available. The system performance was standard in nearly all respects until approximately 73 min after liftoff, when a short circuit occurred in the electrical power distribution subsystem which resulted in the loss of normal solar panel power. This event occurred about 18 min after the attitude control system had completed its normal Sun

acquisition sequence in which it stabilized the spacecraft pitch and yaw axis with the roll axis pointed toward the Sun and transferred the power system from battery to solar panel power. The cause and nature of the power failure are still being investigated, but its effects were the eventual loss of all solar panel power and several malfunctions in the central computer and sequencer. The latter malfunctions included failure to issue the Earth acquisition command (necessary for establishing communications using the high-gain antenna) and issuing the wrong maneuver turn commands. There were also several malfunctions in the data encoder due to abnormal power, but none of these had any significant effect on the outcome of the mission. The subsequent drain on the main battery shortened the useful life of the spacecraft to approximately 8¾ hr from launch when the battery reached depletion.

Prior to battery depletion, a considerable amount of useful engineering telemetry was recovered. In addition, 4 hr of good data from the gamma-ray spectrometer were obtained; these data are expected to verify findings from *Ranger 3*. The loss of power prevented the spacecraft from completing the midcourse maneuver which was attempted, and ruled out any attempt to perform the television experiment or land the seismometer capsule on the Moon. The capsule transmitter with its own battery power supply was tracked by stations of the Deep Space Instrumentation Facility for 11 days after launch, including an accurate measurement of time of signal loss as the capsule was occulted by the Moon.

## 2. Ranger 6–9 Design Status

The existing designs of *Ranger 6–9* are being reviewed for modifications necessary to bring these designs up to the highest level of reliability possible. The aim of the review is to identify changes that could be made to obtain increased assurance of mission success in flights beginning in late 1963. Decisions made to date include removing all ancillary experiments, cancelling requirements for heat and terminal (gas) sterilization, and providing backup commands for Sun and Earth acquisition on *Ranger 6* (formerly beginning with *Ranger 7*).

A contract to perform a reliability study on the *Ranger 6–9* spacecraft was awarded to the Fairchild Stratos Corporation, Bay Shore, New York on October 26, 1962. The contractor is to accomplish the following objectives:

(1) Develop a method and analytical technique for estimating the reliability of the spacecraft and identifying critical areas for reliability development; the calculation of numerical results is of secondary importance in this study.

(2) Determine and describe the methods and procedures in order to obtain the necessary information for estimating the reliability of the spacecraft.

(3) Study the documentation and description material on the spacecraft supplied by JPL and determine what, if any, supplementary materials should be provided in order to describe the spacecraft sufficiently for the purposes of reliability estimation and development.

The milestones in this effort are given by the *Mid-Term Technical Progress Summary Report*, December 1962, and the final oral and written report, due the latter part of January 1963.

## 3. Ranger 6 Test Operations

Test operations on *Ranger 6* during the reporting period consisted of the following:

***a. Flight Model 1 — TV subsystem.*** On November 5, 1962, pictures were taken with the Flight Model 1 (FM 1) subsystem to check camera focus. Examination of the results showed that most cameras were out of focus to some degree. All cameras were removed and refocused. A recent test indicated all cameras to be properly focused.

Two failures occurred during the test: a shutter failure in Camera P4 and a failure in Transmitter B. These failures were repaired and a subsystem test with the spacecraft was satisfactorily performed on November 15. No RF interference or significant interface problems were observed.

Design modifications have been made in the FM 1 TV subsystem to the ×12 multiplier and the emergency telemetry circuits, and new power amplifiers have been installed. During verification of these design changes in the vacuum chamber at JPL, 3 to 5 dbm power losses were observed. The reasons for these losses are not yet known; the failure is under investigation. After a successful vacuum test is obtained, another TV subsystem test will be performed.

***b. Spacecraft.*** On November 26 a leak-check was performed on the attitude control nitrogen gas system. The

leak rate was less than 10 $cm^3$/hr which is considerably lower than the allowable leak rate of 50 $cm^3$/hr.

A third microscopic inspection was performed on all spacecraft modules and harnesses during the weeks of December 10 and 17. The inspection is 90% completed and the results are currently being tabulated.

The *Ranger 6* spacecraft is presently being held in a disassembled state pending the results of the design review currently in progress.

### 4. Ranger 7 Assembly and Test Operations

Assembly operations, subsystem testing, and the initial phase of system testing have been completed. As of November 19, 1962, all formal test effort was suspended pending evaluation of the *Ranger 5* flight and its effect upon the status of current flight hardware.

***a. System Testing.*** The two system tests performed during the period reported revealed the following significant problems:

(1) Gyro heading data did not agree with existing subsystem test data available.

(2) The operational support equipment (OSE) real-time command (RTC) light could not be reset for 30 min during test—a dirty connector pin was found in the ring harness.

(3) Analysis of the transponder spectrum indicated an 800 cps energy component at the time the attitude control system was operating. Preliminary investigation indicated that the *Ranger 7* transponder was susceptible to noise on the regulated 15 v dc line.

(4) Problems noted in the flight scientific equipment involved the data, telemetry, and voltage monitoring; late delivery of the flight experiments to the Spacecraft Assembly Facility (SAF) prevented detection of these problems during the subsystem phase of testing.

(5) During CC&S reset of Command A-5, a Channel B-2 telemetry event was missed; this was accounted for by a capacitor of incorrect value.

***b. Space simulator testing.***

*Test Preparation.* On October 12, 1962, following System Test 2, preparation began for *Ranger 7* space simulation tests. It was noted during these preparations that several of the heat-sterilized cables had developed insulation cracks at the point where the wires enter the potting compound on the Cannon-D connectors. The defective cables were summarily replaced with unsterilized spare cables. However, during installation of the spares, mechanical interference between the new cables and the spacecraft structure developed. Investigation indicated that more adequate definition is required for both assembly and inspection of flight cables.

The *Ranger 7* spacecraft was moved from the SAF to the 6 ft space simulator on October 19.

The available proof test model (PTM) TV system was utilized for this testing phase due to the delay in delivery of the flight model TV subsystem. To avoid again testing nonflight equipment, and because of the physical restraints imposed by use of the 6 ft space simulator, the TV subsystem was assembled outside the chamber and connected to the spacecraft bus via chamber electrical access connectors.

Strip heaters were installed on solar dependent areas to simulate solar radiation and provide proper temperature control of the spacecraft. Temperature monitoring of critical areas was provided by approximately 100 thermocouples. The installation of strip heaters and thermocouples continued throughout the initial electrical verification period. It was found that a time saving could be effected if strip heaters were prefabricated prior to assembly to the spacecraft.

Problem areas encountered during the test preparation period were:

(1) Telemetry showed the battery transducer was open; after the test, the transducer was measured to be 2000 ohms.

(2) The low energy ion detector (LEID) output was missing; a fuse in the transformer rectifier was open. However, the LEID instrument stepped unreliably and was replaced.

(3) The ion chamber occasionally double pulsed; no spare was available.

(4) The $\times 12$ multiplier in the PTM TV subsystem failed due to a shorted transistor.

(5) Several OSE indications were missing at the command decoder and power consoles; intermit-

tent cables were found in the interface between the OSE and the space chamber.

*Mission Verification Test.* A near-space environment was established in the space simulator with cold walls at −300°F and pressure at approximately $6 \times 10^{-6}$ mm Hg. Spacecraft operating time at test start was approximately 166 hr. The mission verification test was performed in accordance with JPL specification starting on October 23, 1962. At test start, the spacecraft was operated in the launch mode with temperature stabilized at approximately 60 to 70°F.

The launch and cruise programmed events occurred as scheduled in real time. Following the Sun acquisition event, the spacecraft temperature was increased in the range of 100 to 150°F to evaluate performance above the nominal design temperatures. The LEID showed abnormal indications similar to those reported during testing at ambient conditions. Since previous failure had not been completely analyzed and a spare unit was not available, it was decided to continue the mission verification test as scheduled.

The midcourse maneuver sequence was performed approximately 18 hr after launch ($A = 0$) The problems reported during this test phase were:

(1) Storage of the midcourse command sequence produced spikes on the monitored transponder functions; investigations following the midcourse maneuver revealed that the spikes were the result of a false phase lock on sidebands of the 890 Mc carrier due to the command subcarrier.

(2) Channel 5 voltage controlled oscillator (VCO) suffered a permanent offset of calibration frequency of approximately 5 cps; the Channel 5 VCO will be replaced at the earliest opportunity.

Real-time evaluation of the spacecraft performance during the post-midcourse cruise period showed the following potential problems:

(1) The low energy plasma detector indicated drifting; the data is currently being analyzed by the cognizant engineer.

(2) Electron flux detector Channel A count rate was extremely high.

Testing continued in the cruise mode until approximately $A + 64$ hr on October 26. At this time the terminal maneuver sequence was initiated. All programmed events occurred as scheduled until a hold was called at approximately $C + 49$ min when the main power failed to the television OSE. After power restoration, the television sequence was repeated to verify proper operation. The only problem reported was the lack of video on television Channel B. An OSE cable was found to be intermittently shorted.

*Low Temperature Evaluation Test.* Upon completion of the real-time mission verification test, the spacecraft temperatures were stabilized below the design nominal values to functionally test the spacecraft at the minimum predicted temperatures (50 to 60°F). Spacecraft running time at this point in the test sequence was approximately 281 hr. The only problem reported during the test sequence was a higher-than-normal offset in the yaw gyro. This offset was the result of the attitude control jet vanes not being set at zero.

*Temperature Control Stabilization Test.* The spacecraft was returned to ambient temperature and pressure, and all of the direct access cables were removed to permit a simulation of flight temperature operating conditions. Spacecraft running time at this part of the test phase was approximately 293 hr. The chamber was again evacuated and the chamber cold walls set at −300°F. The spacecraft cruise mode was established to permit stabilization at cruise temperatures. During the operation period, it was noted that the attitude control Earth sensor would intermittently command a negative roll search. The problem is currently under investigation.

After the test sequence, approximately 1 $cm^3$ of oil was found beneath the midcourse motor. The problem is currently under investigation.

The spacecraft was returned to the SAF for weight and CG measurements on October 29. The running time to date on the spacecraft was approximately 298 hr.

***c. Weight and CG measurements.*** The test was conducted with the spacecraft in flight configuration. Type approval or mechanical equivalent hardware was installed in areas where the actual flight hardware was not available. The weight and CG determination was conducted with no problems encountered during the actual test. The buildup of the spacecraft took more time than was estimated because most of the science experiments

were removed for repair and calibration, and the cabling (ring harness, squib harness, and science harness) was retied and rerouted.

At the conclusion of the weight and CG measurements, an attitude control leak test was conducted. The leak rate was determined to be less than the required 50 $cm^3$/hr.

On November 19, formal test efforts were suspended pending evaluation of the *Ranger 5* flight and current status of existing flight hardware.

### 5. Ranger 8 *Test Operations*

Since the start of *Ranger 8* assembly on September 19, 1962, the only significant testing performed has been the attitude control leak-rate check. This test of the attitude control nitrogen gas system was accomplished from December 7 through 10 and showed a leak rate of less than 5 $cm^3$/hr.

Operations on *Ranger 8* were suspended during fitting of the cases to the spacecraft bus on December 17 and will be held in abeyance until the results of the current design review are known.

### 6. System Design Evaluation

During the past reporting period, assembly of the *Ranger* design evaluation vehicle (DEV) has been completed. The major requirement in assembling the DEV was that it be as electrically identical to the flight vehicle as possible. In order to fulfill this requirement, spare flight subsystems were used wherever they were available, and flight vehicle assembly procedures and techniques were used during the assembly operation. In some areas, flight spares were not available; consequently, nonflight components were used if the electrical integrity of the DEV was not significantly compromised. At the present time the status of the DEV subsystem is as follows:

(1) Command—spares for *Rangers 5* and *7*.

(2) Power—spares for *Rangers 5* and *6*.

(3) CC&S—spare for *Ranger 5*.

(4) Communications—spare for *Ranger 7*.

(5) Attitude control—spare for *Ranger 3* except nonflight gyros and gyro electronics.

(6) Encoder—spare for *Ranger 6*.

(7) Squib firing assembly—nonflight.

(8) Cable harness—flight units that were replaced because splices are of the in-line type instead of butt type.

In order to further ensure that the DEV is representative of a flight vehicle, subsystem and system tests were performed using the *Ranger 6* procedures. After completion of the system test, the DEV was considered ready for design evaluation testing.

The first two tests on the DEV were designed to gather more data about problems that were known to exist in the *Ranger 6* flight spacecraft. The first test was to determine why the dump circuit in one command decoder operating in the *Ranger 6* spacecraft was being triggered when a command was sent. Tests on the DEV revealed that a transient was being introduced into the dump circuit through coupling in the direct access cable.

The second test was to determine the amount and type of noise on the communications 15 v dc. The noise was monitored and recorded as the spacecraft was operated in various modes. It was determined that the 800 cps ripple found on the 15 v dc was being generated by the attitude control 400 cps inverter. The results of these two tests are presently being analyzed by the subsystem personnel.

In order to provide additional data for the analysis of the *Ranger 5* flight failure, several tests were performed on the DEV power system. These tests consisted of observing the telemetry data while:

(1) Varying the input voltage to the booster regulator.

(2) Varying the output voltage of the booster regulator.

(3) Adding resistance in series with the power telemetry return.

(4) Shorting the spacecraft power return isolation resistor.

The data gathered from these tests are presently being analyzed by the power subsystem personnel.

The general procedure planned for the design evaluation tests is to evaluate the system inputs to each subsystem when the subsystem is operating under the influence of the rest of the system. Specific tests are designed to: (1) determine how much the signal can be degraded before the subsystem fails to function, (2) de-

termine how much steady-state and transient noise is present, and (3) determine the amount of noise and transients the subsystem can tolerate. Parameters are never knowingly allowed to attain levels that would cause damage.

Testing of the encoder has been completed. During the encoder tests all dc voltage inputs were increased and decreased beyond the specification limits, and the telemetry data output for a complete commutator cycle was recorded for each voltage increase and decrease. The noise present at each voltage was observed and recorded. For all other system inputs to the encoder, the normal signal characteristics were observed and recorded, the noise present was recorded, and signals were injected to determine the signal input characteristics required for normal operation and the sensitivity of the subsystem to noise. The data gathered during these tests are presently being analyzed by the encoder subsystem personnel.

Detailed procedures have been written for the encoder and the communications subsystem, but due to the experimental nature of the tests, much revising is required as the tests progress.

In order to monitor transients that occur during a flight sequence, a special transient monitor has been developed. This transient monitor provides ten channels of continuous monitoring and records the presence of any transient that exceeds a preset amplitude. The transient monitor was used for the first time during the encoder tests.

### 7. Environmental Test Program Requirements

The environmental specification for assembly-level testing of the *Ranger* spacecraft was generated from past test philosophy and evaluation of expected environments; it contains procedures which establish flight acceptance and type approval environmental test environments. The specification was intended to provide guide lines to aid the cognizant engineer in the writing of the environmental portion of the detail specification for his subsystem. The detail specification, in addition to defining the particular environmental tests applicable, also defined the operating mode of the assembly and criterion for passing or failing the environmental tests. The detail specification then became the controlling document covering environmental and functional tests for a particular subsystem.

The various interpretations by different cognizant engineers not only yielded a non-uniform environmental test philosophy, but resulted in misused or misinterpreted tests, and test interpretations that were contrary to the original philosophy used in generating the specification. The condition was to be rectified by a project requirement that all detail specifications be reviewed by environmental requirements personnel prior to release. The requirement was to be effective on *Ranger 6* and subsequent vehicles; however, in most cases, the environmental testing had been completed prior to review of the detail specification. The sequence resulted in an assembly level test program on *Ranger 6–9* very similar to the one performed on the *Ranger 1–5* assemblies. The environmental test plan for the subsystems must, therefore, be reviewed prior to the performance of environmental testing to be of value to the project.

Specifications for testing complete spacecraft were prepared and released. The spacecraft specifications were of two types, one for testing flight spacecraft, and one for testing the proof test model (PTM). Two PTM specifications have been written to date, one covering *Rangers 1* and *2* and the other covering *Rangers 3, 4* and *5*. Three specifications for flight acceptance of the spacecraft were written; however, no specification was written for *Ranger 2* since the *Ranger 1* specification was applicable.

In support of the specifications, discussions were held with cognizant personnel in the Environmental Test Laboratory (ETL) to clarify the philosophy and intent of the specification and interpret special test requirements. The contact with the ETL provided a useful source of information regarding *Ranger* test progress and facilitated modification of test procedures.

Special tests and investigations were performed in support of the general specification (for assemblies) and the spacecraft specification:

(1) Investigation of shock sources with special emphasis on pyrotechnic shocks, and evaluation of shock isolation devices for pin pullers.

(2) Evaluation and simulation of vibration environment of the spacecraft.

(3) Evaluation and simulation of the radio frequency interference (RFI) environment of the spacecraft at the launch site.

(4) Evaluation and isolation of the RFI associated with the *Ranger 3, 4* and *5* capsule transmitter and JPL receiver.

(5) Evaluation and simulation of the vibration induced in the spacecraft by the midcourse motor.

(6) Evaluation of the test techniques for thermal–vacuum testing of assemblies.

# B. Guidance and Control

## 1. Secondary Power

### a. Ranger 5 *Flight Analysis.*

*Flight summary. Ranger 5* was launched from Cape Canaveral shortly before 17:00 GMT on October 18, 1962. Operation appeared normal until 18:12 GMT, at which time a partial failure occurred in the power system which eventually resulted in depletion of the battery and failure of the mission.

The values of the majority of the power system measurements are plotted versus time in Fig. 1. The gap in the data between 19:00 and 19:23 GMT is apparently a result of a complete power failure and, therefore, a loss of communications. The traces in Fig. 1 extend to about 01:40 GMT on October 19, at which time the battery was depleted. There are several converter monitor voltages which are not indicated in Fig. 1; these appeared to be fairly normal until loss of communications at 19:00 GMT. At 19:28 GMT these monitors were about 10% low, indicating a corresponding drop in the

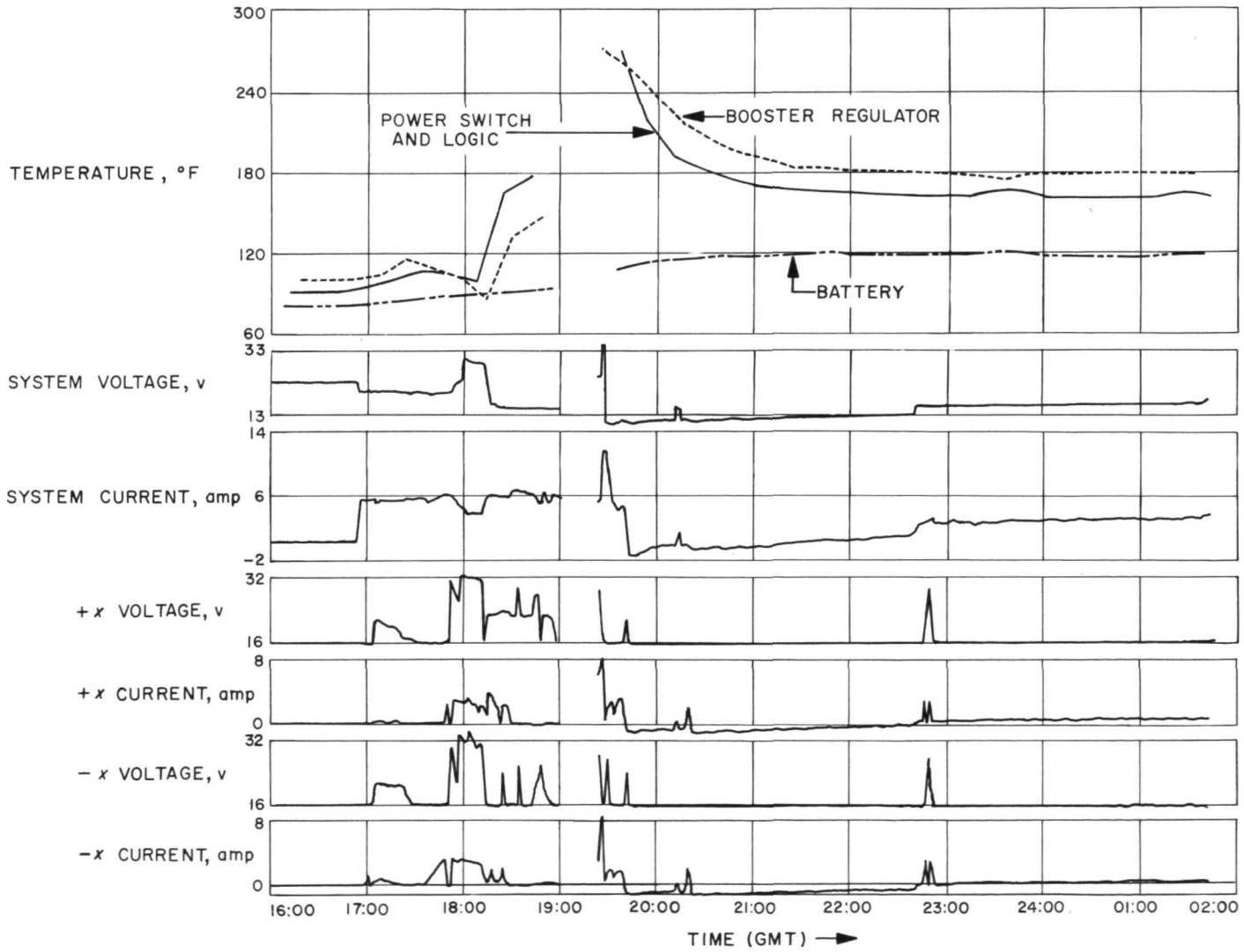


**Fig. 1. *Ranger 5* telemetry plots**

booster output. During the next hour the monitors rose slowly to a level about 5% below normal; this level was maintained until near battery depletion.

The general failure symptoms of the power system exhibited by the telemetry records are summarized as follows:

(1) A period of intense heating in the vicinity of the power switch and logic (PS&L) and booster, followed by abnormally high steady-state temperatures.

(2) Booster apparently operating, but not regulating properly after 19:28 GMT.

(3) Complete loss of power for about 23 min.

(4) Erratic and contradictory power system indications after 18:12 GMT.

(5) Battery depletion after about 8½ hr of operation.

*Failure possibilities.* The initial cause of failure of the power system appears to have been a short circuit within, or adjacent to, the PS&L subassembly. It is estimated from the telemetry records of the PS&L and booster temperatures that a relatively large amount of additional power (about 70–100 w) was dissipated in the PS&L during the period from 18:12 to 19:00 GMT. During the period from 19:00 to 19:23 GMT, the additional dissipation appears to have increased to about 200 w. It appears very unlikely that a partial open circuit in the PS&L power circuits could have generated the dissipations indicated in the period from 18:12 to 19:00 GMT without appreciably affecting the booster output.

It is suspected that a defective or partially loose junction stud for the main power returns in the PS&L may have been the cause of the loss of spacecraft power at 19:00 GMT. The returns for the solar panels, battery, and booster are connected to solder lugs which are bolted together on this stud (Fig. 2). Examination of other PS&L units has revealed that the fiber shoulder washer which insulates the stud from the chassis yields with age, permitting the solder lugs to loosen and thereby increase the resistance of the joints. This results in excessive dissipation at the stud and a corresponding rise in temperature. Tests performed in a vacuum chamber indicated that the temperature rise may be sufficient to melt the solder in the lugs. This could possibly cause the wiring to become disconnected from the lugs, although no such occurrence was noted during the vacuum tests. Additional heating of the junction stud because of the power being dissipated in the short circuit would tend to accelerate the deterioration of the stud.

The probability of a short circuit in the PS&L is increased considerably by the presence of a short circuit to airframe in the squib circuitry. It is estimated that about one squib in eight shorts to the frame with a resistance of less than 10 ohms. Eight squibs are fired

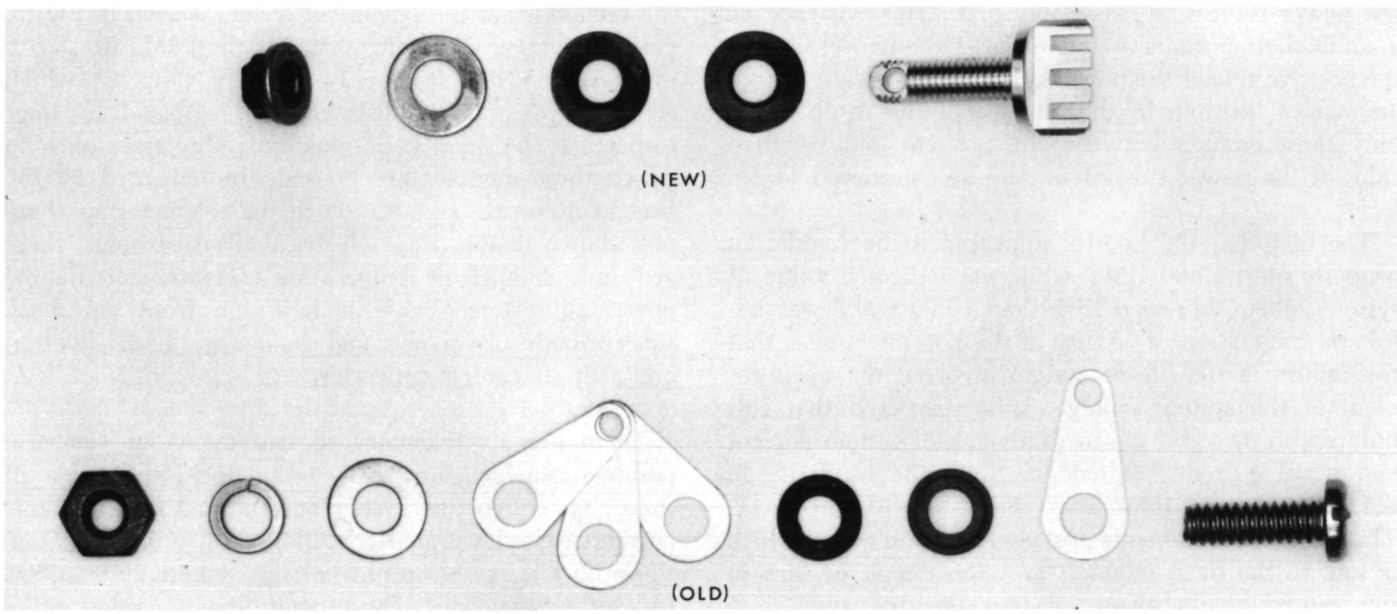


**Fig. 2. Old and new stud designs**

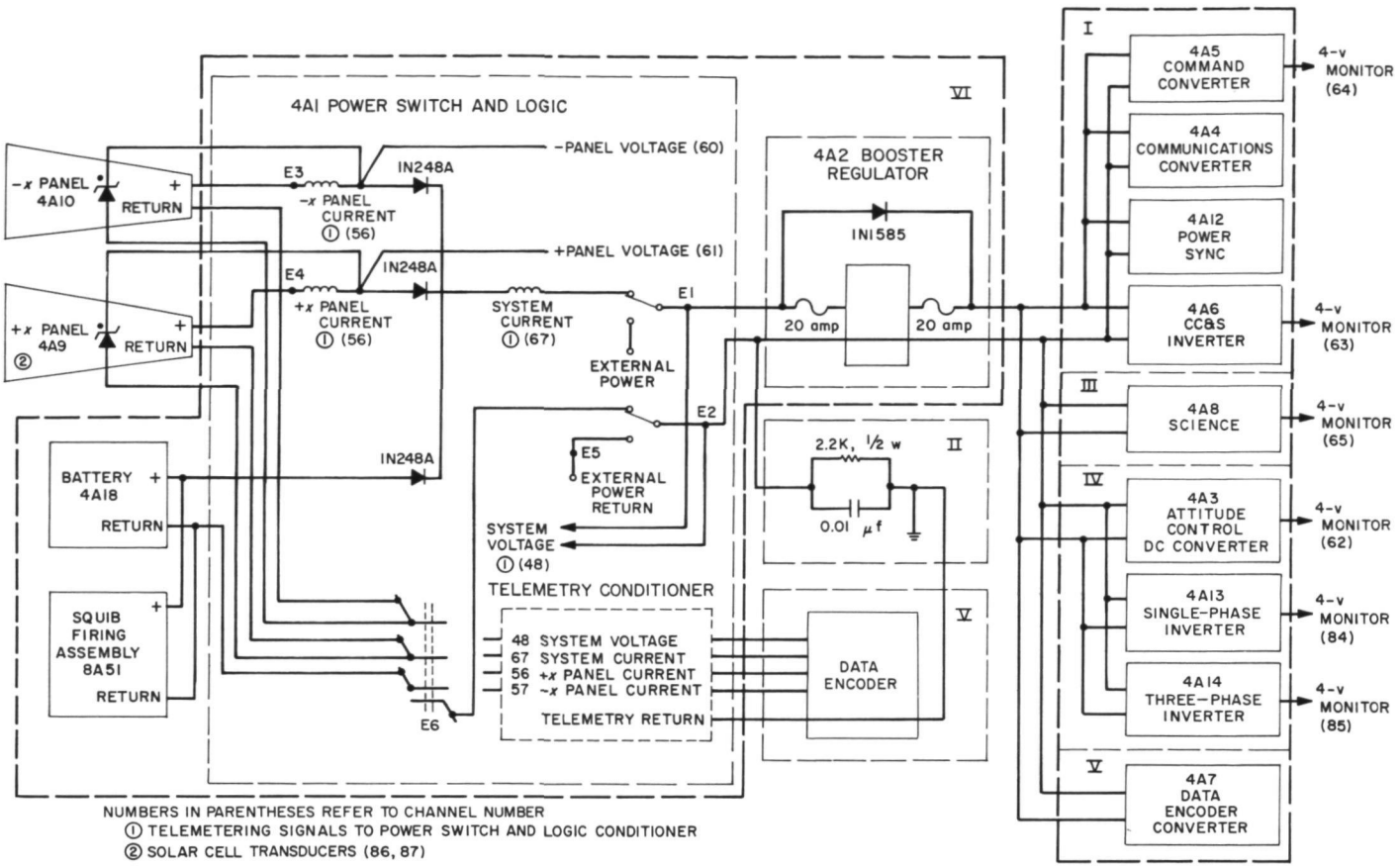


**Fig. 3. Distribution and telemetering signals**

simultaneously when the solar panels are extended; the resulting probability of a short circuit to chassis from the power returns is reasonably high. The existence of a squib short permits a single short circuit to chassis in the positive side of the power subsystem to create a large amount of heating; in the absence of the squib short, only short circuits between the positive and negative sides of the power subsystem may be considered.

The fact that the booster appeared to be regulating properly until 19:00 GMT while the indicated value of system voltage between 18:12 and 19:00 GMT was below the regulation capability of the booster implies that the failure in the power system involved the measurement of the system voltage. It is suspected that this failure also involved the measurement of system current and panel currents, as evidenced by the similarity in the movement of these four traces after 19:40 GMT. These four measurements possess a common return which is sent to the data encoder; an open circuit or bias in this return would affect all four measurements in a similar manner.

*Power system mechanization.* A simplified diagram of the mechanization of the PS&L and its relationship to the remainder of the power subsystem is seen in Fig. 3; various views of the configuration of the PS&L are shown in Figs. 4, 5, and 6. The 14 modules (Fig. 3) which comprise the power subsystem are indicated by their respective "4A" series designations; the assemblies in which these modules are housed are indicated by the Roman numerals. In addition to the telemetering channels shown in Fig. 3 for electrical measurements, there are eight channels of temperature measurements for the power subsystem. These include the front and back sides of both solar panels, and the battery, PS&L, booster, and attitude control converter.

There are six telemetry measurements of electrical parameters which are made within the PS&L. Four of these (system voltage, system current, and the two panel currents) employ signal conditioners in order to obtain the proper range of output voltage, nominally 0 to 5 v, for the data encoder. These conditioners employ either magamps or electronic choppers, depending upon the

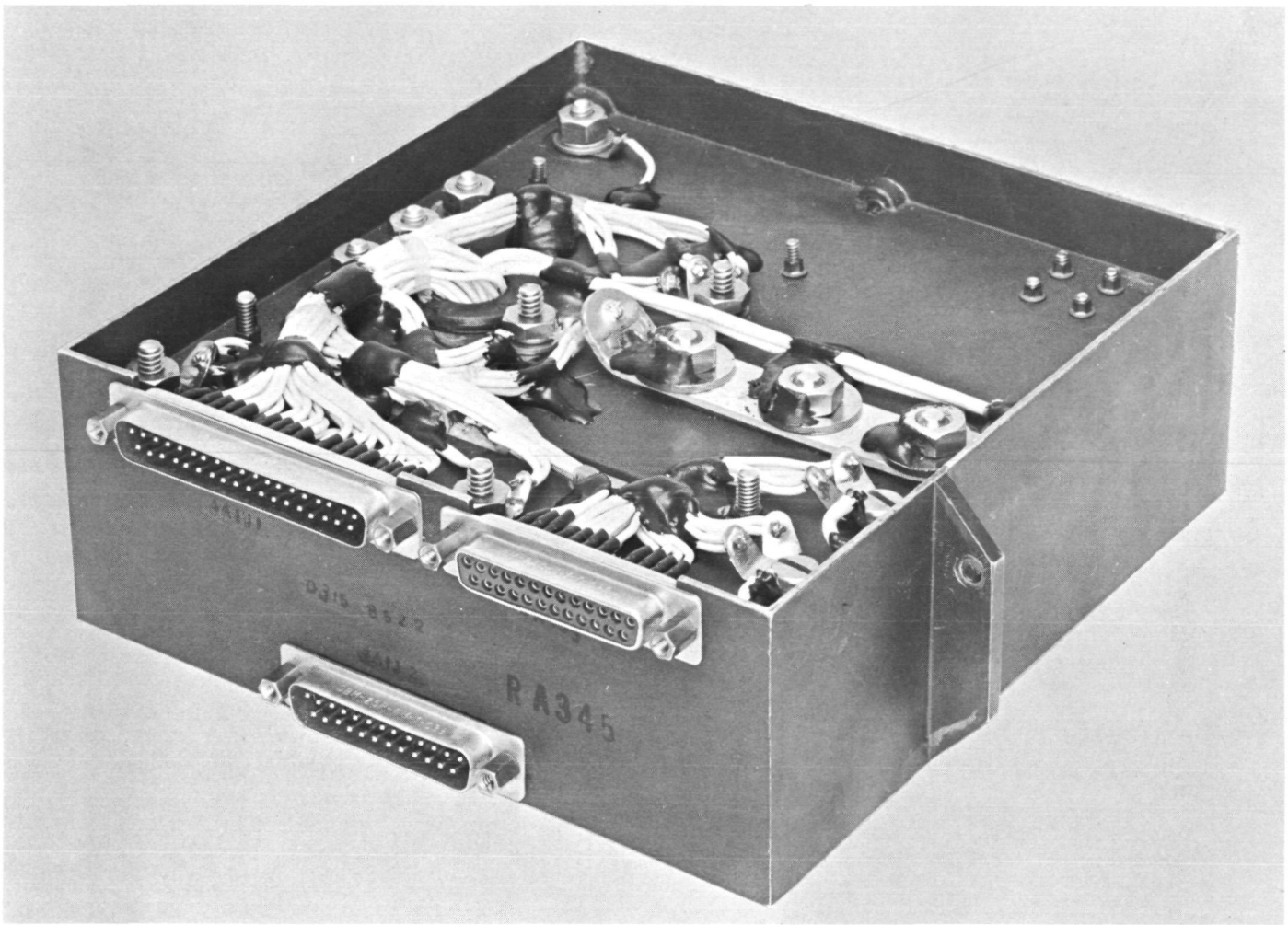


**Fig. 4. Power switch and logic, three-quarter view**

quantity to be measured. The outputs of the conditioners are electrically isolated from their corresponding inputs. A single return is used for all four conditioner outputs; this return is routed to the data encoder and is eventually connected to airframe in Assembly II. The remaining two measurements originating in the PS&L are the solar panel voltage measurements. The full panel voltages are sent directly to the data encoder and attenuated to the proper level by a resistive divider network within the data encoder. The return for these measurements is somewhat devious; it includes the data encoder return to airframe, a 2.2-K isolation resistor for the main power return, two junction studs (E2 and E6), and the internal-external power transfer switch. The purpose of the 2.2-K resistor is to permit static charges to pass to airframe without permitting excessive current drain in case of a short circuit to chassis from the "hot" side of the power subsystem.

During normal operation the current flows from either the battery or solar panels (at certain times from both sources) through their respective blocking diodes to the booster regulator. The current passes through a series of junction studs in the PS&L (indicated in Fig. 3 by the designations E1 through E6). Stud E5 is located in the return for the external power and is, therefore, not used in flight; the remaining five studs are essential for flight operation. The E6 stud carries the returns for both solar panels and the battery; it is this stud that is suspected of having been open for a portion of the flight.

The booster input voltage may vary from 18 to 31 v without exceeding its regulation capabilities. The output voltage is regulated at 31.5 v to an accuracy of $\pm$ 1%. In the event of a severe short circuit within the booster, either the input or output fuse will blow and the raw

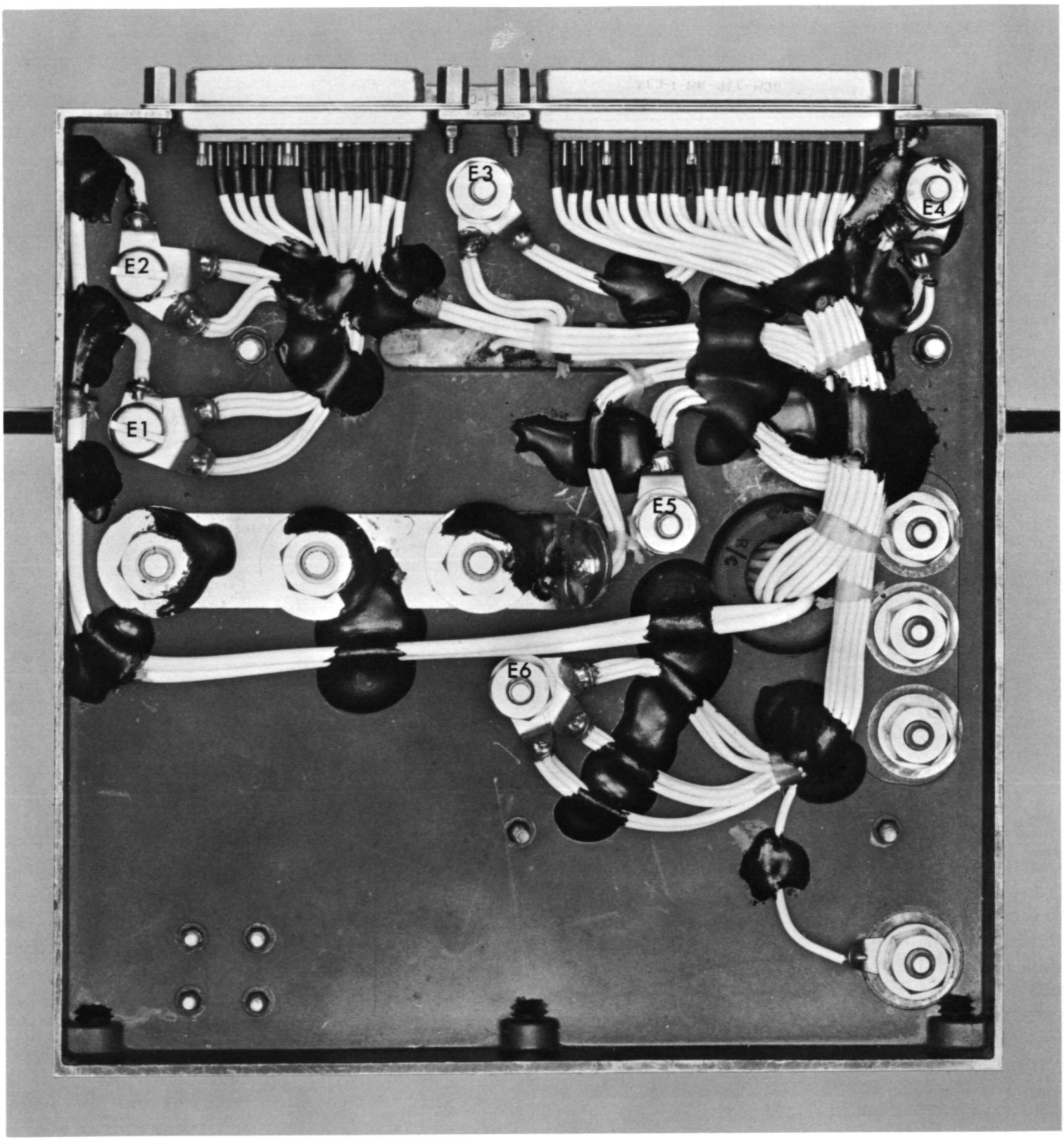


**Fig. 5. Power switch and logic, top view**

input power will bypass the booster and supply the converters directly.

The set of eight converters and inverters operate from the regulated 31.5-v output of the booster, a 9-v bias

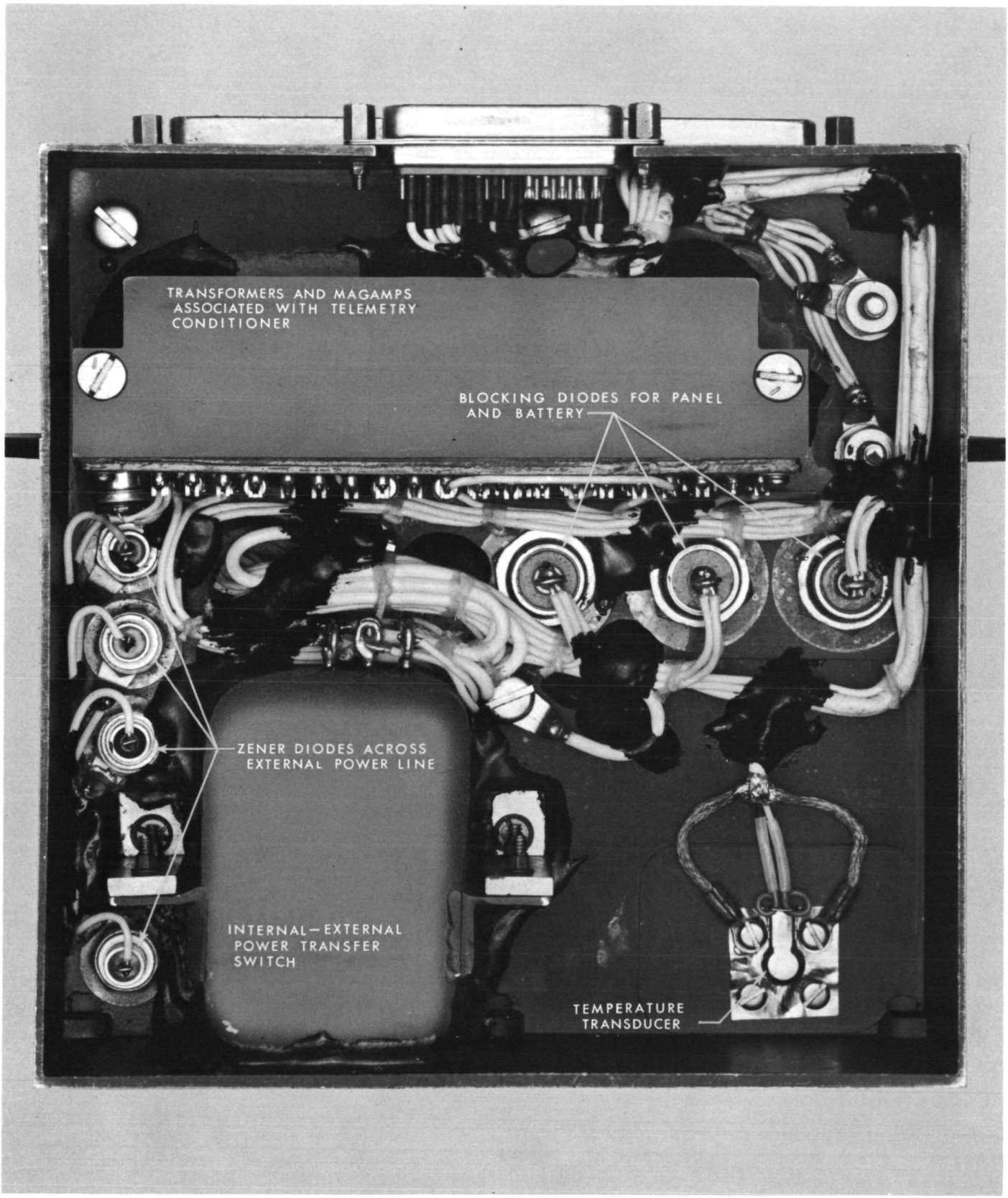


**Fig. 6. Power switch and logic, bottom view**

**Fig. 7. Power switch and logic junction stud**

supply which is also within the booster, and the synchronization signals from the synchronizer. The converters and inverters deliver 23 separate output voltages to the users, as well as monitor voltages to the data encoder.

*Recommended changes.* The junction studs in the PS&L are being replaced with new studs of greatly increased reliability in *Ranger 6* and all subsequent *Rangers*. A comparison of the old and new stud design is given in Fig. 2. The new stud eliminates all electrical connections

which involve only pressure between metal surfaces; all connections to the new stud are soldered. The improved connection should hold voltage drops across the stud to the order of a few millivolts in normal operation. Two shoulder washers will be used to restrict the *lateral* motion of the stud in order to reduce the chances of its shorting to the chassis. The new shoulder washers are made of a material (91LD, glass-filled phenolic) with greatly improved mechanical and thermal properties; this should eliminate the cold flow and cracking exhibited by the washers used previously (Fig. 7). Also, a self-locking nut will be used rather than the hex nut and lock washer combination used in the original design; the former has improved mechanical properties and is now a standard component for fabrication.

All PS&L units will be completely conformal coated (except for connectors and mounting surfaces) when they are reworked for the new stud installation. The *Ranger 3, 4,* and *5* spares had conformal coating only on the terminal boards, since this was the only requirement when they were fabricated.

Several other modifications are recommended for the PS&L in order to improve its performance. The solar panel voltage measurements should be isolated in a manner similar to the system voltage measurement. This change would eliminate the ambiguity which exists in the event of a shift in potential of the power system return relative to airframe. Also, the four zener diodes presently connected across the external power line should be eliminated from the PS&L. These diodes have no function in flight; their sole purpose is to prevent an accidental over-voltage on the external power line from damaging the converters. In practice, they act as a fuse; an over-voltage shorts the zener diodes, which in turn shuts down the system. This function, if required, should be placed in the ground equipment.

### *b.* Rangers 6 *through* 9.

The *Ranger 6* and *7* flight PS&L subassemblies have been modified and again flight acceptance tested. The modifications consisted of replacing the feedthrough stud assemblies with a new design, and reworking the mechanical tie points. The redesigned feedthrough assembly eliminates the mechanical splicing or joining by providing solder terminals at both ends of the stud and replaces the fiber shoulder washer with a new molded washer.

Currently, there appears to be only one problem yet unresolved on the *Ranger 6* power system. This problem involves the newly modified communications converter and the communications transponder. When the converter outputs were modified to supply ± 15 v in place of ± 20 v, some shunt regulators which had previously dropped the 20 to 15 v were removed from the transponder; the loss of the shunt regulators resulted in a loss of filtering. This loss of filtering resulted in the transponder not being able to meet its threshold limits in the spacecraft. This problem will be resolved as soon as the ripple and spike requirements for the transponder can be evaluated, and when it can be determined whether the spikes are being coupled through the power system or through the spacecraft main hex cable.

### *c.* Rangers 6 *through* 8.

Photovoltaic solar cell panels for *Rangers 6, 7,* and *8* have been manufactured and those for *Rangers 6* and *7* have completed flight acceptance testing. The flight acceptance (FA) tests included mechanical vibration, vacuum and temperature, and high temperature sterilization. The high temperature sterilization (125°C for 24 hr) has frequently caused degradation in the solar panel thermal control surfaces and in output electrical power. The thermal control surfaces that are affected are areas covered with a white paint consisting of a titanium dioxide pigment and an alkyd urea base. These surfaces darken due to exposure to the 125°C temperature. The loss in output power is attributed either to a decrease in the transmittance of the filter glass adhesive (Furance Plastics 15E epoxy) or an oxidation at the electrical contacts to the silicon of the solar cell (grids and contracts). As a consequence of the degradation resulting from high temperature sterilization, an engineering change to waive this requirement was requested and authorized by the project office. Under this waiver, the FA temperature sterilization test will not be performed commencing with the solar panels for *Ranger 8.* (A subsequent decision resulted in total removal of *Ranger* sterilization requirements. Effectivity of changes under this new rule is not yet established.)

Nominal values of current versus voltage and power versus voltage are shown in Figs. 8 and 9 for the *Ranger 6* panels. These characteristics were computed using performance data obtained on November 7, 1962, at Table Mountain, California. Nominal values of current versus voltage and power versus voltage are shown for the two *Ranger 6* solar panels measured in parallel with and without a PS&L module.

Nominal values of current versus voltage and power versus voltage for *Ranger 7,* solar panels Serial Nos. 5

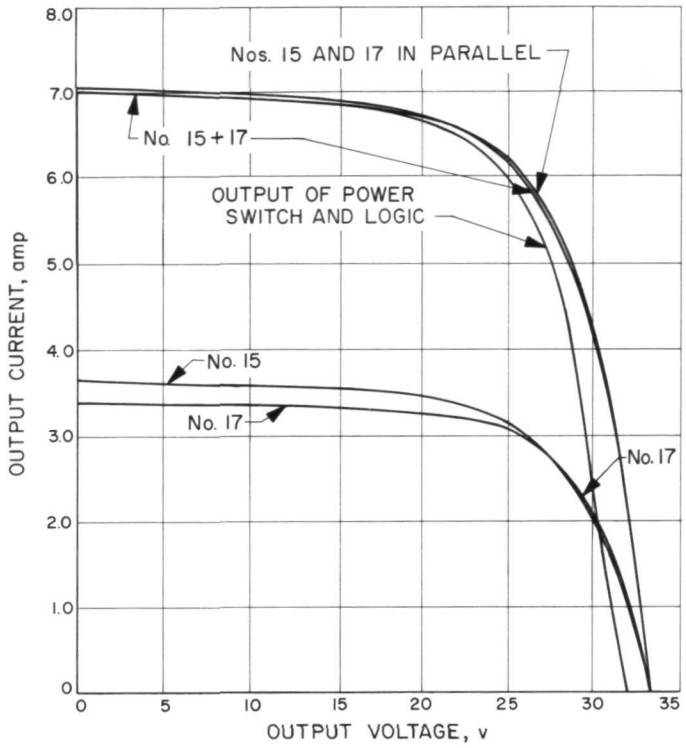


**Fig. 8. Nominal current versus voltage, *Ranger* 6 solar panels**

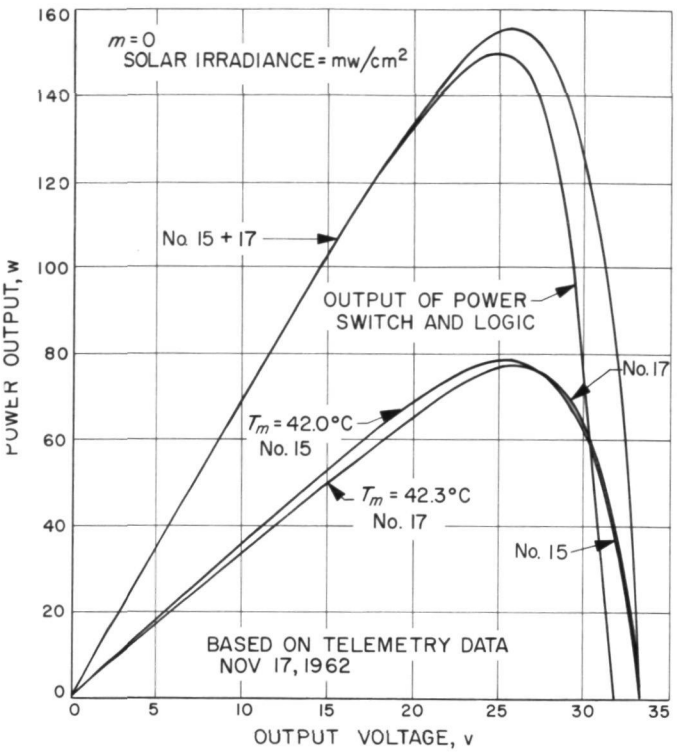


**Fig. 9. Nominal power versus voltage, *Ranger* 6 solar panels**

and 8, are shown in Figs. 10 and 11. These data were computed from measurements performed at Table Mountain on November 27, 1962.

*Mark IV solar panel fabrication.* On November 24, 1962, JPL accepted delivery of the Mark IV sample panel from Electro-Optical Systems, Pasadena, California (Fig. 12). Tests were performed at Table Mountain the same day, but due to cloud conditions, the only result was a qualitative evaluation of the 10 sections of solar cells on the panel.

Further tests were performed on the sample panel on November 26 and 27 at Table Mountain. These tests resulted in a quantitative evaluation of the sample panel. Fig. 13 shows the solar cell submodule layout of the sample panel. Each of the numbered sections contained the following cells:

| | Section | Number of parallel cells | Number of submodules in series | Number of cells | Adhesives and insulation |
|---|---|---|---|---|---|
| Unfiltered cells | 1 | 8 | 35 | 280 | RTV 60, 4-mil epoxy glass |
| | 2 | 8 | 35 | 280 | RTV 60, 4-mil epoxy glass |
| | 3 | 8 | 35 | 280 | RTV 60, LTV 602, 3 Mylar |
| | 4 | 8 | 35 | 280 | RTV 60, LTV 602, 3 Mylar |
| | 5 | 8 | 35 | 280 | RTV 40, LTV 602, 3-mil Mylar |
| | 6 | 8 | 35 | 280 | RTV 40, LTV 602, 3-mil Mylar |
| Filtered cells (410 $\mu$) | 7 | 6 | 30 | 180 | RTV 40, LTV 602, 3-mil Mylar |
| | 8 | 6 | 32 | 196 | RTV 40, LTV 602, 3-mil Mylar |
| | 9 | 6 | 8 | 48 | RTV 40, LTV 602, 3-mil Mylar |
| | 10 | 2 | 70 | 140 | RTV 40, LTV 602, 3-mil Mylar |

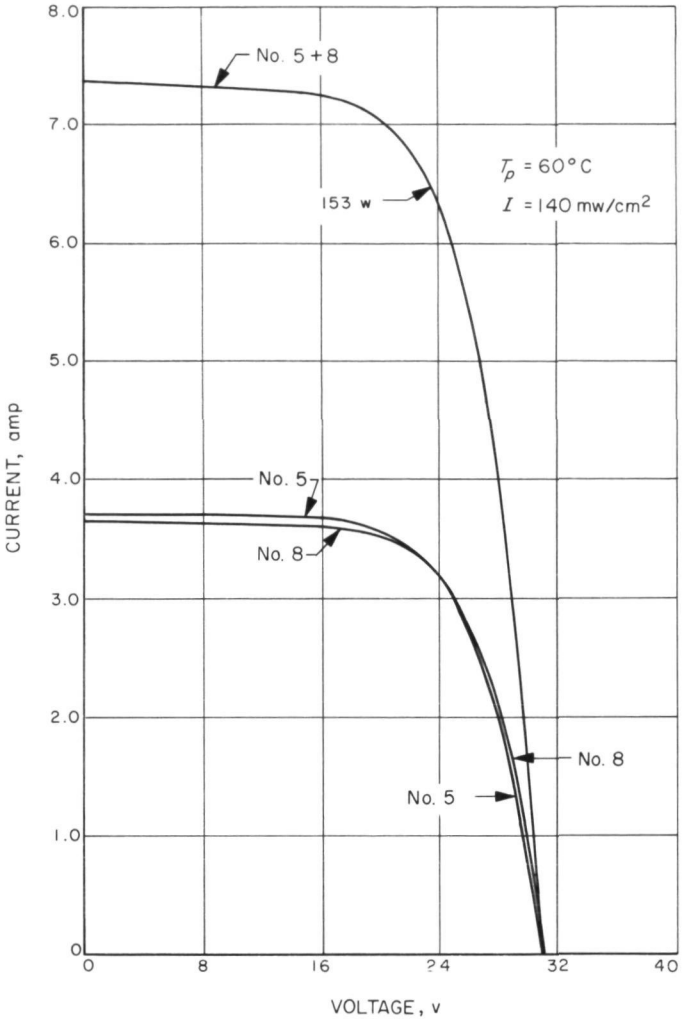


**Fig. 10. Nominal current versus voltage, *Ranger 7* solar panels**

The electrical tests at Table Mountain revealed that only Sections 3, 8, 9 and 10 were free from defective submodules. Table 1 is a list of the defective submodules found in the various sections.

Those sections exhibiting satisfactory performance yielded preliminary efficiency data. Of special interest are: (1) the output of a single cell in Earth space at 140 mw/cm² and 55°C, and (2) the watts/Langley/minute rating at Table Mountain at 50°C. A Table Mountain-to-space spectral correction factor of 0.83 and a power output temperature coefficient of 0.5%/°C were used to compute the performance values. The numbers are scaled up for Item (2) to equal a full size panel; i.e., for Section 3 the power output is scaled up by the factor 5040/280, 5040 being the total number of cells on a fully covered panel. The values of these parameters are shown

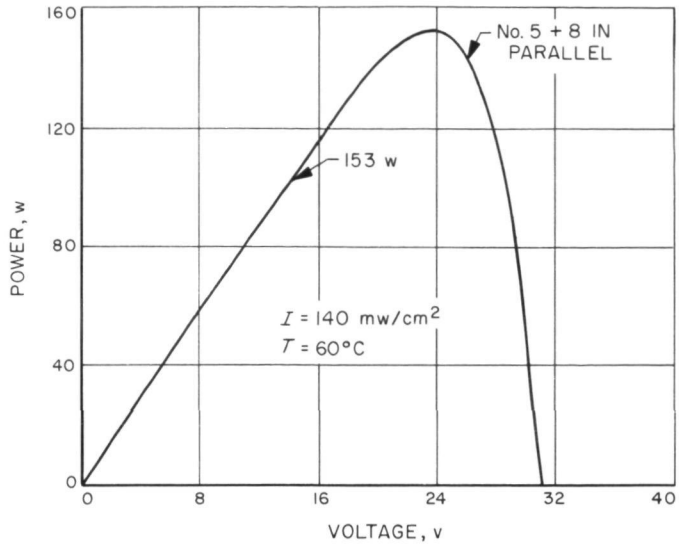


**Fig. 11. Nominal power versus voltage, *Ranger 7* solar panels**

in Table 2 for each of the sections which performed satisfactorily (all with filter covers).

**Table 1. Defective Submodules**

| Section | Defective submodule | Reason |
|---|---|---|
| 1 | 22, 29, 34 | One open cell on each |
| 2 | 27, 34 | 27: three open cells<br>34: one cell open |
| 4 | 23, 24, 30 | 23, 30: one open cell<br>24: two open cells |
| 5 | 8, 27, 32 | 27: partial short<br>8, 32: complete shorts |
| 6 | 13, 14, 20, 26, 27 | 13: one open cell<br>14: partial short<br>20: complete short<br>26: one open cell<br>27: partial short |
| 7 | 18 | One open cell |

**Table 2. Performance values**

| Section | Date | Milliwatts per cell | Watts/Langley/minutes/panel |
|---|---|---|---|
| 3 | 11-26-62 | 18.7 | 58.4 |
| 3 | 11-27-62 | 20.2 | 63.2 |
| 8 | 11-26-62 | 20.0 | 62.6 |
| 8 | 11-27-62 | 20.3 | 63.4 |
| 9 | 11-26-62 | 20.9 | 65.3 |
| 9 | 11-27-62 | 20.8 | 64.9 |
| 10 | 10-26-62 | ..... | ..... |
| 10 | 10-27-62 | 20.0 | 62.5 |
| Average | | 20.1 | 62.9 |

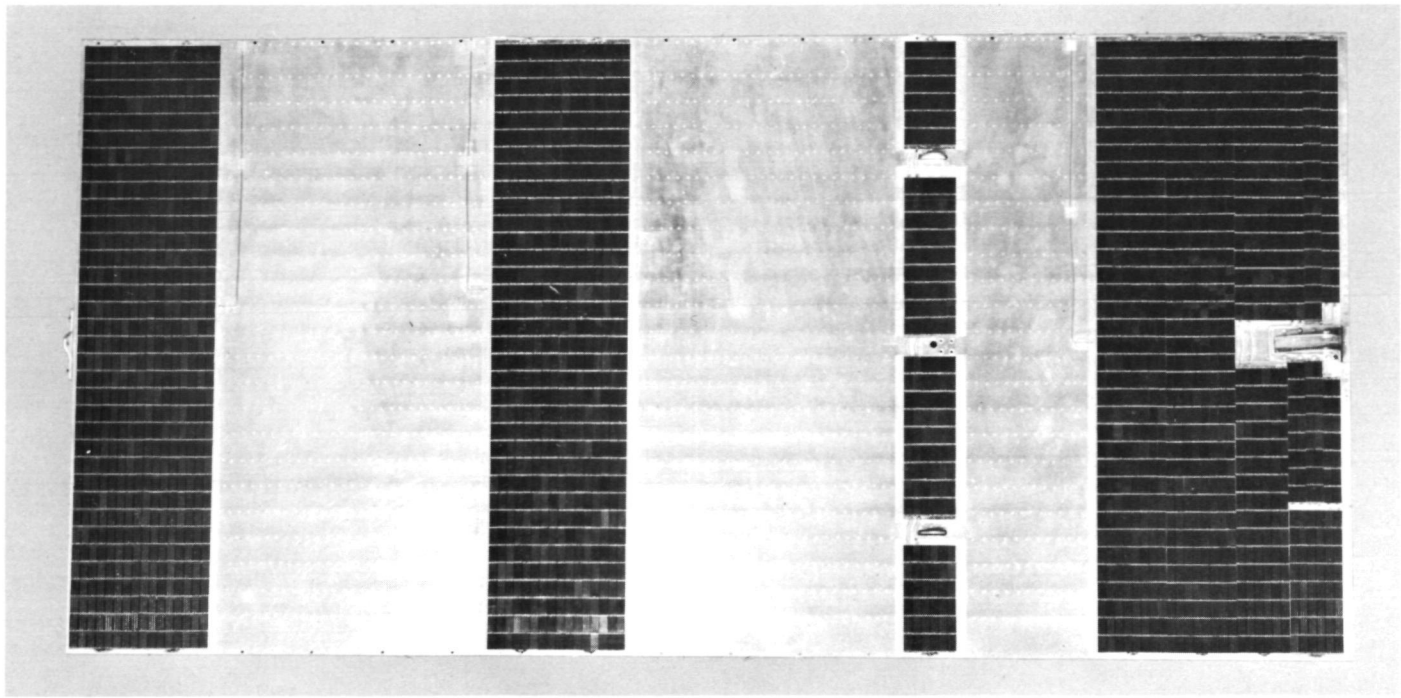

**Fig. 12. Mark IV sample panel**

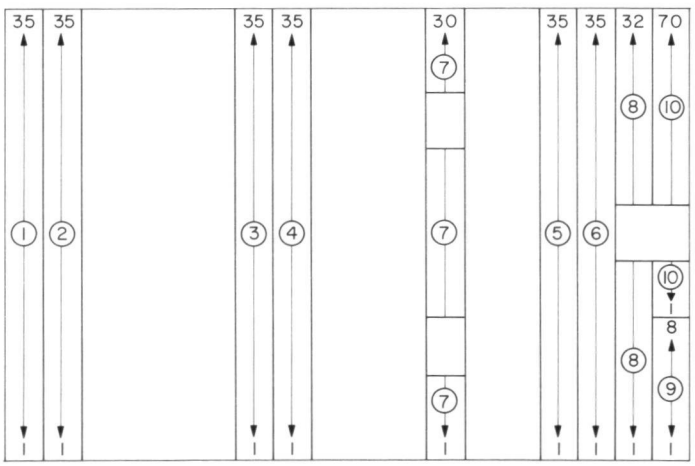


**Fig. 13. Mark IV sample panel submodule layout**

The available power required from two Mark IV solar panels (10,080 cells total) is 174 w at 140 mw/cm² and 55°C in Earth space. The equivalent Table Mountain power output at 50°C is:

$$P_{tm} = \frac{(174\text{ w})}{2\text{ Langley/min }(0.83)\ (0.975)}$$

$$= 107.5\text{ w/Langley/min}$$

where 0.83 = spectral correction factor and 0.975 = temperature correction factor.

The required output from a single panel is:

$$P_{TM} = 53.8\text{ w/Langley/min}$$

at Table Mountain and at 50°C. Assuming a ±7% rms uncertainty in computed output the nominal power required at Table Mountain between air masses 1.5 and 1.8 and at 50°C is:

$$P_{TM} = 57.6\text{ w/Langley/min/panel}$$

The predicted output of 62.9 w/Langley/min/panel shown in Table 2 would satisfy the requirement; however, degradation resulting from type approval or flight acceptance testing and launch has not been considered. The nominal power required from a single cell on the Mark IV panel at 140 mw/cm² and at 55°C in Earth space is 18.6 mw. The average value of 20.1 mw shown in Table 2 is considered reasonable before flight acceptance testing and launch.

On November 27 and 28, all type approval vibration tests (high and low frequency) were performed on the sample panel in accordance with JPL specifications. On November 30, the panel was again tested at Table Mountain. Table 3 shows the post-vibration test performance values:

**Table 3. Post-vibration test performance values**

| Section No. | Milliwatts per cell | Watts/Langley/ minutes/panel |
|---|---|---|
| 3 | 19.8 | 61.8 |
| 8 | 19.3 | 58.5 |
| 9 | 20.2 | 63.2 |
| 10 | 19.8 | 61.8 |
| Average | 19.8 | 61.3 |

These results tend to indicate a 1.0 to 2.5% degradation due to the vibration test. However, the apparent degradation is not necessarily indicative of a change in panel performance, but may be due to atmospheric changes at Table Mountain from November 28 to November 30. The tests on November 30 did not reveal any defective submodules except those previously identified in Table 1.

On November 30 efficiency data were obtained for the Section 1 submodules which contain all unfiltered cells. The average output of these cells extrapolated to 140 mw/cm$^2$ and 55°C in Earth space was 20.8 mw/cell. Compared with the filtered sections of the panel, the maximum power ratio of unfiltered to filtered cells is:

$$\frac{20.8}{19.8} = 1.051,$$

or there is a 5.1% power loss due to the filters on the cells. The cells used on the sample panel were procured on the basis of an average of 22.4 mw/cell at 100 mw/cm$^2$ equivalent Table Mountain solar intensity and 28°C. Normalized to these parameter values, the average bare cell output obtained at Table Mountain on November 30 from the acceptable submodules in Section 1 of the sample panel was:

$$P_{TM} = 20.7 \text{ mw/cell}$$

On the basis of these measurements, the degradation due to (1) handling and assembly of the cells to the panel, (2) cell mismatching, and (3) tungsten to Table Mountain, was a percentage given by the ratio:

$$\frac{22.4}{20.7} = 1.082$$

or a degradation of 8.2%.

On December 3 vacuum and temperature tests were started on the Mark IV sample panel. These tests were continued through December 5. The vacuum and temperature test includes:

(1) A period of 4 hr at −10°C back panel temperature and $10^{-4}$ mm Hg vacuum, or less.

(2) A period of 50 hr at 80°C back panel temperature and $10^{-4}$ mm Hg vacuum, or less.

**Table 4. Results of thermal-vacuum testing**

| Section No. | Defective submodule No. | Reason |
|---|---|---|
| 1 | 22, 29, 34 | 22: twenty open cells; 29, 34: one open cell |
| 2 | 27, 34 | 27: two open cells; 34: one open cell |
| 3 | 24, 31 | One open cell each |
| 4 | 23, 24, 30 | 23, 30: one open cell; 24: two open cells |
| 5 | 27, 23, 35 | One open cell each |
| 6 | 13, 20, 26 | 13, 26: one open cell; 20 shorted |
| 7 | 18 | One open cell |
| 8 | 25 | One open cell |
| 9 | None | |
| 10 | None | |

On December 6, tests were performed on the sample panel at Table Mountain for the purpose of detecting damage and/or degradation of the panel due to the vacuum and temperature testing. The qualitative results of the December 6 testing of the sample panel are given in Table 4.

The defective submodules which appeared in Sections 3, 5 and 8 were not defective prior to the vacuum and temperature tests. Table 4 shows that one open cell in each of the defective submodules is causing the degraded output. In Sections 5 and 6, a total of five submodules (Nos. 8, 27, 32 in Section 5, plus Nos. 14 and 27 in Section 6) which had partial, or complete, shorts prior to vacuum–temperature exhibited satisfactory performance after the vacuum–temperature testing. The only sections which were completely acceptable before and after vacuum and temperature were Sections 9 and 10. This allows a before and after comparison of the Table Mountain performance of these two sections, only. Table 5 shows the comparative Table Mountain results taken on November 30 and December 6 for Sections 9 and 10. On each of these two dates, data was taken with standard cell SM 3-15, the filtered cell contained in standard cell module SM 3 (Fig. 14). This standard cell is one of the

**Table 5. Comparative Table Mountain test results**

| Section No. | Date | Spectral correction factor | Milliwatts/cell | Watts/Langley/minute/panel |
|---|---|---|---|---|
| 9 | 11-30-62 (before vacuum–temperature) | 0.843 | 20.5 | 63.2 |
| 10 | 11-30-62 (before vacuum–temperature) | 0.833 | 20.3 | 63.2 |
| 9 | 12-6-62 (after vacuum–temperature) | 0.831 | 21.7 | 65.9 |
| 10 | 12-6-62 (after vacuum–temperature) | 0.834 | 21.4 | 64.7 |

fourteen flown on ballon Flight 2 for solar cell evaluation (*SPS 37–17*, Vol. IV, pp. 108–110). The air-mass zero-short-circuit-current efficiency ($\eta_0$) based on the balloon flight data for this cell is:

$$\eta_0 = 0.408 \text{ ma/mw/cm}^2$$

The standard cell data taken on the above two dates are used to obtain a spectral correction factor which is applied to the sample panel data. Standard cell SK 3-15 was used since it is a Hoffman cell with a 410-$\mu$ filter, simulating the cells and filters used on the Mark IV sample panel. Table 5 shows the following data:

(1) The maximum power output of a single cell in Earth space at 140 mw/cm$^2$ solar intensity and 55°C temperature based on the performance of Sections 9 and 10 at Table Mountain. The spectral correction factor used is that obtained from the standard cell measurements. A temperature-power correction factor of 0.5%/°C is used.

(2) The maximum power per unit solar intensity at Table Mountain for a full size panel (5,040 cells) at 50°C temperature, based on the performance of Sections 9 and 10. Again, 0.5%/°C is used for a temperature correction factor.

Table 5 shows an apparent increase in efficiency of Sections 9 and 10 of the sample panel after vacuum and temperature testing. Since the spectral correction factor was measured simultaneously with the panel using the standard cells, the change in the milliwatt/cell values would not be regarded as due to a change in the solar

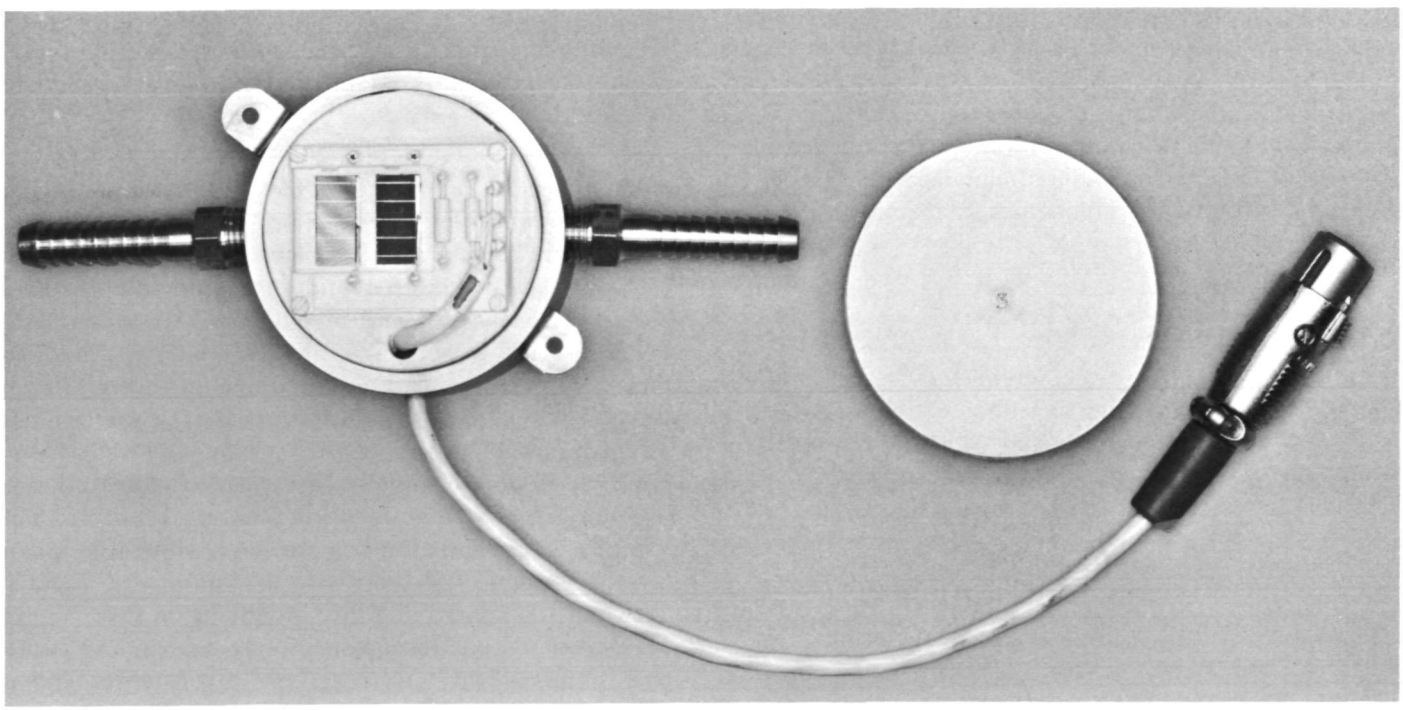

**Fig. 14. Standard cell module SM 3**

spectrum (unless the pyrheliometer is spectrally selective).

There will be a total of 1104 more cells to be mounted on the sample panel for further evaluation.

## 2. Terminal Turns for TV Picture Nesting

*a. Introduction.* Some *Ranger* trajectories may produce impact angles up to 60 deg from the vertical. If it were desired to obtain nested pictures on such trajectories, the motion of the spacecraft with respect to the lunar surface would have to be controlled to minimize: (1) translation of the TV cameras' optical axes with respect to the lunar surface in a direction perpendicular to the optical axes and (2) translation in a direction parallel with the optical axes. The blurring due to the rotation of the camera about axes perpendicular to or parallel with the optical axes is considered negligible.

Since the TV cameras are mounted on the *Ranger* spacecraft with fixed optical axes, for complete picture nesting it would be necessary to cause the spacecraft to turn such that the optical axes continuously point along the line of sight to the point of impact. Figs. 15 and 16 will prove helpful in visualizing the problem. An additional constraint is the requirement that communications be maintained during the descent by tracking the Earth in hinge and roll to point the high-gain antenna at the Earth.

The above-mentioned objectives could be accomplished by rotating the spacecraft during the terminal maneuver so as to point the cameras' optical axes initially at the point of impact and then to maintain the pointing by making simultaneous programmed inertial turns about the pitch and yaw axes during the descent. In general, this would be complicated by the fact that pitch and yaw turns would cause hinge and roll errors in the Earth sensor. The Earth sensor would cause the spacecraft to track the Earth in each of these channels. Consequently, the Earth sensor would cause a roll turn along with the simultaneous pitch and yaw turns.

*b. Methods of solution.* The purpose of this analysis is to determine a means for pointing the optical axis of the camera at the impact point such that complete nesting of the TV pictures results as consecutive pictures of the Moon are taken during the descent. Emphasis on quality is to be placed on those pictures taken closest to

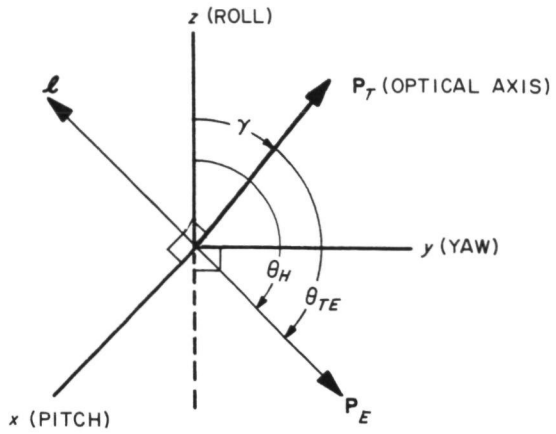


**Fig. 15. Spacecraft coordinate system**

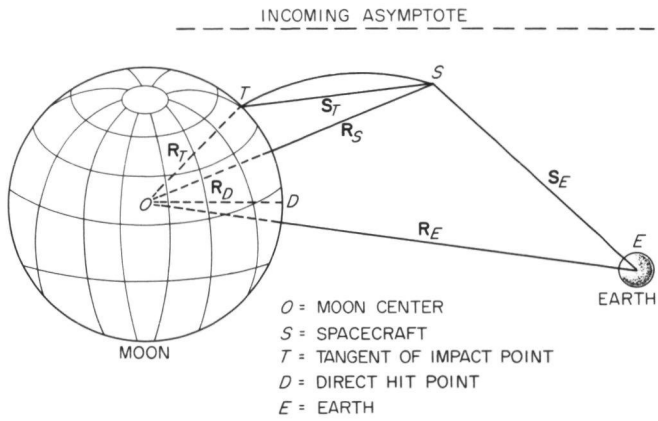


**Fig. 16. Vector configuration showing pertinent quantities**

the Moon's surface. In order to solve this problem, two approaches were taken. First, the question was asked, "What are the necessary variations of the pitch and yaw turns to continuously point the optical axis along the line of sight from the spacecraft to the impact point?" Second, the question of determining the variation of the pointing direction of the optical axis for specified pitch and yaw turns was posed. The first approach will solve the problem generally, but may possibly produce nonphysically realizable results, whereas the second approach will yield practically achievable pitch and yaw maneuvers but will produce an error. In other words, the second method guarantees a solution to the problem which can be implemented. The first method does not.

In the second method, the resulting error in the pointing direction of the optical axis will be determined and the pitch and yaw turns selected to produce optimum results.

*First method.* The solution in the first approach to the problem (i.e., obtaining the time variations of the pitch and yaw turns in order to keep the optical axis continuously pointed along the line of sight from the spacecraft to the impact point) consists essentially of solving the vector configuration shown in Fig. 16 as a function of time. In Fig. 16, the vectors are defined as follows:

$\mathbf{R}_T$ = point of impact vector

$\mathbf{R}_S$ = spacecraft vector

$\mathbf{R}_E$ = Earth vector

$\mathbf{R}_D$ = direct hit point vector

$\mathbf{S}_T$ = spacecraft to point of impact vector

$\mathbf{S}_E$ = spacecraft to Earth vector

It should be noted that any vector associated with the spacecraft is trajectory-dependent.

Referring to Fig. 16, it may be seen that the spacecraft must be turned about an axis perpendicular to the trajectory plane. It is convenient to use the incoming asymptote as an inertial reference for the turn so that the variation of the angle between the incoming asymptote and the line of sight from the spacecraft to the impact point would be indicative of the turning rate required of the spacecraft. Quantitatively, the turn rate can be obtained as follows:

$$-\cos\theta_A = \frac{\mathbf{S}_T \cdot \mathbf{R}_D}{|\mathbf{S}_T||\mathbf{R}_D|} = \mathbf{s}_T \cdot \mathbf{r}_D$$

and the magnitude of the turn rate is:

$$|\Omega_A| = \frac{d|\theta_A|}{dt} = \frac{d}{dt}\left|\cos^{-1}(-\mathbf{s}_T \cdot \mathbf{r}_D)\right|$$

The turn rate vector is completely defined by

$$\Omega_A = |\Omega_A|\eta_T$$

where

$$\eta_T = \mathbf{r}_D \times \mathbf{r}_T$$

It should be mentioned that lower case letters denote unit vectors.

The vector $\Omega_A$ is composed of three components, the pitch, yaw, and roll rates. Pitch and yaw are along the spacecraft $x$ and $y$ axes, respectively. The required pitch and yaw turns are put into the spacecraft by means of programmed signals sent to the pitch and yaw gyros in the attitude control system. The third component is put into the spacecraft by the automatic tracking of the Earth sensor in roll. Consequently,

$$\Omega_A = \Omega_P + \Omega_Y + \Omega_R$$

where

$\Omega_P$ = pitch turn rate vector

$\Omega_Y$ = yaw turn rate vector

$\Omega_R$ = roll turn rate vector

The individual turn rate vectors can be written in the form:

$$\Omega_P = (\Omega_A \cdot \mathbf{x})\mathbf{x}$$

$$\Omega_Y = (\Omega_A \cdot \mathbf{y})\mathbf{y}$$

$$\Omega_R = (\Omega_A \cdot \mathbf{z})\mathbf{z}$$

In the above set of equations, it was necessary to represent the spacecraft coordinate axes $(x,y,z)$ in the lunar inertial cartesian coordinates $(a,b,c)$. This was accomplished by using the vectors $\mathbf{s}_E$ and $\mathbf{s}_T$ in the following manner:

$$\mathbf{x} = \mathbf{s}_E \times \mathbf{s}_T$$

$$\mathbf{l} = \mathbf{x} \times \mathbf{s}_T$$

The vector $\mathbf{l}$ lies in the $y$–$z$ plane at an angle of (180 deg $-\ \gamma$) from the $+\ y$ axis. The angle $\gamma$ is the angle between the optical axis (which is coincident with $\mathbf{S}_T$) and the $+\ z$ axis. The direction of the $+\ y$ axis is then readily determined by noting the angles between the $+\ y$ axis and the vectors $\mathbf{l}$, $\mathbf{x}$, and $\mathbf{s}_T$. the $z$ axis is defined by:

$$\mathbf{z} = \mathbf{x} \times \mathbf{y}$$

At this stage, the pitch, yaw, and roll turns have been defined in such a manner as to turn the spacecraft so that the optical axis is continuously pointing at the impact point during the descent. All that remains is to determine the motion of the hinge during the final descent. This can be accomplished by noting that the hinge motion is entirely in the $y$–$z$ plane. The optical axis, which is coincident with the line-of-sight xector $\mathbf{S}_T$, and the antenna axis, which is coincident with the spacecraft to Earth vector $\mathbf{S}_E$, are both in the $y$–$z$ plane. The angle between $\mathbf{S}_T$ and the $+\ z$ axis is denoted by $\gamma$. The angle between the optical axis and the antenna is $\theta_{TE}$. Consequently, the antenna hinge angle $\theta_H$ is determined from the expression

$$\theta_H = \gamma + \theta_{TE}$$

where $\gamma$ is a fixed angle and $\theta_{TE}$ is determined from the relation

$$\theta_{TE} = \cos^{-1}(\mathbf{s}_T \cdot \mathbf{s}_E)$$

Since the hinge angle $\theta_H$ is mechanically constrained between $\gamma$ and 180 deg, the angle $\theta_{TE}$ is unequally defined by its cosine. Fig. 15 illustrates the mentioned configuration.

*Second method.* This method differs from the first in that instead of specifying the continuous pointing direction of the optical axis along a particular line and then determining the required pitch and yaw turns, the pitch and yaw turns are specified, and the resulting pointing direction of the optical axis is determined. The resultant pointing of the optical axis is then compared with the desired pointing in order to generate an error.

In the following development, Fig. 17 will prove of value. To begin, the initial conditions in the spacecraft coordinate system $(x,y,z)$ must be determined and then reflected into an inertial system $(a,b,c)$ centered at the origin of the Moon. The initial conditions in the $x,y,z$ system can be found in a manner discussed in the first section. What is required is a knowledge of $\mathbf{s}_E$, the spacecraft to Earth unit vector, and $\mathbf{s}_A$, the unit vector denoting the initial pointing direction of the optical axis. In order to relate the body-fixed Cartesian coordinate system to the inertial coordinate system, three successive angular rotations must be defined. These angles, of course, are known as the Euler angles and the stated transformation is depicted by the matrix equation:

$$\begin{pmatrix} x \\ y \\ z \end{pmatrix} = A \begin{pmatrix} a \\ b \\ c \end{pmatrix}$$

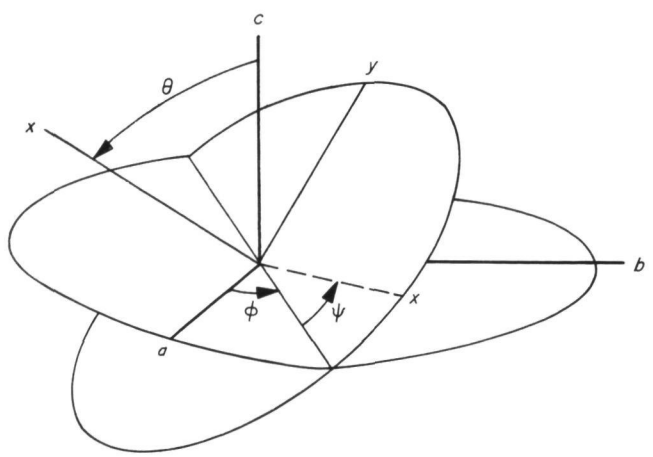


**Fig. 17. Relationship between body-fixed coordinate system and inertial coordinate system**

where

$$A = \begin{pmatrix} \cos\psi\cos\phi - \cos\theta\sin\phi\sin\psi & \cos\psi\sin\phi + \cos\theta\cos\phi\sin\psi & \sin\psi\sin\theta \\ -\sin\psi\cos\phi - \cos\theta\sin\phi\cos\psi & -\sin\psi\sin\phi + \cos\theta\cos\phi\cos\psi & \cos\psi\sin\theta \\ \sin\theta\sin\phi & -\sin\theta\sin\phi & \cos\theta \end{pmatrix}$$

The angles $\theta$, $\phi$, and $\psi$ are the Euler angles.

It remains now to determine the variation of the Euler angles with time. It is noted, first of all, that the various turn rates about the spacecraft pitch, yaw, and roll axes can be written in the following form:

$$\Omega_P = (\Omega_P)_\phi + (\Omega_P)_\theta + (\Omega_P)_\psi$$
$$\Omega_Y = (\Omega_Y)_\phi + (\Omega_Y)_\theta + (\Omega_Y)_\psi$$
$$\Omega_R = (\Omega_R)_\phi + (\Omega_R)_\theta + (\Omega_R)_\psi$$

The observation is then made that the time derivative of the Euler angles is related to the various components of the pitch, yaw, and roll turns in the following manner:

$$\frac{d\phi}{dt}(t) = \left[\Omega_P(t)\right]_\phi + \left[\Omega_Y(t)\right]_\phi + \left[\Omega_R(t)\right]_\phi$$
$$\frac{d\theta}{dt}(t) = \left[\Omega_P(t)\right]_\theta + \left[\Omega_Y(t)\right]_\theta + \left[\Omega_R(t)\right]_\theta$$
$$\frac{d\psi}{dt}(t) = \left[\Omega_P(t)\right]_\psi + \left[\Omega_Y(t)\right]_\psi + \left[\Omega_R(t)\right]_\psi$$

The components of the various turn rates, the terms on the right-hand side of the above equations, can in turn be defined in terms of the Euler angles and the turn rates about the pitch, yaw, and roll axes. It becomes a question then of integrating the resultant equations in order to obtain the time variation of the Euler angles. The pertinent expressions are shown below:

$$\phi(t) = \int_0^t \Big[\sin\psi(t)\csc\theta(t)\,\Omega_P(t) + \cos\psi(t)\csc\theta(t)\,\Omega_Y(t)\Big]dt$$

$$\theta(t) = \int_0^t \Big[\cos\psi(t)\,\Omega_P(t) - \sin\psi(t)\,\Omega_Y(t)\Big]dt$$

$$\psi(t) = \int_0^t \Big[-\sin\psi(t)\cot\theta(t)\,\Omega_P(t) - \cos\psi(t)\cot\theta(t)\,\Omega_Y(t) + \Omega_R(t)\Big]dt$$

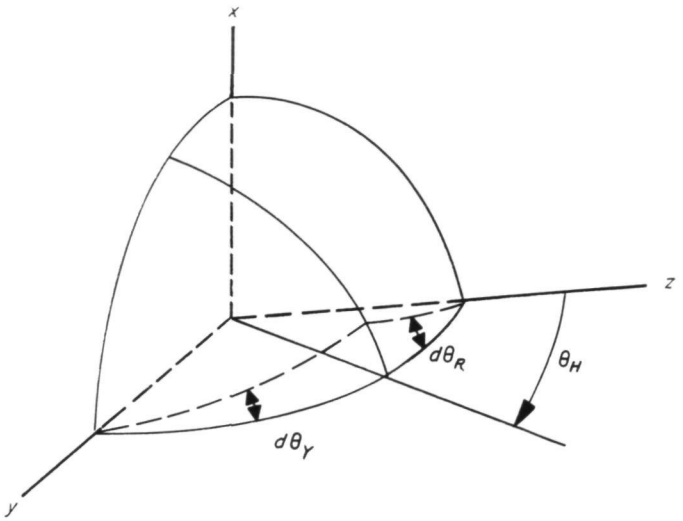


**Fig. 18. Effect of yaw-channel error on roll channel**

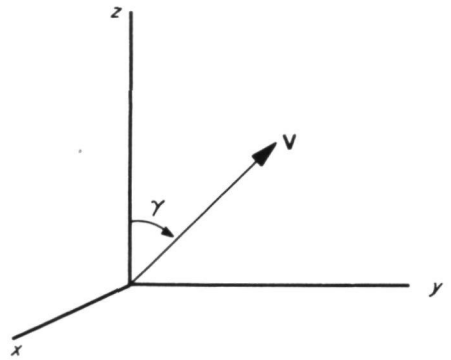


**Fig. 19. Body-fixed coordinate system showing fixed optical axis**

where $\Omega_P$ and $\Omega_Y$ are specified, and $\Omega_R$ is related to $\Omega_Y$ in the following manner:

$$\Omega_R = \Omega_Y \cot \theta_H$$

The above expression is obtained from consideration of the effect on the roll channel due to an error in the yaw channel. Fig. 18 illustrates this effect.

From Fig. 18, the following relation can be obtained:

$$d\theta_Y \cos \theta_H = d\theta_R \sin \theta_H$$

where $d\theta_Y$ and $d\theta_R$ designate the errors in yaw and roll respectively. Differentiation of the above equation will yield the previous expression relating $\Omega_R$ and $\Omega_Y$.

Now that the variation of the Euler angles with time has been defined, it becomes a question of defining the pointing direction of the optical axis, denoted by **v**, as a function of time. The unit vector **v** is given in the body-fixed coordinate system by the spacecraft design. In other words, the optical axis is mechanically fixed in the spacecraft as shown in Fig. 19.

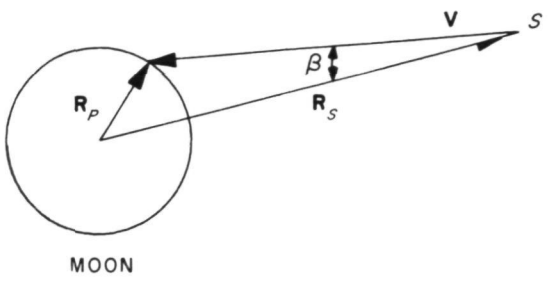


**Fig. 20. Vector configuration showing viewing point of camera**

The pointing direction in the inertial coordinate system is then obtained from the following equation:

$$\begin{pmatrix} v_a \\ v_b \\ v_c \end{pmatrix} = A^{-1} \begin{pmatrix} v_x \\ v_y \\ v_z \end{pmatrix}$$

The matrix $A$ has previously been defined.

In reviewing what has been done, it is noted that the pointing direction of the optical axis has been defined in terms of the Euler angles which in turn are defined in terms of the pitch, yaw, and roll turns. The pitch and yaw turns are specified at the outset and all the other quantities are subsequently defined. The question that remains is to determine the error resulting from such a means of pointing the optical axis. In this regard, Fig. 20 is of value.

In Fig. 20, the viewing point of the TV camera on the Moon's surface is denoted by $\mathbf{R}_P$. Consequently, the vector $\boldsymbol{R}_P$ can be determined and an angular measure of the error obtained from the following relation:

$$\theta_E = \cos^{-1}\left(\frac{\mathbf{R}_P \cdot \mathbf{R}_T}{|\mathbf{R}_P||\mathbf{R}_T|}\right)$$

### 3. Gas Actuator System Development

*a. System.* Design studies for future *Ranger* gas actuator systems include consideration of a two-part, unitized, strap-on gas system. Each half section would be capable of providing the required control torques autonomously,

in the event of a component failure in a half section. Each section would be composed of an 8-in. pressure vessel (*Mariner type*), regulator subassembly, and six jet valves—two valves on each axis providing plus and minus torque control. The solar panel bays would serve as the packaging area for the vessel, regulator subassembly, associated plumbing, and the yaw jet assemblies. The yaw valves would be mounted approximately 2 in. off the pitch axis, adjacent to the solar panel actuator, to reduce crosscoupling when a half section is operating. The angular acceleration requirement of 0.28 millirad/sec$^2$ would be provided by each section, thereby being compatible for commanded turn acceleration requirements in the event the spacecraft is operating on a half system. The total fuel capacity for this system is 4.34 lb. In the event of a half system failure during launch the remaining half system would be left with 1.45 lb of $N_2$. This figure is based on reasoning that 1½ units of gas flow from the half system which has failed (i.e., worst case) until the gas supply is exhausted. During this period, ½ unit is given up by the second half system. A review of *Ranger* 3 and *Mariner* 2 gas system flight performance indicates that 1.45 lb of $N_2$ would be sufficient to complete the mission. The weight penalty for this system is approximately 7 lb. The total gas system weight including gas weight is approximately 23 lb.

***b. Jet valve development.*** A new design version of an attitude control thrust valve is presently undergoing evaluation tests. Fig. 21 shows a dual valve unit which is miniature compared to past standards. These valves contain a soft seat, Teflon, which offers a distinct advantage. With a valve containing a metal-to-metal seal, clean contamination-free systems are paramount for low leakage. In a valve having a soft seat, contamination influence is less pronounced and may be fail-safe (i.e., based on leakage criteria) when exposed to particle contaminants in the size range up to 50$\mu$. Criteria for metal-to-metal valves presently require clean levels below 10$\mu$.

The units perform with exceptionally fast response times. The smaller coil and lower winding inductance provide for opening and closing times of 2.5 and 1.5 msec when excited with normal voltage.

Extensive testing is programmed during the first 3 months of 1963 with similar units.

***c. Fill manifold and filter.*** The *Ranger* gas subsystems utilize conditioned nitrogen gas as the working fluid. The inlet manifolding to the gas system has included (Fig. 22) a bacteria filter rated at 0.22 $\mu$ absolute to meet sterilization requirements formerly imposed. Included also in the fill manifold assembly are two shutoff valves, a check valve, a pressure port for calibration and leak testing and associated plumbing. A new compact

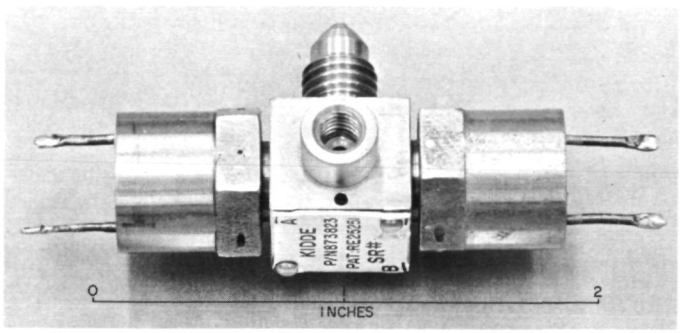


**Fig. 21. Dual valve unit, Kidde Co.**

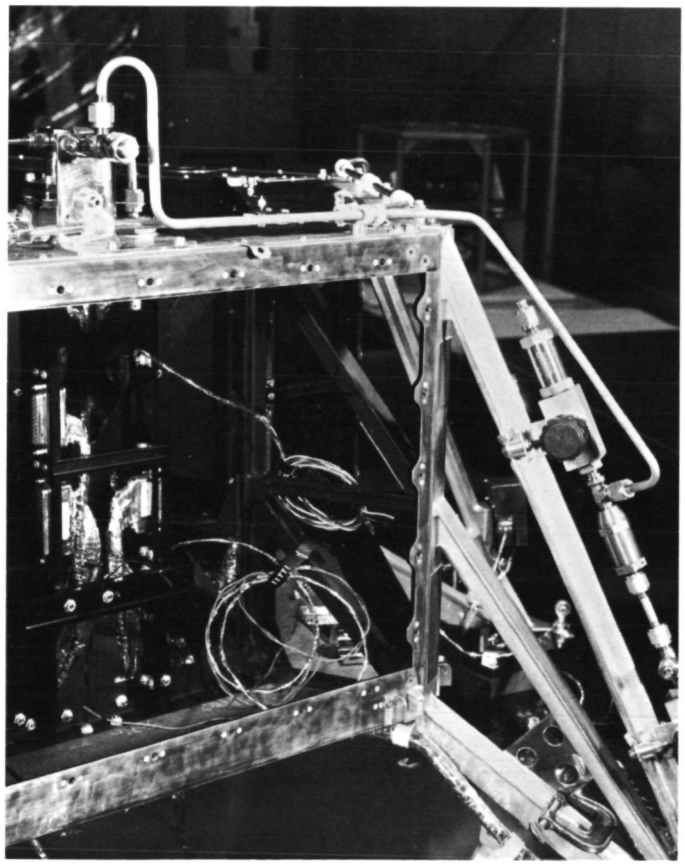

**Fig. 22. Present manifold fill assembly used on *Ranger***

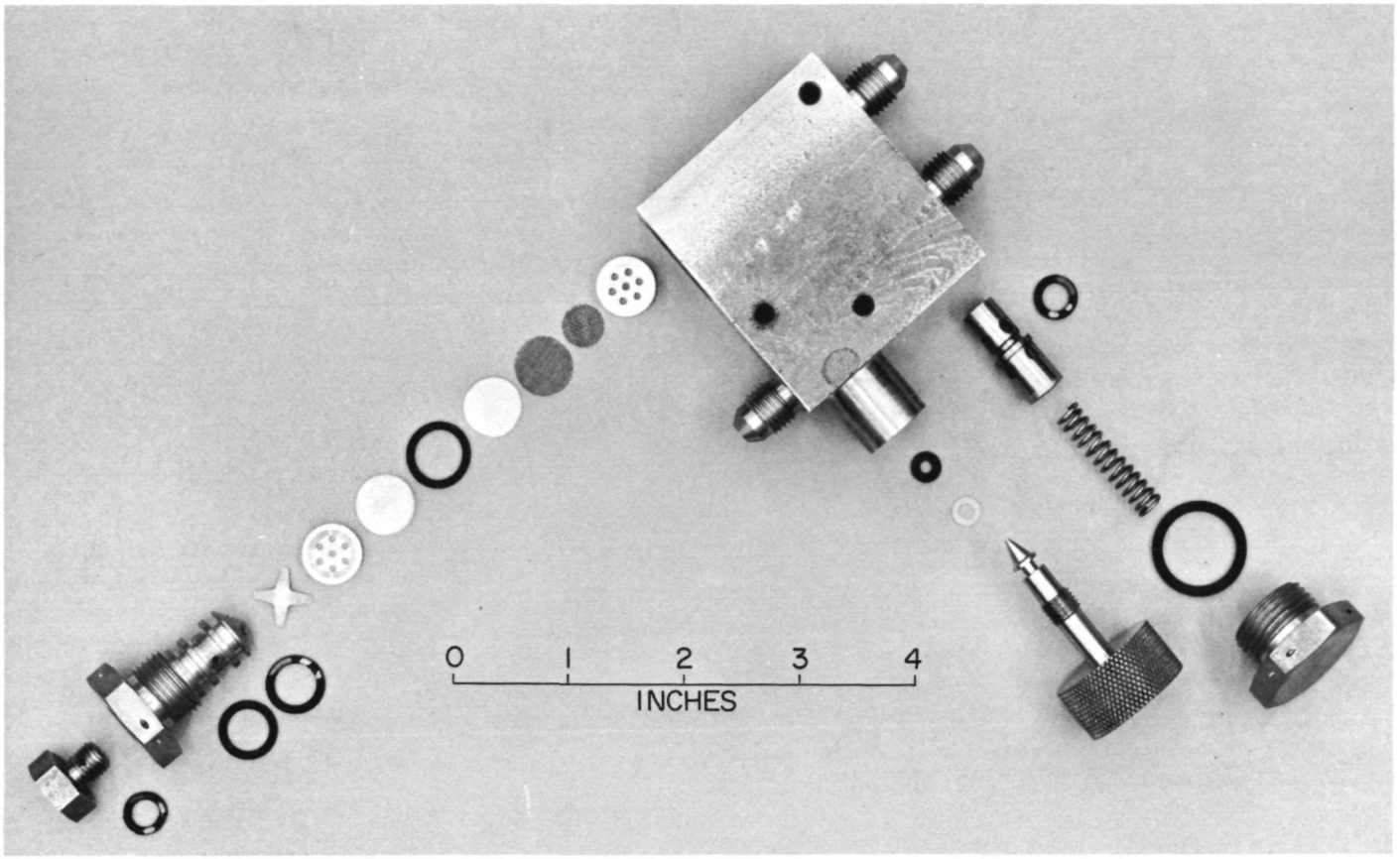


**Fig. 23. New compact fill manifold assembly**

fill manifold assembly has been designed to improve upon this subassembly (Fig. 23).

The compact filter assembly provides all of the basic utilities of the old system, in addition to fail-safe protection. A check valve in parallel with the filter limits the reverse flow pressure drop which would otherwise puncture the filter membrane. One needle-point shutoff valve replaces the previous two. The fill assembly is removed from the spacecraft after the final flight charging operation.

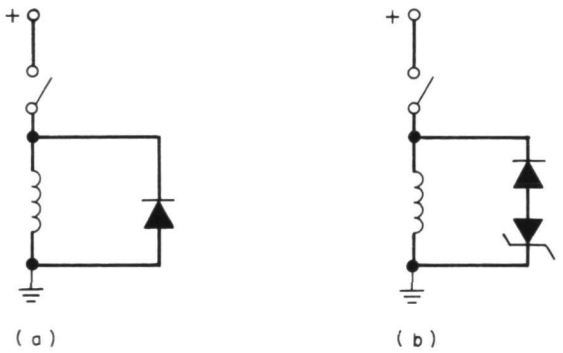


**Fig. 24. Solenoid switching circuit protection**

### 4. Gas-Valve Solenoid Improvement

In the gas attitude control used on the *Ranger* and *Mariner* spacecraft, a source of impulse error in correcting the position of the spacecraft is the slow and variable closing time of the solenoids used on the gas valves. Because of this error, gas wastage results, and more gas must be stored aboard the spacecraft for any particular mission. This is a problem inherent in cell solenoids, as holding current level is well below pull-in current level, and the associated switching circuitry must be protected from the high voltages that can be induced by the solenoid upon disconnecting the circuit. The commonly used circuit protection is shown in Fig. 24(a).

In the relationship $L\ di/dt + iR = 0$ (which is the equation that describes what happens in an inductive circuit when the outside energy is removed), $R$ is the coil resistance and the forward resistance of the protective

diode in Fig. 24(a). The voltage developed across the coil in this circuit is less than 1 v.

To speed the current drop, more resistance is needed in the diode circuit. This results in higher voltages being induced across the coil. The limit is the voltage level that the controlling switch can stand. In the *Ranger* and *Mariner* attitude controls this is a transistor switch and little real aid can be obtained in adding resistance to the diode circuit. A more promising means of speeding current drop and solenoid closing time is the addition of a zener diode in the circuit [Fig. 24 (b)]. This increases the resistance in the circuit and places a limit on the induced voltage, protecting the control switch. Experimental results are:

(1) *Ranger*-type solenoid valve with protective diode —40 to 95 msec.

(2) *Ranger*-type solenoid valve with zener protection —8 msec.

The reason for the large variation in solenoid drop-out time for the circuit of Fig. 24 (a) is that it takes in excess of 5 time constants of the circuit for the solenoid valve to close. The case for the circuit of Fig. 24 (b) is that the solenoid valve closes in less than 1 time constant of the circuit.

In the gas attitude control system used aboard the spacecraft, the addition of the zener diode allows a much more accurate prediction of gas consumption, a better prediction of impulse imparted to the spacecraft, and less gas required for any particular mission.

Further investigation is in progress to establish the relationship of zener dynamic resistance to valve closing time as well as a reliability of higher order for this use of a zener diode.

### 5. Electronic Component Reliability

***a. The Space Parts Working Group.*** The Aerospace Industry has long been confronted with a serious electronic component reliability problem. This difficulty is due to the fact that most of the industry companies and agencies procure and use only small quantities of any single given type component; yet, the reliability of the few components per type must be extraordinarily high. High reliability demands on the one hand, coupled with a low use factor on the other, are not economically compatible, with the result that superior components are extremely scarce. Only in the areas where considerable effort and money have been expended are improved parts available. One such area is the *Minuteman* Program; however, many of these parts are difficult to obtain due to demand.

In the Fall of 1961, the action and encouragement of Lockheed Missile and Space Company resulted in a conference of twenty aerospace companies and agencies at the Marshall Space Flight Center. This group had one common problem: how to obtain electronic component reliability in small lot purchases. This meeting constituted the first gathering of the Space Parts Working Group (SPWG). This organization, which is in the process of receiving official recognization as an active Air Force consulting committee, has grown during the last 14 months to include approximately 40 companies and agencies. The charter of the group stipulates that the chairman must be a full-time government employee or an officer in the armed services.

The SPWG, since its inception, has been working toward one goal. That is, the producing of a series of high reliability component procurement specifications. It was early recognized that the specifications must be sufficiently definitive to yield a truly high reliability component. However, a means must be provided in the documentation to allow the individual participating companies and agencies to express specific requirements.

To provide for these variables, the specification format has taken the form of three documents. The Top Document or Document I contains information of a general nature pertaining to all electronic components. This includes environmental and reliability requirements, process control, failure analysis and corrective action statements, quality assurance provisions, delivery requirements, and a section devoted to application notes. The Top Document has been written as a combined effort of six subcommittees within the SPWG. It is currently being circulated to the full participating membership for comment and correction. Following correction, the document will be submitted to the component manufacturing industry for comment. When all meaningful corrections and comments are incorporated, the document will become an active operating specification. It will be identified by an assigned Air Force number. One day this specification may become a standard military specification. However, the current Air Force identification is adequate until further steps can be taken.

The SPWG is continuing aggressive action in the electronic component specification area. The second in the series of three high reliability documents is currently being written. The second document, really a group of several specifications, is known as the Generic Specifications. These documents will detail the specifics of the various classes of components, such as diodes, capacitors, and transistors. It is expected that the group will contain between 15 and 30 specifications. The generic documents should be available about mid-1963.

Following the generic specification effort, the SPWG plans to prepare the third group of documents. This group will be known as the Item Requirement Sheets. These will detail the requirements of individual component types within the various classes. This series of documents will not be available until late in 1963.

JPL has been an active participating member of the SPWG since its inception. The Laboratory is particularly interested in the Top Document effort. JPL has been procuring a number of types of electronic components to Laboratory-prepared Hi-Rel specifications. Many of the nontechnical requirements, such as vendor process control and documentation have been conducted by verbal agreement. The SPWG Top Document will formalize this area in the immediate future.

JPL will continue to contribute to the SPWG effort. A high reliability transformer specification will be submitted for inclusion in the generic document group in January of 1963.

The total efforts of the SPWG have been met with very encouraging results. The users of components have been able to cooperate successfully to the extent that the first document has been produced. The component manufacturers have expressed considerable interest because the number of imposed specifications promises to decrease. It is expected that satisfactory and meaningful documentation will continue to be generated through the SPWG endeavor.

***b. Spacecraft multipin connectors.*** The interconnection of assemblies is one of the major reliability problems in spacecraft electronics. The reliability of interconnecting devices, particularly connectors, is a major problem because of two important factors: (1) the quality of the connector itself (2) the human factors associated with the assembly of the connector into the equipment and its handling thereafter.

The quality of connectors is gradually improving as manufacturers and users more fully understand the functional requirements that lead to improved reliability and reflect such requirements in the design of the connector, manufacturing process control, and users' procurement specifications. However, any connector, even though of the highest quality when received from the manufacturer, must be protected from handling damage and from environmental contamination.

The multi-pin connectors currently used in the majority of the spacecraft applications are round bayonet-lock (pygmy type), manufactured by Bendix and others now entering the field, and the rectangular D-series connector manufactured by Cannon and Cinch. These two types of connectors are now covered by JPL Hi-Rel specifications which require the manufacturer to provide minor design changes and to perform stringent quality control. The latest revisions of the specifications are in the final stages of negotiation with the manufacturer. Procurement for electronic stores will begin in the near future.

Features of these specifications that are common to both types are requirements for 100% inspection of contact mating forces and a careful inspection for workmanship with particular emphasis on contacts and inserts.

The inspection will be performed by the manufacturer who will also provide an inspection record with *each* individual connector. Sample inspection at JPL will serve to monitor the manufacturers' performance with regard to the quality requirements of the specification. Each connector will be marked with a date-code and serial number.

Design changes for the bayonet-lock type of connector consist of changing the wafer spring in the coupling ring to a nonmagnetic material, irridite shell finish, a heavier gold plating, and the prohibition of the use of cadmium and certain other materials. The part numbering will be changed to a JPL nomenclature. This will permit procurement of connectors from other manufacturers (when they qualify) with a minimum stocking confusion.

In the case of the D-series, the major design change involves control of the orientation of the socket contacts. Some changes in the design of contacts to improve their reliability are being considered; however, no agreements have been reached with the manufacturers. Other features of the existing design have been more definitely specified.

The future of multi-pin connectors tends toward higher contact density and smaller contacts. Two designs are now

being investigated. The first, Cannon's Micro-D, is similar in design to the D-Series with a substantial size reduction. A new concept in contact design is utilized consisting of a spiraled, multi-wire pin and a springless cylindrical contact. Preliminary tests indicate the need for refinement of process control for contact mating forces and a design change to strengthen the connector body. The second is Microdot's 43-series which is a high density, round, push-pull type. No performance data are available as yet.

## C. Telecommunications

### 1. Ranger Data Encoder

The basic system for encoding data in a form suitable for modulation of the RF carrier is a pulse amplitude modulation/frequency modulation (PAM/FM) or time division multiplex/FM subcarrier method. In this system many data points are periodically sampled and the sampled data then frequency-modulate an oscillator. The outputs of several FM oscillators, each being modulated with sampled data, is linearly mixed and the composite signal then modulates the transponder. Pulses generated in the spacecraft operate the encoding device.

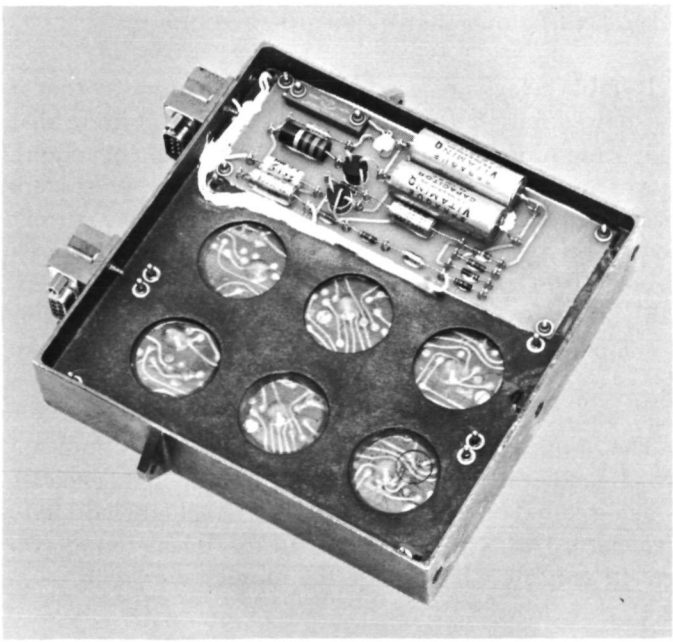

Fig. 25. Auxiliary clock

*a. Auxiliary clock.* After the central computer and sequencer (CC&S) clock pulses on *Ranger 4* ceased to occur, it was not possible to read out of the spacecraft any events or sampled data. In order to avoid this in the future an auxiliary clock (Fig. 25) which will provide pulses if the primary CC&S pulses are not present was designed and installed in *Ranger 5* and subsequent *Ranger* spacecraft.

The auxiliary clock circuit is shown in Fig. 26. A unijunction transistor is used as a relaxation oscillator. If the primary CC&S pulses are present, the 0.68-$\mu$f condenser is discharged by these pulses through the switching transistor which prevents the auxiliary clock pulses from being generated. If the primary CC&S pulses do not occur, the 0.68-$\mu$f condenser charges up to a predetermined voltage level and discharges through the unijunction transistor and the switching transistor. At this time, the current flowing through the 68-ohm resistor produces an output voltage pulse.

Note that no elements in series with the CC&S line are necessary and that either both diodes or the 6800-ohm resistor or the 0.47-$\mu$f capacitor must short in order to prevent the primary CC&S pulses from occurring. To distinguish the auxiliary clock pulses from the primary CC&S pulses, the auxiliary clock pulse repetition rate is adjusted for 24 pps, while the CC&S pulse repetition rate is 25 pps.

If the 1-msec CC&S pulse becomes too narrow the auxiliary clock will generate its pulse rather than be inhibited

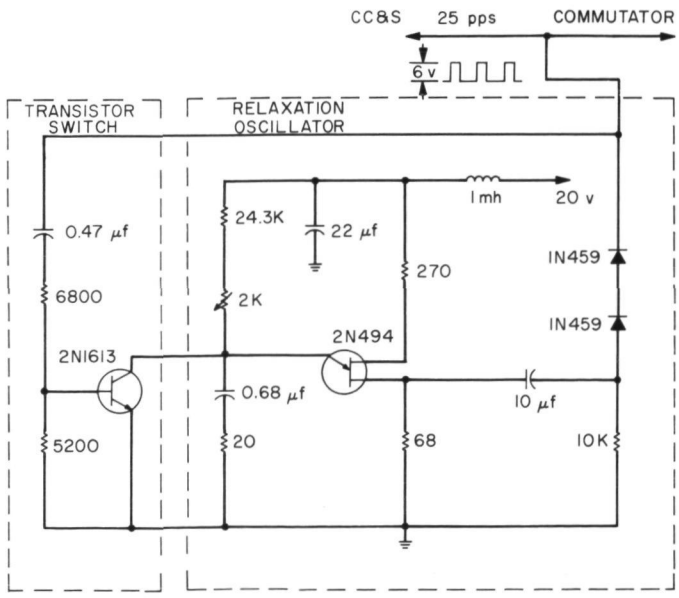


Fig. 26. Auxiliary clock circuit

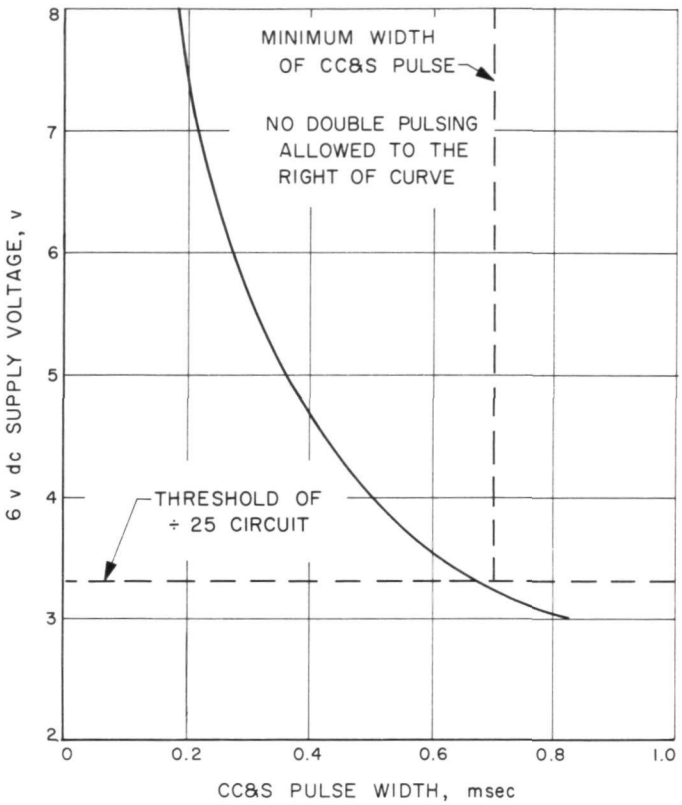


**Fig. 27. Standard voltage-width curve**

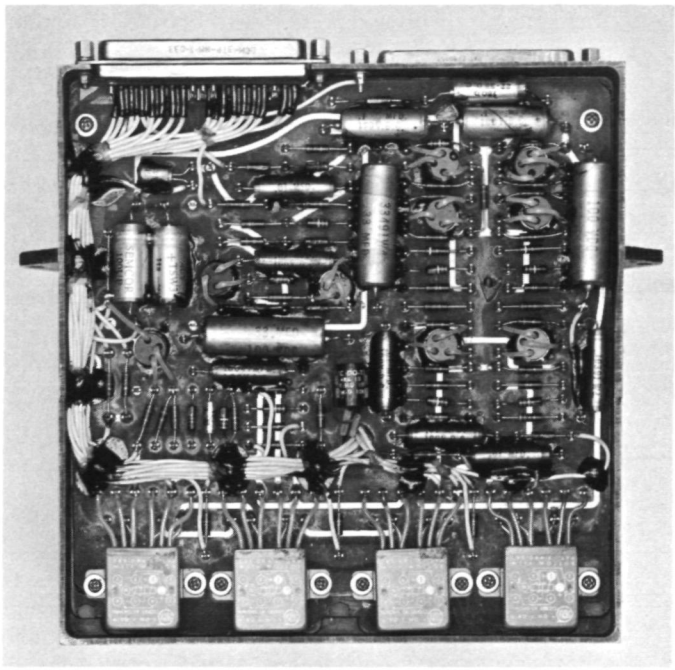

**Fig. 28. Data encoder programmer**

by the CC&S signal. This is known as double pulsing. If double pulsing occurs in flight the commutator will not operate properly; to avoid this, the CC&S pulse width and amplitude limits are specified. As the positive 6-v supply voltage decreases the clock becomes more sensitive to the pulse narrowing effect. The graph of Fig. 27 shows how the supply voltage varies with the pulse width at which double pulsing occurs as illustrated by the dashed lines. The minimum pulse width is 0.7 msec and the minimum pulse amplitude is 3.3 v.

***b. Programmer.*** During *Ranger* flights the importance of the individual signals being telemetered varies with the maneuvering characteristics of the spacecraft. So that the most important events and measurements will be telemetered at the proper time, four different modes of telemetering are employed. The data encoder mode is determined by the programmer shown in Fig. 28.

As shown in the block diagram of Fig. 29, the programmer consists basically of a pulse divider, a relay commutator, a pulse forming circuit, and the data relays. An incoming mode changing pulse triggers the flip-flop which immediately advances the relay commutator one step. The commutation is accomplished by connecting bistable relays so that they will advance one step at a time from pulses which alternate from one side of the flip-flop to the other. 1-msec clock pulses spaced 1 sec apart trigger the pulse forming circuit which widens the clock pulses to 10 msec. These modified clock pulses are then wide enough to reliably pulse the bistable relays. The relay commutator then determines which of the data relays will be operated by the 10-msec pulses.

Bistable relays are used in the programmer so that if the power fails the relays will stay in the position that they were in initially. Also, because relays do not require power to hold them in either position, only pulses are used to operate the relays rather than continuous current flow. The average power dissipation is very much reduced. If the positive 20-v supply voltage fails momentarily, the power failure reset circuit assures the transistor flip-flop of being set in the same position as it was before the power failure.

The terminals labeled *Test Output* are used to indicate which mode the programmer is in when the data encoder is being tested on the ground. The terminal labeled *Mode Telemetry Output* is connected to the telemetering system to indicate which mode the programmer is in.

Three mode change inputs are located on the programmer. Normally, the mode change pulse originates from

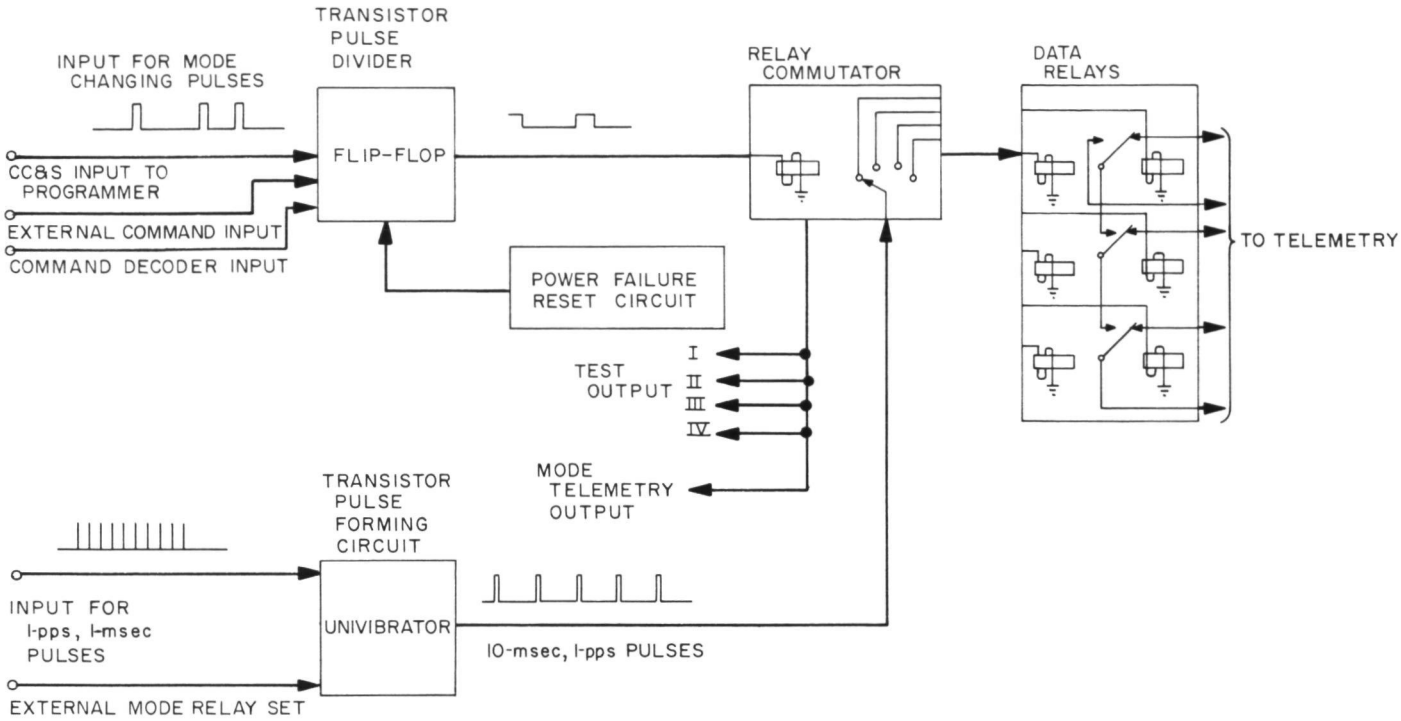


**Fig. 29. Programmer block diagram, Module 6A14**

the CC&S located on the spacecraft. This signal is applied to the terminal marked CC&S Input to Programmer. When testing the spacecraft on the ground an external signal is applied to the terminal marked External Command Input. If the mode is to be changed from the ground while the spacecraft is in flight a signal from the command system is sent to the programmer through the terminal marked Command Decoder Input. After a mode change pulse occurs, the terminal marked External Mode Relay Set is pulsed externally to change modes without the normal clock pulse.

# D. Space Sciences

## 1. Ranger TV System: Ground Recovery Equipment, Calibration, and Ground Data Handling

*a.* **Ranger 5** ***ground data handling.*** The primary receiving station for *Ranger 5* television data was the Echo Station at Goldstone, California. It was necessary to locate all ground data handling equipment at the receiving site in order to minimize photograph degradation due to land-line noise or standard instrumentation tape wow and flutter. The onsite equipment used for the *Ranger 5* operation consisted essentially of a specially modified Ampex FR-600 tape recorder, ground support equipment racks containing all necessary program and sync logic, scan converters and video monitors, and special 35-mm kinescope film recorders. In addition to this ground handling equipment, the services of a commercial Video Tape Van were secured for NASA public release of the photographic data as presented through the scan conversion equipment and from on-site processed film. The ground handling equipment (Fig. 30) was housed in a special room which had controlled access; the activities inside were visible through windows from an adjacent experimenters' room.

Seven tracks of data were recorded on the FR-600 magnetic tape recorder. This was comprised of the following: Two tracks of analog FM recording were used for the outputs of the two video demodulators, while one track was used for the common predetection signal into the video demodulators. The remaining four tracks were used to record the 400-cps Channel 1 output from telemetry, the motor drive sync signals for magnetic transport control, the horizontal sync pulses from the ground data rack, and the 1-kc tone burst GMT signals for real-time identification of any portion of the recorded tape. Because

**Fig. 30. Ground handling equipment at Goldstone for *Ranger 5* TV data**

absolute transport stability is essential to prevent signal degradation, the magnetic recorder was run at 30 in./sec. This was the fastest tape speed which would accommodate the 3-$\sigma$ maximum mission length and give the lowest flutter.

Five kinescope film recorders were utilized in the ground data handling equipment. This large number of units would allow for on-site development of two films for immediate viewing, editing, and cutting while allowing three records to be developed later for detailed experimenter analysis and archive storage. These cameras were developed specifically for the *Ranger* 3–5 mission and are a continuous film transport with single line scan on the modulated cathode ray tube. With this technique, it was possible to incorporate dynamic focus capability such that all portions of the kinescope record are of equal quality with no soft-focused corners. A large system simplification resulted from the fact that no frame pull-down pulse is required. The camera framing is accomplished by the continuous film transport, and it is only necessary to drive the cameras with a horizontal sync pulse. Because sync pulses are obtained from the output of Channel 1 phase lock discriminators, it is possible to maintain absolute synchronization in frame and line even if the video signal-to-noise ratio should drop below unity, as in the *Ranger* 3 mission failure.

The primary functions served by the control racks (two were used for redundancy) are the maintenance of synchronization of ground and flight cameras, and video processing for display purposes. The flight cameras derived line sync by counting down the 400-cps spacecraft clock telemetered back on Channel 1. Thus, while a vestigial sync pulse was combined with the telemetered video, it was necessary only to use the narrow band clock for ground synchronization since the spacecraft camera always used every 20th zero crossing for line sync even during camera erase mode. Of course, in the event of a Channel 1 failure, it was possible to use standard synchronization techniques. In practice, the 400 cps from telemetry was used to phase-lock an internal oscillator in the ground rack. This internal oscillator was made to zero-beat against Channel 1 prior to phase-lock, and phase-lock is interruptable with a front panel switch so that an interruption of Channel 1 would not throw the system out of sync or cause excessive noise. By using a triggered sweep sawtooth generator as opposed to flywheel sync, it was possible to count down by any integer and, if necessary, use random sync signals for line lock. By thus using this nonstandard approach, it was possible to maintain synchronization and hence retain video for any spacecraft failure that would allow video of any sort to be transmitted. A further spacecraft backup was provided by using internally generated free-running oscillators which were locked by the central computer and sequencer. Should a clock failure occur on the spacecraft, the flight cameras would revert to their free-running mode allowing data transfer.

Video processing was restricted to the minimum functions of gain set, dc restoration, and horizontal shading. The video signal as recovered from telemetry demodulators contains a dc term; however, simplicity of gain adjustment and polarity inversion were required, which necessitated ac coupled amplifiers and a very simple dc restoration of the video prior to feeding to the film recorders and scan converter. It is a characteristic of the storage vidicons used on the *Ranger* program that a near-parabolic background shading appears superimposed on the video. This is of such a nature as to render the center of a line lighter than its edges. A simple additive shading potential was provided on the ground rack for smoothing this background. A low light level magnetic tape recording of the *Ranger* 5 flight camera was available for presetting this control, and almost any realistic level of this parabolic shading as well as shading tilt was provided, should it be found that a change occurred in the lighting of the flight camera. The shading potential was in no way added to the FR-600 magnetic tape, but was an operator

option separately on the film cameras and the scan converter as determined by repetitive oscilloscope display of flight camera line video.

The scan converter allowed the 10-sec frame time to be written in and held at a standard television rate so that operating personnel and experimenters could comfortably view the experiment in progress, while a standard video tape recording might be made for rapid public release. No qualitative data were expected from scan conversion pictures, and their maximum contribution was an immediate assessment of system operation. Frame lock for the scan converter was derived from a vertical triggered sweep generator with automatic free run to prevent losing a frame.

*b. Video performance through telemetry.* Since the success or failure of the lunar impact photography experiment depended upon the telemetry link, every opportunity was taken to monitor performance through the receiver. A test tape was generated for this purpose which consisted of three sections. The first section contained Channel 1, Channel B-2, and an unmodulated Channel V carrier of 3.6 kc. This first section allowed for setup of the test transponder and corresponded to the Mode IV signal from *Ranger* 5. The second section of tape was used for telemetry signal-to-noise calibrations and contained the same signals as the first section with the exception that the Channel V signal was modulated from band-edge to band-edge with a 100-cps square wave. The final section of tape contained the Mode IV signals with a test pattern modulation of Channel V.

The calibration tape thus represented a real-time simulation of the signal used to modulate the spacecraft transmitter. In operation, the output of this tape was fed via land line to the Echo Station collimation tower approximately a mile from the receiving antenna. A transponder was modulated by this test signal, and the modulation index was adjusted for the proper carrier suppression by the first section of tape. The receiving antenna was used to pick up the transponder signal, and carrier signal strength was monitored at the receiver. The demodulated signal from telemetry was sent to the television control room and there displayed on an oscilloscope, recorded on kinescope film recorders, and recorded on an instrumentation magnetic recorder. As soon as the proper modulation index and carrier strength were established, the square-wave test pattern was fed through the system and photographs were taken of the resultant output for various carrier strengths. By this means, it was possible to reduce the data at leisure for interpretation in terms of

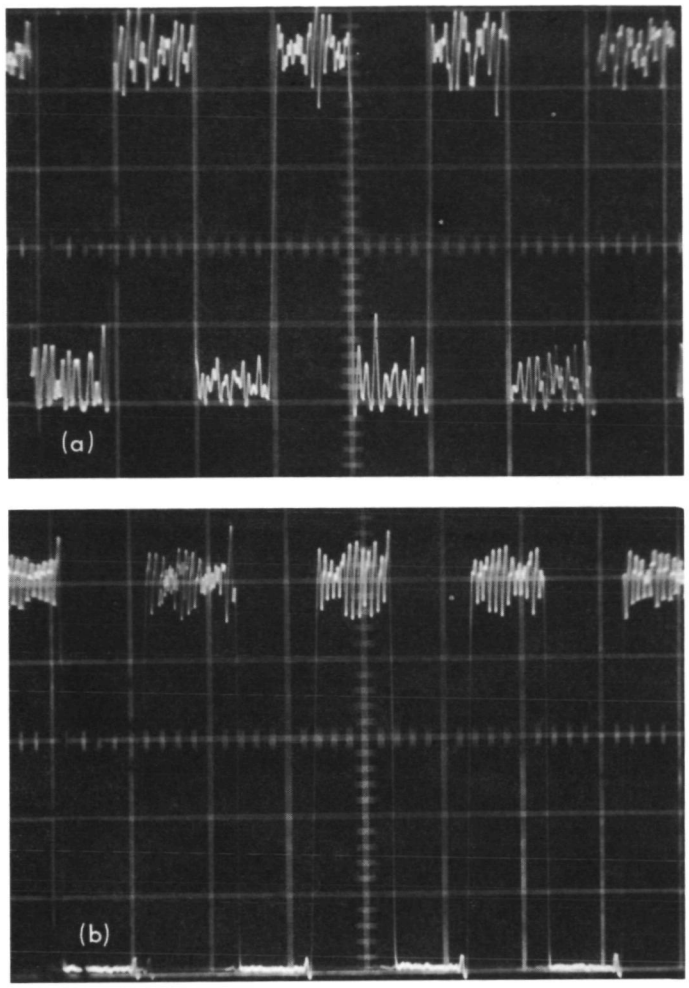


**Fig. 31. Square wave (a) calibration signal at — 125 dbm and (b) response through the intersite microwave link**

effective demodulated signal-to-noise ratio as a function of carrier strength. This interpretation was aided by using the square-wave signal as opposed to normal test charts, because the peak-to-peak signal was known quite accurately and the test signal could be quite readily subtracted from system noise. A typical sample of such a resultant signal is shown in Fig. 31(a). Every opportunity was taken to monitor performance in this manner. Although minor variations in signal-to-noise ratio were discerned, performance as a whole was consistently high. Table 6 summarizes representative system performance. Anticipated nominal carrier strength was of the order of −122 dbm.

The final portion of test tape containing a test pattern was then fed through the system, and a photographic record was made of this signal at each of the test carrier

**Table 6. Typical performance through Echo Station receiver**

| Carrier strength, dbm | Ratio of peak-to-peak signal to rms noise, db |
|---|---|
| −110 | 36 |
| −115 | 34 |
| −120 | 30 |
| −122 | 27 |
| −125 | 23 |
| −130 | 18 |

signal strengths. Fig 32 represents a typical set for a standard test pattern and an imitation lunar landscape. The jitter in these photographs is due to wow and flutter in the particular instrumentation tape recorder used to play back the test tape for system performance checks at Goldstone. The jitter is not representative of actual system performance, but it does illustrate the inadequacies of recordings made on standard instrumenation machines without motor drive stability control.

The primary data recording site for *Ranger 5* was Echo Station with a parametric amplifier in the receiver. However, Pioneer Station is equipped with a maser amplifier and was to simultaneously monitor the TV signal when data was first received. If for any reason the spacecraft signal fell below its nominal strength and the extra margin of sensitivity was required, the signal from the receiver at Pioneer Station would be sent over a microwave link to Echo Station telemetry and processed in the TV room. A normal signal strength on the other hand would free Pioneer Station to track the capsule transmitter. Checks were made of the microwave link to determine degradation, if any, of the predetection signal so as to incorporate this data in the over-all signal-to-noise calculations. The second portion of test tape with a 100-cps band-edge to band-edge square wave was sent from Echo to Pioneer and back to Echo Station over the microwave link with no discernible degradation. An oscillograph made of the resultant demodulated square wave is shown in Fig. 31(b). The small amount of periodic signal seen at one extreme of the square wave is a leak of the 2.2-kc carrier through the 6-pole 2.0-kc Butterworth filter in the demodulator. This would correspond to an extreme white signal and would be a rare event. The other extreme is the 5.0-kc carrier, corresponding to maximum sync pedestal and is a good illustration of two-way microwave noise.

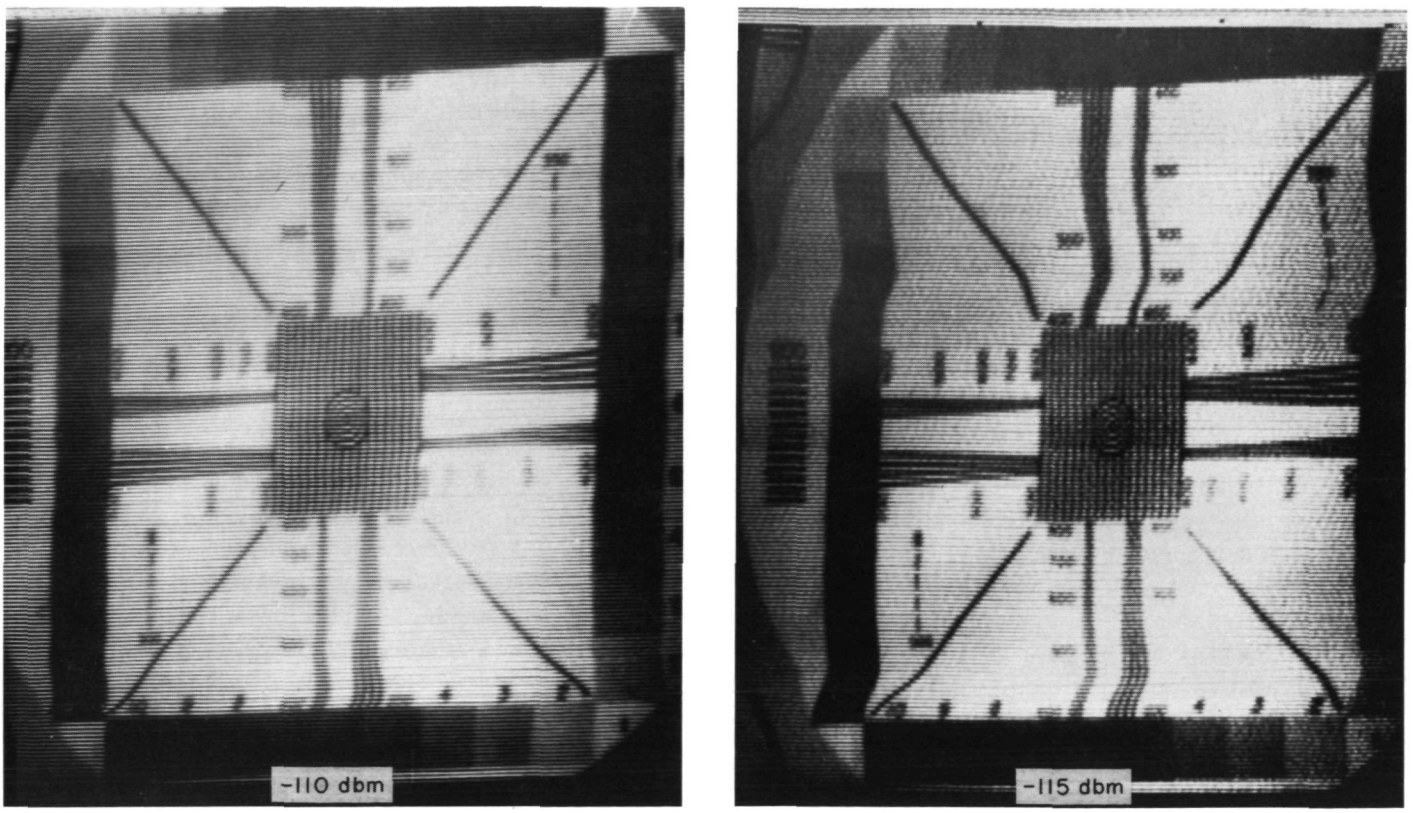


**Fig. 32. Test pattern and simulated lunar landscape through Echo Station receiver at various carrier strengths**

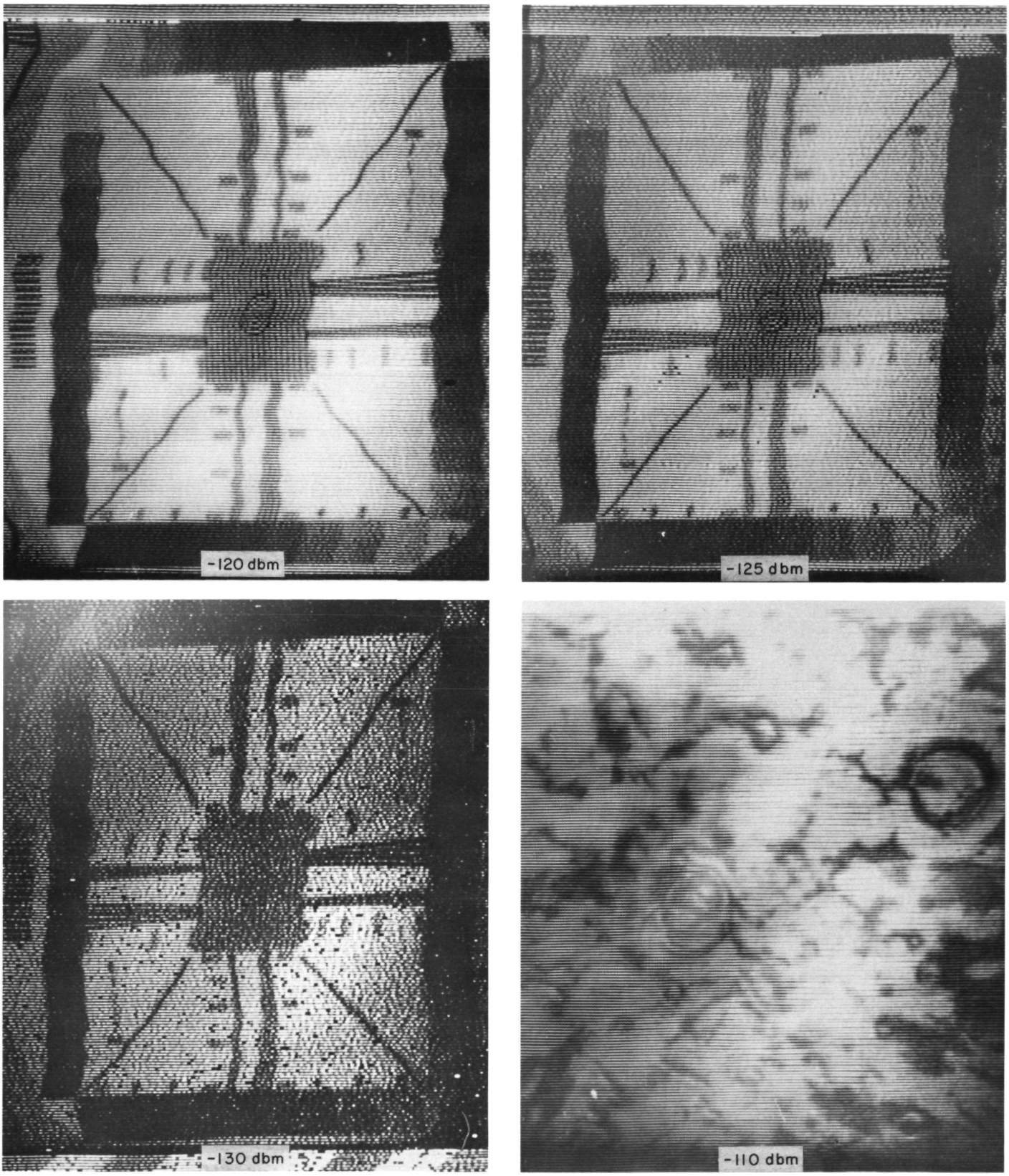


**Fig. 32. (Cont'd) *Test pattern and simulated lunar landscape through Echo Station* receiver at various carrier strengths**

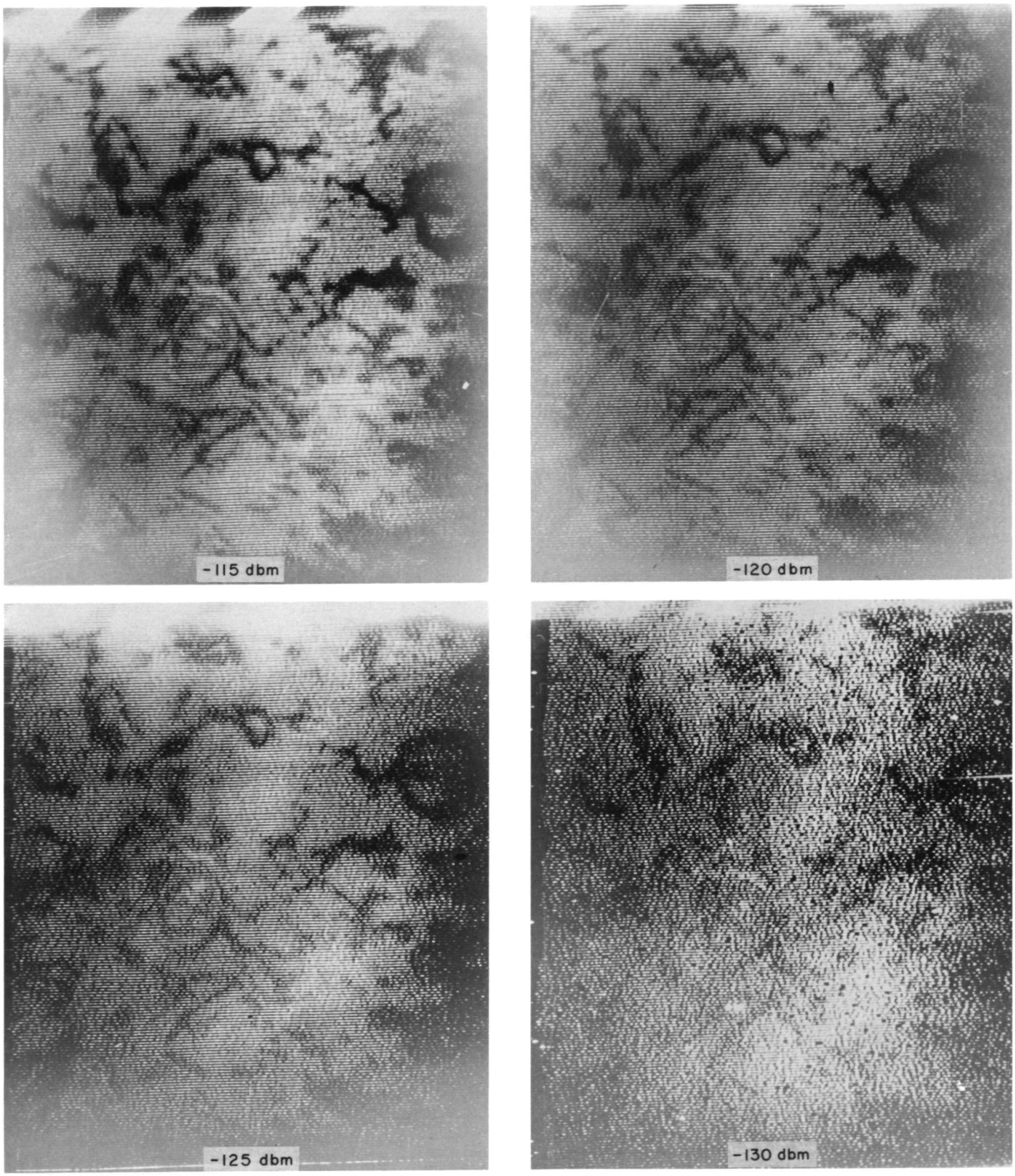


**Fig. 32. (Cont'd) Test pattern and simulated lunar landscape through Echo Station receiver at various carrier strengths**

### 2. *Lunar-Surface-Characteristics Measurement Techniques*

Orbiting spacecraft are of great interest in the exploration of the Moon and planets because they provide extended periods of relatively well defined orbits for reconnaissance purposes. A picture, representing shades of gray of countless image points, would appear to be the classical approach to lunar and planetary reconnaissance missions. A picture has always been the ultimate reconnaissance tool, but its transmission over large distances requires that a substantial portion of the payload be devoted to communications and communications support subsystems. It was decided, then, to investigate other approaches in order to provide similar data for early space missions in an attempt to acquire meaningful data sooner. Relaxing the design requirements of the spacecraft (which is usually overburdened with tasks because of the always present booster limitations) could be accomplished at the same time.

Spatial sensors and decision testers were considered candidates for obtaining surface data from orbiting spacecraft. Aerojet-General/Azusa conducted a parametric study to determine the tradeoffs involved in communications bandwidth versus these techniques for the specific problem of a lunar orbiting spacecraft.

The obvious application of similar techniques to Mars reconnaissance missions was not investigated in the study. The decision was made to look at the feasibility of the approach within the earliest mission constraints. Additional applications, such as the Mars mission, could be considered for follow-on studies after the feasibility has been established for lunar orbiters.

It was assumed that the spacecraft would be injected into a 100 km circular orbit for an expected 30 day lifetime. The spacecraft attitude accuracy was assumed as $\pm\frac{1}{2}$ deg off the local vertical with maximum spacecraft drift rates of 0.02 deg/sec. The study was constrained within techniques rather than to a particular bandwidth(s). In this manner, the techniques were evaluated at the conclusion of the study by their degree of usefulness and inherent bandwidth requirements.

Questions that were asked to assist in the analysis of the techniques were:

(1) What kind of lunar surface information does each technique provide?

(2) What are the roughness resolution limitations of each technique?

(3) What are the bandwidth requirements?

(4) What are the weight and power requirements?

(5) What are the relative reliability figures?

(6) To what extent is each detector output amenable to onboard processing to increase the information-to-transmitted bandwidth ratio?

(7) Will the use of detectors responsive to more than one portion of the spectrum improve the information content of the technique?

(8) Are any of the techniques useful in providing surface material characteristics?

Particular techniques and principles were investigated and evaluated in the laboratory at Aerojet. The primary purpose of the techniques investigated in the study was to detect the presence or absence of surface anomalies on the Moon. The information detected and transmitted from the spacecraft to Earth would permit analysis of the comparative suitability of specific surface areas for manned or instrumented spacecraft landing.

Laboratory experiments during the study revealed that sufficiently distinct signatures of lunar surface features derived from detector outputs could possibly permit accurate and repeatable classification of the features. Quantitative uncertainties in lunar feature signature analyses require that additional study be directed toward clarifying this area.

The parametric study led to the conclusion that the most useful technique for early lunar surface reconnaissance from an orbiter was that of the *spatial sensor*. The detection of specific features under alternative lunar lighting and albedo conditions was most simply performed by this system. Curves indicating the utility versus surface resolution were generated and the maximum point of the utility curve was found to be around 1.5 m, corresponding to a 5-inch, $f/5$ optical system. The telescope design considered imaging on both visible and infrared detectors. The visible spectrum sensor would consist of a set of independent detectors as shown in Fig. 33. A mask assembly functioning as a field stop of the telescope would divide the image of a strip of the lunar surface of width $A$ and over-all length $W$ into three functional sections with five detectors.

The central detector would sense the energy emitted from an area $A \times A$ of the lunar surface. Two detectors,

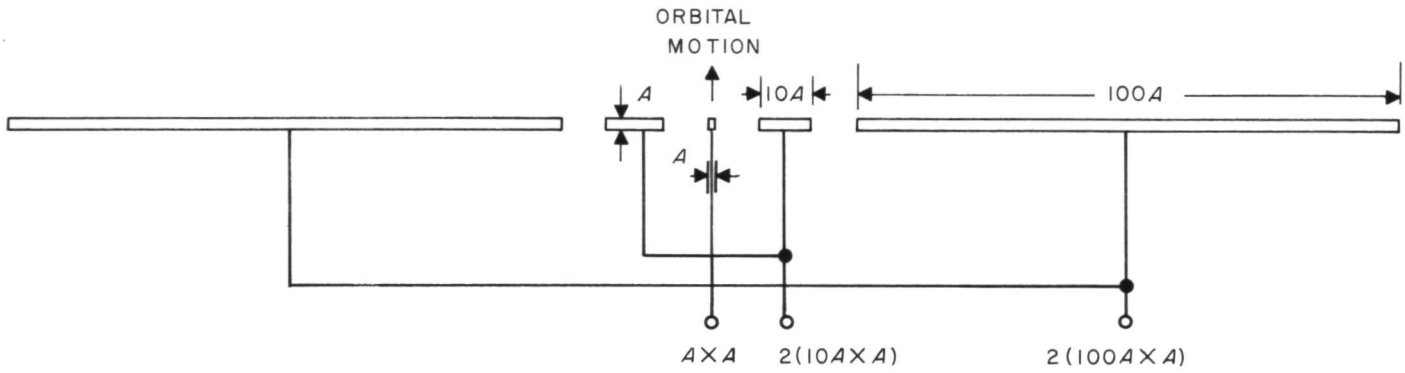


**Fig. 33. Visible spectrum sensor**

one on each side of the central detector, would sense the energy emitted from an area $2 \times (10A \times A)$. Additional detectors could be utilized if increased bandwidth requirements were tolerable. The forward orbital motion of the spacecraft would create the required scanning effect.

The signal detected by the sensors as the spacecraft moves forward would vary according to the energy received from successive areas of the Moon. While passing over smooth areas, the amplitude of the detectors' signal would remain nearly constant. However, when passing over rough areas, amplitude variations would occur due to the presence of bright and shaded areas caused by the uneven terrain. The central detector would indicate the density of roughness within the $A$ meter resolution. The detector on either side of the center detector would indicate the width of the roughness within the $10A$ meter resolution. This roughness would be checked additionally by the outboard detectors.

Additional detectors responsive to the longer wavelength, infrared region could supplement the system. Emissivity variations could be distinguished from surface roughness by correlating data from this detector with the

An all-reflective telescope design has been considered which would not have different image planes for different wavelengths of radiation. This is a requirement if more than one portion of the spectrum is to be analyzed. The detector configuration precludes the assembling of three photomultipliers on the image plane as close as is required by the image size. A bundle of fiber optics has been suggested to transport the optical information from the image plane to the appropriate photomultipliers. The use of fiber optics in this application appears feasible. The critical position of the image panel and the thermal expansion and contraction of the telescope body as the visible spectrum responsive detectors.

spacecraft passes alternately over the bright and dark side of the Moon requires a complete thermal analysis to preserve image sharpness.

The performance of this technique, assuming that diffraction and aberration images are much smaller than the field of view, depends on the light level of the lunar surface under observation. The amount of energy received by the telescope is a function of (1) the radiant energy from the Sun, (2) the Sun inclination, (3) the surface area projected normal to the line of sight, (4) the reflectivity characteristics of the Moon's surface, (5) the telescope aperture area, and (6) the altitude of the spacecraft above the surface. The variable parameters are the photometric characteristics of the Moon's surface and the incident angle. The photometric characteristics of a surface depend on the angle of incidence, the angle of view, and the nature of the material. Curves indicating the photometric characteristics of the lunar surface for different Sun angles and local slopes were drawn, and the coefficient of brightness of the surface deduced.

The electronics in this technique amplifies the photomultiplier outputs and conditions them for spacecraft telemetry. Selection of the amplifier design criteria was based on the photomultiplier levels and signal-to-noise ratio (SNR) characteristics in the operating range of interest, and on the imposed spacecraft telemetry input level and resolution capability. The SNR function has been plotted for the three-detector configuration. An efficient amplifier characteristic would make use of these approximately parabolic or square-root SNR functions to reduce the dynamic range of the transmitted signal by reducing noise bits.

A dc amplifier characteristic was selected as the design objective for follow-on study for the central detector

processing which, because it is the fine resolution detector, has the least signal dynamic range. The two high-aspect-ratio detectors have so large a dc signal dynamic range that their dc signal cannot be adequately resolved with the fixed telemetry resolution. AC processing was, therefore, chosen for these two channels and is inserted to the telemetry at several different levels of amplification for each detector.

The maximum information rate at which this technique could collect data is related to the number of channels, their bandwidths, the number of stages of amplification, and the number of differentiable signal steps. A central detector, monitoring 2 $m^2$ of the lunar surface, has a bandwidth of 800 cps, and one stage of amplification, with 20 distinguishable steps of telemetry level or about 3200 bits/sec transmitted to Earth. The intermediate detector, viewing a $2 \times 40$ m strip, also has an 800 cps bandwidth, but has three stages of amplification each with 20 telemetry steps or 9600 bits/sec. An outboard detector of $4 \times 400$ m has a bandwidth of 400 cps and four amplifier stages or an information rate of 6400 bits/sec. The total transmitted information rate is, at most, then, about 20,000 bits/sec. In 10 days of viewing $\pm 20$ deg lunar latitude by $\pm 50$ deg lunar longitude with a 15% duty cycle and a 60 deg inclined orbit, $2.5 \times 10^9$ bits will be transmitted.

A second technique, *decision testing,* was also investigated in the study. Spatial filtering theory has shown that for any given spatial signal pattern there is one spectral filter, or reticle, that will maximize the SNR. This principle could be applied to the exploration of the surface features of the Moon if laboratory experiments provided favorable results. Several reticle detector assemblies could be built, and each tuned to respond to radiation from a certain surface feature of predicted radiance configuration, and discriminate heavily against all other features. The occurrence of maximum correlation would provide a large signal resulting in identification of the surface configuration being sought. It must be noted that lunar feature characteristics are not defined below 1 km, but could be extrapolated from large configurations to higher resolutions commensurate with decision testing resolutions. The surface features undergo large variations in radiance pattern as a function of Sun illumination angle. Even if a satisfactory space filter model could be contrived, a great many matched-reticles per given-surface-feature would be required to account for all Sun angles. A compromise leads to false indications and an inaccurate count.

This technique was investigated only briefly during the study. The difficulties of matching a spatial filter to the wide variation of surface radiation features resulted in the formulation of a conceptual Moon model of fairly unpredictable light and shadow configuration. This precludes the selection of a preferred reticle pattern. A set of rectangular slits was chosen as having adequate response to a large variety of radiance patterns. The slits would exploit the full resolution of the optical system in the direction of scan. Their several widths average over several lengths in a direction perpendicular to the scan and would respond preferentially to monotonic variations in radiance over those widths.

In summary, the study established the feasibility of the spatial sensors technique for providing meaningful lunar surface data with a bandwidth of approximately 5 kc. The application of the same technique to Mars missions was not investigated but has obvious related uses. The decision testing technique showed promise but would require additional experimental and analytical study before it could reach the same state of confidence as the spatial sensors technique.

## E. Propulsion

Accomplishment of the *Ranger 6–9* high-resolution television investigation of the lunar surface and terrain requires the spacecraft to undergo a single midcourse propulsion maneuver to remove or reduce *Agena* injection dispersion errors. This maneuver is accomplished through the use of a small monopropellant-hydrazine-fueled propulsion system of 50-lb vacuum thrust. The unit is capable of delivering a variable total impulse in response to signals from an integrating accelerometer circuit. A more detailed description of the propulsion system, the operational design philosophy, and a system schematic are contained in *SPS 37-3;* development progress is reported in *SPS 37-3* through *37-18.*

All drawings of the midcourse propulsion system for *Rangers 10* through *14* which incorporate the product improvement changes specified in *SPS 37-18,* Vol. I have been released; orders are currently being placed for fabrication of components. Since there are several changes being made, a type-approval system will be procured and sent through complete type-approval testing. A test specification covering this testing is currently being prepared.

# F. Supporting Activities and Engineering Facilities

## 1. Summary of Ranger Environmental Test Program

During November and December a total of 49 experimental, 50 type-approval, and 89 flight acceptance environmental tests associated with the *Ranger* project were performed by the JPL Environmental Test Laboratory (ETL) (Table 7).

## 2. Vibration Testing

*a. Hydrostatic bearing.* During November, ETL added a second hydrostatic bearing to the facility for vibrating spacecraft systems (*SPS 37-18*, Vol. II) to further reduce the cross-axis motion during vibration testing. The modified system is now being evaluated.

*b. Ballistic shock machine.* A ballistic-type shock machine is being developed by ETL for the testing of spacecraft components.

## 3. Space Simulation Testing

*a.* Ranger 6 *TV subsystem test.* The RCA Flight Model 1 TV subsystem for *Ranger 6* was flight-acceptance tested in the 6-ft space simulator during December (Fig. 34). The subsystems weighed about 370 lb. There were three pumpdowns, each lasting about 16 hr. The pressure was $1 \times 10^{-4}$ torr, or better; most of the time, the shroud was at ambient temperature. The equipment was operated during the last hour of each run when the shroud temperature was lowered to prevent overheating due to internal power dissipation.

**Table 7. *Ranger* usage of environmental test facilities during November and December**

| Facility | Number of tests |
|---|---|
| Space simulation | 4 |
| Vacuum | 8 |
| Vacuum–temperature | 40 |
| Vibration | 57 |
| Low-frequency vibration | 7 |
| Centrifuge | 24 |
| Shock | 7 |
| Temperature | 24 |
| Temperature humidity | 3 |
| Gas sterilization | 12 |
| Explosive atmosphere | 1 |
| Salt fog | 1 |
| Total | 188 |

Lowering the shroud temperature dropped the chamber pressure to the mid-$10^{-6}$ torr range. Difficulty was experienced with the operation of flight gear during each test. Plans are being made to repeat the tests with modified flight gear.

## 4. 25-ft Space Simulator

During the reporting period, the contractor-furnished optical system was modified (*SPS 37-19*, Vol. II) to produce a 5-ft D off-axis beam. The intensity and uniformity of distribution meet the requirements for *Ranger* spacecraft testing. Preparations are under way to test the *Ranger* temperature control model in the simulator early in 1963.

**Fig. 34. *Ranger* 6 TV subsystem mounted in 6-ft space simulator**

# III *Ranger* TV Subsystem

The primary objective of *Rangers 6, 7, 8,* and *9* will be to produce high-resolution TV pictures of the lunar surface. To implement this objective, a TV subsystem is being developed for *Rangers 6–9* by RCA under contract to JPL. The subsystem will mate with the JPL bus as does the lunar capsule of the *Ranger 3–5* series.

The subsystem structure consists of three major assemblies: (1) the central box which houses the main electronic components, (2) the camera subassembly with associated bracketry and equipment, and (3) the thermal shield. Camera view apertures are provided in the thermal shield.

The following material relating to the subsystem development is abstracted from the RCA report, *Ranger TV Subsystem, Eighth Bimonthly Progress Report,* December 15, 1962:

Flight Model 1 (FM 1) was delivered to JPL on October 18, 1962, after successfully completing environmental and electrical testing at AED. At JPL, the FM 1 subsystem was mated with the *Ranger 6* spacecraft and has successfully undergone subsystem and system tests. The FM 1 subsystem is presently being modified to incorporate several product improvements in the communications system and in the "free-running" camera. After it has been brought up to desired configuration, the TV subsystem will be tested in the vacuum chamber at JPL.

The mechanical test model 2 (MTM 2) subsystem was delivered to JPL on October 18, 1962, and is being prepared for a series of qualification-level vibration tests to be conducted at JPL. The proof test model (PTM) was used at JPL for match-mate tests and for weight and cg determinations with the *Ranger 7* spacecraft. It also served as a signal generator for the *Ranger 7* thermal–vacuum tests. The engineering test model (ETM) was returned from JPL to RCA during this reporting period for evaluation of certain product improvements.

The assembly of the FM 2 subsystem was completed and preliminary system tests were performed. Environmental testing of FM 2 was delayed until the next reporting period to allow time for the evaluation of certain improvements designed to reduce noise interference in the vidicon camera. The acceptance testing of the spare assemblies for FM 1 and 2, and of the assemblies for FM 3 and 4 subsystems continued to progress satisfactorily during this reporting period.

# A. Structure

## 1. Design Effort

The design effort during this reporting period consisted primarily of (1) re-evaluation of the structural acceptability of the camera bracket support, (2) static testing of the solar-panel support bracket No. 1703494 for *Mariner R* solar panels, and (3) redesign of the battery mount for FM 4 to accommodate the new lightweight battery. Numerous drawing changes resulting from integration requirements as well as drafting errors were made.

The castings for the camera bracket support are not meeting strength and radiographic requirements. A re-evaluation of the loads, actual and allowable stresses, and other applicable design criteria is in progress. JPL has been requested to supply AED with the accelerometer data on the castings. This data, to be obtained from the forthcoming qualification test of the MTM 2 at JPL, may show that some of the existing castings are acceptable. A second-source vendor has been contacted for additional castings. The re-evaluation may result in possible relaxing of the prescribed requirements.

A Stresscoated solar-panel support bracket was subjected to a preliminary static test. The assembly satisfactorily withstood specified test loads.

The battery mount for FM 4 is presently being redesigned to accommodate the new lightweight (12-cell) battery. The new configuration will be similar to that currently in use but, because of the reduced length of the new battery, will not require the "belly band." The connector locations and external configuration will remain the same as in the present mounting arrangement.

The final assembly drawings for the *Ranger* TV subsystem have been completed.

## 2. Test And Flight Models

Vibration testing of MTM 2 was completed and the unit was shipped to JPL. Except for the external clevis fittings, the *Mariner R* truss assembly was installed on this unit. The clevis fittings were scheduled for delivery to JPL in December 1962.

FM 1 was shipped to JPL on October 16. The weight of the TV subsystem without batteries was 277.99 lb. This weight included that of the omni-antenna cable (1.25 lb). With the addition of the batteries, the complete *Ranger* TV subsystem will weigh:

| | |
|---|---|
| Subsystem without omni-antenna cable | 276.74 lb |
| Battery | 43.00 |
| Battery | 43.00 |
| Mounting hardware | 0.21 |
| | 362.95 lb |

FM 2 was assembled and delivered for electrical testing on October 24. The final work and component fitting of the structure of FM 3 has been completed and is awaiting assembly.

# B. Electrical Integration

## 1. Test And Flight Models

Both the ETM and PTM were at JPL during this period. The ETM was returned to AED after the arrival of FM 1 at AED.

Debugging and alignment of FM 1 subsystem components was continued during this reporting period. Noise spikes in the video were the major problem. The subsystem showed satisfactory operation during the thermal–vacuum test except for an occasional intermittent noise during abbreviated runs which was traced to an arc-over inside a transmitter standoff connector. Evidently, sufficient air was retained in the insulator to allow arc-over to occur in the abbreviated mission where the out-gassing period was several hours instead of several days, as for a 66-hr real-time mission. These hollow-core insulators have been replaced with solid-core insulators. Thermal-vacuum testing and the acceptance test were completed and FM 1 was shipped to JPL on October 18.

The mechanical integration of FM 2 was completed during this reporting period. Checkout and alignment of the subsystem progressed through the vibration and thermal-vacuum environmental test stages.

The emergency-mode telemetry of FM 1 and 2 had shown fluctuations that made interpretation extremely difficult at times. Changes were made to assure the stability of a zener diode-controlled voltage level after

switching to emergency-mode telemetry. Circuit constants are being altered to optimize the TV subsystem-to-GSE link.

Modified power amplifiers were installed.

The cameras, working as a group in the TV subsystem mounting, showed a degree of sensitivity not exhibited in previous testing on the bench. The shutter pulses were fed back mechanically to microphonic components, causing variations in the emergency-mode telemetry. These variations or peculiarities were corrected. Several vidicons require special connection treatment for either or both excessive dimensional variations and microphonic sensitivity. Slightly over-length deflection coils compounded the dimensional problem.

### 2. Electrical Harness

The harness design has continued through minor evolutionary changes primarily to compensate for mechanical vidicon variations. Specific changes include:

(1) Reconsideration of the camera vidicon cable because of the decrease in length of a new lot of vidicons and increase in microphonic sensitivity of the vidicons.

(2) Shifting of the vidicon cable lay by 90 deg to facilitate recabling to a specific tube orientation which is dictated by the type of mask used on the vidicon.

(3) Redesign of the battery connection on FM 4 to accommodate the new lightweight battery.

A temporary alteration of the vidicon connector for short vidicons successfully passed qualification-level testing. The existing mounting flange was carefully cut from the potted vidicon connector and a clamp-on flange was epoxied in place giving a greater projection of the socket beyond the flange.

The transmission of the shock from the P-camera shutters to microphonic full-scan vidicons through the potted vidicon connector, was noted in FM 2. The design of a connector insert with low shock transmission has been initiated.

Cabling for the lightweight battery was developed to utilize the existing harness and to facilitate the making of battery charging connections while the TV subsystem is mounted on the bus. The battery is brought out to a Pigmy connector on the back ring of the structure for easy access in charging. The connection to the high-current regulator, which must be broken during charging, is brought out on one side of the -*Y* axis Leg C to be routed to the connector on the other side.

The monitoring connections used both during charging and during flight will go through a connector on the ring. It will thus be possible to connect them directly to the charging equipment. For flight configuration, a plug with jumpers will be placed on the monitor connector to return those connections to the flight harness.

The external connections have been placed about the $-y$ axis in order to shorten the cable length in the TV subsystem and to remain well away from the front of the camera and the larger *Mariner B* solar panels.

## C. Environmental Testing

*Flight Model 1.* The environmental testing of FM 1 was completed with the final acceptance test in thermal–vacuum. This test consisted of an abbreviated mission with collimators installed, the purpose of which was to verify the electrical integrity of the FM 1 subsystem in the thermal–vacuum environment.

*Acceptance testing.* All acceptance testing on the component level has been completed except for the batteries for FM 1 and 2. Work is progressing on the testing of these batteries.

*Qualification testing.* Qualification testing of the communications components has been delayed because of the incorporation of product improvements.

## D. Electronics

### 1. Video System

The exposure time of the FM 1 partial scan (Type P) cameras for *Ranger 6* has been increased to 4 msec. This

additional exposure time was required to increase the signal-to-noise ratio of the camera system to an acceptable level for the lower scene luminances which are expected near the lunar terminator. To support the field operations in making this change on the *Ranger 6* TV subsystem, the two spare P-cameras have also been fitted with 4-msec shutters. In addition, four spare P-shutters have been fabricated with the 4-msec exposure capability for use in *Ranger 6*, if necessary. All other P-cameras, including those for *Ranger 7*, are presently equipped with 2-msec shutters. If present plans are maintained, the modification of the remaining cameras and shutters for *Ranger 7* and subsequent flight units will be dependent upon the results obtained from *Ranger 6*. All cameras are presently set to be white-clipped at a brightness level of about 1250 ft-lamberts.

As the plans to alter the trajectory for an impact closer to the Moon's terminator became firm, the usefulness of the blue filter (and hence the color television experiment) became questionable because of the anticipated reduction in scene luminance near the terminator. It was consequently decided to remove the color wheel. A secondary effect of the deletion of the color experiment is the removal of the capability for variable exposures by means of the effective transmissions of color filters.

The evaluation of the TV subsystem parameters has continued at both RCA and JPL. One of the more interesting discoveries was the effect of the change in shutter speed on system performance. As has been noted previously, the rate of increase of "shades of relief" as the terminator is approached is much faster than the corresponding decrease in the signal-to-noise ratio of the camera system. This is true if published data on the photometric function are accepted. The published data was gathered with telescopes having a level of resolution at least two orders of magnitude lower than the cameras in *Rangers 6* to *9*. This difference in resolution may be significant, especially over the limited areas covered by the P-cameras. The camera settings have been made consistent with the published data on photometrics. This is an area requiring further consideration before the camera settings are finalized.

The following discussion is concerned only with those aspects of the shutter change related to smear, resolution, and contrast. In recognition of the importance of contrast as one of the system parameters that will significantly increase the information content of the resulting picture, altered trajectories are presently being considered which will ensure a minimum of two to three shades of relief. The increase in exposure to 4 msec was necessary to provide a signal-to-noise (rms) ratio of at least 21 db at the brightness level where the desired contrast is achieved. It is felt that this signal strength is required for the vidicon to reproduce adequately this degree of contrast at the relatively low light level expected. Further system studies are currently in progress in an effort to determine the precise contrast and signal-to-noise ratio in the vidicon required to produce a usable picture. Part of this analysis must include a judgment as to the certainty of achieving the desired trajectory.

With the exposure time of the P-cameras increased to 4 msec, it is necessary to review the image degradation due to smear. Fig. 1 shows the ratio $\gamma_p$ of the translational $\beta_p$ to the intrinsic resolution $R_I$ as a function of the height above the lunar surface, the misalignment of the common optical axis $(\psi + \zeta)$, and the velocity vector. This function is linear for small angles of $(\psi + \zeta)$ and for small changes in exposure time $\Delta t$. With the stipulation that the ratio $\gamma_p$ should not exceed 0.5, the smear-free area on the last picture with a 4-msec exposure is contained within a circle of 0.5 deg radius about the velocity vector. Fig. 2 shows a graphical analysis of the first-order effects of this decreasing smear-free area for the P-cameras designed for *Ranger 6* to *9*. With the present

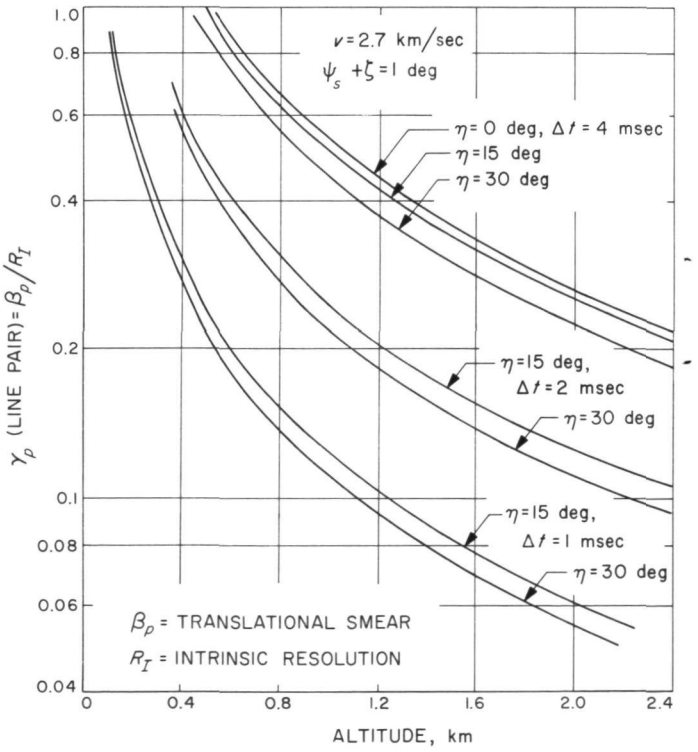


**Fig. 1. Image degradation due to smear**

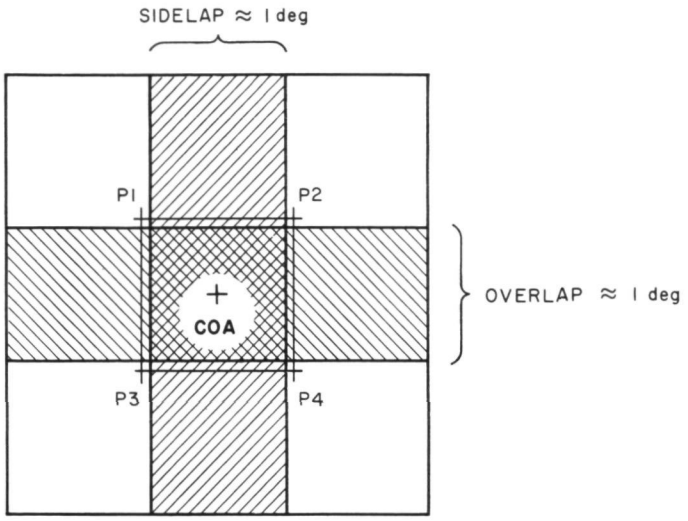


**Fig. 2. P-camera arrangement**

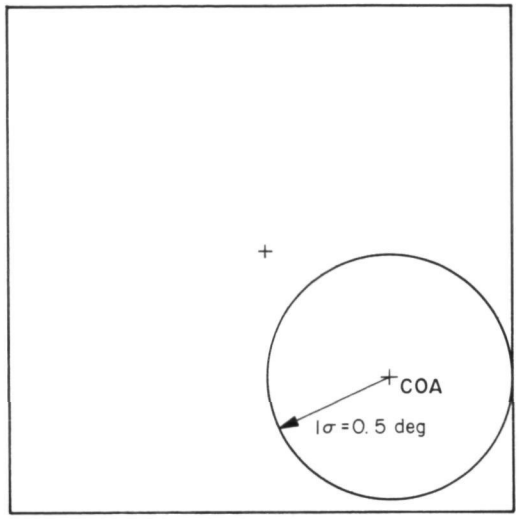


**Fig. 3. Velocity vector error 1σ with respect to the composite optical axis**

program of sequential exposure and readout of the four P-cameras, each has an equal probability of being exposed at the 600-m altitude where the resolution of 0.2 m per line-pair is achievable, and each can still be read out in real time.

Figs. 3 through 5 show the 1-, 2- and 3-$\sigma$ error circles of the velocity vector misalignment with the common optical axis. It is possible to construct on each of these error circles a locus of points on which at least half of the 0.5-deg smear-free circles can be drawn and be contained in the field of view. The probability of this occurring is approximated by the following relation:

$$\sigma_1 p_1 + (\sigma_2 - \sigma_1) p_2 + (\sigma_3 - \sigma_2) p_3 = p_{1A}$$

where the probability integrals are

$$\sigma_1 = \sigma$$
$$\sigma_2 = 2\sigma$$
$$\sigma_3 = 3\sigma$$

and $p_1$, $p_2$, $p_3$ are the probabilities of the error occurring in a direction which will permit at least one-half of a

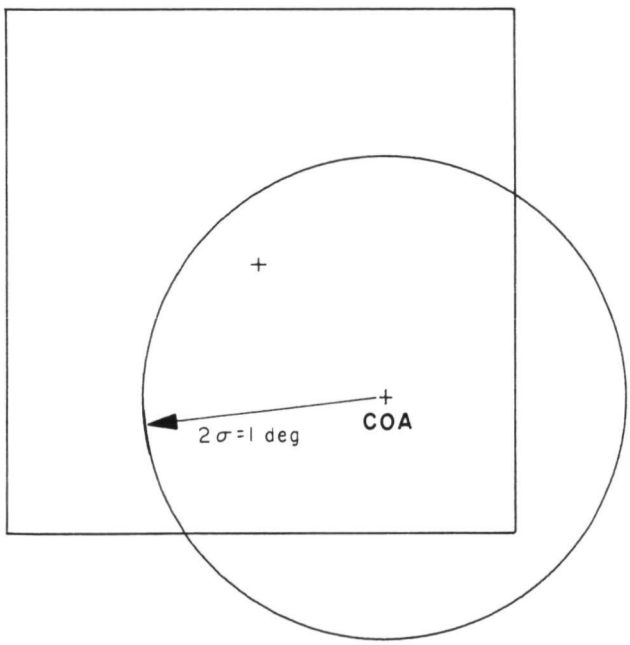


**Fig. 4. Velocity vector error 2σ with respect to the composite optical axis**

smear-free circle to be contained in the field of view of the last frame for each of the end possibilities of misalignment. In a similar manner, a probability can be computed for the containment of a full smear-free circle in the final frame ($p_{2A}$). Table 1 shows these probabilities ($p_{1A}$ and $p_{2A}$) as well as the probabilities ($p_{1B}$ and $p_{2B}$) computed for a camera arrangement where the camera optical axis coincides with the composite optical axis (Fig. 6).

**Table 1. Computational results for the probabilities $p_{1A}$, $p_{2A}$, $p_{1B}$, and $p_{2B}$**

| Probability | Smear-free circle | Spread field—A | Common axis—B |
|---|---|---|---|
| $p_1$ | At least 1/2 | 0.80 | 0.95 |
| $p_2$ | Complete | 0.32 | 0.68 |

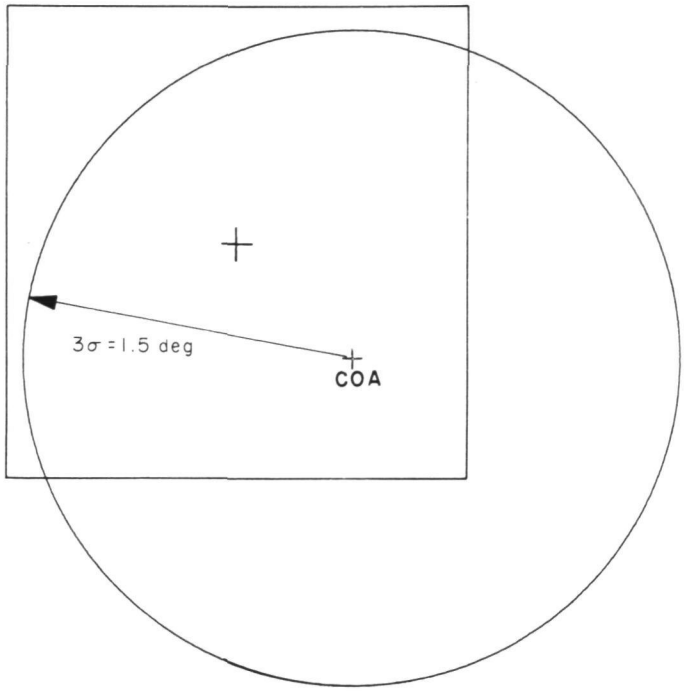


**Fig. 5. Velocity vector error $3\sigma$ with respect to the composite optical axis**

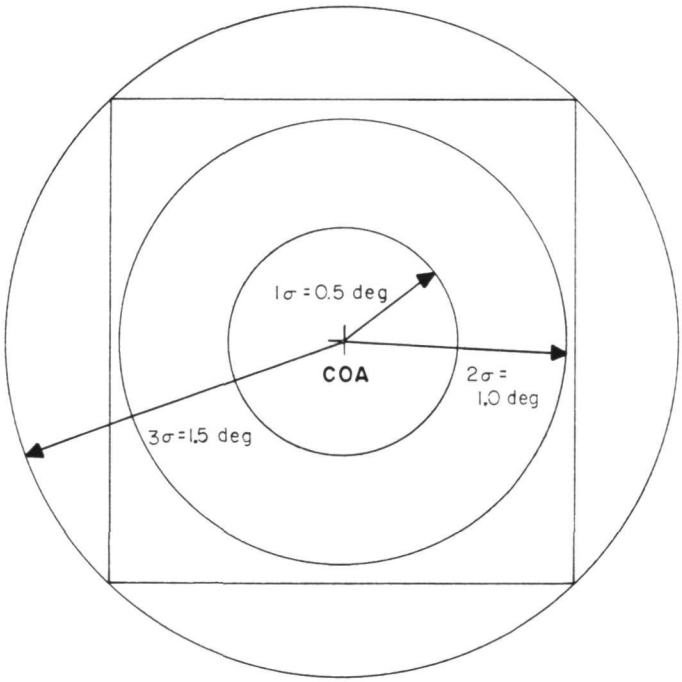


**Fig. 6. Composite optical axis coincident with the camera optical axis**

The data shown in Table 1 indicate that there is a reasonable probability of obtaining at least a portion of a smear-free image in the last frame. The data also indicate that this probability can be increased with a modified pointing arrangement indicated in Fig. 6. To keep these probabilities in their true perspective, it is necessary to see what they mean in terms of actual smear-free area when the 4-msec exposure is compared to the 2-msec exposure. This comparison is shown in Table 2.

**Table 2. Comparison of smear-free areas resulting from the 2- and 4-msec exposure times**

| Area | $\Delta t = 2$ msec | $\Delta t = 4$ msec |
|---|---|---|
| Smear-free circle | 300 m$^2$ | 75 m$^2$ |
| ½ smear-free circle | 150 m$^2$ | 37.5 m$^2$ |

Continued study effort is also being concentrated on an error-analysis of the location of the optical axes with respect to the velocity vector in order to determine their effect on the probability of achieving the final resolution in the region of 0.2 to 0.3 m per optical line-pair. This analysis is considering:

(1) The pointing error due to uncertainty in the location of the velocity vector with respect to the four spacecraft body axes.

(2) The additional pointing error due to gyro drift $\theta$.

(3) The camera bore-sight error which accounts for the misalignment of the vidicon center reticle with respect to the optical-mechanical axes.

(4) The error in the camera bracket which accounts for the misalignment of the camera's optical-mechanical axes with respect to the desired common optical axis (**COA**).

(5) The roll misalignment error of the vidicon reticle with respect to horizontal and vertical axes constructed on the optical axis.

Also being considered in this analysis is the effect of the black-mask area and the loss of active field in the horizontal-scan direction (sidelap) while compensating for the black mask to maintain an overall one-to-one aspect ratio. Fig. 7 shows the amount of black mask covered with respect to the active scan time for the three camera types.

The above discussion indicates that it may be desirable to change the pointing arrangement of the P-cameras when modified to the 4-msec exposure configuration, in order to increase the probability of obtaining some area

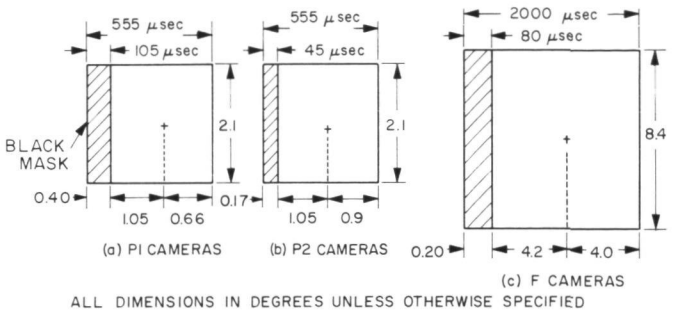


**Fig. 7. Active side fields of view for the Ranger 6 – 9 cameras**

at 0.2 m. The area that can be obtained is about 75 $m^2$. This is an area of such extent and viewed at such a resolution that, if the basic lunar photometric model can be assumed to hold, then the picture may have no shade relief whatsoever. In other words, such resolution cannot be achieved with this model with any reasonable probability. Conversely, if conditions are assumed which yield the desired resolution, a lunar model is thereby suggested with considerable detailed contrast and possible highlights. There are no direct data to support such a model, but the difference in resolution is such that details of this sort are not inconsistent with photometric data observed at presently achieved resolution.

## 2. Cameras

Assembly-level flight acceptance tests of all cameras for FM 2 and five of the six cameras for FM 3 were completed. Acceptance testing of the remaining cameras is scheduled for completion by the end of December.

*a. Video amplifier.* Modification to the reference filter for the first differential amplifier to minimize circuit noise has been incorporated on the FM 2 units and all subsequent units. This modification was not required for the FM 1 unit since low-noise zener diodes had been selected for its circuit.

*b. Vertical sync generator.* Modifications to all P-1 or free-run flight cameras have been made to enable the use of the P-sync-disable mode of sequencer operation and allow demonstration of the free-run capability of the P-1 cameras. This change minimizes the interface loading effects which had previously caused a lockup of the free-running portion of the P-1 camera.

*c. Shutter and lamp drive.* Modifications to the lamp-drive circuit have been made to eliminate continuous lamp operation in the event of a loss of external drive (such as may occur during the sequencer P-sync-disable mode of operation). A capacitor-coupled network was required to prevent long periods of continuous lamp operation. To incorporate this change in the camera subsystem, a modification to the sequencer was also required.

All flight cameras have been modified with the exception of those in FM 1. For this case, the P-sync-disable demonstration must be made with the preamplifier cables disconnected in all P-cameras except the P-1 camera.

*d. Shutter microphonics.* The most critical arrangement of the camera subsystem is in the integrated payload configuration. In this configuration, microphonics are induced in the vidicon and the nuvistor preamplifier when the shutter shocks in adjacent cameras are transmitted through the camera bracket. An evaluation of this problem has been undertaken using the FM 2 camera subsystem. The encapsulation of the preamplifier nuvistor in a soft potting material was one of the modifications attempted to desensitize the camera elements to shutter-induced shocks. Pending further evaluation, this modification has been incorporated in the FM 2 cameras only.

Other possible modifications being investigated are the isolation of the vidicon cable assembly from the vidicon and the isolation of the preamplifier housing from the camera.

Proposals to eliminate the shutter cross-talk effect by altering the shutter program of the P- and F-cameras are being considered. The proposed changes would remove the microphonic cross-talk by time-sharing rather than by concurrent operation of the shutters.

*e. Vidicons.* The problem of obtaining an adequate supply of acceptable vidicons for the completion of FM 3 and 4 has received considerable attention. The main areas of difficulty concerned cathode emission and life expectance of the heaters. A careful review of all vidicons tested earlier on the *Ranger* program has yielded sufficient tubes to complete FM 3 and 4.

## 3. Control Programmer And Camera Sequencer

A change in resistor value to provide more lamp pulse drive was required as a result of the change in the camera electronics to provide lamp burnout protection during loss of sequencer lamp drive. This change has been incorporated in all units with the exception of that for FM 1.

A failure in the power telemetry point at high temperature during thermal–vacuum testing was experienced in the sequencer for FM 3. Insufficient automatic-reset pulse duration was determined as the cause of failure; the duration of this pulse has been extended from 1 to 6 msec to eliminate this problem. This change will be applied to the unit for FM 3 and all subsequent units.

All other modifications have been completed on the units at AED. With the exception of thermal-vacuum test on the unit for FM 4, acceptance testing on flight units of the control programmer and sequencer have been completed.

### 4. Video Combiner

All video combiner units are complete with the exception of the Unit 005 which failed during the acceptance-level thermal-vacuum test as a result of excessive P-amplifier drift. The failure was traced to a mismatch in the input differential amplifier. A temporary solution was effected by selecting the transistors for this stage. Also, a selection procedure was established and distributed to the test personnel. A review of the design of this circuit is under way to minimize the drift and eliminate the necessity for part selection.

### 5. Telecommunications

During this reporting period there have been design changes in the transmitter, telemetry chassis, and transmitter power supply. The transmitter and telemetry chassis have been modified to improve the emergency-mode operation of the TV subsystem. In addition, the commutators on the telemetry chassis are being reworked to increase reliability and operational life-times. The 500-v dc bridge for the transmitter power supply has been replaced with a 1000-v dc bridge.

Transmitter and telemetry chassis modifications to improve emergency-mode operation have been incorporated on FM 1 and 2. In addition, the 500-v dc bridges have been replaced in both units. Modified power amplifiers were received, acceptance tested, and mounted on the FM 1 and 2 subsystems.

Explosive atmosphere and liquid sterilant tests were conducted on the telemetry chassis. With the satisfactory completion of these tests, the telemetry chassis is now completely qualified. The remainder of the TV transmitter subsystem was subjected to the following qualification tests:

(1) Explosive atmosphere.

(2) Liquid sterilant.

(3) Thermal storage.

(4) Thermal humidity.

(5) ETO compatibility.

With the satisfactory completion of these tests, all units (except the transmitter chassis) of the TV transmitter subsystem, including the new power amplifier, have completed the qualification cycle. The transmitter chassis still requires vibration, shock, and acceleration testing to complete the qualification tests for this unit.

The transmitter power supply, 4-port hybrid ring, dummy load, second intermediate power amplifier, and telemetry processor of the spare FM 1 subsystem have been acceptance tested and released during this period. Two transmitter chassis, a modified power amplifier (with signal sampler), and a telemetry chassis are required to complete the system. The transmitters are being modified to incorporate the changes in the emergency-mode circuitry in the modulator and will then be subjected to the acceptance test cycle.

Several units of the spare FM 2 subsystem were started through the acceptance test cycle during this reporting period. However, due to modification of the transmitter and the commutators, this system will not complete the acceptance test cycle until January.

Assembly of the FM 3 subsystem (formerly spare FM 1) has been completed, and the transmitters have been modified. Modified power amplifiers have not yet been received for this system, nor have the modified commutators. This subsystem will receive modified components ahead of spare FM 2 and will complete the acceptance test cycle about the middle of January.

The FM 4 subsystem will be the last subsystem to complete the acceptance test cycle. All RCA-manufactured units have been completed and have undergone the latest modifications. Preliminary electrical tests have also been completed. The following vendor-supplied items are still required before acceptance tests can begin: (1) two modified commutators, (2) two modified power amplifiers, (3) one dummy load, and (4) two 225-kc VCO's. The delivery of these items will delay the start of acceptance tests until January.

*a. Commutators.* During the 66-hr simulated mission in the thermal-vacuum test, there occurred a failure of the 15-point commutator of the FM 1 subsystem. The unit was subsequently returned to the manufacturer for examination. The manufacturer's report indicated that the bearings were dry, with the possible cause being that the 125°C sterilization cycle caused the grease to run out. The bearings were initially filled to only 10% of capacity by the motor manufacturer in order to meet a specification imposed by the manufacturer of the commutators. That specification concerned an operation test of the commutators at −55°C.

The life-test commutators had satisfactorily completed their tests and were operated again to check their performance before opening one of the units for visual examination at AED. During the performance check, one of the units began to operate erratically. Upon opening this unit it was found that carbon from the motor brushes had accumulated around the motor bearing, and the bearings showed signs of overheating due to lack of lubrication. The other life-test commutators were also opened and the same conditions were found to exist. It was decided that the motor manufacturer would increase the grease fill of the bearing to be compatible with a −10°C operating requirement instead of −55°C and the brushes would be changed to a harder material, matched to the commutator, and run in. After the run-in, the motor would be examined for excessive carbon and cleaned up. The possibility of using a sealed bearing would also be investigated. In addition, the commutator vendor was to investigate the possibility of changing the configuration of the filter used on the −27.5-v dc line. The manufacturer had found from previous tests that a different filter configuration would increase the life of the motor by a factor of three.

Work has progressed in the modification of QTM commutators to incorporate the above recommendations. In addition, a suitable sealed bearing will also be incorporated. With the removal of the requirement of sterilization at 125°C, the resulting modified commutators should be more reliable and should meet the manufacturer's quoted lifetime of 1000 hr.

Upon receipt of the first two modified units, vibration, shock, acceleration, and thermal-vacuum tests will be conducted. The unit will then undergo a shortened life test and be re-examined. In the meantime, units for spare FM 1 and 2 and FM 3 and 4 have already been returned for modification.

*b. Emergency-mode modification.* During this reporting period, emergency-mode operation of the subsystem was re-evaluated. Previously, tests had been made without the cameras being present or they were mounted on the structure but not operating. With the cameras mounted and operating, the emergency-mode data received by the ground station showed excessive low frequency noise at the output of the phase-lock detector. This was traced to shutter pulses getting into the modulator on the −27.5- and 100-v dc lines. Since the pulse rate of the shutters is approximately the same as the data rate (3 cps), and the commutator output directly frequency modulates the transmitter at a low deviation (1 kc peak-to-peak), the combined result was excessive low frequency noise at the output of the GSE phase-lock detector (PLD). The shutters draw a 2-amp surge from the battery when operated, and cause a slight instantaneous drop at the input to the −27.5- v dc regulator. This drop appeared as a 50-mv change at the output of the regulator. Although the −27.5 v dc was further filtered and zener-controlled in the modulator, the shutter pulses were still observed in the B+ lines inside the modulator. It was then observed that the operation of the emergency-mode relay in the modulator changed the −20-v dc bus (derived from the −27.5-v dc supply) by approximately 0.5 v, indicating that the zener diode was not bleeding enough current in the emergency mode to regulate properly. This was corrected by taking the power for the emergency-mode relay directly from the −27.5-v dc bus, instead of from the zener-controlled point in the modulator.

This modification reduced the low frequency noise considerably. The shutter pulses, however, continued to contaminate the data. This residual contamination was eventually traced to the +100-v dc supply line. The +100 v dc is generated by the transmitter power supply directly from the battery voltage. Since there is no active regulation in the transmitter power supply, variations in the battery voltage directly affect the output voltage of the power supply. Although the +100 v dc is filtered and zener-controlled in the power supply, the time-constant was found to be too short to sufficiently reduce the shutter pulses entering the modulator. This condition was corrected by increasing the time-constant of the filter on the dc reference used by the varactor modulator.

This second modification, together with the first, improved the emergency-mode data output of the PLD to the extent that approximately 90% of the data points now corresponded with the normal 225-kc telemetry

specifications. Even with these modifications, however, certain points continued to produce erroneous data—as much as five times expected value, in some cases. These points were determined to be high impedance points (greater than $10^5$ ohm), with the result that input to the modulator was almost open-circuited, causing the baseband amplifier to return to its own dc operating point. It was found that if the emergency-mode data was ac-coupled into the modulator and the baseband amplifier was allowed to operate at a constant dc bias, then all the emergency-mode data points would correlate with the normal 225-kc telemetry.

Simultaneously with the analysis of the telemetry problems, the operation of the PLD was also re-evaluated. It was found that two minor modifications would improve the operation of this unit and aid in reducing data. First, it was discovered that the signal into the PLD was below the limiting level under certain conditions. This was due to the fact that the IF signal to the PLD passed through only four of the eight IF-limiter amplifier stages. The change in the signal level to the PLD caused a change in the loop bandwidth of the unit resulting, in turn, in a very narrow lock-in range for low signal levels. This situation was corrected by changing the source of the PLD input signal from the output of the fourth IF stage to the output of the seventh IF stage (the output of the eighth IF stage was not utilized in order not to affect the operation of the on-line discriminator during the normal mode of operation). This modification increased the GSE emergency-mode sensitivity −22 db, from −88 to −110 dbm.

Next, the bandwidth of the PLD was increased to be more compatible with the actual threshold (due to the finite IF gain of the system) rather than the theoretical threshold defined by the information bandwidth. For the rate-limited FM emergency-mode data transmitted by the subsystem, the theoretical noise bandwidth required by the PLD is 320 cps, giving a corresponding signal threshold of −128 dbm. Thus, for the GSE sites the noise bandwidth of the PLD could theoretically be increased by +18 db (from −128 to −110 dbm), corresponding to a noise bandwidth of 20 kc. Actually, as a reasonable compromise, the bandwidth of the PLD was increased by only 5 to 7 db, giving a theoretical threshold of −121 dbm. This gives sufficient bandwidth to enable the reproduction of transmitted data with an error of less than 2% without the use of correction factors.

***c. Transmitter power supply.*** During the integration of the FM 1 subsystem at AED, there occurred a failure of the 500-v bridge. This failure could not be traced to any permanent external overload. Since the failure occurred when the operate relay was thrown, it is believed that the bridge failure was caused by a temporary short external to the modulator. As there are current-limiting resistors in the high-voltage lines, the failure could not have been due to excessive surge current external to the power supply. However, since the −500 v is generated by a +250-v supply tied to the −750 v, a short on the −750-v supply could place a high reverse voltage across the current-limiting resistors and thus the 500-v bridge. This would exceed the breakdown voltage rating of this bridge. Therefore, to avoid any more failures due to a similar situation, the voltage rating of the 500-v bridge was increased. The 1000-v bridge has the same mechanical configuration as the 500-v bridge and will be installed in its place on all flight model transmitter power supplies.

## 6. Power Supplies

***a. Voltage regulators.*** All of the high-current voltage regulators produced for *Ranger 6* to 9 have been completed and are in mechanical integration with the exception of the Unit 008. This unit is to be final acceptance tested early in December 1962.

***b. Batteries.*** Four of the Model 202 (22-cell) battery units were received from the vendor early in November. These units have been subjected to acceptance tests and are to be used in systems testing.

The new Model 230 (12-cell) batteries will be of a monobloc design and will weigh approximately 26 lb each. Two of these units in series will be used for each flight to replace the present two large 22-cell units that are connected in parallel.

The 12-cell battery offers the following advantages:

(1) The total weight of the in-flight batteries will be 52 lb compared to the present weight of 85.4 lb, a weight saving of 33.4 lb.

(2) The volume saving of the pair of new batteries over the present pair of batteries is approximately 1000 $in^3$.

(3) The reliability and storage life of the batteries are improved by the use of a four-layer cellophane separator per plate compared to the present three layers per plate.

(4) A new lead-wire sealing technique will be incorporated into all of the 12-cell batteries.

(5) A tap terminal has been provided on the eleventh cell in each battery unit to allow the use of either a 22-, 23- or 24-cell payload configuration and still retain the interchangeability feature. A bolt-on sealing cover will be provided on each unit to blank off the terminals not in use, thereby preventing any possible errors during installation.

(6) A simpler harness will be required because the cellmonitoring connections will be brought to a 25-pin plug on each of the battery units. The main battery leads will be brought to a fixed plug on the structure to simplify the connection of the external power supply and the battery monitor harness to the batteries. The fixed plug is also where the system load will be connected.

# E. Thermal Control

## 1. Thermal Shield Finish

In an effort to make the finish of the thermal shields more uniform, the surfaces are now being polished to a bright aluminum finish. Irriditing the aluminum resulted in streaking, spotting, and blemishing which could not be repaired. Oxidation problems have been found to be negligible and easily overcome. Tests of the optical properties of the polished aluminum have been carried out. Results of these tests indicate the average values for the solar absorptivity $\alpha$ and emissivity $\epsilon$ of the polished aluminum are: $\alpha = 0.200$ and $\epsilon = 0.057$.

Irridited aluminum provided an $\alpha = 0.33$ to 0.40, and an $\epsilon = 0.077$. The polished aluminum, therefore, offers a reduction in the thermal input by a factor of 2 when the vehicle experiences the solar maneuver.

## 2. Instrumentation and Simulation

*a. Thermocouples.* During the reporting period, a new thermocouple configuration was designed. The newly designed thermocouples react more efficiently to transient conditions and have been incorporated into the thermal–vacuum instrumentation.

*b. Environmental test wiring.* Standardized connections and wiring to all the environmental test area facilities were established after the testing of FM 1 was completed. This necessitated rework of all wiring harnesses used for simulation and thermocouple instrumentation. Since no further changes are anticipated, these harnesses will be used for all future flight models.

*c. Temperature sensors.* Temperature sensors for FM 2 through 4 have been fabricated, tested, accepted, and delivered to mechanical integration. Testing has been completed on the two spare sensor units and the thermistors corresponding to these units. These too have been accepted and delivered to mechanical integration.

# F. Ground Support Equipment

## 1. TV Recording and Display

As of this date all TV recording and display units have been installed and checked out at their respective field locations. Units 1 through 4 (the checkout units) have been integrated into the GSE complex and are being used in the integration and testing of the various TV subsystem models. The operational unit at DSIF is undergoing extensive system testing in the GSE configuration.

Design of the TV recording and display equipment has been finalized with the recent incorporation of the vertical-sweep-direction change.

Units 1 and 2 are being used at AED for FM 2 integration and checkout as well as for the training of RCA field personnel. Unit 2 has been checked out prior to shipment to JPL. Units 3 and 4, at JPL, are being used in the testing program for the FM 1 and the PTM of the *Ranger* TV subsystem. Unit 3 is undergoing final checkout prior to shipment to AMR. Unit 5 is being integrated into the GSE configuration at DSIF.

## 2. Communications

All units have been installed and are in operation at their respective field locations. The unit at Goldstone (Fig. 8) is undergoing extensive system testing. Integration tests with the antenna system were to begin soon

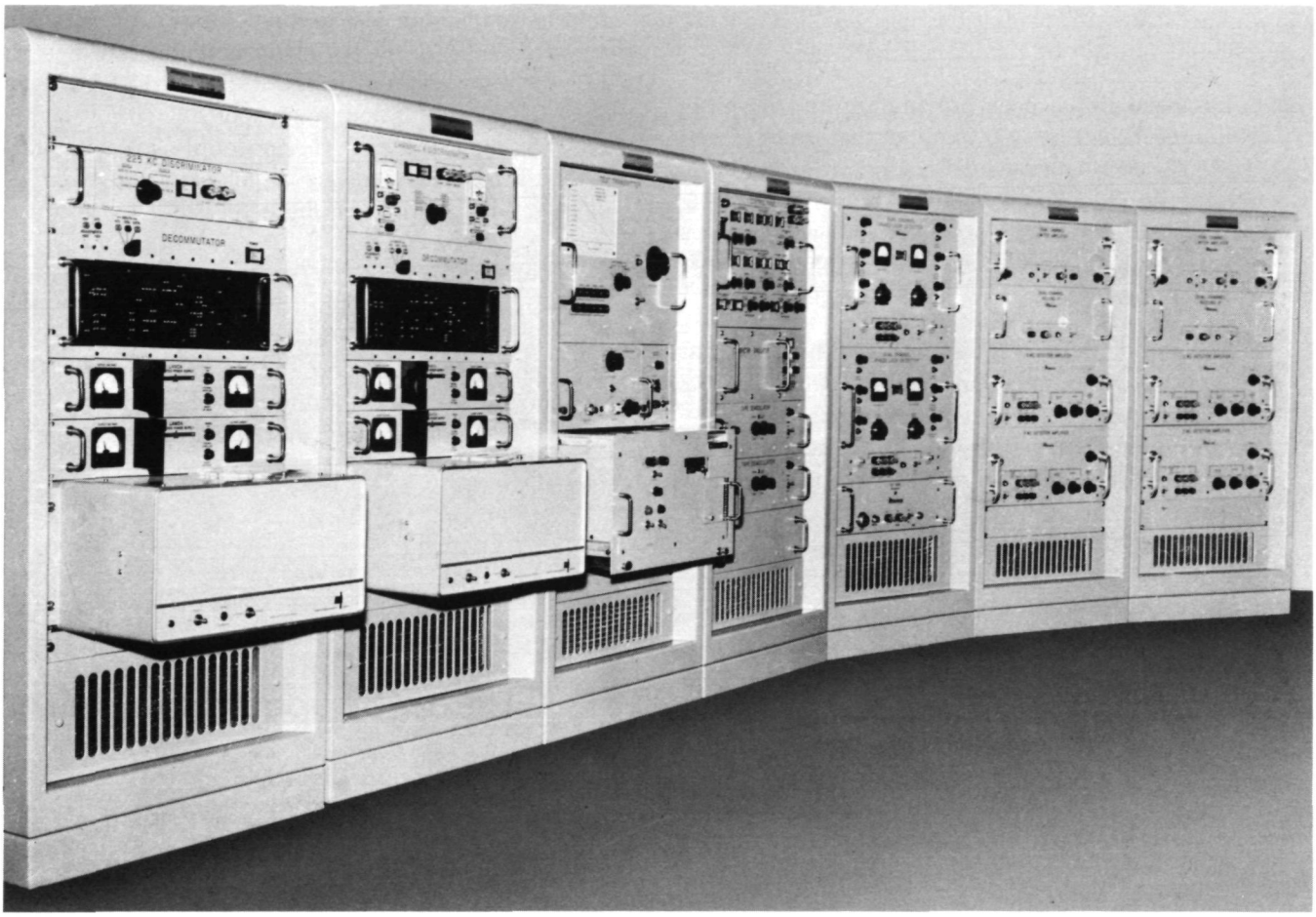


**Fig. 8. DSIF communications subsystem**

after December 14, 1962. Several modifications have been incorporated in the checkout units:

(1) Improvement of the emergency-mode telemetry system to provide better performance at threshold levels.

(2) Replacement of crystal ovens in the RF head with those having closer temperature tolerances for better tracking of the emergency-mode data during system test.

(3) Modification of the 225-kc discriminator to improve temperature stability.

The equipment for the RF links to the gantry and Explosive Safe Area has been delivered to AMR and is awaiting installation by JPL.

# IV. *Surveyor* Project

## A. Introduction

*Surveyor* is a lunar-surface-investigation project which includes seven missions for soft landing modest scientific payloads on the lunar surface in 1963, 1964, and 1965. The project is managed by the Jet Propulsion Laboratory for the National Aeronautics and Space Administration. Hughes Aircraft Company (HAC), under JPL Contract, is responsible for design, development, manufacture, and operation of the *Surveyor* spacecraft system.

The launch vehicle system will be the *Atlas–Centaur* involving the cooperation of Lewis Research Center at Cleveland, Ohio, and during the launch phase, the Launch Operations Center, Cape Canaveral, Florida. Tracking and spacecraft control will involve the cooperative use of the JPL Deep Space Instrumentation Facility and the Space Flight Operations Facility.

A group of approximately a dozen scientists is participating in the scientific activities of *Surveyor*.

## B. Scientific Experiments

### 1. Surveyor *Scientific Instruments Status Summary*

*Surveyor* scientific payload instruments which are at various stages of development are as follows:

(a) X-ray diffractometer.

(b) X-ray spectrometer.

(c) Gas chromatograph.

(d) Physical parameter instruments.

(e) Soil mechanics instrument.

(f) Television system.

(g) Surface sampler.

(h) Geiger counter.

(i) Seismometer.

(j) Micrometeorite ejecta detector.

(k) Alpha-particle-scattering experiment.

In November 1962, a decision was made to reduce the payload of the *Surveyor* appreciably so as to include only the X-ray diffractometer (a), the soil mechanics instrument (e), the two-camera television system (f), surface sampler (g), and the micrometeorite ejecta detector (j). The alpha-particle-scattering experiment is being evaluated for possible inclusion. It was decided at that time that all other instruments would be placed on an extended time schedule and extensive evaluation tests, both scientific and engineering, would be performed. In addition, it was decided that emphasis should be placed on a single-axis seismometer, a surface magnetic susceptibility instrument, and a surface thermal diffusivity instrument as alternates. Detailed descriptions of the status and program for each of the *Surveyor* scientific instruments follow:

***a. X-ray diffractometer.*** The X-ray diffractometer (being fabricated by Philips Space Development, Mount Vernon, New York) is one of the items of the scientific payload receiving maximum emphasis at this time since it is scheduled to fly on the first *Surveyor* launches. Prototypes 1 and 2 have been accepted and delivered to JPL.

At the completion of the Prototype-2 (P-2) phase of the contract, it was decided to change the design to effect several desirable innovations. The third prototype was to have a smaller X-ray tube, an improved detector, a superior power supply, improved packaging, and an improved dust cover design. The over-all configuration of this instrument was to be much smaller than the P-1 or P-2 models.

The third prototype X-ray diffractometer has been extensively tested. To allow an unstressed instrument to be delivered to JPL for type approval testing, a developmental model of the P-3 was authorized. This developmental model (P-3D) has successfully undergone all developmental tests as called for in the HAC type approval specification. This model is identical to the P-3 model, and no difficulty is foreseen in the ability of P-3 to undergo type approval testing.

P-3 was functionally tested prior to the acceptance tests and found to far exceed the requirements called for in the design specification. This instrument has just passed acceptance testing and delivery is expected at JPL before the first of the year. The type approval testing of the P-3 model is scheduled for January 1963. A design freeze on the instrument will be invoked immediately after type approval testing.

***b. X-ray spectrometer.*** The first prototype of the X-ray spectrometer (being fabricated by Philips Space Development) did not successfully pass acceptance testing. The basic reasons for this failure were electrical cross-talk problems and insufficient high voltage isolation.

The second prototype (P-2) was constructed using a new packaging design. A different readout scheme for P-2 allowed a reduction to be made of approximately 8000 electrical components. This design was extensively tested to determine its ability to eliminate the cross-talk and high voltage arcing problems that the first prototype experienced. These tests show that the new packaging design was indeed feasible. This prototype is scheduled for delivery to JPL in February 1963.

Since scientific studies have dictated further evaluation of the technique used in this instrument, the second prototype is due to undergo extensive scientific testing in the future. This instrument is not scheduled to fly on the early *Surveyor* spacecraft, so an extended evaluation schedule is possible.

No type approval tests are planned for the X-ray spectrometer. The contract will be completed at the completion of the second prototype.

***c. Gas chromatograph.*** The gas chromatograph being built by Beckman Instruments, Inc., is not scheduled to fly on any of the early *Surveyor A* flights. Two prototypes have been constructed under this contract. The first prototype (P-1) was accepted by JPL with some waivers. The P-2 has recently passed acceptance tests and has been delivered to JPL; the gas chromatograph contract is being completed.

Plans for this instrument call for type approval testing as well as extensive scientific and engineering evaluation. The instrument is essentially in flight configuration, and a minor amount of redesign is anticipated for the flight models.

***d. Physical parameter instruments.*** The physical parameter instruments consist of the following:

*Subsurface probe:*

(1) Subsurface thermal diffusivity.

(2) Subsurface magnetic susceptibility.

(3) Acoustic velocity.

(4) Caliper.

(5) Subsurface temperature.

*Surface instruments:*

(1) Surface thermal diffusivity.

(2) Surface temperature.

(3) Surface magnetic susceptibility.

(4) Acoustic velocity.

(5) Penetrometers.

A stop work order has been issued to Texaco Experiment, Inc., the vendor for these instruments. This was necessitated because of over-run conditions, re-evaluation of scientific goals, and an extension in the time schedule. It is anticipated that the physical parameter instruments to be delivered will not be in fully completed form; rather, the semicomplete instruments will be modified and evaluated by the JPL cognizant engineers and scientists. Contract negotiations to complete the contract are scheduled for January 1963. An extended evaluation schedule will be entered into; no type approval of these instruments is planned at this time.

***e. Soil mechanics instrument.*** This instrument is slated to fly on the first *Surveyors* and hence is on a very high priority schedule. The breadboard and first prototype (P-1) were delivered and accepted by JPL and are now being evaluated by the JPL scientific staff.

The developmental model for the second prototype (P-2D) has been undergoing extensive developmental tests. A failure in the P-2D deployment mechanism during vibration has necessitated considerations of redesign of this particular mechanism in the second generation prototype. Thermal–vacuum testing will continue for the remainder of December 1962. It was decided that acceptance testing of the instrument would be performed on P-2D. The second prototype (P-2), which is to undergo type approval some time early next year, is being studied for its design characteristics.

The associated test equipment for the instrument has been completed and has been accepted by JPL. This equipment is to remain at GMC for the duration of the acceptance testing of P-2D. The acceptance testing of P-2D is slated to begin in January 1962. It is anticipated, however, that work on P-2 will begin before the acceptance testing for P-2D is completed.

The vendor for this instrument, General Motors Corporation (GMC) Defense Research Laboratories, is making a proposal on desired modifications in the soil mechanics instrument. It is anticipated that a modification to the existing contract will be issued during the first part of next year.

***f. Television system.*** The *Surveyor* television system is being built by HAC under JPL cognizance. A recent demonstration of this system indicated that the resolution requirement may be met. The ability of this instrument to perform photometric and polarmetric observations is still uncertain. The problems involved in each of these measurements is now being studied to determine their specific complexity. The stereoscopic coverage of the television system has not as yet been demonstrated to JPL. No serious problems are seen, however, in providing the television system with the capability to perform stereoscopic measurements.

***g. Surface sampler.*** This instrument, which is the primary sample gathering instrument for the alpha particle experiment and the X-ray diffractometer is currently being studied for desired modifications. Due to the fact that the payload of the early *Surveyor* spacecraft will be limited as far as science data gathering ability is concerned, all means of optimizing specific experiments are being investigated.

It was discovered that several interesting bits of scientific information could be gained from the surface sampler if certain modifications were made. These modifications, for example, consist of:

(1) Strain gages to measure the frictional and cohesive properties of the lunar surface.

(2) More precise maneuverability of the instrument to enable the instrument to—(a) manipulate lunar rocks or interesting lunar objects under the scrutiny of the television system and (b) dig a furrow into the lunar surface to gain some information concerning the subsurface layer of the lunar surface.

HAC, the manufacturer of the surface sampler, is studying the problems involved with making the changes enumerated.

***h. Geiger counter.*** The first prototype of the Geiger counter has been received at JPL and is undergoing scientific and engineering evaluation. The second prototype

is slated for delivery early next year. This second prototype differs from its predecessor only in respect to thermal shielding and thermal control properties. An extended evaluation schedule is contemplated for this instrument; no type approval is planned. The contract for the instrument with Electro-Optical Systems, Inc., will be completed after the delivery of the second prototype.

***i. Seismometer.*** The first prototype of the seismometer has been completed and accepted by JPL several months ago. Since that time it has been undergoing extensive scientific and engineering evaluation. It was determined that a standby payload item for the first *Surveyor A* launches would be a single axis seismometer. No contract for the development of this instrument has been awarded as yet. However, proposal instructions are being prepared, and it is expected that a contract for this instrument will be let soon.

***j. Micrometeorite ejecta detector.*** A micrometeorite experiment has been approved for inclusion in the *Surveyor* payload. The purpose will be to determine initially the flux and momentum distribution and eventually velocity measurements. Instruments proposed by groups at Goddard Space Flight Center and Ames Research Center are being evaluated.

***k. Alpha particle experiment.*** An instrument under development at the University of Chicago for quantitative elemental analysis of the lunar surface employing alpha-particle-scattering techniques is being evaluated. A breadboard model has been furnished to JPL by the University and has undergone functional testing.

In addition to work on scientific instruments, work has also been performed on planning experimentation to take place at JPL on the *Surveyor* scientific instruments. A plan describing the total laboratory program for the *Surveyor* scientific instruments is being prepared.

Systems testing and ground support equipment philosophies are now being formulated. It is expected that specifications concerning systems tests will be available by mid-January 1963. In addition, a complete description of desirable ground support equipment is expected by mid-February 1963.

Data handling activities concerning engineering evaluation and needs for the *Surveyor* scientific instruments are just beginning to be formalized. The X-ray diffractometer group data handling techniques, however, are at a fairly advanced stage of development.

# V. *Surveyor* Spacecraft System

*The following material relating to the* Surveyor *Spacecraft System was prepared by the Hughes Aircraft Company:*

*Scientific payload.* The scientific palload for the A-21 spacecraft has been defined as the following: (1) television, (2) surface sampler, (3) sample transport and processor, (4) X-ray diffractometer, (5) alpha particle scattering device, (6) soil mechanics experiment, and (7) micrometeorite ejecta detector. Payload interfaces with the spacecraft are being defined and instrument test plans are being formulated. The television electronic modules for the T-21 spacecraft have been built and tested. A demonstration of the television system operating in conjunction with the command and data handling console was made. A surface sampler modified to meet current requirements is being tested.

*System analysis.* A study of launch window for the case of direct ascent trajectories shows that from an operational viewpoint they compare very unfavorably with the parking orbit method. Television capability, such as resolution, instrumentation viewing, and descent phase coverage, has been assessed on the basis of tests of a developmental system. A preliminary design mission sequence corresponding to the redefined payload has been formulated.

*Flight control.* An all-spur-gear train for the roll actuator is being designed to replace the final-stage worm gear design. Thermal-vacuum tests of the flight control sensor group indicate that only minor changes will be needed to meet thermal control requirements. An evaluation indicates that the $3\sigma$ error in roll axis orientation during retroengine burning will be less than 0.3 deg. Acceptance testing of the Canopus sensor for the T-21 spacecraft was completed. Changes in the flight control electronics unit for T-21 are being incorporated, based on test results with the unit for T-2.

*Electronics.* The engineering model planar array antenna for the T-21 spacecraft has been fabricated and preliminary tests made. Initial pattern tests of the omnidirectional antennas on the full-scale MA-2 spacecraft were completed following a change in the orientation of the Antenna 1. A traveling-wave tube which meets flight-acceptance requirements is available for the type-approval transmitter. Most of the spacecraft electronic components are in the fabrication, final assembly, or test phase; the electronic subsystems laboratory is in operation to check interaction between units. Problems with warping of the altitude marking radar dish are believed solved. An interim version of the X-1 radar altimeter and doppler velocity sensor was delivered to Hughes in early December for initial system testing; this development has

encountered serious delays and extensive modification has been necessary.

*Electrical power supply.* Thermal-vacuum tests of the second developmental solar panel were completed. A developmental battery exceeded requirements in charge-discharge cycling tests. Calibration of a solar simulator for solar cell tests has been completed. Testing of the T-2 power control system revealed a need for modification of boost regulator converter.

*Thermal control.* An IBM study of the thermal response of Compartment A to the lunar day mission sequence has been completed, and preliminary results of a similar study have been obtained on Compartment B for transit and a portion of the lunar day sequence. Thermal analysis of the main retro-engine using a new estimate of case emittance factor is under way, and several improvements were made in thermal control provisions of the vernier propulsion propellant lines and attachment fittings. Simulated lunar night tests of the MT-1 Sector 2 spacecraft thermal mockup were completed.

*Engineering mechanics.* Further studies of landing stability of the A-21 spacecraft have been made and preparations are nearly complete for a new series of drop tests using a reduced-weight version of the T-1 vehicle. The first static tests of the structural type-approval vehicle (S-2) were completed. The substructure-to-spaceframe joint design is being evaluated in static and fatigue tests.

*Propulsion.* Detailed data from two firings of the main retro-rocket engine confirmed that modification of the nozzle gave the necessary improvement in specific impulse. The first flight-weight retro-engine case produced by Lycoming proved satisfactory in a hydrostatic burst test. Injector clogging in the vernier propulsion system has been corrected, and thrust chambers have been delivered to support the T-2 test program.

*Spacecraft vehicle and mechanisms.* The T-21 prototype spacecraft was fitted with the vernier engines early in the report period and is now in the component installation stage of assembly. The S-2 structural test vehicle is being upgraded with T-21 type compartment support structure. The thermal test vehicle MT-1 Sector 2 is being prepared for transit and lunar day tests. An improved footpad design will be evaluated in the next series of drop tests with the T-1 vehicle. As a result of thermal-vacuum tests of the antenna-solar panel positioner, improvements are being made in the potentiometer and polar axis drive.

*Reliability and system test.* Integration and checkout of items for the T-21 system test equipment assembly is nearly complete. Detailed system test procedures have been prepared and are being converted to the use of automatic data processing techniques. A detailed schedule for implementing the reliability assurance test program has been formulated.

*Mission operations.* As a step in studying countdown requirements, a launch pad countdown sequence chart has been prepared. Data processing techniques are being applied in the system for organizing and revising detailed test procedures. The command and data handling console for the first system test equipment assembly has completed system tests, and system test of the prototype console is in the final stages.

# A. System Engineering Summary

## 1. Configuration

A redefinition of the scientific payload for the first flight spacecraft was received in late October, and details of the spacecraft configuration to accommodate this payload are being worked out. The current preliminary configuration is shown in Figure 1; most of the payload is clustered in the sector opposite leg 1. The instruments included in the payload are listed in Section B and are shown in Figure 2.

Since the weight of the entire desired payload is estimated to bring the spacecraft separated weight above the 2100-lb maximum allowed, studies have been made to determine a configuration which will permit instrument offloading with minimum shifts in the lateral center-of-gravity location.

## 2. Weight Summary

The current weight summary is given in Table 1. A detailed breakdown of spacecraft weight, including the new scientific payload is given in Table 2.

**Table 1. Spacecraft weight summary**

| Item | Maximum allowable weight, lb | Current design weight, lb |
|---|---|---|
| Total separated weight | 2100.00 | 2128.65 |
| Basic bus | 653.82 | 651.06 |
| Usable propellant | 1331.69 | 1347.69 |
| Scientific payload | 114.49 | 129.90 |

## 3. Explosive Squibs

At the request of JPL, Hughes investigated the effects of converting to the use of 1-w/1-amp no-fire squibs in the *Surveyor* spacecraft; after the results of the investigation had been submitted to JPL, they directed that all squibs used in the flight units of the *Surveyor* spacecraft system should meet the no-fire requirements of 1-w/1-amp for 5 min. Hughes is presently implementing this directive.

All Category A and Category B explosive devices will be converted to the 1-w/1-amp design. These include the main retro-engine explosive nut release mechanism, the main retro-engine igniter, the helium valve squib, the nitrogen valve squib, the mast extension gas release valve squib, the landing gear shock absorber locks, and various pin pullers. In general, this change will involve removal and replacement of the present squibs with the new ones, as well as some retesting to confirm compatibility. A design optimization and squib qualification program will also be required to ensure that the reliability requirements are met. Because procurement and testing of the explosive nuts for the main retro-rocket release mechanism has not begun, at present the conversion will involve only the revision of the specification; however, the higher resistance of the 1-w/1-amp squibs makes their firing by present circuitry impossible and the firing circuits must therefore be modified. Some wiring harness changes will also be necessary. The two pyroswitches that are used to remove power from the radar altimeter and doppler velocity sensor (RADVS) and the flight control systems after touchdown will not be converted to the 1-w/1-amp design. Instead they will be replaced with two solid-state switches, which will give added flexibility in test.

Increasing the no-fire requirements for pyrotechnic devices tends to degrade system reliability for three major reasons:

(1) Since increasing the no-fire requirement also increases the all-fire current and voltage, the margin of power available is somewhat depleted and a larger transient is put on the power supply.

(2) The circuitry required to fire the main retro-rocket explosive nut release mechanism is somewhat more complex.

(3) Because some redevelopment of squibs will be required, there is some loss of the confidence gained by the present system.

It is planned to incorporate the capability for firing the 1-w/1-amp squibs into the spacecraft during the March–April 1963 upgrade period.

CONFIDENTIAL

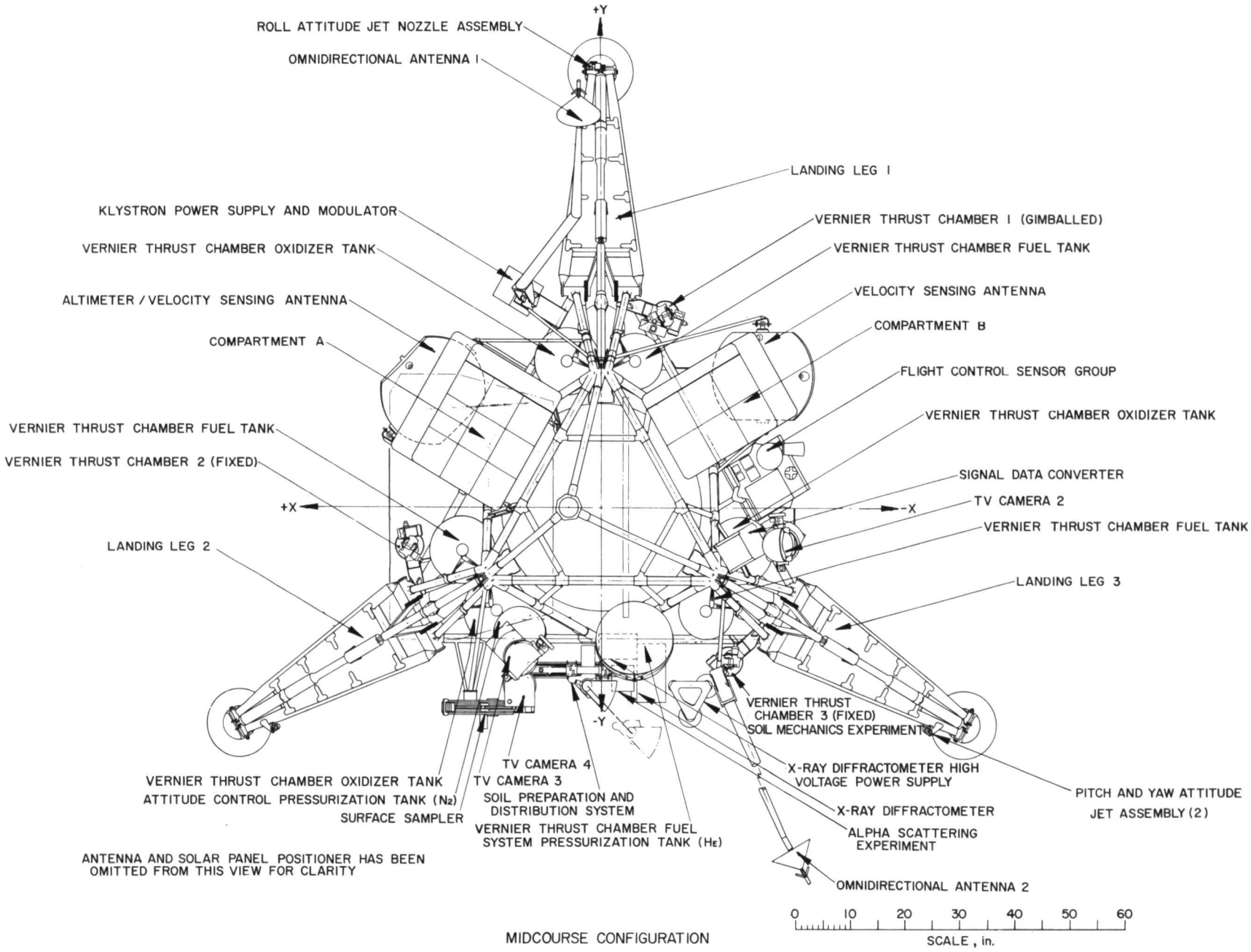


**Fig. 1. General arrangement of spacecraft**

CONFIDENTIAL

### 4. Sterilization

Late in the report period, JPL informed Hughes that the sterilization requirements would be reworded in part as follows:

> "Objective – Every effort shall be exerted to maintain a thoroughly clean and decontaminated spacecraft. As a final operation the complete spacecraft shall be encapsulated in the nose fairing and be subjected to a surface gas sterilization procedure. Complete internal biological sterilization as obtained by heat radiation or aseptic assembly is not required."

Hughes was directed to proceed immediately to implement these changes. All requirements to sterilize by heat, radiation or aseptic assembly have therefore been removed from all Hughes developed equipment, and all subcontracts are also being reviewed. Whenever any dollar saving is possible, the heat, radiation, and aseptic assembly sterilization requirements are being removed.

### 5. Wiring Harness

Each circuit exiting from the thermally controlled compartments has recently been reviewed to determine both satisfactory circuit operation and the effect of the nichrome wire used in these circuits to minimize thermal losses from the compartments. The review showed that a number of circuits including the squib ignition circuit, flight control circuits, and TV camera power circuits would not function properly with the additional impedance from the nichrome wire thermal barriers to the harness. Consequently, in thirty harness circuits these barriers were replaced with a length of copper wire. The use of copper inserts in place of nichrome allows the circuits to operate properly electrically; however, thermal losses from the compartments are substantially increased, jeopardizing the night survival capability of the spacecraft. Investigations are therefore being conducted to determine means whereby the compartment thermal losses can be minimized. These investigations cover two main areas:

**Table 2. Spacecraft weight breakdown**

| Item | Maximum allowable weight, lb | Current design weight, lb |
|---|---|---|
| 1.0 Basic bus (total) | 653.82 | 651.06 |
| 1.1 Flight control | 51.77 | 52.07 |
| Sensor group | | |
| Secondary solar sensor | | |
| Attitude control system | | |
| 1.2 Electronics | 95.18 | 102.29 |
| Data link (antennas, RF switches, transmitter-diplexer, command receiver and transponder) | | |
| Central command decoder | | |
| Central signal processor | | |
| Altitude marking radar | | |
| Doppler velocity sensor and altimeter | | |
| Power control system | | |
| TV Camera 4 | | |
| Engineering data processing | | |
| Mechanisms auxiliaries | | |
| Heater control | | |
| 1.3 Electrical power | 54.50 | 54.50 |
| Solar panel | | |
| Battery | | |
| 1.4 Mechanisms | 30.32 | 29.50 |
| Positioner, antenna/solar panel | | |
| Antenna mechanism, omni-directional | | |
| Separation sensing and arming provisions | | |
| 1.5 Spacecraft vehicle | 198.65 | 196.97 |
| Spacecraft basic structure | | |
| Equipment attaching hardware | | |
| Landing gear installation | | |
| Paint | | |
| Equipment compartments A and B | | |
| Electrical wiring | | |
| Pneumatic lines, attitude control | | |
| Release mechanism, retro-rocket | | |
| Engineering measurement sensors | | |
| Spacecraft-to-*Centaur* latch | | |
| Thermal control | | |
| 1.6 Spacecraft propulsion (not including usable propellant) | 223.40 | 215.73 |
| Rocket engine, main retro | | |
| Vernier propulsion system | | |
| Unusable vernier propellant | | |
| Helium | | |
| Insulation, main retro-engine | | |
| Safety and arming device, main retro | | |
| 2.0 Usable propellant (total) | 1331.69 | 1347.69 |
| 2.1 Retro-rocket propellant | | 1196.40 |
| 2.2 Vernier propellant | | 150.69 |
| 2.3 Pyrogen propellant (igniter) | | 0.60 |
| 3.0 Scientific payload (total) | 114.49 | 129.90 |
| 3.1 TV Cameras 2 and 3 and auxiliaries | | 39.20 |
| 3.2 Surface sampler and auxiliaries | | 10.00 |
| 3.3 Lunar soil properties measuring device and auxiliaries | | 14.10 |
| 3.4 Sample processor and auxiliaries | | 16.20 |
| 3.5 X-ray diffractometer and auxiliaries | | 16.30 |
| 3.6 Alpha scattering instrument and auxiliaries | | 7.10 |
| 3.7 Micrometeorite ejecta detector and auxiliaries | | 13.00 |
| 3.8 Engineering instrumentation | | 2.00 |
| 3.9 Electrical wiring | | 12.00 |

(1) Moving some switching functions outside the insulated compartments to minimize the number of wires passing through the compartment wall

(2) Disconnecting those wires exiting from the compartments that are not required after the first lunar day.

These investigations will be completed during the next report period.

## 6. Telecommunications Decibel Control Margins

The Surveyor spacecraft receives and transmits data to Earth in a variety of modes; these modes utilize the flexibility of the telecommunications link by changing such parameters as antenna gain, transmitter power, and data bandwidth. To provide assurance that the telecommunications link will adequately transmit and receive under all conditions, the transmission equation has been calculated for each case. Table 3 indicates newly calculated center margins and tolerances; Table 4 lists the parameters used in obtaining the center margins. A revised decibel allocation and margin summary for the telecommunication subsystem has been released. This revision includes DSIF acquisition modes along with new television modes.

## 7. Commands

A summary of A-21 spacecraft commands is given in Table 5. The basic bus contains a total of 7 subsystem decoders, which provide a total of 224 commands. Of these, 144 are presently in use and the additional 80 are spares.

The scientific payload auxiliaries contain a total of 7 subsystem decoders, which provide a total of 128 commands. The anticipated number of commands required by the payload is 83. A total of 45 additional commands is also available for future needs.

## 8. Data Channels

The A-21 basic bus data channels are summarized in Table 6. Basic bus commutated channels that are available for use by the scientific payload are included. Several of the payload auxiliaries will contain additional commutators or subcarrier oscillators; the signal processing details of the revised payload, however, are not sufficiently defined to permit their inclusion.

## 9. SNAP-11 Radioisotope Thermoelectric Generator (RTG)

At the request of JPL, Hughes has reviewed available information on the use of the SNAP-11 RTG power source for Surveyor, and has evaluated the effect of this

**Table 3. Telecommunications center margins**

| Calculation[a] | Center Margin, db | Tolerance, db |
|---|---|---|
| A. Earth to spacecraft | | |
| DSIF acquisition mode command phase | 8.0 | 5.4- 6.4 |
| DSIF acquisition mode phase lock | 17.8 | 7.0- 8.4 |
| Transit phase transponder modes | 35.1 | 7.2-14.2 |
| Transit phase command mode | | |
| Carrier | 28.3 | 8.8-16.2 |
| Subcarrier | 17.3 | 6.0-13.0 |
| Lunar phase command mode | 17.5 | 6.0-13.0 |
| B. Spacecraft to Earth | | |
| DSIF acquisition mode | 4.4 | 5.4- 4.4 |
| Transit phase transponder mode | 15.7 | 7.8-11.8 |
| Transit phase recorded data playback | | |
| Carrier | 63.2 | 7.2-11.4 |
| Subcarrier | 18.7 | 8.4-12.4 |
| Data from spacecraft during midcourse correction | | |
| Carrier | 33.9 | 8.8-13.2 |
| Subcarrier | 21.1 | 8.2-11.9 |
| Real-time engineering data | | |
| Transit phase | | |
| Carrier | 27.9 | 9.4-13.8 |
| Subcarrier | 15.0 | 7.9-12.2 |
| Lunar phase | | |
| Carrier | 27.89 | 9.4-13.8 |
| Subcarrier | 18.0 | 7.0-12.5 |
| Television transmission | | |
| Terminal descent | 4.2 | 6.4- 4.5 |
| Primary mode | 4.2 | 6.4- 4.5 |
| Emergency mode[b] | 6.6 | 7.8- 5.8 |
| Emergency mode (special[c]) | 0.9 | — — |
| High data rate transmission of scientific data | | |
| Carrier | 33.0 | 8.0- 6.5 |
| Subcarrier | 14.0 | 6.5- 4.9 |
| Low data rate transmission of scientific data | | |
| Carrier | 27.8 | 9.4-13.8 |
| Subcarrier | 18.0 | 7.9-12.5 |
| Lunar phase recorded data playback | | |
| Carrier | 59.0 | 6.6- 4.6 |
| Subcarrier | 40.9 | 7.4- 5.4 |

[a]The calculations are based upon the assumption that rapid switching polarization diversity is used at the DSS.
[b]The emergency mode for television transmission is restricted to a 60-degree cone angle relative to the spacecraft vertical.
[c]The spacecraft transmitter, upon command, can provide a higher peak deviation for television video; only nominal parameter values are considered for this mode.

RTG on the 2100-lb spacecraft. As a result, Hughes does not at present recommend replacing the present solar panel-battery power system with a solar panel/battery/RTG system as the primary source of electrical power on the *Surveyor* spacecraft. The RTG does offer several significant advantages for *Surveyor* and therefore would be a useful alternate or backup power source to be used to increase the reliability or extend the performance of later spacecraft.

The advantages of using an RTG on the 2100-lb spacecraft are listed below:

(1) *Lunar night survival:* The night survival of the A-21 spacecraft depends on whether or not enough electrical energy is available to maintain the thermally controlled compartments above the minimum temperatures required by the battery and electronics. The present solar panel/battery system is marginal in this respect, but the RTG assures a safe margin for survival through the lunar night.

(2) *Payload flexibility:* With the present system, all available energy is used to maintain the compartment temperatures during the lunar night. Therefore, no energy is available for heating remote instruments or operating any scientific equipment at night. The energy supplied by the RTG would allow experiments to be conducted at night without jeopardizing survival of the spacecraft. During the lunar day, the available electrical energy would be increased with the RTG from approximately 65 w to approximately 80 w. This would allow greater flexibility in the spacecraft sequence of operations.

(3) *Reliability:* Present A-21 power system design does not provide redundant battery charging capa-

**Table 4. Decibel values used for calculations**

| Parameter | Value | Tolerance, db |
|---|---|---|
| DSS transmitting power (maximum) | 70 dbm | 0-1.0 |
| DSS transmitting antenna gain | 50.0 db | ±1.0 |
| DSS antenna gain (at spacecraft transmit frequency measured at DSS mixer) | 51.0 db | ±1.0 |
| Spacecraft transmitting power | | |
| High | 40 dbm | 1-0 |
| Low | 20 dbm | 1-0 |
| Transmitter cable and switch loss | —0.4 db (max) | |
| Interconnection cable and transfer Switch 1 | 0.46 db (max) | |
| Antenna cable | | |
| 16-ft planar array | —1.9 db (max) | |
| 8-ft omnidirectional | 0.95 db (max) | |
| Spacecraft antenna gain | | |
| Planar array | 27.0 db | ±0.5 |
| Omnidirectional | 2.0 db | ±2.0 |
| Polarization loss (1-db axial ratio on transmit and receive — planar array) | 0 db | ±0.1 |
| Pointing loss (0.25 deg) | 0 db | 0-0.1 |
| Spacecraft omnidirectional antenna pointing and polarization loss (with DSS polarization diversity) | 0 db | 0-6 |
| Spacecraft receiver diplexer and interconnecting cable loss | —1.5 db (max) | |
| Spacecraft receiver phase-locked loop bandwidth ($2B_{LO}$ = 500 cps) | —27 db | ±1.7 |
| Path alternation (384,500 km at carrier frequency) | —211.4 db | ±0.4 |
| Spacecraft receiver noise figure | 13 db | ±1.0 |
| DSS phase-locked loop bandwidth ($2B_{LO}$ = 20 cps) | 13 db | |
| Noise bandwidth (3.3 mc) | 65.18 db | |
| Phase-locked loop threshold | 7 db | ±1.0 |
| Threshold (FM) | 10.5 db | ±1.0 |
| Boltzmann's constant | —198.6 dbm/°K/cps | |
| Effective noise temperature (on lunar surface) = 160.8°K ± 1.2 | 22.1 | ±1.2 |
| Spacecraft receiver bandwidth (FM) | 41.1 db | ±0.5 |

bility, since this mode of operation depends on successful operation of both the optimum charge regulator and the solar panel. Use of the RTG in the power system would enable redundant charging capability and increased lunar day power since it serves as a second prime power source on the regulated 29-v bus. Redundant battery charging from the RTG is enabled through the boost regulator to the unregulated bus and the battery. A block diagram of the RTG power system is shown in Figure 3. Reliable spacecraft operation can be achieved by use of the RTG in the event of battery failure although operations would be limited to a maximum power demand of 25 w.

The disadvantages and problems associated with the use of the RTG are listed below:

(1) *Weight:* The weight of the present power system is 63.3 lb. The RTG system would weigh 71.1 lb,

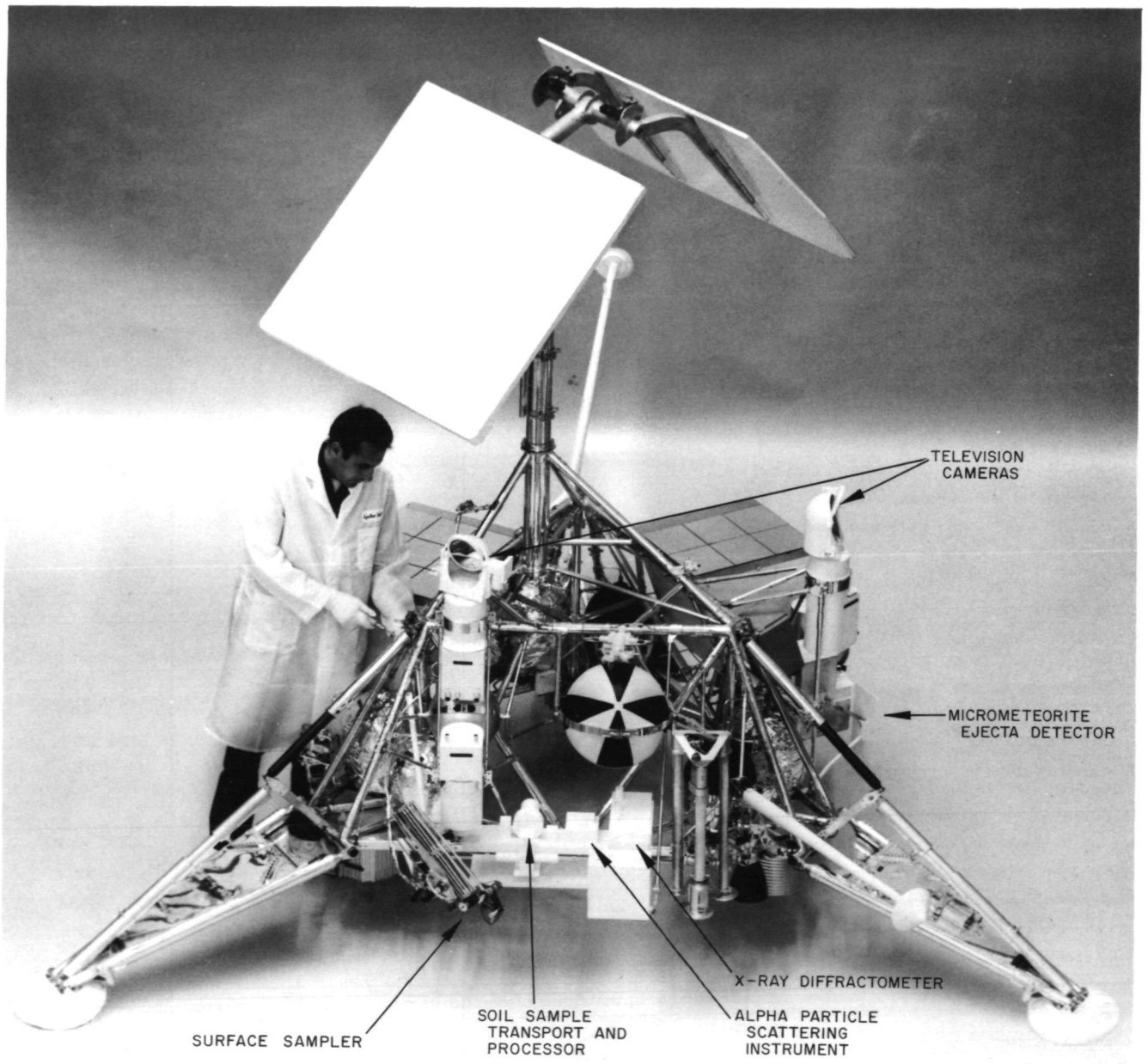


**Fig. 2. Scientific payload items on M-12-21 spacecraft mockup**

an increase of 7.8 lb. A weight breakdown is listed in Table 7.

(2) *Thermal radiation:* The thermal problem is caused by the large amount of heat that must be radiated from the RTG for proper operation. The spacecraft thermal control system is largely passive, depending upon the proper selection of surface thermal characteristics for temperature control. With this type of thermal control system, the temperatures of spacecraft units are sensitive to the complex thermal radiation and reflection characteristiscs of the remainder of the spacecraft. Introduction of a large thermal source into such a system causes difficult thermal problems. To some degree these thermal interactions can be treated with extensive thermal shielding. In the case of the RTG, however, extensive shielding degrades the

**Table 5. Spacecraft command channels**

| Subsystem command decoder | Number of commands assigned | Number of commands available |
|---|---|---|
| Basic bus | | |
| Data link and TV camera 4 | 30 | 32 |
| Signal processing | 29 | 32 |
| Electrical power | 12 | 32 |
| Mechanisms and vehicle | 14 | 32 |
| Basic bus spare | 0 | 32 |
| Engineering mechanisms auxiliary | 29 | 32 |
| Flight control | 30 | 32 |
| | 144 | 224 |
| Scientific payload | | |
| Television | 30 | 32 |
| Soil sample preparation and distribution | 13 | 20 |
| Surface sampler | 10 | 20 |
| X-ray diffractometer | 14 | 20 |
| Lunar soil properties measuring device | 8 | 20 |
| Micrometeorite ejecta detector | 3 | 8 |
| Alpha particle scattering | 5 | 8 |
| Total | 83 | 128 |
| | 227 | 352 |

**Table 7. Power system weight summary**

| ESTIMATED SNAP-11 RTG INSTALLATION WEIGHT, LB | |
|---|---|
| RTG | 30.0 |
| DC-DC converter | 1.0 |
| Shunt regulator | 0.3 |
| Attach brackets | 3.0 |
| Shielding on mechanisms | 3.0 |
| Wiring additional | 1.0 |
| | 38.3 |

| SYSTEM WEIGHT COMPARISONS (A-21) | |
|---|---|
| **System** | **Weight, lb** |
| Solar panel/battery | |
| Solar panel (9.2 $ft^2$) | 8.5 |
| Battery | 46.0 (2700 w-hr) |
| Central power control | 8.8 |
| | 63.3 |
| Solar panel/RTG/battery | |
| Solar panel (9.2 $ft^2$) | 8.5 |
| Battery | 15.0 (700 w-hr) |
| RTG total | 38.8 |
| Central power control | 8.8 |
| | 71.1 |
| Weight difference using RTG | (+) 7.8 |

**Table 6. Basic bus data channels**

| Item | Commutated data (PCM) | | | | High-frequency or continuous data (PM or FM) via subcarrier oscillators |
|---|---|---|---|---|---|
| | Digital | Analog | | | |
| | | Voltage | Current | Temperature | |
| Data link | 7 | 8 | — | 2 | 1 |
| TV Camera 4 | 2 | 1 | — | 1 | — |
| Signal processing | 2 | 2 | 3 | — | — |
| Mechanisms | 4 | 4 | — | 3 | — |
| Propulsion | — | 2 | — | 15 | — |
| Vehicle | 4 | 3 | — | 25 | 4 |
| Electrical power | — | 5 | 10 | 3 | — |
| Radar | 14 | 6 | — | 6 | — |
| Flight control | 46 | 25 | — | 7 | 1 |
| Basic bus channels Available to payload | 8 | 10 | 1 | 9 | — |
| Total | 87 | 66 | 14 | 71 | 5 |

RTG performance. For these reasons, the RTG probably will have to be extended from the spacecraft (approximately 5 ft) after touchdown, in addition to being thermally shielded from the spacecraft. The thermal problem also requires that cooling gas be delivered to the RTG at all times while the spacecraft is enclosed in the *Centaur* shroud, complicating the installation, sterilization, and testing of the spacecraft in the shroud.

(3) *Nuclear radiation:* The nuclear radiation problem is caused primarily by the limited radiation tolerance of some of the scientific instruments, primarily the X-ray diffractometer. The radiation limits finally established for the instruments will affect the shielding weight and also to some degree the fuel processing. The nuclear radiation problem is eased somewhat by extending the RTG from the spacecraft as described above.

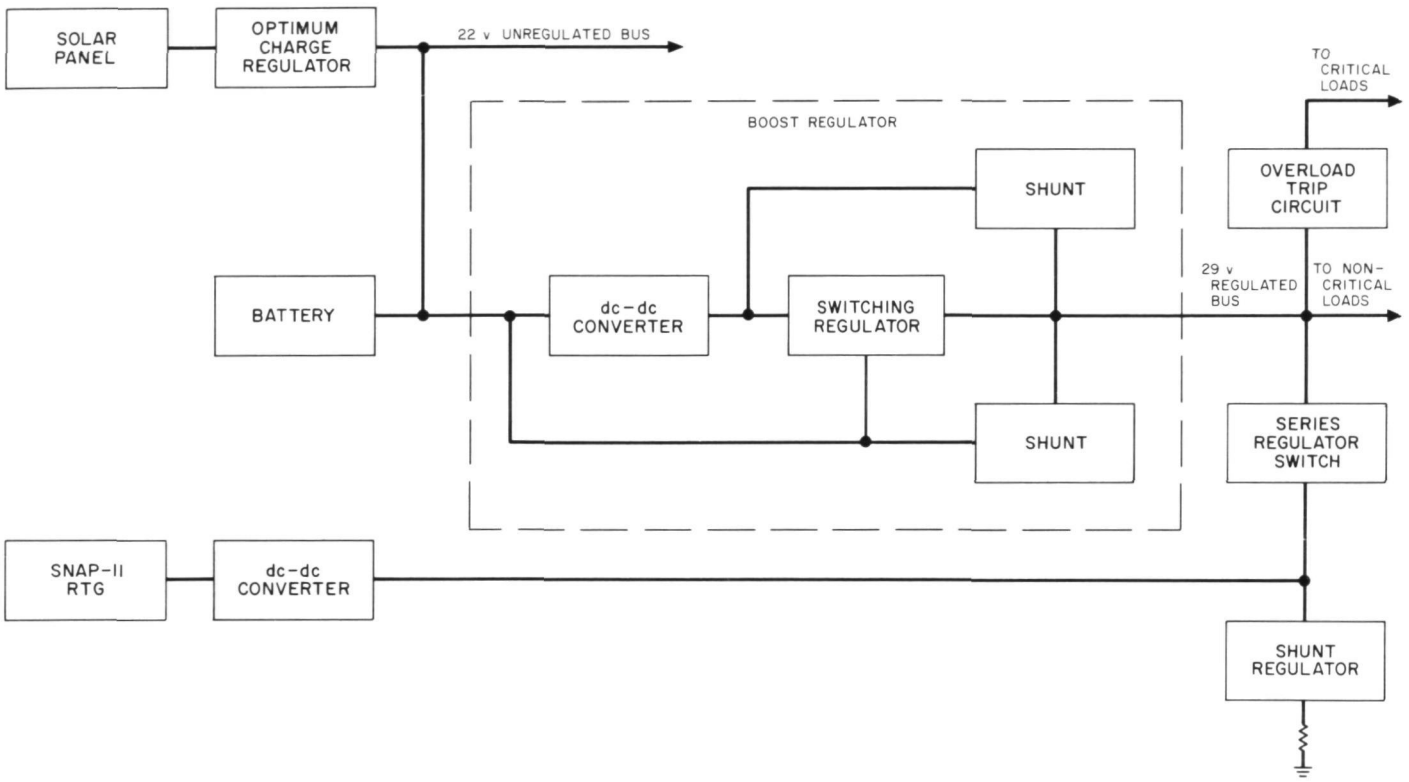


**Fig. 3. Solar panel/battery/SNAP-11 RTG power system**

# B. Scientific Payload

## 1. Payload Definition

On October 29, JPL transmitted to Hughes the definition of the scientific payload planned for use on the A-21 (2100-lb) *Surveyor* spacecraft. The payload includes the following units:

(1) Television, including Panoramic Cameras 2 and 3 (Camera 4 is presently included as part of the basic bus)

(2) Surface sampler

(3) X-ray diffractometer

(4) Soil mechanics experiment

(5) Micrometeorite ejecta detector

(6) Alpha particle scattering device

(7) Sample transport and processor (not in itself an experiment but necessary to provide samples for both the X-ray diffractometer and the alpha particle scattering device)

The total weight of these units, including their auxiliaries, is presently estimated to be 132 lb, and it may be necessary to delete one or more items to restrict the spacecraft weight to the required value. The spacecraft design will incorporate all these payload items unless it becomes apparent as the design progresses that a portion of the payload must be deleted. In that event, it appears possible simply to omit an instrument and its associated mechanical and electronic auxiliaries without changing any portion of the basic bus. It is planned that should a payload item be eliminated, no wiring harness provisions will be deleted, inasmuch as the weight penalties are negligible and stripping out instrument wiring provisions is very difficult.

## 2. Payload System Integration

The primary requirement in defining the means by which the instruments are to be integrated into the spacecraft design is to establish a firm interface definition between the instrument and the spacecraft. The interface specification will serve as a design guide for both the instrument developer and the Hughes activities involved in integration and development of mechanical and electronic auxiliaries. The principal elements to be included in the individual interface specifications are as follows:

(1) Weight and center of gravity

(2) Outline and mounting

(3) Electrical power

(4) Signal processing

(5) Thermal control

(6) Soil sampling

(7) Instrument manipulation

(8) Television viewing

(9) Command control

The block diagrams for the surface sampler auxiliary, sample processor auxiliary, X-ray diffractometer control auxiliary, soil mechanics auxiliary, alpha particle scattering auxiliary, and micrometeorite ejecta detector auxiliary are presented in Figures 4 through 9.

During the past 2 mo following announcement of the current payload, considerable effort has been devoted to system design leading to experiment autonomy and independence between the payload and the basic spacecraft. Under this concept, the payload equipment will be designed in such a manner that all functions applying to successful accomplishment of a particular experiment (e.g., power, signal conditioning, commands, manipulation, etc.) will be provided by equipment located in separate units; when such units are removed from the system, all functions required by the designated experiment are also removed. It is a further objective that removal of the units for any experiment should not remove any function required by other experiments of the payload or by the basic bus.

To this end, preliminary outline and mounting information on each experiment auxiliary has been specified and a preliminary layout of equipment within thermally controlled compartments completed. Preliminary command and data channel allocations for each experiment have been made and power allocations for each experiment have been started. Interconnections data between elements of the new payload are partially complete. A close examination is being made of the effects of line drop between units in the payload. Wire sizing and harness design will follow these studies and are scheduled for completion during the next report period.

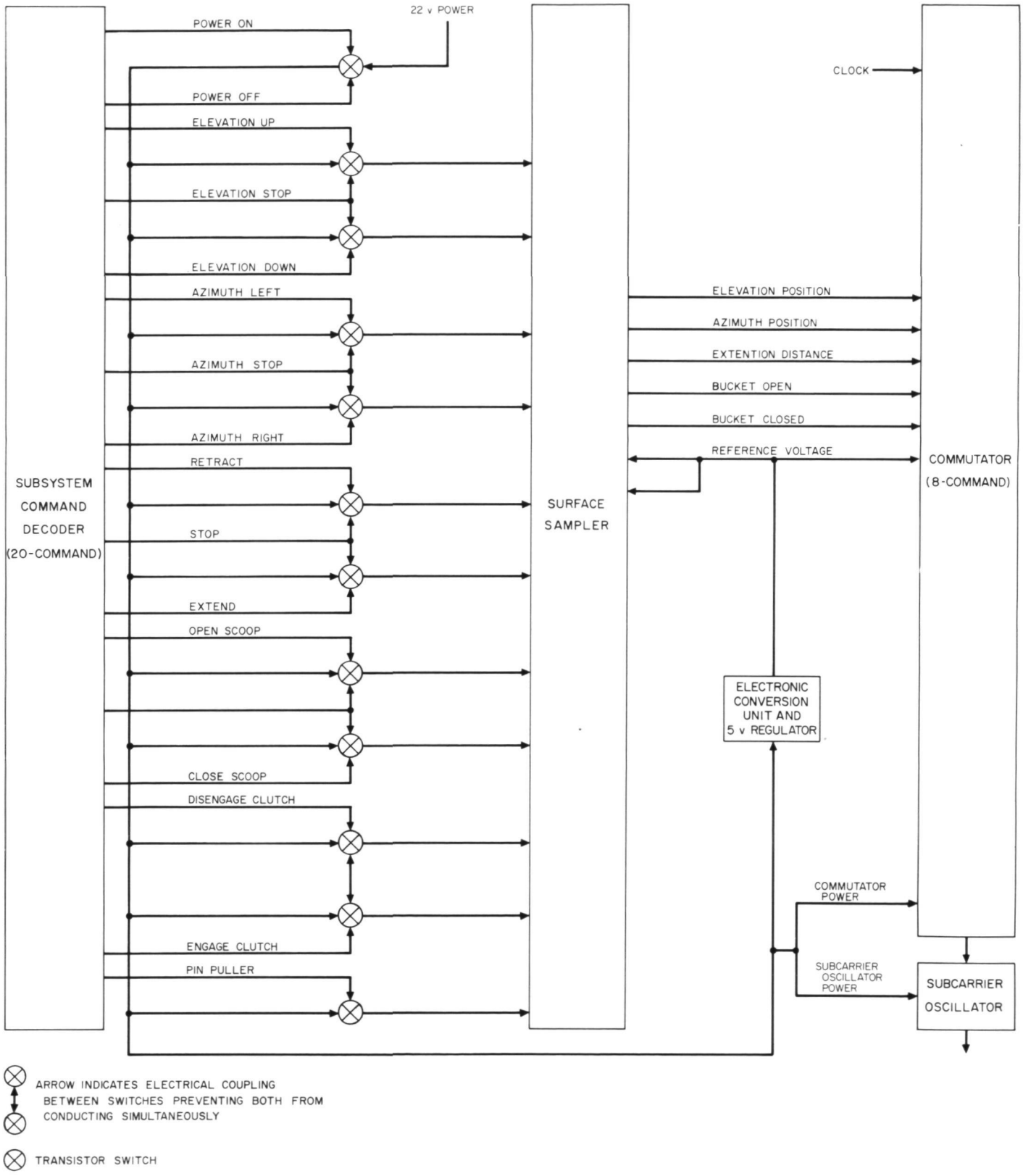


**Fig. 4. Surface sampler auxiliary**

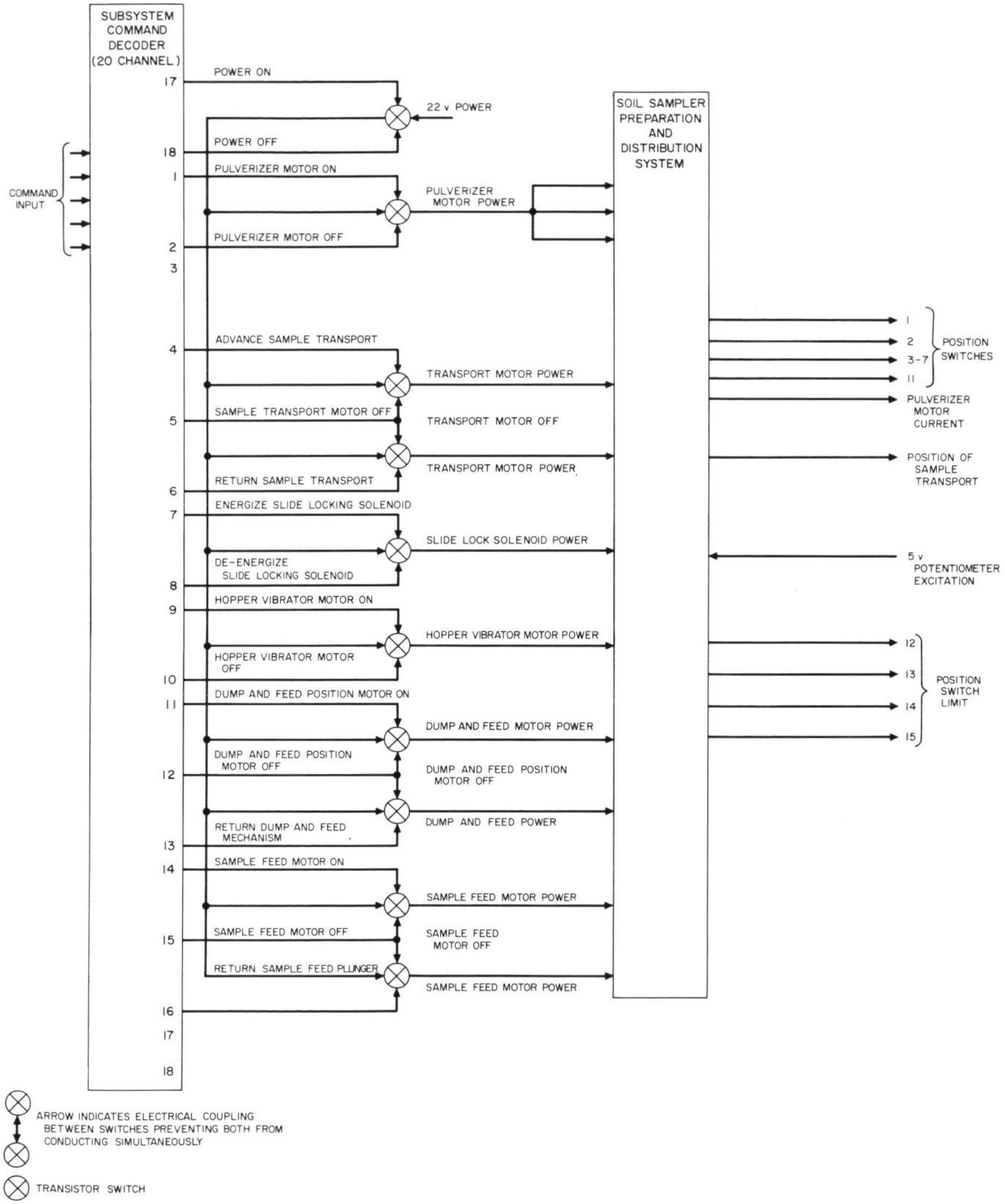


**Fig. 5. Sample processor auxiliary**

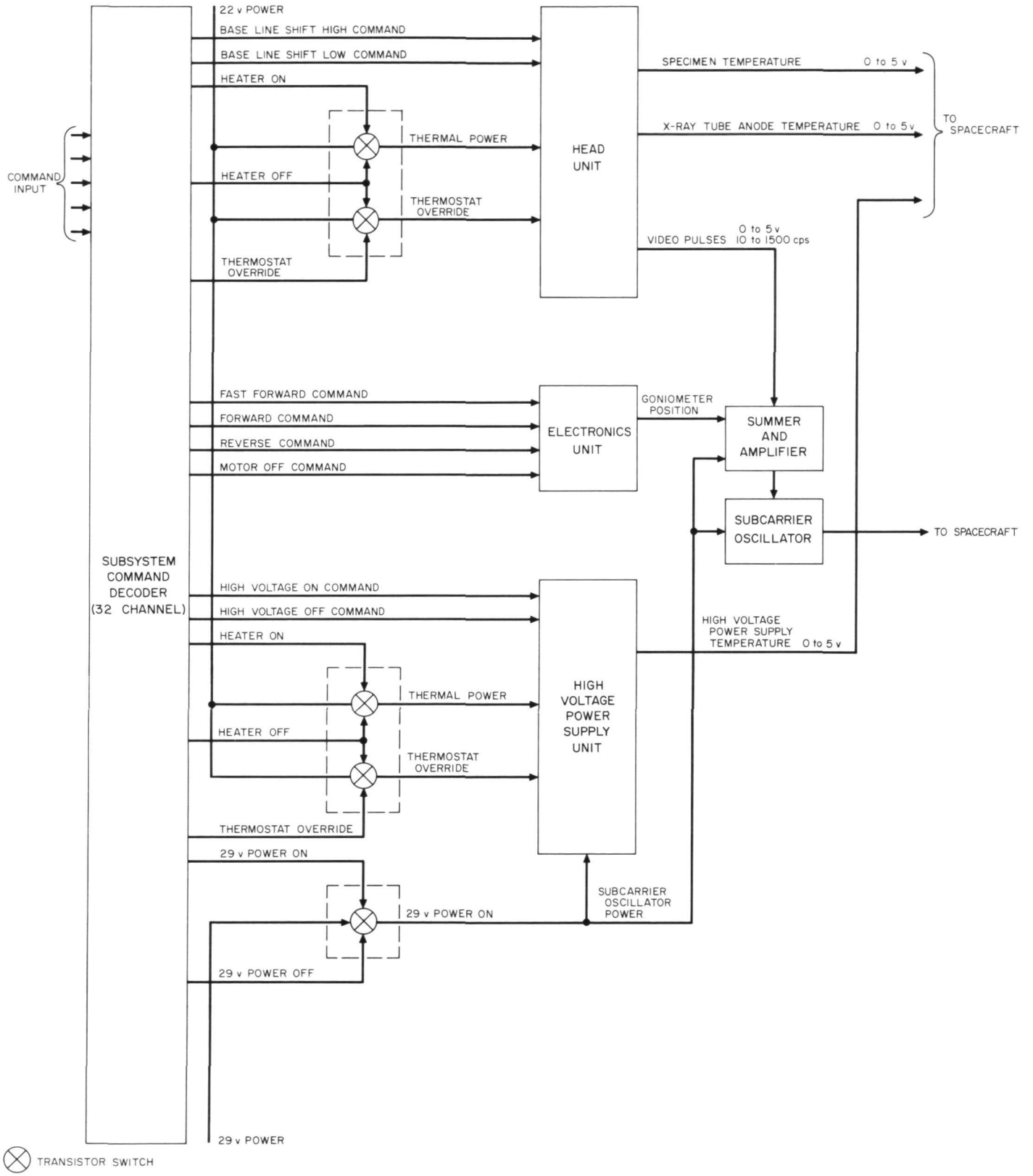


**Fig. 6. X-Ray diffractometer control auxiliary**

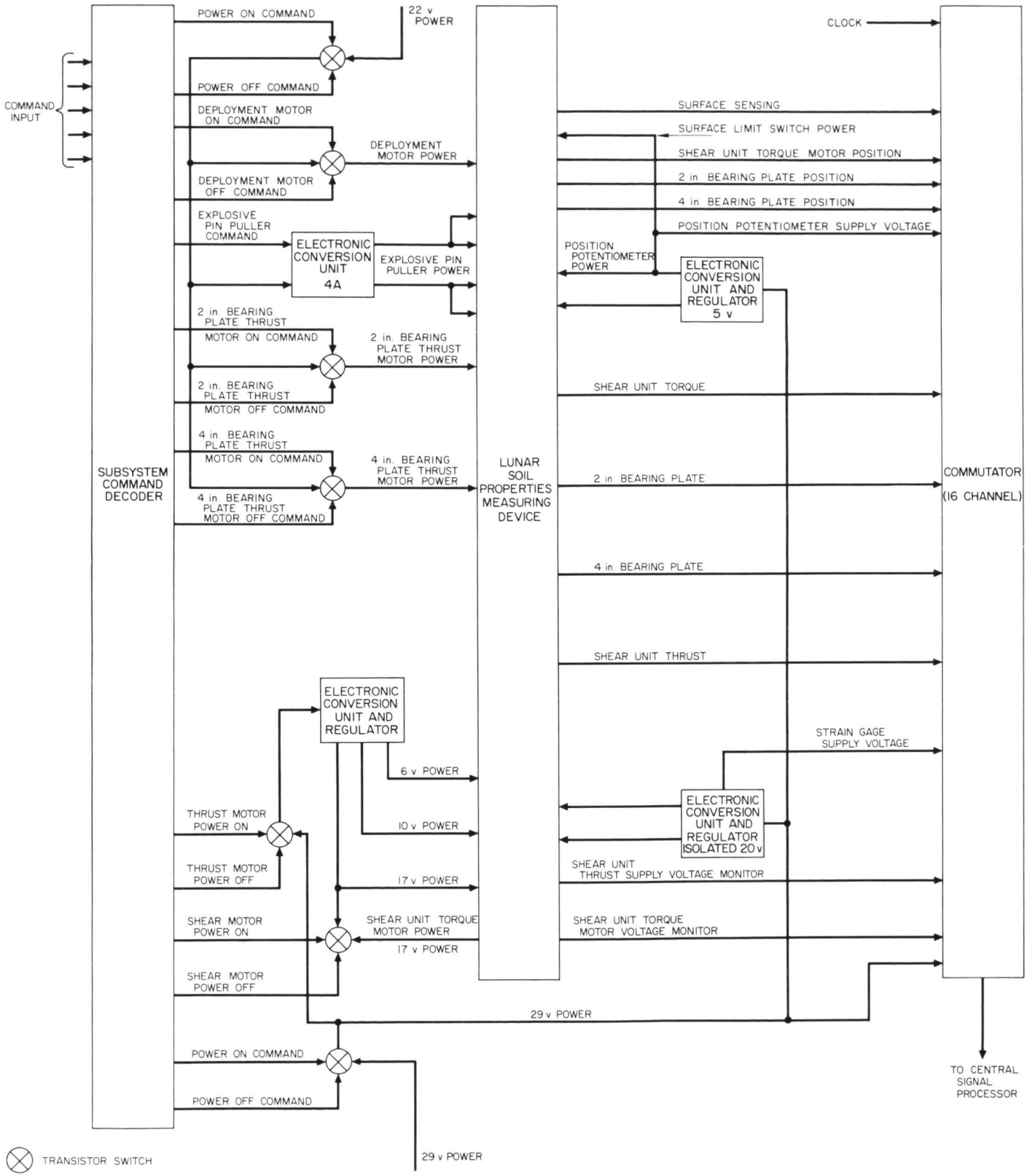


**Fig. 7. Soil mechanics instrument auxiliary**

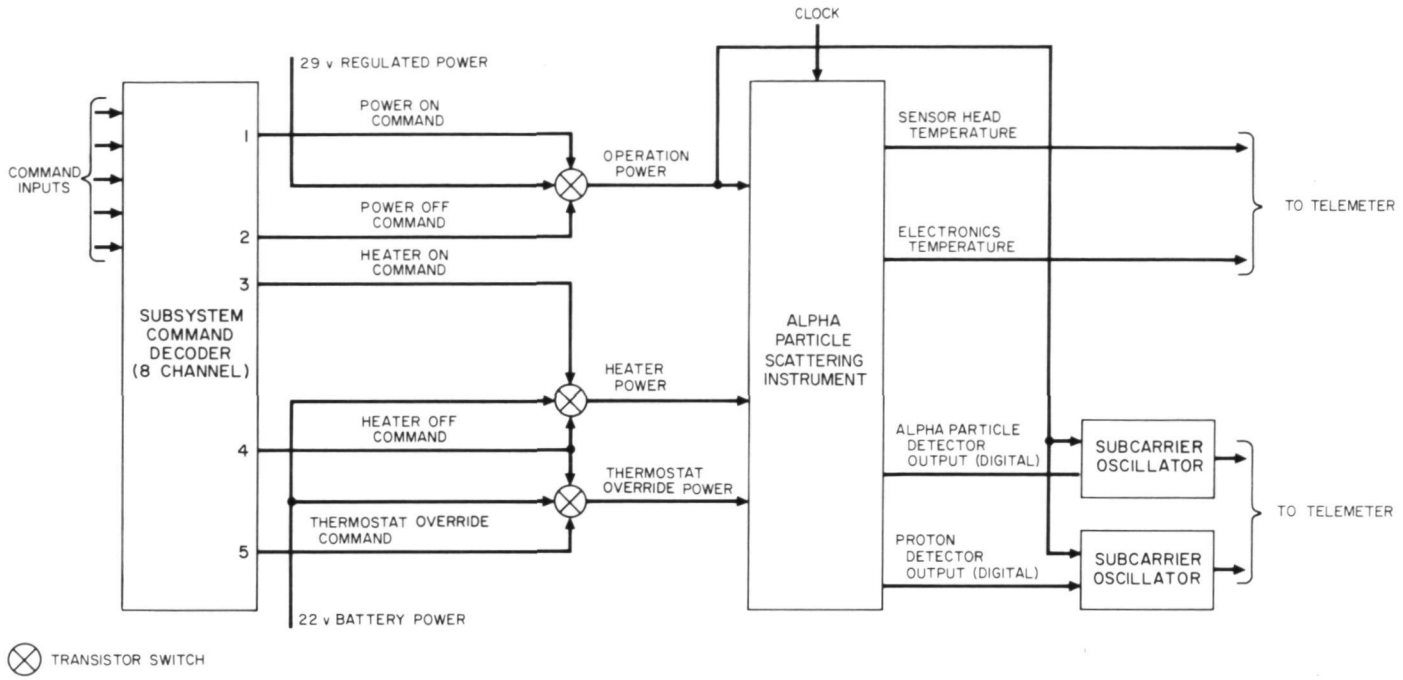


**Fig. 8. Alpha particle scattering instrument auxiliary**

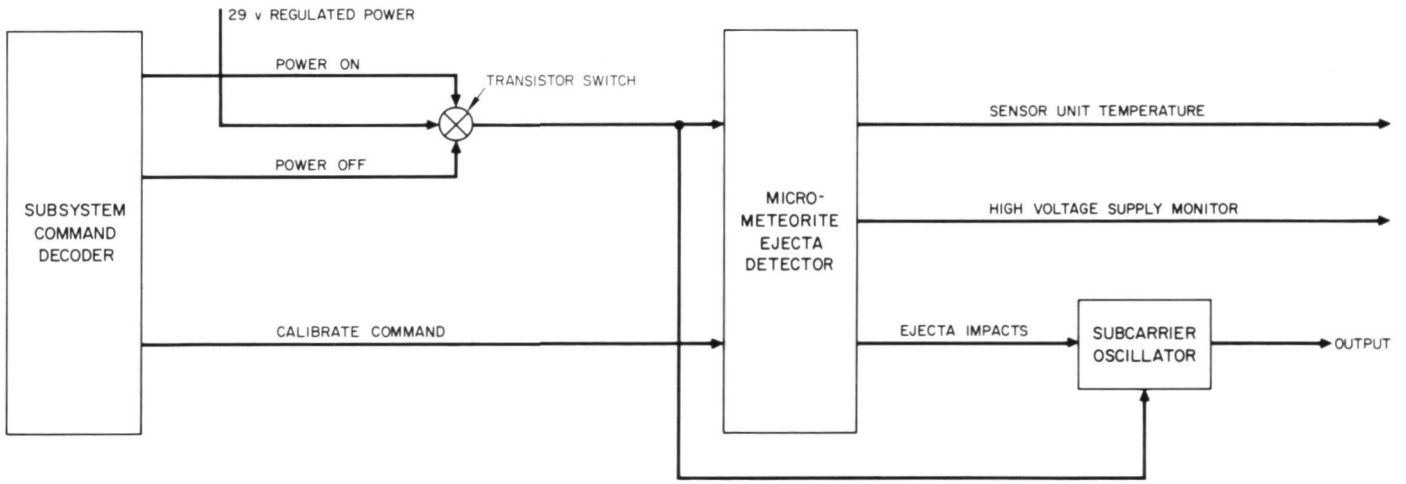


**Fig. 9. Micrometeorite detector auxiliary**

### *3. Payload Systems Evaluation*

Payload evaluation activities have centered around (1) formulating an overall payload test program which will provide high assurance of operation of scientific experiments on the Moon, (2) test planning for off-spacecraft integration testing of the experiments scheduled for flight spacecraft, and (3) investigating scientific instrument viewability by television cameras.

A subsystems and systems scientific payload testing plan has been formulated, so that sufficient subsystem developmental testing to assure that interface and experiment requirements have been complied with will be completed prior to installation of instruments and auxiliaries on the spacecraft for overall system testing. This method should allow a majority of integration problems to be detected and solved prior to spacecraft systems testing. Testing plans for individual experiment subsystems are under preparation; from these plans the requirements for stimuli, commercial test equipment, and special test equipment can be determined.

To determine the extent to which scientific instruments can be viewed by spacecraft television cameras and what changes might be necessary to accomplish desired viewing, an Exakta 35 mm camera was mounted with its focal plane approximately coincident with the mirror horizontal axis of TV Cameras 2 and 3. Installation of this test fixture in television mounting brackets for Camera 2 is shown in Figure 10. This fixture permitted horizontal and vertical movement of the Exakta camera as well as simulated tilting of the television camera housing. Instruments viewed were the soil mechanics group, surface sampler, and soil processor. Other scientific instruments scheduled for the A-21 do not at present have TV viewing requirements.

Initial tests with this setup revealed that some redesign would be required to achieve TV views of the specified payload items. Effort in this area is continuing.

### 4. Television

The television system for the A-21 spacecraft employs two cameras for visual surveillance of the lunar surface and a third camera for obtaining approach pictures of the Moon during the descent phase. The lunar surface surveillance cameras employ variable focal length lenses for wide or narrow angle capability. Scanning is accomplished by means of moving mirror assemblies mounted on each of the two cameras. Both surveillance cameras include a filter wheel with clear, red, blue, and green color segments. The third or approach camera utilizes a fixed focal length lens without color filters.

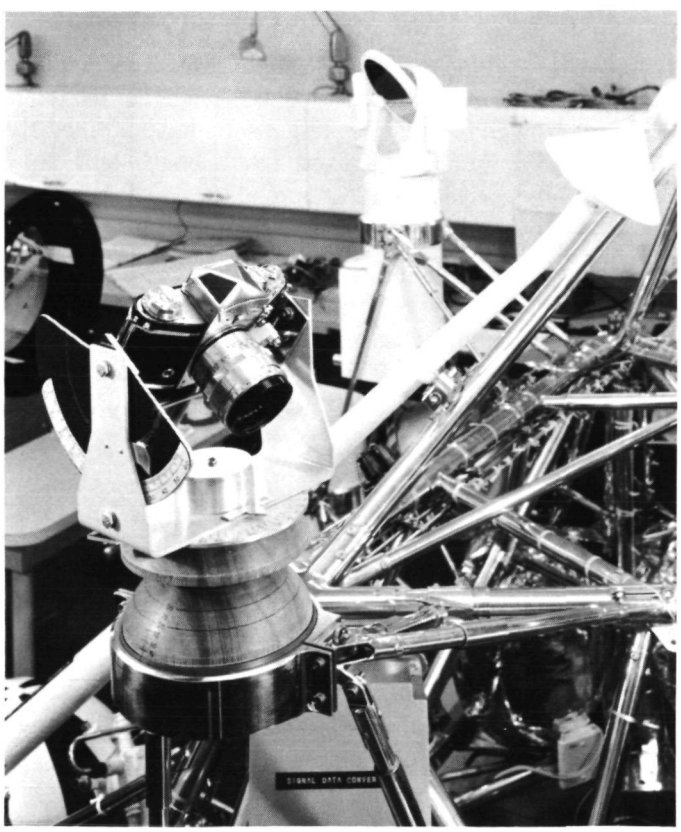

**Fig. 10. Test jig mounted in TV Camera 2 position**

Each camera contains the electronic circuitry necessary to process the image formed on a vidicon tube. The modes of operation, normal and emergency, are provided in each camera except for the downward-looking approach camera, which has normal mode only. Under normal operation, single-frame pictures can be produced at a maximum rate of one every 3.6 sec. The sweep circuits in the camera free-run continuously. Shutter operation and picture readout, including identification code, are initiated by command from Earth at the proper time in the sweep cycle and synchronized by video logic circuitry in each camera. Prior to a succeeding shutter and readout cycle, time is allotted for vidicon erasure, effected by the continuous sweeping of the tube, and for operation of mirror and lens mechanisms by Earth commands. Control circuitry for the mechanisms is also included in each camera.

Emergency mode operation is similar to normal mode except for a reduction in sweep rate and open-shutter operation. In this mode, the picture rate is reduced to one in about 62 sec. The emergency mode will be used if a failure in the communications link requires the use of the omnidirectional antenna.

*a. Drawing status.* All of the drawings necessary to build the TV cameras have been released for fabrication.

*b. Fabrication and test.* A total of 68 cordwood-type modules have been built and tested. This is the required number of modules to be installed in the TV system of three cameras for the T-21 type-approval test spacecraft. Twenty-nine of the modules have been installed on six chassis and in the electrical conversion unit. The six chassis and electrical conversion unit for T-21 Camera 2 have been built and tested. The conversion unit had to be modified because low-intensity magnetic leakage from the assembly degraded the TV picture. This condition was noted during the testing of the flight configuration engineering model. Additional filtering was added to the output of the voltage regulators, and the material of the assembly housing was changed from aluminum to a conetic alloy. The change in housing material results in attenuation of the radiated interference by an order of ten. Four of the chassis for T-21 Camera 3 have been built and tested.

*c. Structural studies.* A structural test model of Cameras 2 and 3 has been constructed and is shown in Figure 11 along with a mockup of the television electrical conversion unit with the covers removed. The model is constructed so that it has the same weight distribution as the actual unit. The test fixture has also been completed and the unit is awaiting installation of accelerometers prior to shock and vibration testing. A transmissibility plot covering a frequency range of 20 to 1500 cps will be made. This information will later be reviewed in terms of the vibration levels at the camera supports as determined from a vibration test of the S-2 structural test vehicle. In this way, the specific vibration environment existing at the cameras will be defined and can be examined.

*d. Thermal studies.* A complete thermal analysis of the television cameras is presently in progress. The analysis is being made to determine the non-operating, steady-state temperatures of each camera during all periods of the lunar day under the following conditions:

(1) Shaded at 65 deg latitude landing site
(2) In direct sunlight at 65 deg latitude landing site
(3) Shaded at the lunar equator
(4) In direct sunlight at the lunar equator
(5) During the lunar night

With this information, by means of a series of transient thermal analyses, it will be possible to determine the duty cycle limitations (if any) on the camera system with the present design and the changes that could be made to the present design to increase operating capabilities. With this type of thermal study, not only will the extremes of the television camera operation be defined but also many specific questions concerning operating conditions within these extremes can be answered.

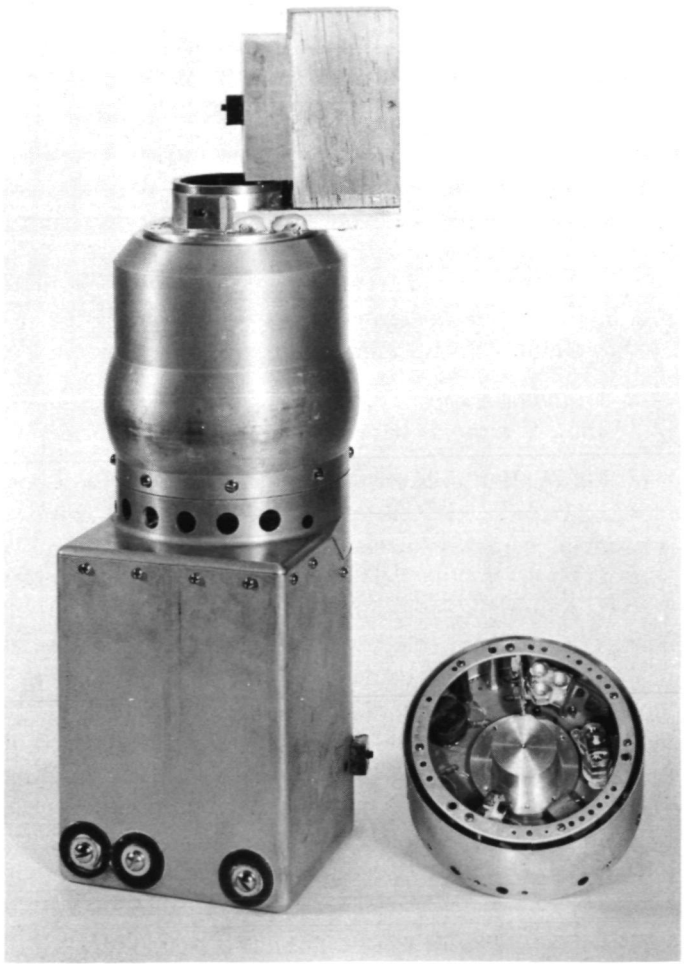

**Fig. 11. Structural model of camera with electrical conversion unit**

*e. Variable focal length lens.* Bell and Howell has delivered X-1 through X-7 of the first eight development model variable focal length lens. X-8, the lens for the type approval test camera, has not yet been delivered nor has TA-1, the Bell and Howell type approval test lens. Both lenses are awaiting parts shipped November 30 from Hughes to Bell and Howell. The T-21 models, X-5 and X-6, are included in the units already delivered.

*f. Fixed focal length lens.* Model X-1 fixed focal length lens, to be used on Camera 4 on T-21, has been delivered. Bell and Howell reports that test results have verified the mechanical design of the fixed focal length lens. Spot diagrams for verification of optical design have been furnished to Hughes.

Bell and Howell will start type approval tests in the near future. A copy of their test procedures has been reviewed by Hughes and conditionally approved. Complete approval will be withheld pending addition of tests to cover operation of the shutter in the 20 ms mode during vibration.

*g. TV auxiliary.* The TV auxiliary provides command decoding, switching, and signal processing for the television cameras. A block diagram of the auxiliary is shown in Figure 12.

The subsystem command decoder of the TV auxiliary receives digital information from the central command decoder. The subsystem decoder in turn supplies actuating or command signals to the cameras. It has the capability of handling 32 commands, although only 28 commands are used presently. Five modules perform this function. The modules are of welded-encapsulated construction and are 1.5 by 1.0 by 0.5 in. in size.

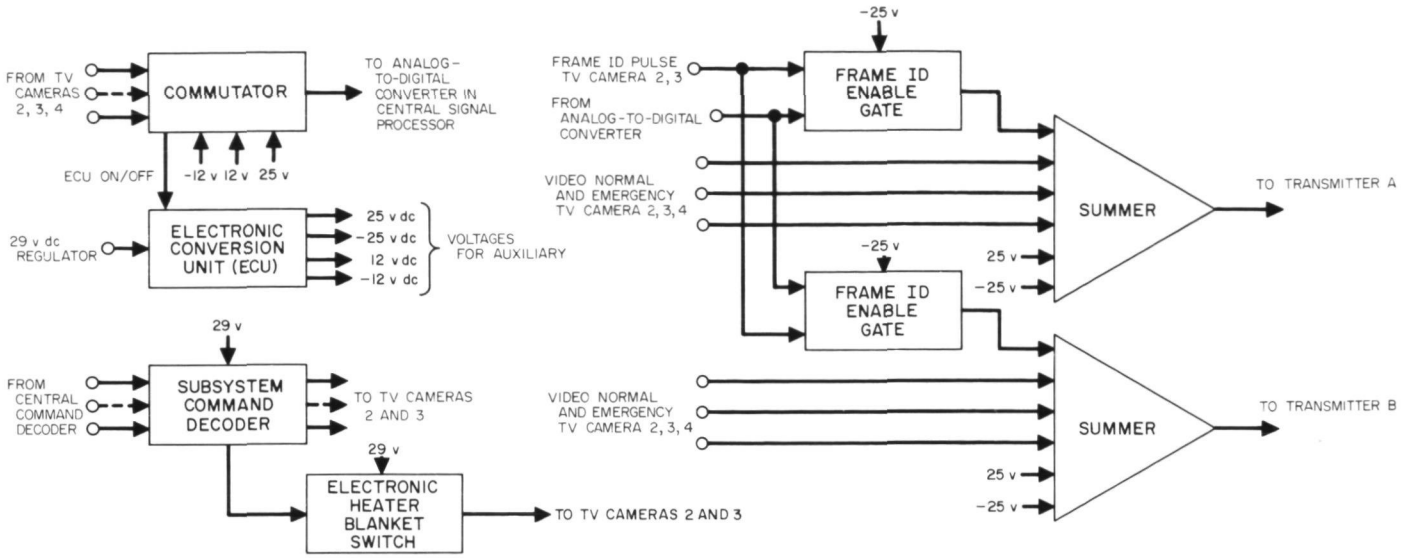


**Fig. 12. TV auxiliary**

The commutator commutates the data from the television cameras. The data, called frame identification (frame ID), are descriptive of the orientation or functional state of camera optics or mechanisms and of vidicon and electronics temperature. The processing scheme consists basically of logical gating and diode summing. Logical gating is used where high accuracy data would suffer from the use of normal summing. Diode summing is used on the remaining incoming data. The frame ID is sampled sequentially and gated to the master switch located in the central signal processor. The output from the master switch goes to the analog-to-digital converter. The commutation rate can be at either 4400, 1100, or 550 bps. The rate is controlled by the analog-to-digital converter clock oscillator located in the central signal processor. The frame ID signals are in the 0 to 5 v range. Seven modules perform the commutation, of welded-encapsulated cordwood construction and 1.5 by 1.0 by 0.5 in. in size.

The video summing amplifier receives the video and the frame ID enable pulse from the camera and the analog-to-digital converter output from the central signal processor. These signals are summed in the two parallel-connected, weighted, summing amplifiers and gated to Transmitters A and B. There are two modules for this function, of solder-freeze coated cordwood construction and 1.5 by 1.0 by 0.5 in. in size. Figure 13 shows the circuitry in the video summing amplifier for Transmitter A.

The electronic heater blanket switch delivers power to the resistors mounted on the chassis in the camera. The heat from the resistor preheats the electronic circuitry before power is applied to the camera. The switch receives the on-off command from the subsystem command decoder. The switch is not completely modularized; larger components are mounted on the chassis board. There is one module (1.25 by 1.0 by 0.5 in.), of solder-freeze coated cordwood construction. Figure 14 is a schematic diagram of the switch for Cameras 2 and 3.

The electrical conversion unit provides voltages for signal processing 25, —25, 12, and —12 vdc with a total regulation of ±2% over the load current range. The unit consists of a dc-to-dc converter (transistorized square-loop oscillator, with appropriate output rectification and filtering). The unit is turned on when the camera is turned on, and off when the camera is turned off. The components for the electrical conversion unit are mounted on the chassis board. Figure 15 is a schematic diagram of the unit.

The television auxiliary circuitry is on two chassis (5.0 by 7.6 in.) of sandwich construction. The modules and large components are mounted on the plate side; components too large to be packaged in modules are mounted on the board side. Chassis 1 holds the subsystem command decoder circuitry and the electrical conversion unit, and Chassis 2 holds the commutator, video summing amplifiers, and electronic heater blanket switch.

The construction of the two chassis for T-21 Spacecraft is complete. Electrical checkout is in process.

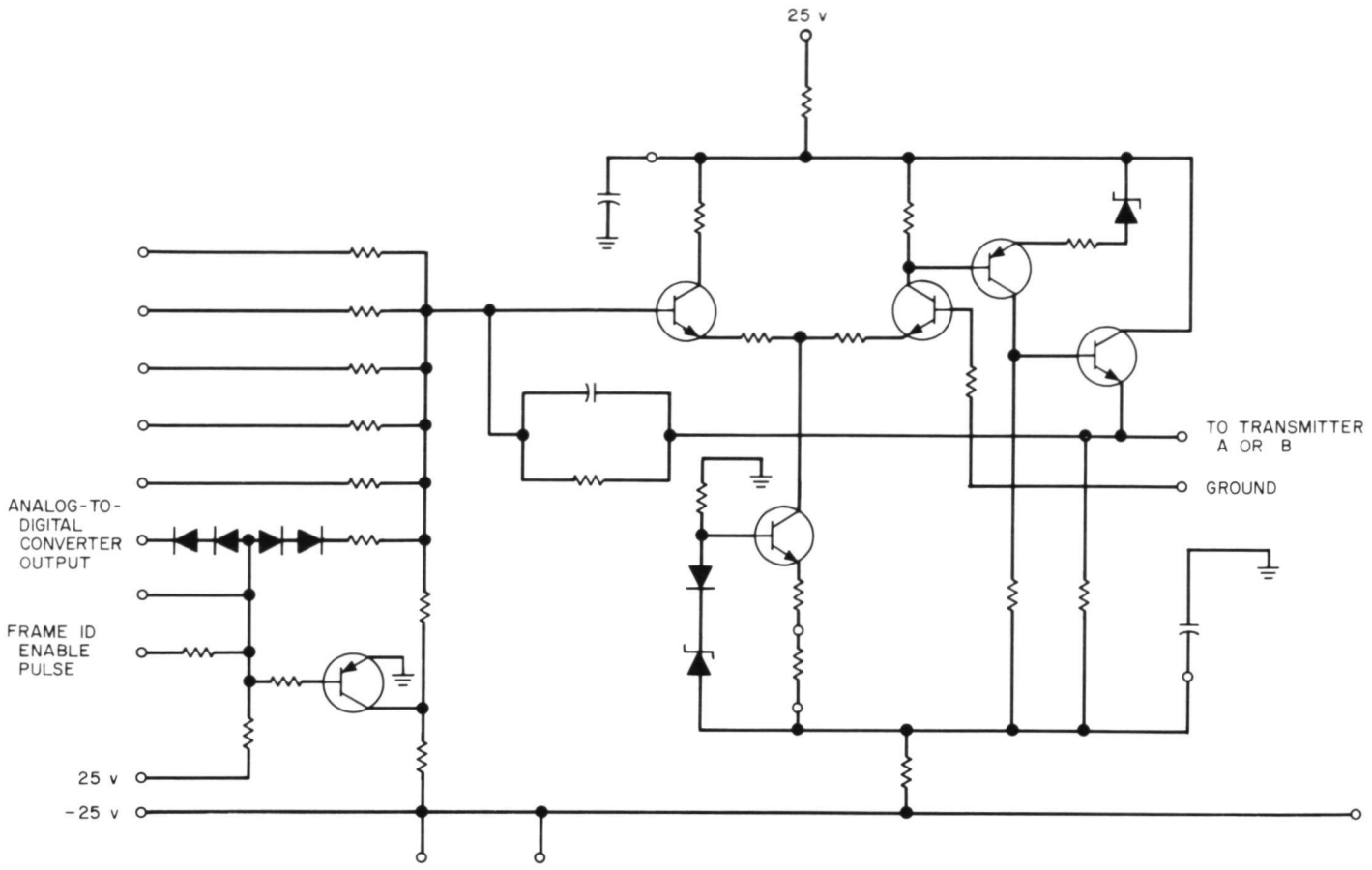


**Fig. 13. Video summing amplifier and frame ID enable gate for Transmitter A**

### *5. Demonstration of Mated TV Camera and Command and Data Handling Console*

A demonstration was made of a television system generally representative of the spacecraft and ground display TV subsystem. Hard-line connections from the surveillance-type TV camera to the command and data handling console (CDC) were used in lieu of the RF link.

The TV camera was placed outdoors near a building housing the CDC. The camera, together with the surface sampler, is shown in Figure 16, and the CDC in Figure 17. The photorecorder was operated throughout the demonstration; sections of film were quickly developed and enlarged for examination during the course of the demonstration. In addition, a Polaroid land camera was provided to swing down and photograph the monitor as desired.

The TV camera was operated by remote control through the CDC in the manner planned for actual lunar operations. The commands required for changing the angular location of the field of view in elevation and azimuth, angular size of the field of view (choice of focal length), focal distance, etc., were introduced into the command generator unit of the CDC by either manual punching of the octal keyboard or punched tape. The punched tapes had been prepared in advance for one 90-frame wide-angle survey covering 360 deg azimuth at each of three elevation angles and for two 18-frame narrow-angle surveys of selected portions of the scene. Each survey was conducted at the rate of one frame each 3.6 sec – the maximum rate that allows time for two vidicon-erase scans following the readout scan.

Manual keypunch entry was used for the commands needed to view the resolution and gray-bar charts, display the surface sampler to two sample-pickup positions (both wide-angle and narrow-angle modes for each position), and similar operations, including use of the emergency mode (20-sec scan.) Sample Polaroid photographs of the CDC television monitor are shown in Figure 18.

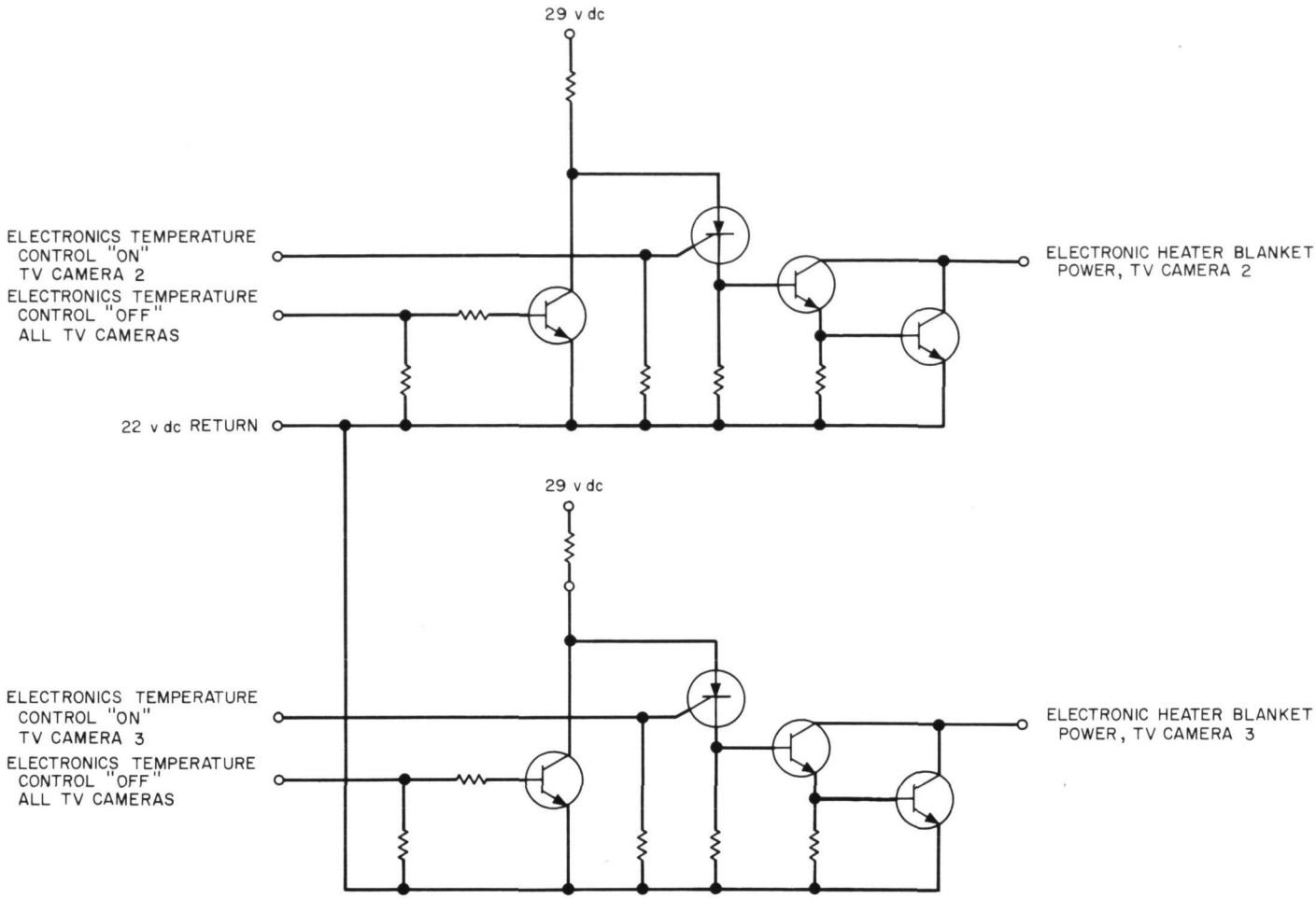


**Fig. 14. Electronic heater blanket switch**

The system capability for color differentiation was demonstrated qualitatively by showing, in juxtaposition, swatches of pink and light blue cloth. The samples appeared alike when no color filter was employed but were readily distinguishable on the monitor when, for instance, the red camera filter was moved into place, when the pink sample appeared to be markedly lighter than the blue sample. Subsequent determinations at JPL yielded the following values for the chromaticity coordinates of these samples:

Pink sample
x-coordinate 0.352
y-coordinate 0.304

Blue sample
x-coordinate 0.284
y-coordinate 0.266

These coordinates indicated color purities of approximately 15%.

The television system for the demonstration differed from the complete system in several respects, all stemming from the use of hard-line connections instead of an RF link. This system is represented in Figure 19, compared to the *Surveyor* system itself in Figure 20. Apart from the coaxial cable, the special tie-in equipment of Figure 19 makes up three principal chains: (1) command chain, beginning at the printer in the CDC and ending at the TV camera, (2) camera parameters chain, a multiwire cable leading from the TV camera to the telemetry display console; and (3) the synchronizing chain, which begins at the TV camera and terminates at the tape reader entry in the CDC.

### 6. Tape Recorder

Development and manufacture of the tape recorder is under subcontract to Data Recorders Division of Consolidated Electro-dynamics Corporation (CEC). In August, 1962, a stop-work order was placed on the effort at

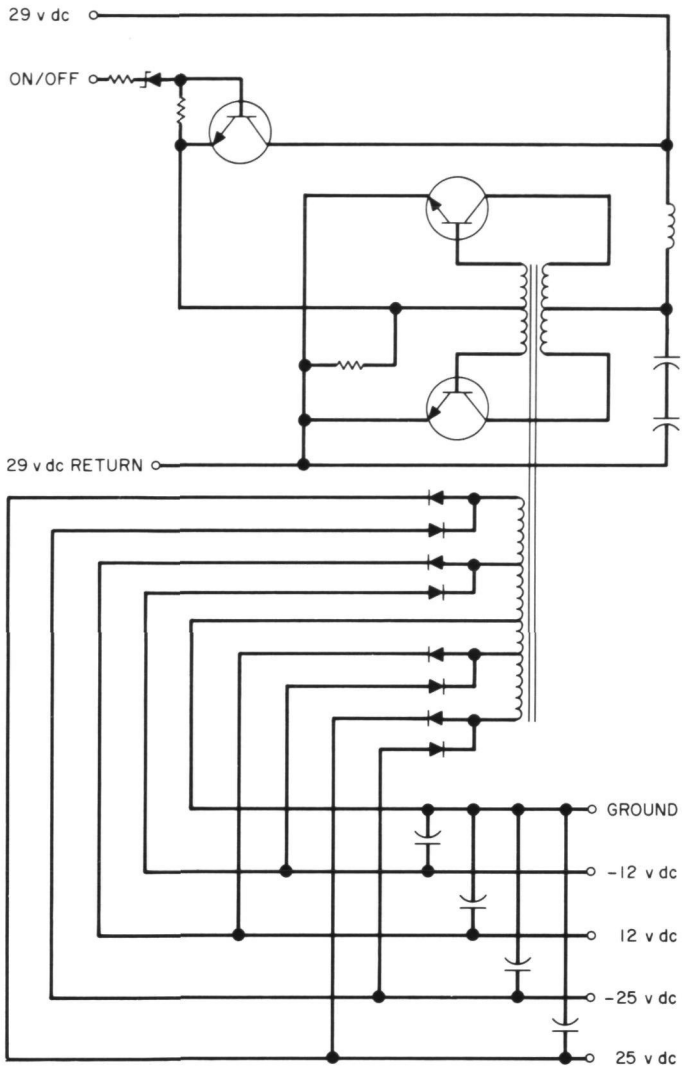


**Fig. 15. Electronic conversion unit**

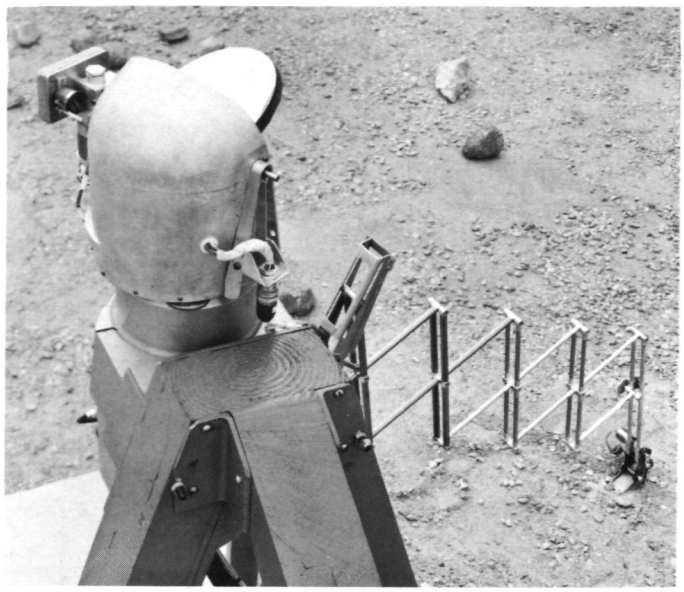

**Fig. 16. TV camera and surface sampler**

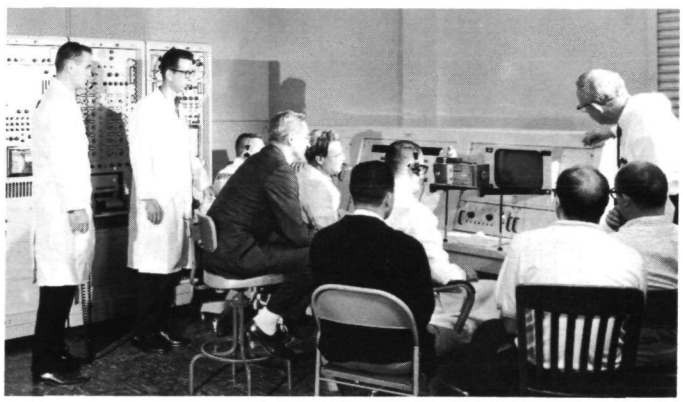

**Fig. 17. TV/CDC demonstration**

CEC pending a decision concerning the *Surveyor* A-21 payload. CEC was subsequently directed to complete a recorder using an existing preprototype model of the tape transport with electronic circuitry in accordance with T-21 hardware except that the circuitry is dip-sealed and the case is not sealed. This model is suitable for testing in the event that the tape recorder is included on the spacecraft at a later date. This model has been completed and was demonstrated on November 15. Figure 21 shows the recorder with signals being reproduced on three of the analog channels. Further development effort has been suspended.

### 7. Ionization Chamber Assembly

The ionization chamber assembly development and fabrication contract at Electro-Optical Systems, Inc., was stopped on August 1, 1962, because of the impending *Surveyor* reprogramming and payload redefinition. The program was reactivated on November 5, but at a reduced level of effort.

Because a substantial amount of development had been accomplished, it was considered economically sound to culminate the work in operating prototypes capable of satisfactorily completing prototype acceptance tests. The revised program reduced the number of prototypes from five to two, eliminated the type approval test effort, eliminated the requirement for flight articles at this time, but maintained the level of engineering development envisioned at program inception in February, 1962. The present plan is based on type approval test effort being conducted by JPL.

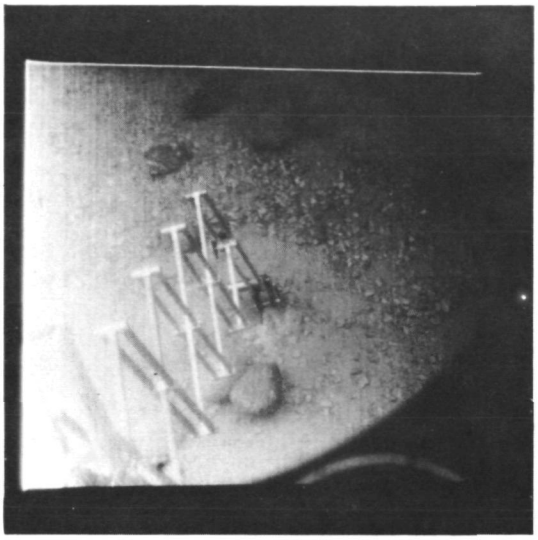

(a) Wide-angle lens at 6 ft focal distance

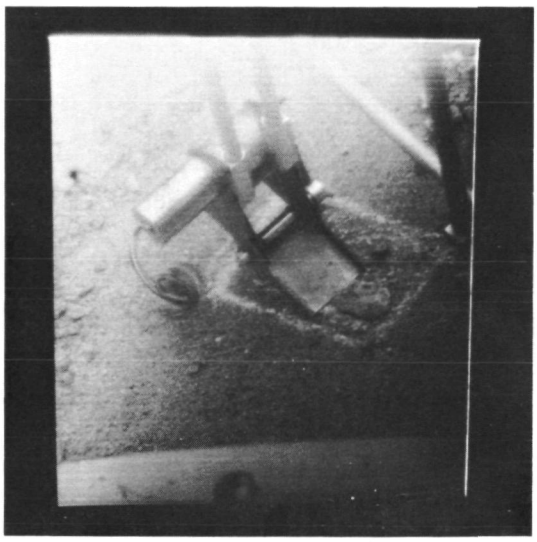

(b) Narrow-angle lens at 6 ft 3 in. focal distance

**Fig. 18. Television views of surface sampler**

A number of technical changes were introduced in the development concurrent with the resumption of the effort:

(1) Inclusion of a thermostat to regulate the nighttime operating temperature of the ion chamber preamplifier. Provisions for bypassing the thermostat with ground commands are also included.

(2) Clarification of the in-process tests, functional tests, and criteria for acceptance-rejection.

(3) Reduction of the pressure level applied during in-process testing of the ion chamber welded sphere.

Several development tests remain to be completed:

(1) Electronic circuit boards have been successfully cycled and operated throughout the temperature range of −50 to 125° C. The minimum survival temperature remains to be determined from actual tests.

(2) Twelve quartz electronic charge collector rods (integrating assemblies) have been successfully vibrated at levels above those to be experienced in actual flights. Each of these rods has further been vibrated to failure, which occurred at input loads between 15 and 37 *g*. Twenty-four more collector rods will be tested in similar fashion and additional rods will be tested to determine the failure level and failure modes under shock loadings.

(3) Welded sphere and neck subassemblies have been successfully vibrated. Four additional units will be used in vibration tests, shock tests, and subsequently burst tests.

The development program, fabrication, and acceptance testing of two prototypes will be completed in the early part of February, 1963.

### 8. Mechanisms for Scientific Payload

*a. Sample processor.* The sample processor consists of a hopper and measuring device into which coarse lunar soil will be fed by the surface sampler, a pulverizer which will grind up this coarse lunar material for the experiments, and a distribution system which will transport the ground-up material to the alpha scattering experiment and the X-ray diffractometer. Provisions are also made to transport standard Earth soil samples to these instruments.

Primarily because of design changes in the X-ray diffractometer, made during the period when no Hughes effort was being expended on the sample processor, there is a requirement now to modify the previous processor design. This design modification is progressing with the preparation of design layouts. A significant improvement from the preceding design is the use of a simplified sample measure and feed. The double arm linkage with four motors has been replaced by a single motor-driven rotary device. This is possible because the sample recovery and feed requirements have been simplified with the removal of the subsurface sampler and the gas chromatograph from the payload. Detail drawings of the pulverizer for the engineering model have been completed and parts are being fabricated. Electrical wiring and schematic diagrams and a preliminary outline and mounting drawing have been completed.

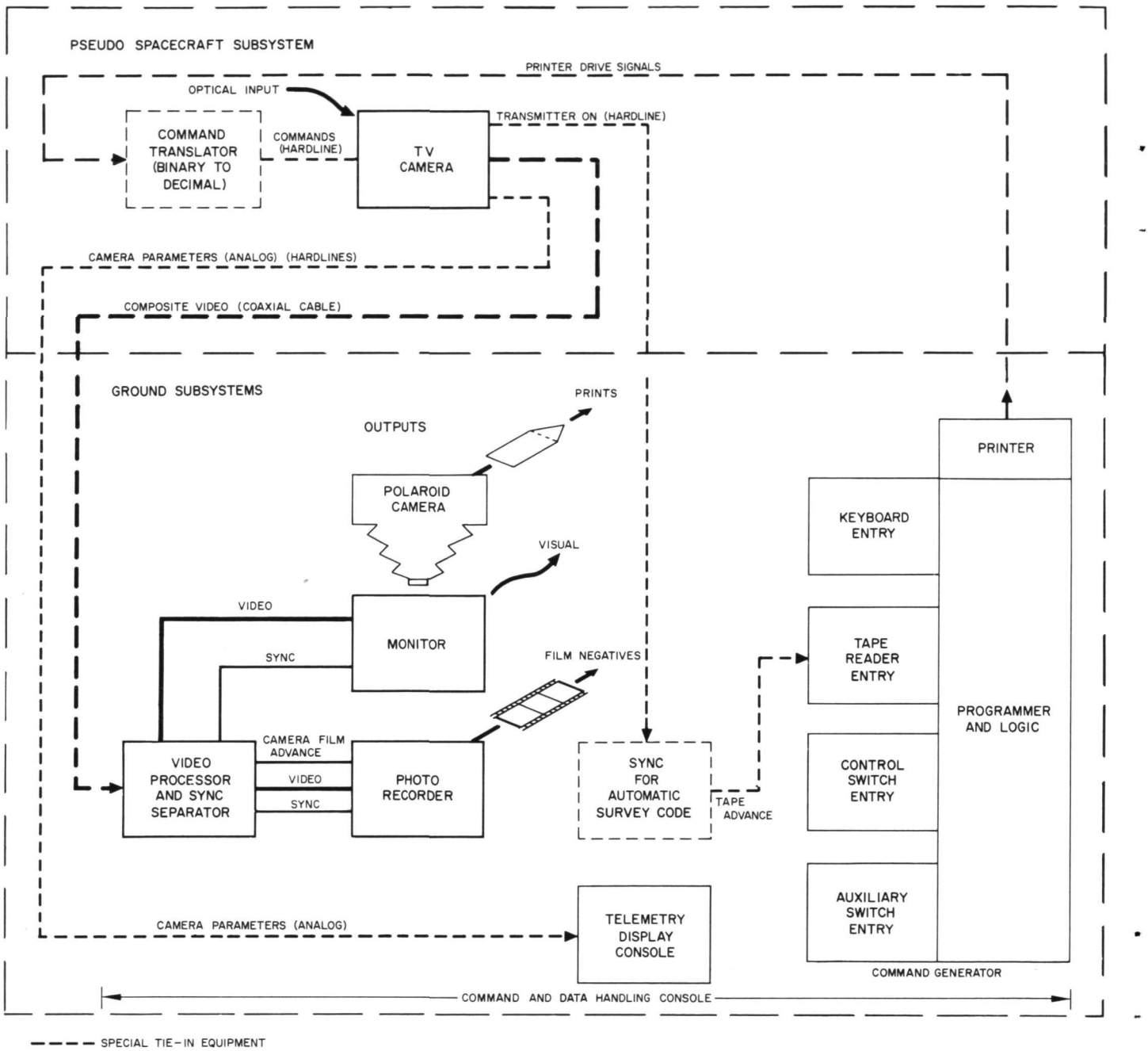


**Fig. 19. Demonstration TV system**

*b. Surface sampler.* The surface sampler is a device capable of scraping, digging, manipulating, and collecting lunar surface material near the spacecraft. A motor-driven clamshell collection device is attached to one end of a pantograph extension arm. The other end is mounted on a horizontally and vertically hinged base attached to the spacecraft frame. Electric motors are used to move the arm in azimuth, elevation, and retraction.

The breadboard unit has been reworked and is in operation (Figure 22). The original extension drive screw was replaced by a coil tension spring to extend the arm and a winch drive to retract the arm, for more efficient operation. In addition, the movable portion of the clamshell was slightly modified to better retain the collected sample. Investigatory tests are being conducted to determine the capabilities of the breadboard unit in various soil models.

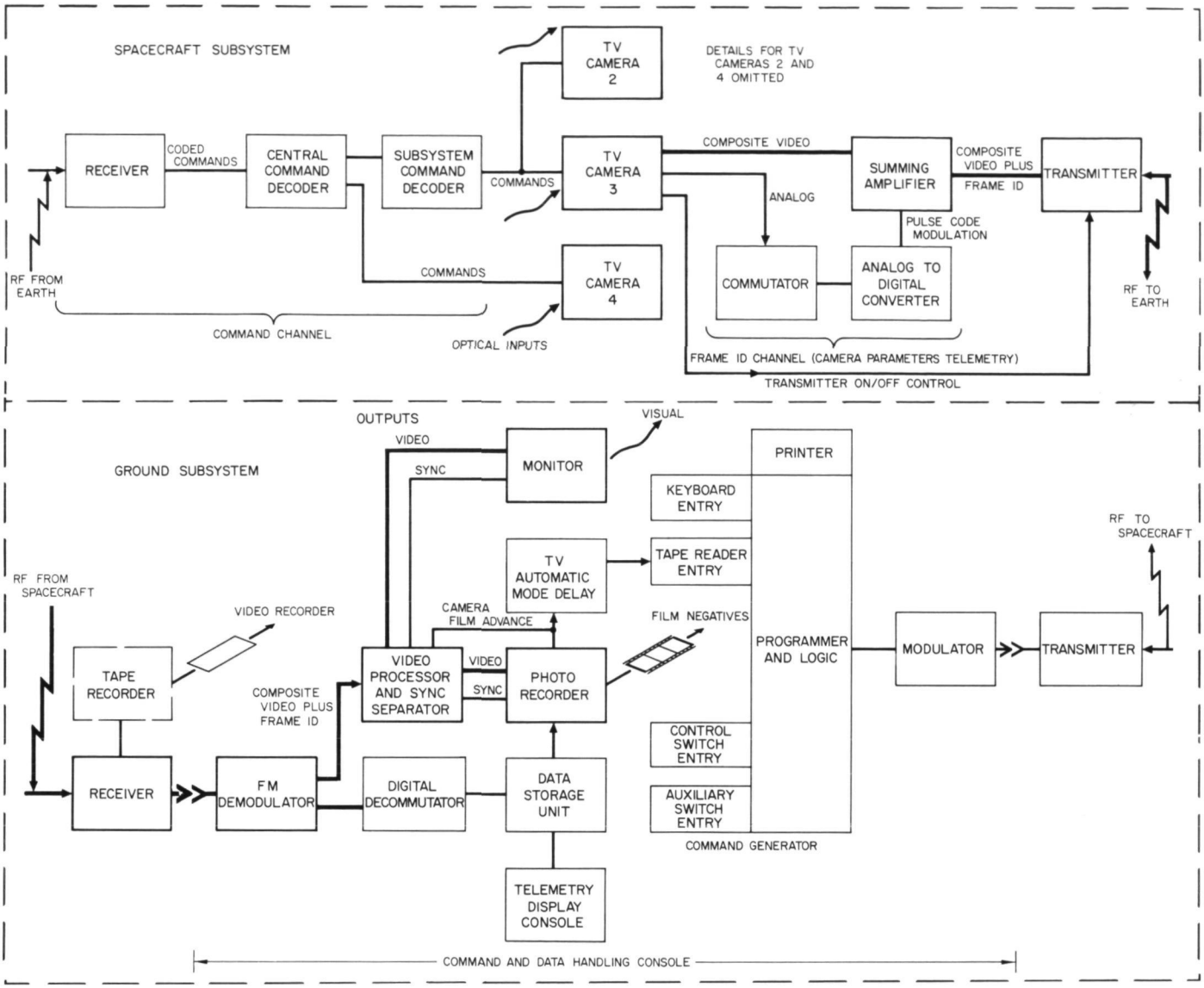


**Fig. 20. Spacecraft TV system**

Design layouts and detail drawings are being prepared for the engineering model. Studies have been conducted for proposed changes in surface sampler operating requirements. Many motor vendors have been contacted in advance of a decision on the type of prime mover to be used. If at all feasible, the same motors as used for the sample processor will be selected.

*c. TV mirror units.* The TV mirror units provide azimuth and elevation scanning for the television system. The initial prototype units have been assembled, functionally checked, and delivered to the television for the T-21 vehicle. The engineering model of the protoype configuration has been reassembled and again subjected to vibration tests.

As before, no problems were experienced in the thrust axis sweeps. However, during vibration in the lateral axis perpendicular to the elevation pilot axis, large amplitudes of mirror movement were noted. This movement is a result of the mirror unbalance about the elevation pivot axis; at mirror resonant frequencies this unbalance produces loads resulting in stress levels above the yield point of the aluminum worm wheel in the elevation drive mechanism.

No attempt had been made previously to balance the mirror about the elevation pivot axis since unbalance

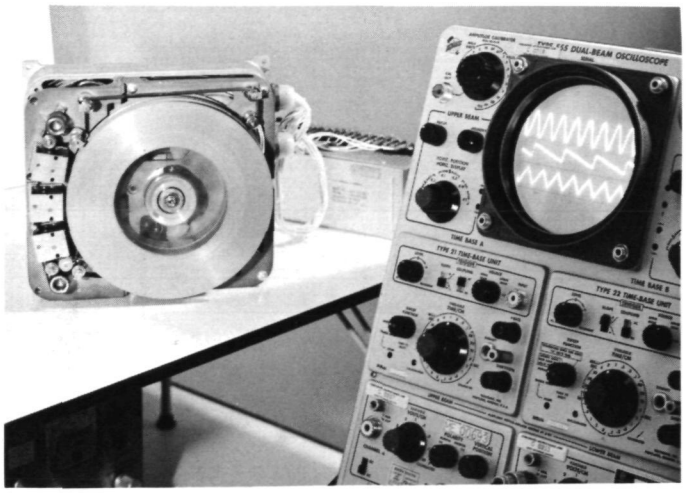

**Fig. 21. Tape recorder demonstration**

provides a unidirectional loading in this axis that favorably influences the stepping accuracy by tending to remove backlash. However, as a result of vibration tests, the lightening hole pattern on the backside of the beryllium mirror has been changed and the mirror itself reworked to provide a balanced assembly. This results in a net weight increase in the mirror of 0.07 lb, approximately one-third the weight which would be required for an explosive latch assembly to lock the mirror during vibration. The engineering model is being reassembled with the balanced mirror and will undergo further vibration tests.

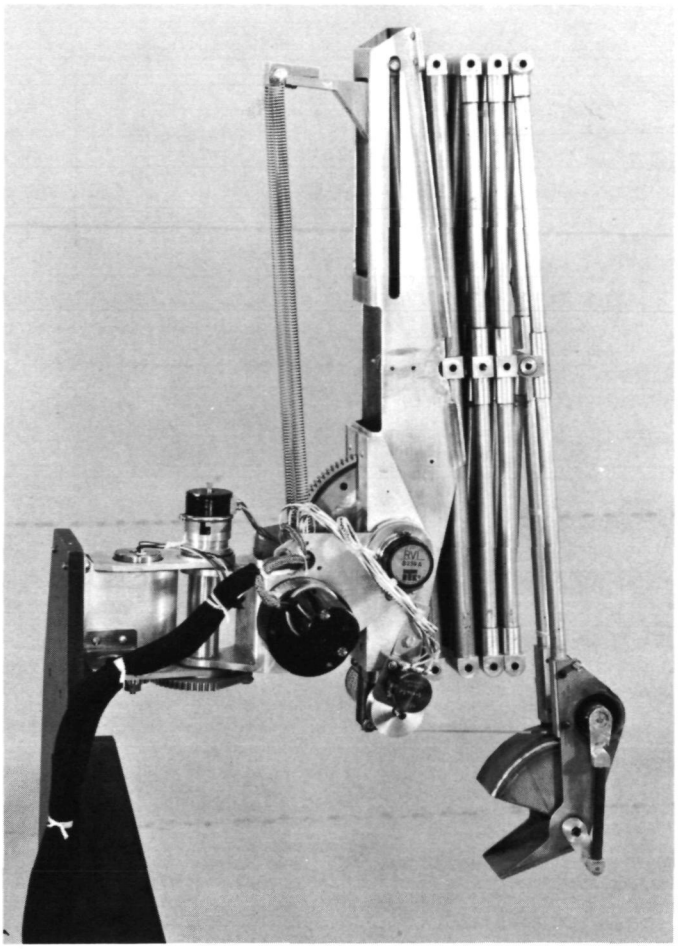

**Fig. 22. Reworked surface sampler breadboard**

# C. System Analysis

## 1. Launch Window Considerations for Direct Ascent Trajectories

At the request of JPL, a brief study was made concerning the feasibility from the launch window point of view of using direct ascent trajectories for the *Surveyor* mission. Certain hardware and system simplification may be made for the *Centaur* vehicle if such a boosting concept is utilized, although it appears that no substantial payload advantage will result from it.

In order to study this problem, it is important to recognize a few essential factors concerning the entire launch-to-impact trajectory in the case of direct ascent:

(1) The total central angle between the launch site, Atlantic Missile Range, and the Moon remains strictly a function of the geometry described by the following equation:

$$\sin \delta_m = \sin \lambda \cos \theta_s + \cos \lambda \sin \theta_s \cos \sigma_L$$

where

$\delta_m$ = declination of pseudo-asymptote $\approx$ lunar declination

$\lambda$ = latitude of AMR

$\sigma_L$ = launch azimuth

$\theta_s$ = central angle between launch site and pseudo-asymptote $\approx$ central angle between launch site and Moon

(2) For a given flight time or energy level for the transit trajectory, the true anomaly of the pseudo-asymptote is essentially constant. In other words, the central angle between the perigee of the outgoing Earth conic and the Moon is essentially constant. This angle is defined as $\theta_s'$.

(3) The boost arc for injection into the Earth conic must remain essentially constant in order to retain payload capability. This arc angle is designated $\theta_b$.

Since the $\theta_b + \theta_s'$ generally does not equal $\theta_s$ for an arbitrary geometry, injection or thrust cutoff of the booster cannot in general be at the perigee point. In fact, in order to have any launch window at all, the true anomaly $\theta_i$ of the injection point must be a continuously adjustable variable obeying the relation:

$$\theta_i = \theta_b + \theta_s' - \theta_s$$

which will vary with the geometry as $\theta_s$ varies.

The *Centaur* vehicle can be designed to inject at different values of $\theta_i$ by shaping the boost trajectories accordingly. However, payload consideration again dictates that the permissible variation in $\theta_i$ be kept within a reasonably small range near zero.

For the purpose of the study, the following values have been assumed:

$$\theta_b \approx 29 \text{ deg}$$

$$\theta_s' \cong 170 \text{ deg}$$

These values are considered reasonable for the present *Centaur* design and the 66-hr type transit trajectory adopted.

Since $|\theta_i|$ must be a small value, it is found that for the range of launch azimuth to be considered (90 to 114 deg E), only high negative values of $\delta_m$ yield possible launchings. Figure 23 is a plot of launch azimuth versus lunar declination for different values of the total central angle $\theta_s$. At $\theta_s = 199$ deg, the true anomaly of injection is zero; at $\theta_s = 205$ and 193 deg, it is $-6$ and 6 deg, respectively. The implication of this graph is that for a practical lower bound on $\theta_i$, say $-6$ deg, lunar declinations more positive (northerly) than $-16$ deg will give no launch possibility at all.

The launch time duration for a particular range of $\theta_s$ and any specific lunar declination was examined. In Figure 24, the ordinate is the launch time interval reckoned from 90 deg azimuth to any particular azimuth greater than 90 deg, and the abscissa is the lunar declination. The solid curves are the launch time intervals for fixed upper limits in $\sigma_L$, obtained through computer means. The curves of Figure 23 may be transcribed as loci of constant $\theta_s$ shown as dotted curves in Figure 24. Thus, supposing that a certain launch date has a corresponding impact date $\delta_m$ of $-22$ deg and that the limits on $\theta_s$ are 205 and 193 deg corresponding to $\theta_i$ of $-6$ and 6 deg, respectively, the minimum launch azimuth would be 99 deg, corresponding to $\theta_s = 205$ deg. The maximum azimuth remains at 114 deg because even at this azimuth

the value of $\theta_s$ is still somewhat larger than 193 deg. The net launch time interval, represented by the difference in the ordinates, is 50 min.

Figure 25 shows the launch interval versus lunar declination at impact for the assumption stated. It is seen that the maximum interval is about 55 min. Table 8 shows the allowable lunar declination limit as a function of the minimum launch interval or window desired.

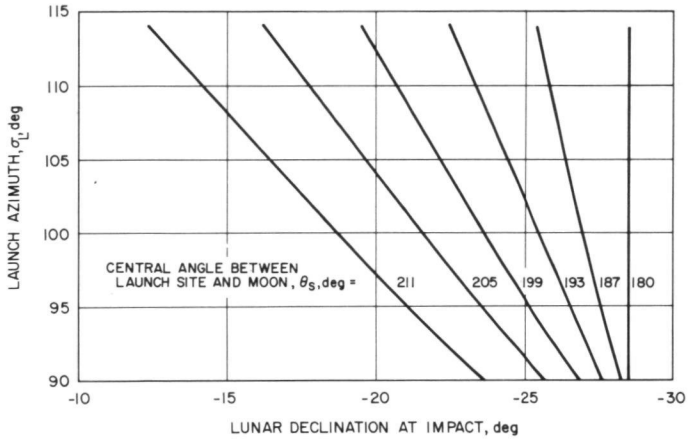


**Fig. 23. Launch azimuth vs lunar declination at impact**

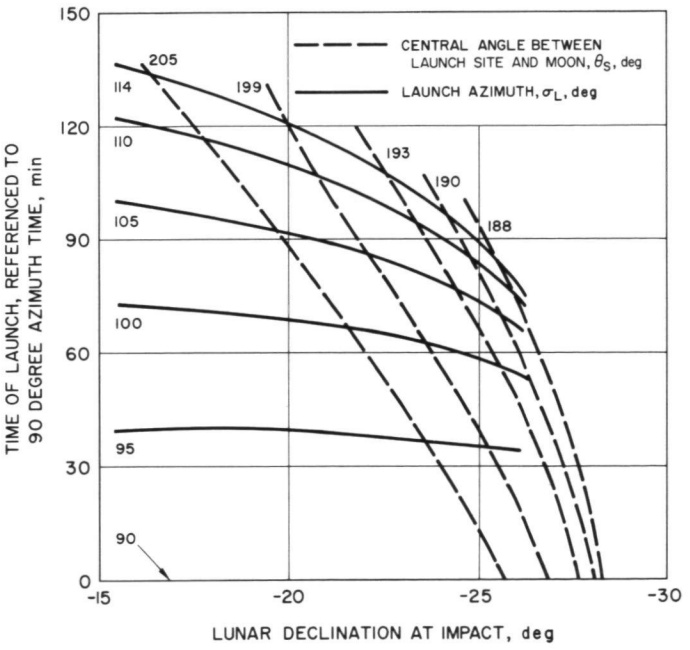


**Fig. 24. Universal launch window curves**
Launch site latitude = 28.47 deg

**Table 8. Minimum launch window vs lunar declination**

(193 deg $\leq \theta_s \leq$ 205 deg, 90 deg $\leq \sigma_L \leq$ 114 deg)

| Minimum launch window, min | Lunar declination limits, deg |
|---|---|
| 50 | −22.0 to −25.9 |
| 40 | −20.8 to −26.3 |
| 30 | −19.6 to −26.7 |
| 20 | −18.5 to −27.1 |

The lunar ephemeris tables for the time period of interest, e.g., January 1964 to December 1965, are correlated with Table 8 and the desired lighting condition to check the impact dates offering suitable windows. The lighting condition is determined by the phase of the Moon as well as the landing site. Thus, if a particular landing site is chosen — for instance, that corresponding to a normal incidence approach on a 66-hr trajectory (approximately 45°W longitude) — it may be found that some or all of those days in a particular month with favorable declination are ruled out because of either complete darkness or insufficient postlanding sunlight duration. This condition is alleviated somewhat if the landing site is allowed to "follow the Sun" within the landing incidence capability of the spacecraft system. Table 9 is a summary of the results of the study for 1964 and 1965.

The feasibility of this concept depends to a considerable extent on the question of the minimum daily launch window required for a substantial probability of getting off a shot. In addition, there is the question of arranging

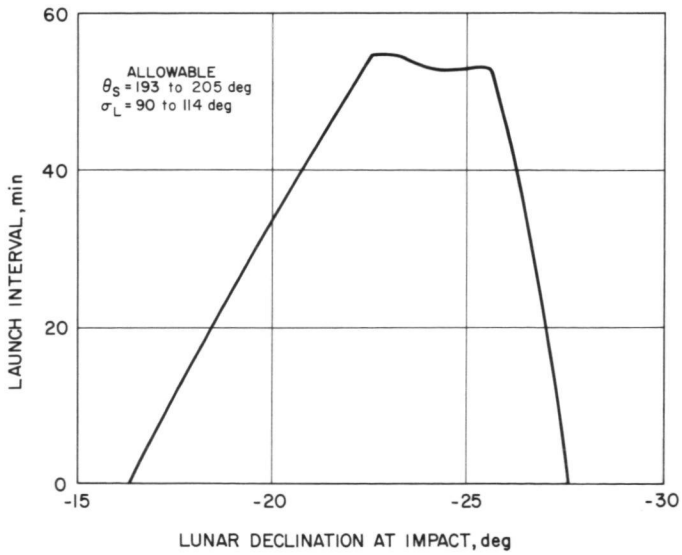


**Fig. 25. Launch interval vs declination at impact**

**Table 9. Launch opportunities for direct ascent[a]**

| Window / Month | (A) "Follow the Sun" in selecting landing site: Postlanding sunlight duration > 150 hr | | | | | | | | (B) Landing at 45° W longitude: Postlanding sunlight duration > 100 hr | | | | | | | |
|---|---|---|---|---|---|---|---|---|---|---|---|---|---|---|---|---|
| | > 20 min | | > 30 min | | > 40 min | | > 50 min | | > 20 min | | > 30 min | | > 40 min | | > 50 min | |
| | (A) | (B) | (A) | (B) | (A) | (B) | (A) | (B) | (A) | (B) | (A) | (B) | (A) | (B) | (A) | (B) |
| 1964 JAN | 0 | 0 | 0 | 0 | 0 | 0 | 0 | 0 | 0 | 0 | 0 | 0 | 0 | 0 | 0 | 0 |
| FEB | 1 | 0 | 0 | 0 | 0 | 0 | 0 | 0 | 3 | 0 | 2 | 0 | 1 | 0 | 0 | 0 |
| MAR | 2 | 0 | 2 | 0 | 1 | 0 | 1 | 0 | 4 | 1 | 4 | 1 | 3 | 0 | 2 | 0 |
| APR | 4 | 1 | 4 | 1 | 3 | 0 | 3 | 0 | 6 | 3 | 6 | 3 | 5 | 2 | 5 | 2 |
| MAY | 6 | 4 | 5 | 3 | 5 | 3 | 3 | 2 | 6 | 6 | 5 | 5 | 5 | 5 | 3 | 3 |
| JUN | 6 | 5 | 5 | 5 | 5 | 4 | 4 | 4 | 6 | 6 | 5 | 5 | 5 | 5 | 4 | 4 |
| JUL | 6 | 6 | 6 | 6 | 4 | 4 | 4 | 4 | 6 | 6 | 6 | 6 | 4 | 4 | 4 | 4 |
| AUG | 6 | 3 | 5 | 3 | 5 | 3 | 3 | 2 | 6 | 3 | 5 | 3 | 5 | 3 | 3 | 2 |
| SEP | 6 | 2 | 6 | 2 | 4 | 1 | 4 | 1 | 6 | 2 | 6 | 2 | 4 | 1 | 4 | 1 |
| OCT | 4 | 0 | 4 | 0 | 4 | 0 | 3 | 0 | 4 | 0 | 4 | 0 | 4 | 0 | 3 | 0 |
| NOV | 2 | 0 | 2 | 0 | 1 | 0 | 1 | 0 | 2 | 0 | 2 | 0 | 1 | 0 | 1 | 0 |
| DEC | 0 | 0 | 0 | 0 | 0 | 0 | 0 | 0 | 0 | 0 | 0 | 0 | 0 | 0 | 0 | 0 |
| 1965 JAN | 0 | 0 | 0 | 0 | 0 | 0 | 0 | 0 | 0 | 0 | 0 | 0 | 0 | 0 | 0 | 0 |
| FEB | 0 | 0 | 0 | 0 | 0 | 0 | 0 | 0 | 1 | 0 | 0 | 0 | 0 | 0 | 0 | 0 |
| MAR | 3 | 0 | 3 | 0 | 2 | 0 | 2 | 0 | 5 | 2 | 5 | 2 | 3 | 1 | 3 | 1 |
| APR | 5 | 2 | 4 | 1 | 4 | 1 | 3 | 0 | 6 | 3 | 6 | 3 | 6 | 3 | 5 | 2 |
| MAY | 6 | 3 | 6 | 3 | 5 | 2 | 5 | 2 | 7 | 5 | 7 | 5 | 6 | 4 | 5 | 3 |
| JUN | 7 | 6 | 6 | 5 | 5 | 5 | 5 | 5 | 7 | 7 | 6 | 6 | 5 | 5 | 5 | 5 |
| JUL | 6 | 6 | 6 | 6 | 6 | 6 | 4 | 4 | 6 | 6 | 6 | 6 | 6 | 6 | 4 | 4 |
| AUG | 7 | 5 | 6 | 4 | 5 | 4 | 5 | 4 | 7 | 5 | 6 | 4 | 5 | 4 | 5 | 4 |
| SEP | 7 | 3 | 7 | 3 | 5 | 2 | 4 | 1 | 7 | 3 | 7 | 3 | 5 | 2 | 4 | 1 |
| OCT | 5 | 0 | 5 | 0 | 5 | 0 | 4 | 0 | 5 | 0 | 5 | 0 | 5 | 0 | 4 | 0 |
| NOV | 3 | 0 | 3 | 0 | 2 | 0 | 2 | 0 | 3 | 0 | 3 | 0 | 2 | 0 | 2 | 0 |
| DEC | 0 | 0 | 0 | 0 | 0 | 0 | 0 | 0 | 0 | 0 | 0 | 0 | 0 | 0 | 0 | 0 |

[a]Indicated launch opportunities are numbers of consecutive days in which windows exceed specified values.

favorable launch schedules. These questions must be considered in conjunction with the results of this study, although it is clear that the direct ascent trajectory concept compares very unfavorably with the parking orbit concept in the operational sense.

## 2. *Alternate Vernier Propulsion Systems*

As part of a continuing study of advanced alternative vernier propulsion systems, an analysis has been made of the payload benefits to be gained from one such system, presently under development at Space Technology Laboratories, Inc. This system is capable of a throttling ratio as high as 10:1 and has a specific impulse of 311 sec. Several combinations of maximum and minimum thrust levels were chosen for comparison with the present vernier system being developed by the Reaction Motors Division of Thiokol Chemical Corporation. The characteristics of the systems considered are shown in Table 10, along with the dry landed weight.

The results show that STL engines with maximum and minimum thrust of 150 and 20 lb provide 21 lb more payload capability than the present RMD vernier engines. Increasing the maximum thrust level of the STL engines to 200 lb provides an additional increase of 14 lb. Further increase in the thrust level without changing the throttling ratio is of no benefit.

The specific impulse of the STL engines was taken as 311 sec, independent of thrust, while that of the RMD system depends on thrust as shown in Figure 26, based on the latest data.

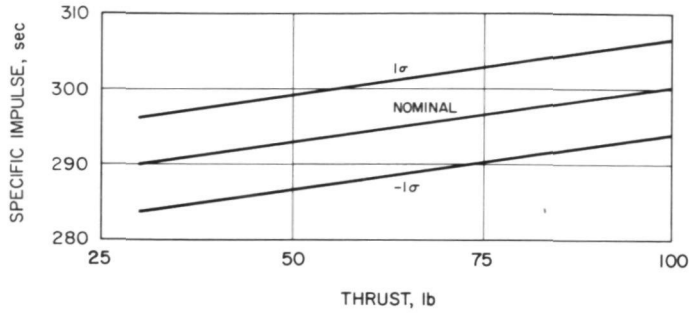


**Fig. 26. Vernier propulsion system performance**

**Table 10. Vernier system characteristics**

| Characteristic | Current RMD | Engine with thrust range, lb | | | |
|---|---|---|---|---|---|
| | | STL | | | |
| | | 20-150 | 20-200 | 25-250 | 30-300 |
| Maximum thrust, lb | 104 | 150 | 200 | 250 | 300 |
| Minimum thrust, lb | 30 | 20 | 20 | 25 | 30 |
| Specific impulse, sec | 290-301 | 311 | 311 | 311 | 311 |
| Maximum thrust acceleration, g | 2.35 | 3.43 | 4.58 | 5.72 | 6.87 |
| Minimum thrust acceleration, g | 0.96 | 0.59 | 0.57 | 0.72 | 0.88 |
| Dry landed weight, lb | 590 | 611 | 623 | 622 | 624 |

As in previous vernier system designs, the maximum and minimum acceleration levels were determined from the maximum and minimum thrust levels, modified by an 11% safety factor, and the greatest or least weights occurring during the maximum or minimum thrust phases. The maximum weight occurs for burnout on the maximum acceleration curve with no midcourse fuel consumed and maximum unbraked impact velocity. The minimum weight occurring during the minimum thrust phase corresponds to minimum unbraked impact velocity, maximum midcourse fuel consumed and main retro burnout on the 99% dispersion ellipse in the region of greatest altitude and least velocity. For this case, the minimum weight occurs at the end of the minimum thrust phase, thus requiring an iteration procedure for the determination of the minimum acceleration.

For purposes of this study, the main retro dispersion ellipses were assumed to be unchanged from previous studies, but the specific impulse of the main retro was reduced from 294 sec to the estimated value of 288 sec. (More recent data indicate the somewhat higher value of 290 sec may be achieved.) The ellipses were located sufficiently above the maximum acceleration parabola to

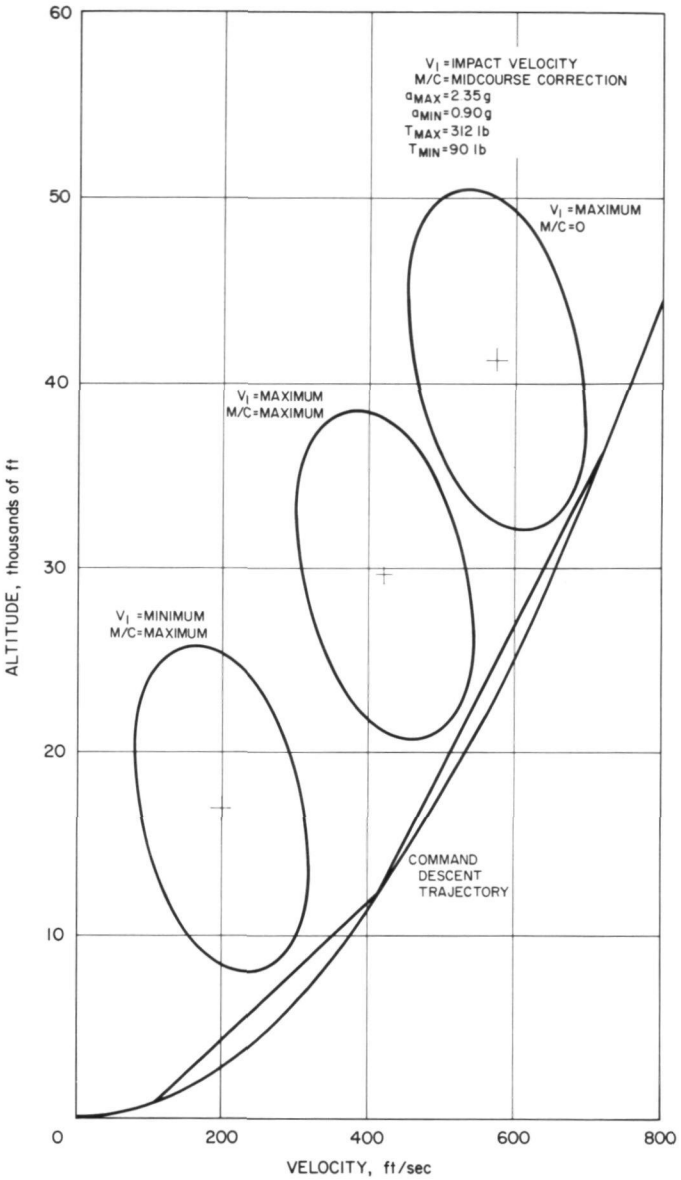


**(a) RMD engine (30 to 104 lb thrust)**

**Fig. 27. Burnout ellipses**

ensure sufficient time for attitude reorientation after a 45 deg burnout angle at the minimum altitude. Figure 27 shows the ellipses as located in the altitude-velocity plane.

The landed dry weight is determined from the maximum fuel consumption based on descent from the critical point on the dispersion ellipse corresponding to maximum impact velocity. For the RMD engines and the high-thrust STL 30-300 engines, the case of minimum impact velocity actually results in a greater fuel consumption. However, in these cases the injected weight capability is greater than in the maximum impact velocity

case, and it will be possible to ballast the spacecraft with additional vernier fuel, thus increasing the main retro burnout velocity to the point where this condition is no longer critical.

Table 11 shows the complete weight breakdown for the five systems, including the nominal fuel consumption (maximum midcourse correction, maximum impact velocity) and the amount required for dispersions. The dispersions include (1) the difference between vernier fuel required for the nominal and 99% burnout conditions, (2) a 2.6-lb variation in the touchdown phase, (3) 3.0-lb vernier dispersion in the main retro-phase, and (4) 9.1-lb required for vernier engine performance variations such as specific impulse. Since better information was not available for the STL engines, Items 2, 3, and 4 were taken as the currently estimated RMD values. These sources of dispersion are root-sum-squared to give the values listed in Table 11.

### 3. Surveyor Television Performance

Some development tests have been performed on the engineering development TV system to check performance specifications. Test data and performance estimates are presented which are derived from these tests. Limited data are available on the flight configuration camera, and there has not been time to reflect spacecraft configuration details which are now becoming firmed up as a result of the recent payload definition. Thus the performance estimates presented must be regarded as preliminary and quite approximate in many cases. Summary tables are included which compare present performance with that specified in the documents which established the design requirements.

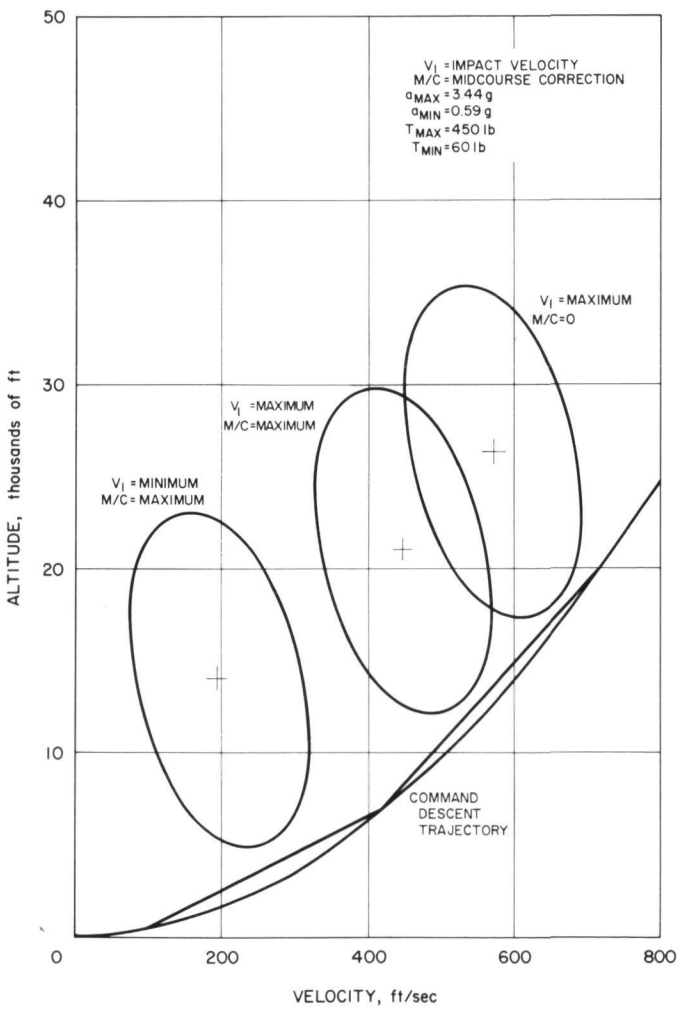


(b) STL engine (20 to 150 lb thrust)

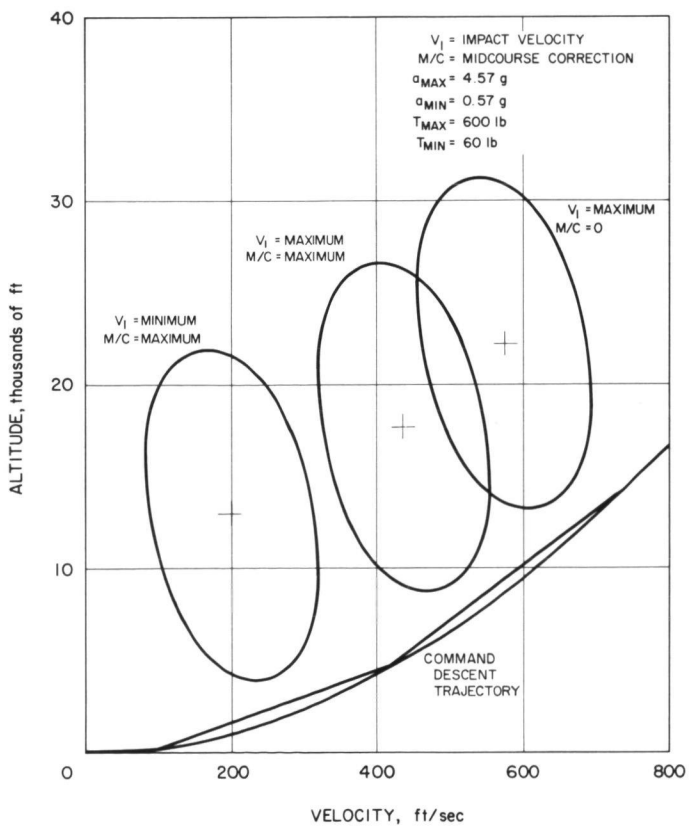


(c) STL engine (20 to 200 lb thrust)

**Fig. 27. Burnout ellipses (continued)**

*a. Resolution and signal-to-noise ratio.* Horizontal square-wave amplitude response data taken recently from a breadboard camera are shown in Figure 28 and summarized in Figure 29. The test chart employed in these measurements is shown in Figure 30. The first trace in Figure 30 shows the video voltage for a single horizontal sweep across the chart. Traces 2, 3, and 4 are expansions of the central portion of the sweep which permit better estimation of the amplitude response at the three line frequencies employed. The fourth trace shows the black-level noise at increased sensitivity. The rms noise was estimated from this and similar traces. The data were obtained by passing the camera output through a sharp cutoff low pass filter of the type used in the ground station equipment and do not represent the signal as actually transmitted.

It is important to note that a horizontal response as shown in Figure 28 is meaningless without a statement of the corresponding signal-to-noise ratio since, without noise, an indefinite amount of electronic peaking or aperture correction could be used to improve the response. The signal-to-noise ratio as defined here, i.e. peak-to-rms, is one-half the black-level to white-level

**Table 11. Weight breakdown**

| Item | RMD 30-104 | Engine and thrust range, lb STL 20-150 | STL 20-200 | STL 25-250 | STL 30-300 |
|---|---|---|---|---|---|
| Injected weight | 2100.0 | 2100.0 | 2100.0 | 2100.0 | 2100.0 |
| Marker radar | 8.8 | 8.8 | 8.8 | 8.8 | 8.8 |
| Main retro | 1345.0 | 1345.5 | 1345.5 | 1345.5 | 1345.5 |
| Propellant | 1200.5 | 1201.0 | 1201.0 | 1201.0 | 1201.0 |
| Case | 144.5 | 144.5 | 144.5 | 144.5 | 144.5 |
| Vernier fuel | 148.9 | 127.9 | 116.2 | 116.5 | 115.2 |
| Midcourse correction | 22.0 | 21.0 | 21.0 | 21.0 | 21.0 |
| Main retro descent | 29.3 | 27.8 | 27.8 | 27.8 | 27.8 |
| Case separation | 9.9 | 9.4 | 9.4 | 9.4 | 9.4 |
| Nominal minimum thrust | 14.2 | 5.1 | 5.0 | 6.5 | 8.4 |
| Nominal maximum thrust | 51.5 | 44.4 | 32.6 | 31.4 | 28.3 |
| Touchdown | 1.9 | 1.8 | 1.8 | 1.8 | 1.8 |
| Dispersions | 11.9 | 12.4 | 12.6 | 12.6 | 12.5 |
| Outage | 4.2 | 2.0 | 2.0 | 2.0 | 2.0 |
| Allowance | 4.0 | 4.0 | 4.0 | 4.0 | 4.0 |
| Nitrogen | 4.5 | 4.5 | 4.5 | 4.5 | 4.5 |
| Helium | 2.5 | 2.5 | 2.5 | 2.5 | 2.5 |
| Dry landed weight | 590.3 | 610.8 | 622.5 | 622.2 | 623.5 |

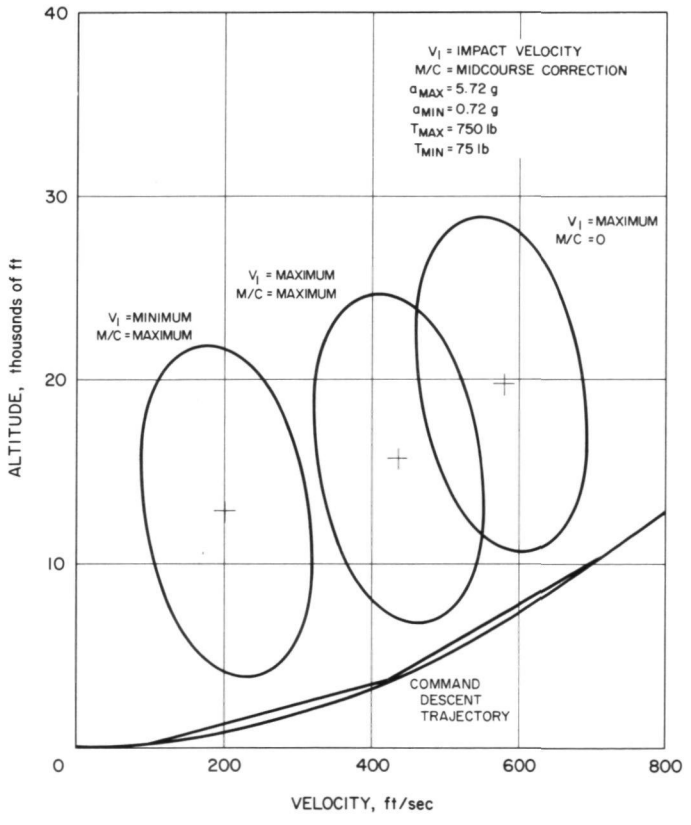


(d) STL engine (25 to 250 lb thrust)

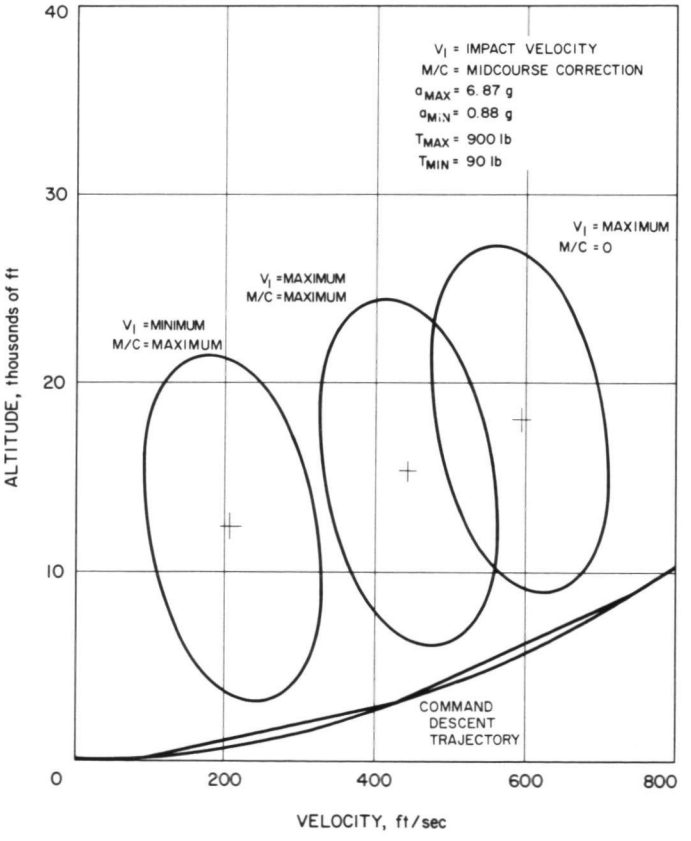


(e) STL engine (30 to 300 lb thrust)

**Fig. 27. Burnout ellipses (continued)**

voltage difference divided by the rms noise. The sometimes used peak-to-peak-to-rms ratio is 6 db higher, or 30 db in this case.

The data presented are subject to qualification by several factors: (1) difficulty of precise estimation from available records, (2) variation in vidicon performance, and (3) superiority of breadboard camera lens response to the flight configuration variable focal-length lens for most lens settings. These factors are illustrated in Figure 31 which compares square-wave response for two RCA tubes (one from Figure 29), a Westinghouse tube, and a theoretical sine-wave response for the Bell and Howell lens. While a potential degradation caused by this lens is apparent, the actual degradation in the flight configuration will have to be determined in further tests. The RCA tube has been selected for the T-21 cameras. However, the Westinghouse tube has some advantages and is still under consideration for later cameras.

Estimated response in the vertical direction is presented in Figure 32. Measurement of vertical response is somewhat more difficult than horizontal response, since without aperture correction it is considerably lower at the high line frequencies. The results presented here are based on published vidicon data and a spot diagram of the variable focal length lens (same conditions as Figure 31). In order to combine the vidicon square-wave response with the lens sine-wave response and obtain a resultant square-wave response, approximate transformations were employed.

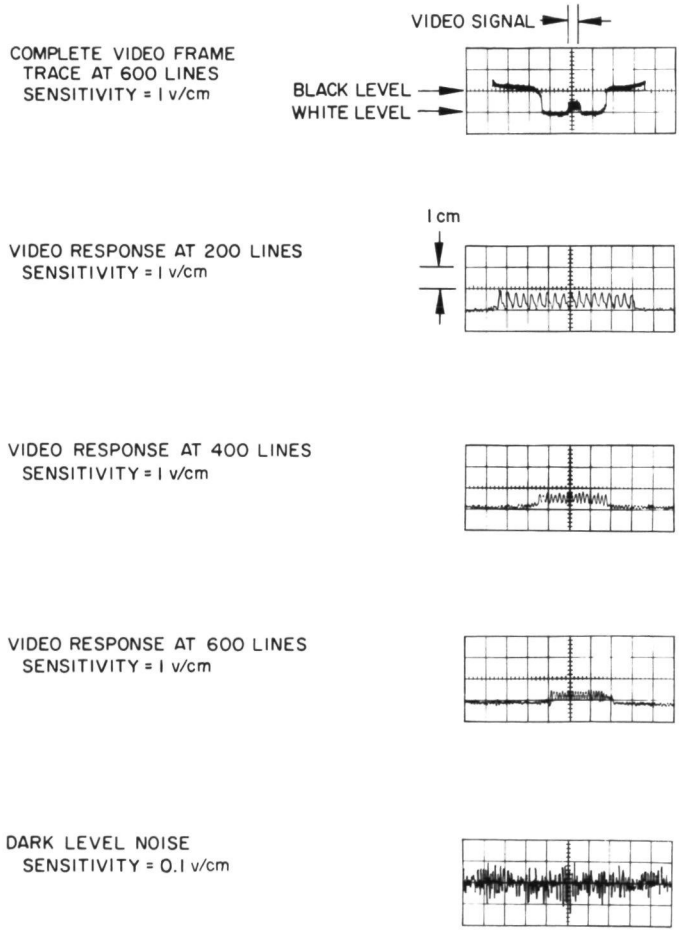


VIDICON = C74098, X-20
SHUTTER = 150 msec
HIGHLIGHT LUMINANCE = 100 ft-LAMBERTS
APERTURE = f/4.5
TARGET VOLTAGE = 26 v
INPUT = SQUARE WAVE

**Fig. 28. Line frequency response and noise level**

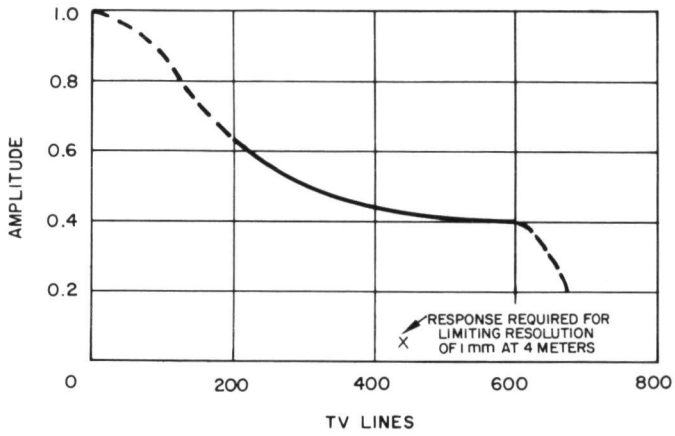


**Fig. 29. Camera square wave amplitude line frequency response**

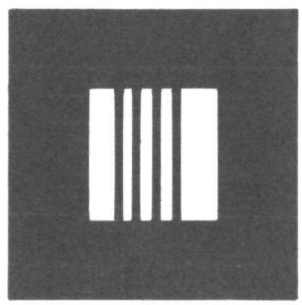

VIDICON = C 74098, X-20
SHUTTER = 150 msec
HIGHLIGHT LUMINANCE = 100 ft-LAMBERTS
APERTURE = f/4.5
SIGNAL-TO-NOISE = 24 db PEAK, TO rms
CONTRAST RATIO = ~60 TO 1

**Fig. 30. Test chart arrangement**

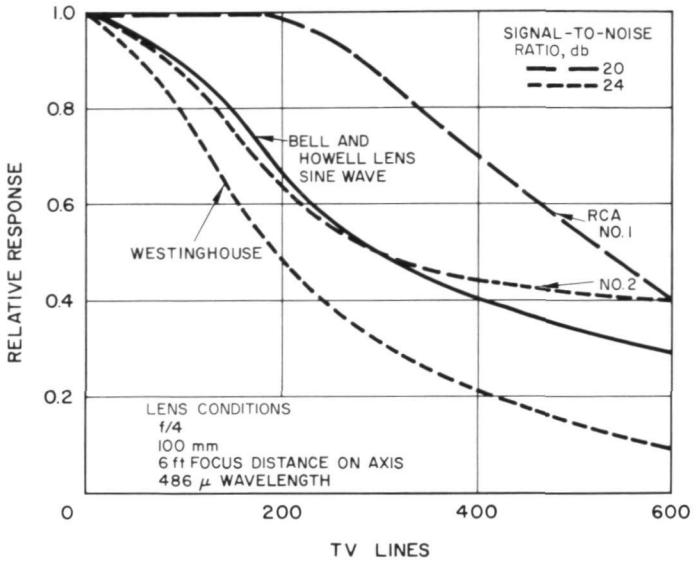


**Fig. 31. Vidicon and lens responses**

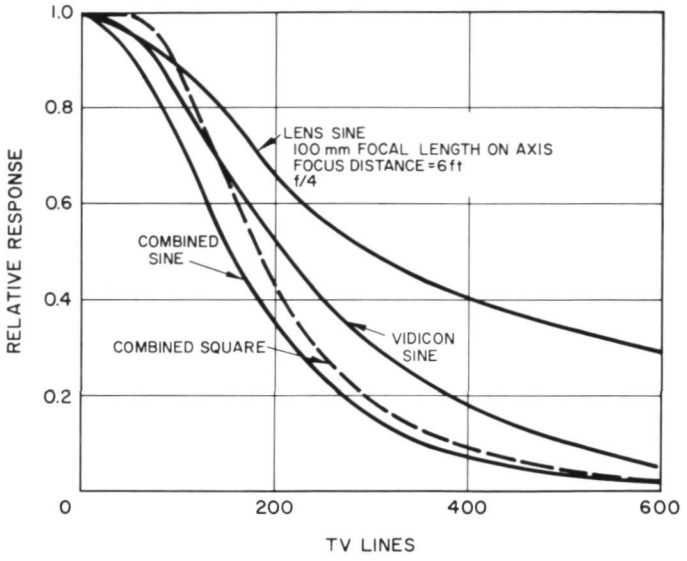


**Fig. 32. Estimated vertical response without raster**

*b. Instrumentation viewing.* The limitations on television viewing of the soil mechanics and surface sampler experiments were determined with the aid of pictures taken with an ordinary camera from the mirror positions of TV Cameras 2 and 3. The instrument locations are shown in Figure 33.

The location of the soil mechanics experiment planned previously (Configuration A in Figure 33) proved to have inadequate viewing from either television camera. It is now planned to locate this instrument as shown in Configuration B with the instrument extended to the point marked Position 3. Position 1 of Configuration B was inadequate, as shown in Figure 34a. The clear view of the instrument as extended to Position 3 is shown in Figure 34b.

In these pictures the crosshatched area represents that portion of the view which would be obscured by the camera in the actual television picture. The obscurations shown are the worst possible in the sense that they represent the edge of the blurred region for an *f/4* aperture. The square shown in dashed lines describes the approximate field of view in the narrow angle mode. The full field of view of these pictures is roughly that of the television cameras in the wide-angle mode. No attempt was made to simulate resolution or depth of field. TV Camera 3 had a 13.5-deg tilt.

Position 4 of the surface sampler as viewed from Cameras 2 and 3 is shown in Figure 35. These views do not give an impression of the large area in which surface sampler operation can be viewed, since Position 4 was chosen to illustrate a near-limiting condition.

*c. Azimuth stereo coverage.* Azimuth coverage for two configurations is presented in Table 12 based on an effective baseline as defined in Figure 36. To illustrate the restriction which results from the use of only two cameras, percentage coverage is given for both 360 deg and the maximum possible with the actual baseline in the configuration.

*d. Performance summary for survey cameras.* A comparison of some important system parameters, as specified in JPL TM 33-13, the Hughes design study, and JPL 30240B, as well as current performance data is presented in Table 13. The horizontal resolution data are considerably better than required for limiting resolution at 1 mm. However, the camera used for these data did not include

**Table 12. Approximate stereo azimuth coverage**

**(0.6 m effective baseline)**

| Elevation angle, deg | Original configuration of 2100-lb spacecraft | | A-21 configuration of August 16, 1962 | |
|---|---|---|---|---|
| | % of 360 deg | % of maximum possible (240 deg) | % of 360 deg | % of maximum possible (252 deg) |
| +15 | 42 | 63 | 67 | 95 |
| 0 | 42 | 63 | 65 | 93 |
| −15 | 42 | 63 | 64 | 92 |
| −30 | 19 | 29 | 32 | 46 |
| −45 | 17 | 27 | 27 | 39 |

the variable focal length lens which will probably degrade resolution under some conditions.

*e. Descent phase coverage.* Descent phase events as related to the approach TV are shown in Figure 37. Approximately 100 pictures will be taken between the time the terminal attitude maneuver is complete at about 1000 mi until the TV must be turned off at 80 mi to permit telemetry of the altitude mark. A 20-mi margin is required because of trajectory uncertainty. During main retro burning, approximately two pictures will be taken, subject to exhaust interference. A final picture will be taken after main retro burnout but before separation subject to vernier exhaust and attitude motions. Loss of the high-gain antenna beam from Earth will probably preclude further useful picture data at lower altitudes.

The geometry for non-normal incidence is shown in Figure 38. The locations of the camera field of view on the surface with respect to the nominal touchdown point at several approach angles are shown in Figure 39. Since many more frames will be taken than are

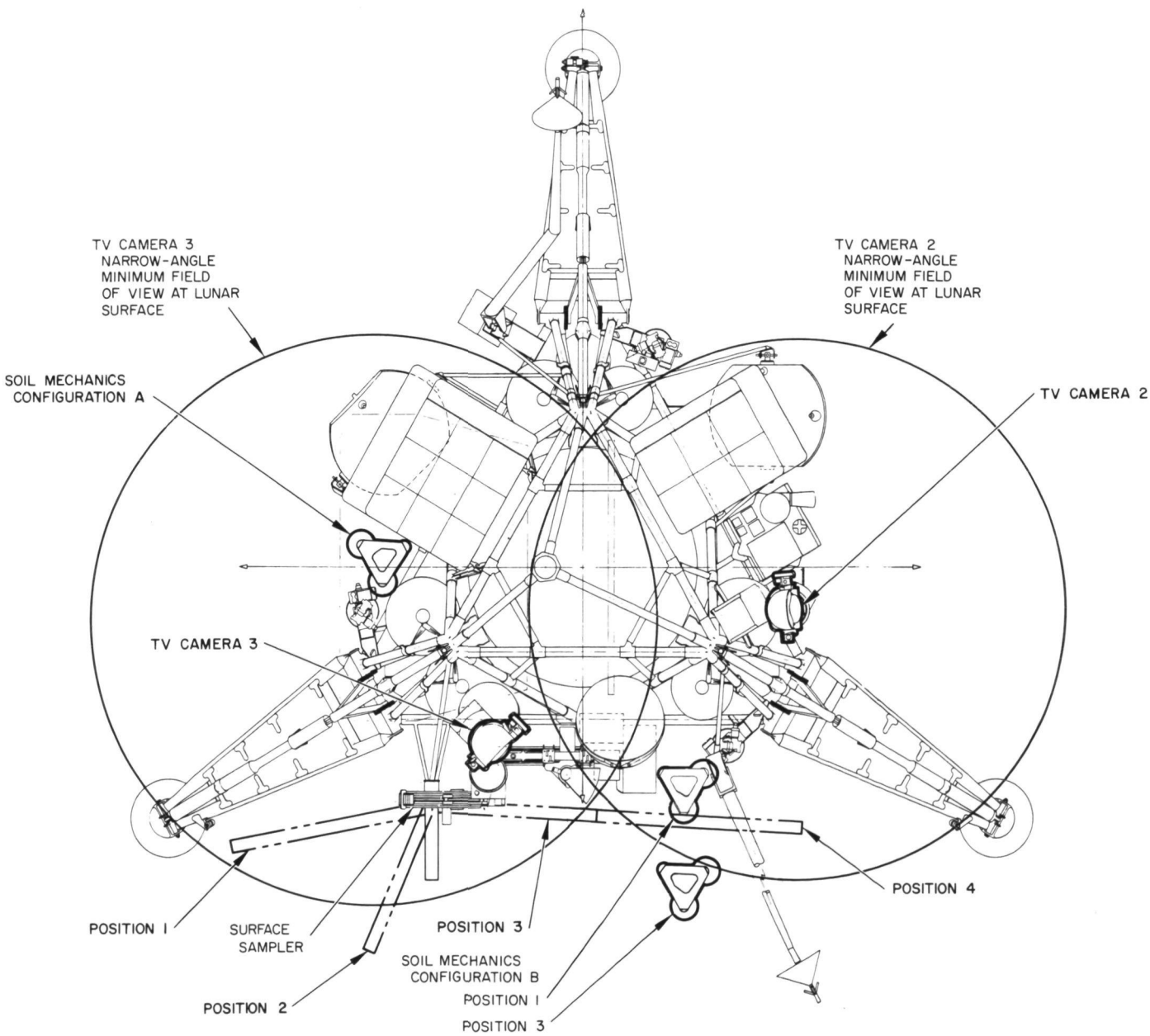


**Fig. 33. *Spacecraft configuration and instrument position for visibility photographs***

illustrated, it is apparent that adequate overlap will be obtained. Figure 40 illustrates the field of view for the final frames for a 45-deg angle of unbraked impact. In this case the landing site will nominally be within the field of the last frame before retro ignition but not in the field of the postretro picture. Dispersion in camera alignment and thrust axis to velocity vector alignment will modify this coverage somewhat.

*f. Descent picture quality.* Signal-to-noise ratio as a function of days after local terminator at touchdown is shown in Figure 41. Three possible $f$ numbers are considered. Since highlight saturation occurs at 4-1/2 days with $f/4$, a setting of approximately $f/5.6$ would be required to go through the whole lunar day without adjustment. This results in a signal-to-noise ratio of about 15-db peak-to-rms, 21-db peak-to-peak-to-rms, one day away

**Table 13. Survey TV performance comparison (Cameras 2 and 3)**

| | JPL TM 33-13 | Hughes design study | JPL 30240B | Present estimate (breadboard camera) |
|---|---|---|---|---|
| Resolution at 4 m (narrow angle) | Approximately 1 mm | 1.05 mm | 600-line raster | Vertical: 0.74 mm/raster line<br>Horizontal: 40% response at 1 mm for 23 db overall signal-to-noise |
| Elevation coverage | Within 45 deg of vertical | 15 to — 45 deg in spacecraft coordinates | — | Wide angle: 20 to —45 deg } spacecraft<br>Narrow angle: 45 to —54 deg } coordinates[a] |
| Highlight luminance for full signal-to-noise | — | — | — | 100-ft-lambert |
| Colorimetry | — | Filters included for color pictures | Colorimetric measurements required | Feasibility, accuracy not yet assessed |
| Photometry | — | — | Photometric measurements required | Accuracy not yet assessed; feasibility of simple calibration standards under study |
| Minimum focus distance | To meet instrument viewing reqjurements | 6 ft | — | 6 ft |
| Number of frames in narrow angle survey | — | 1900 | — | 1100 (15 to — 45 deg<br>Stereo overlap for August 1952 configuration) |

[a]Camera tilt for instrument viewing will affect the coverage with respect to the local vertical accordingly.

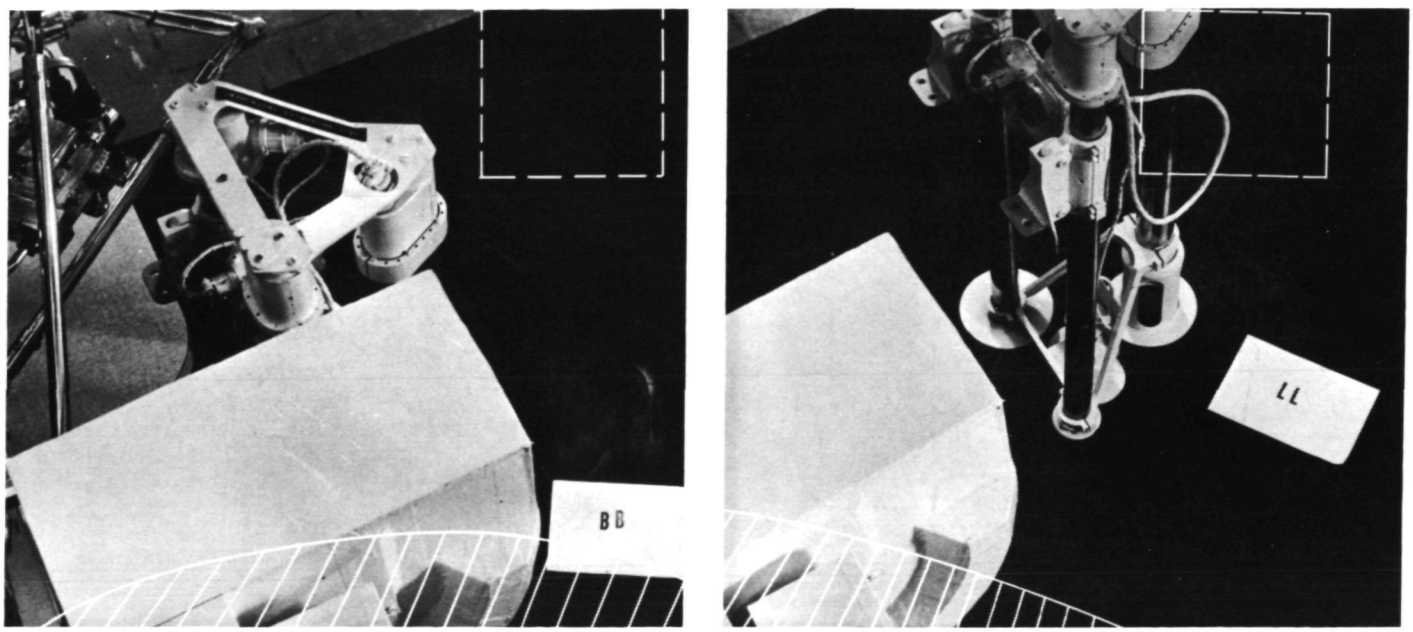


**(a) Position 1** **(b) Position 3**

**Fig. 34. View from Camera 3**

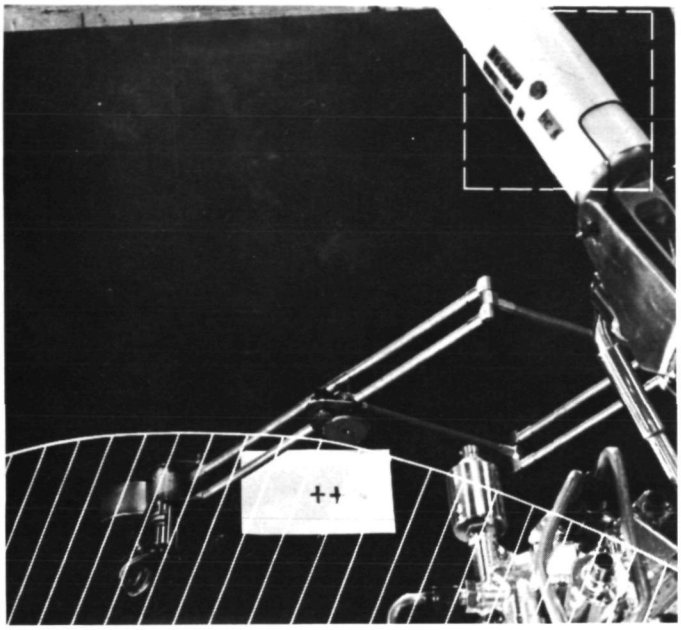

(a) Camera 2

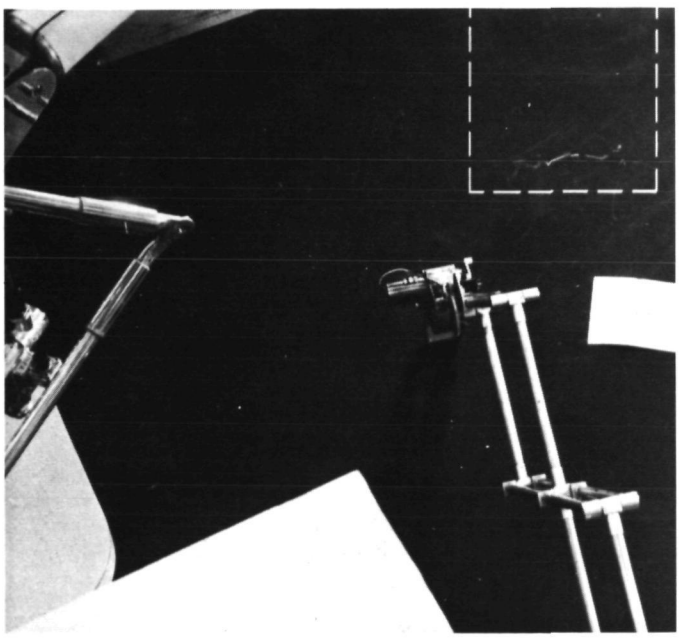

(b) Camera 3

**Fig. 35. View of Position 4**

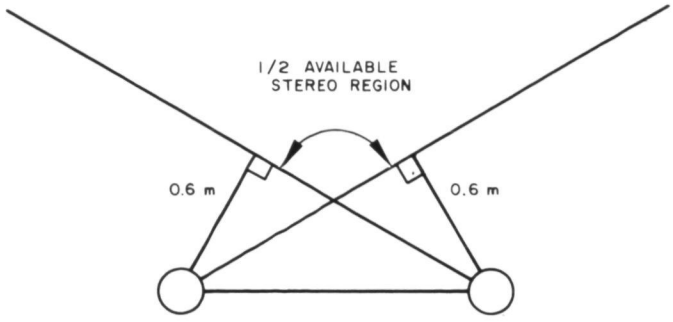


**Fig. 36. Effective baseline**

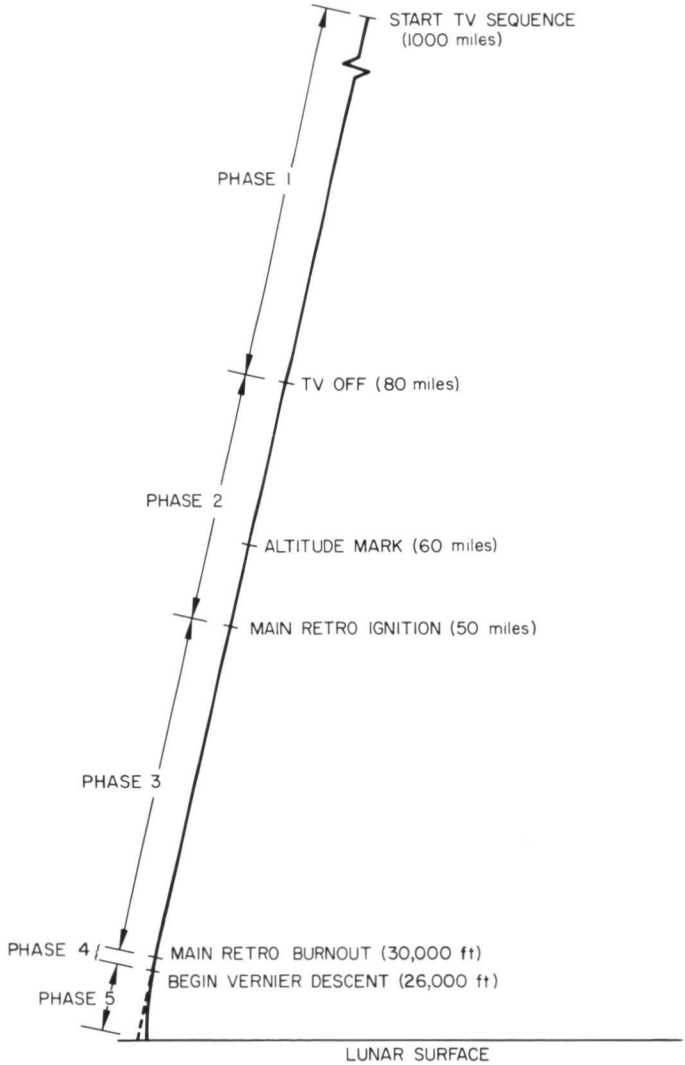


**Fig. 37. Descent phase events**

from terminator. Because high contrast scenes are expected at low illumination angles, it is believed that this picture quality is adequate to determine the landing location.

A performance comparison for the approach TV is presented in Table 14. Because of the additional degradation in resolution due to smear resulting from linear and angular motions and closure, detailed response curves are not appropriate to the approach camera resolution.

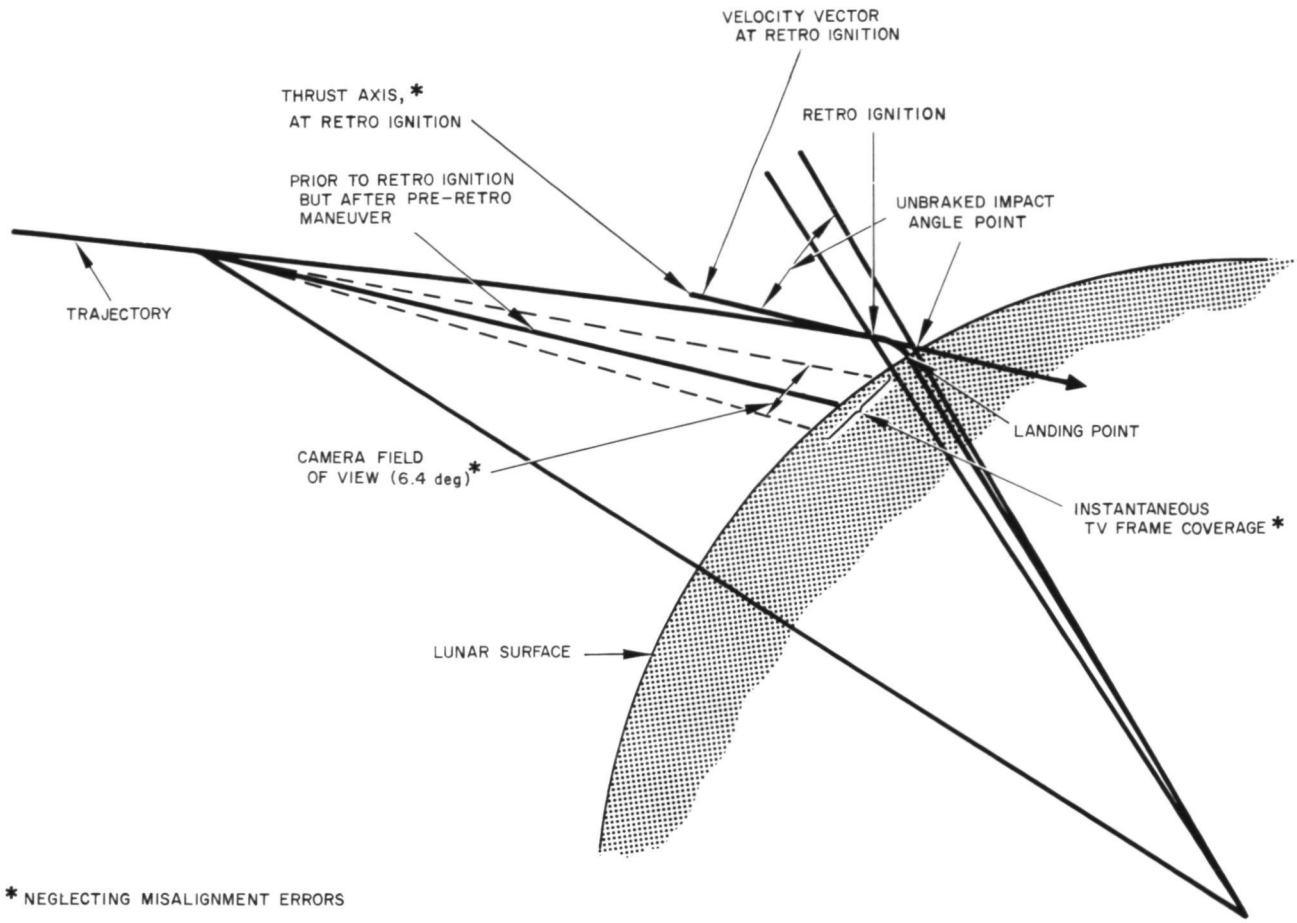


**Fig. 38. Geometry of descent phase TV coverage**

### 4. Design Mission Sequence

A design mission sequence for the A-21 spacecraft has been prepared to illustrate the experiments which may be performed during the first lunar day for the case of an eighth day launch with a touchdown at 0° selenographic latitude and —35° selenographic longitude. The standard trajectory selected results in a 156-hr lighting interval between touchdown and the day-to-night terminator.

The mission was designed to satisfy the requirements of the current scientific instrument – spacecraft interface specification but is idealized to the extent that problems remain to be resolved that may result in changes in the operations indicated. The elements of the scientific payload and spacecraft still in question are discussed in in subsequent paragraphs. The mission profile illustrated in Figure 42 will consist of the following operations:

(1) Six lunar-surface soil-sampling operations.

(2) One wide-angle and ten narrow-angle black and white TV mapping surveys.

(3) Five narrow-angle color TV mapping surveys.

(4) Six X-ray diffractometer lunar soil analysis experiments.

(5) Six alpha-scattering lunar soil analysis experiments.

(6) Six alpha and proton channel reaction lunar soil analysis experiments.

(7) A lunar soil mechanics experiment.

(8) Two surface sampler soil tests.

(9) Nearly continuous measurement of micrometeorite ejecta impacts.

(10) Hourly engineering measurements of critical spacecraft parameters.

(11) 50-hr nighttime engineering thermal test (not illustrated by Figure 42).

Current predictions of the solar panel temperature profile indicate that approximately 6500 w-hr of energy

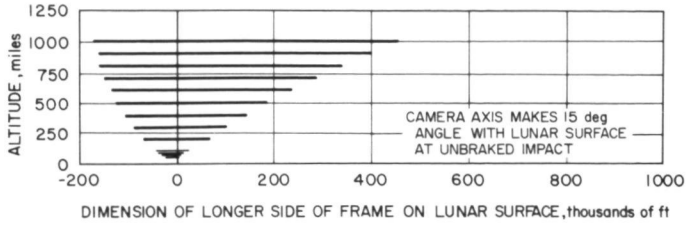


(a) 15-deg approach

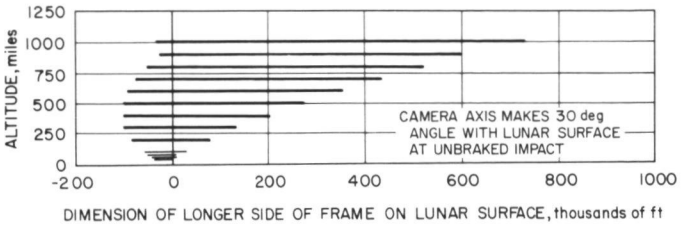


(b) 30-deg approach

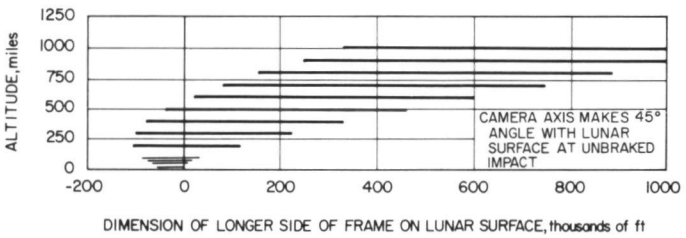


(c) 45-deg approach

**Fig. 39. Camera field of view**

**Table 14. Approach TV performance comparison**

| | TM 33-13 | Hughes design study | JPL Specification 30240B | Present estimate |
|---|---|---|---|---|
| Resolution | 1 m for final picture | 1400 ft at 1000 mi | 600-line raster subject to spacecraft motion and engine exhaust | 330 m per line at 1000 mi<br>27 m per line at 80 mi<br>3 m per line at 30,000 ft subject to exhaust interference |
| Number of frames | — | 25 | Time-shared with real-time telemetry from 12 min before retro ignition to staging | 100 from 1000 to 80 mi<br>Two during main retro<br>One between burnout and separation |
| Highlight luminance for full signal-to-noise | — | — | — | 750 ft-lambert |

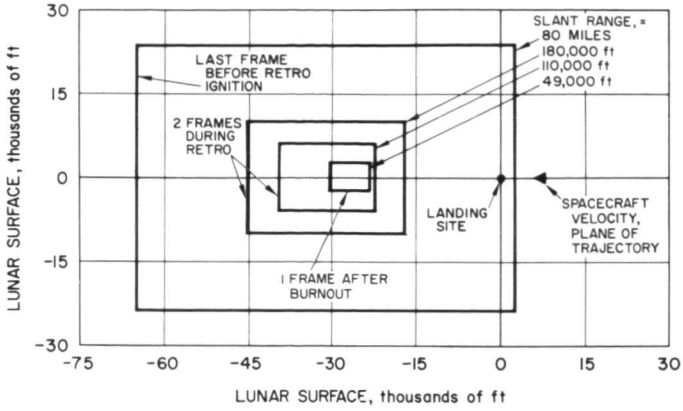


**Fig. 40. Descent phase TV coverage — final frames**

**Typical for 45-deg unbraked impact trajectory**

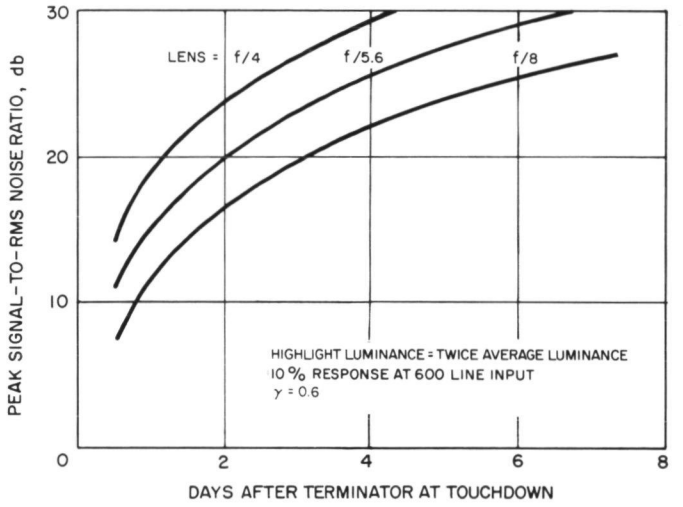


**Fig. 41. Effect of launch day on signal-to-noise ratio**

will be available for use by the scientific payload. The energy consumed by the operations named is within this allocation. The transit energy deficit is currently less than 200 w-hr, such that the basic bus allocation of approximately 900 w-hr is sufficient to supply the needs for the transit deficit and the basic bus during lunar operation. The mission is designed to provide for a full battery charge at the day-to-night terminator.

In order to facilitate the interpretation of Figure 42, the operations illustrated are defined in the following paragraphs.

### *a. Surface sampler*

*Sample procurement.* During sample procurement, the surface sampler will select a sample of lunar material for use by the soil analysis experiments. Since these opera-

CONFIDENTIAL

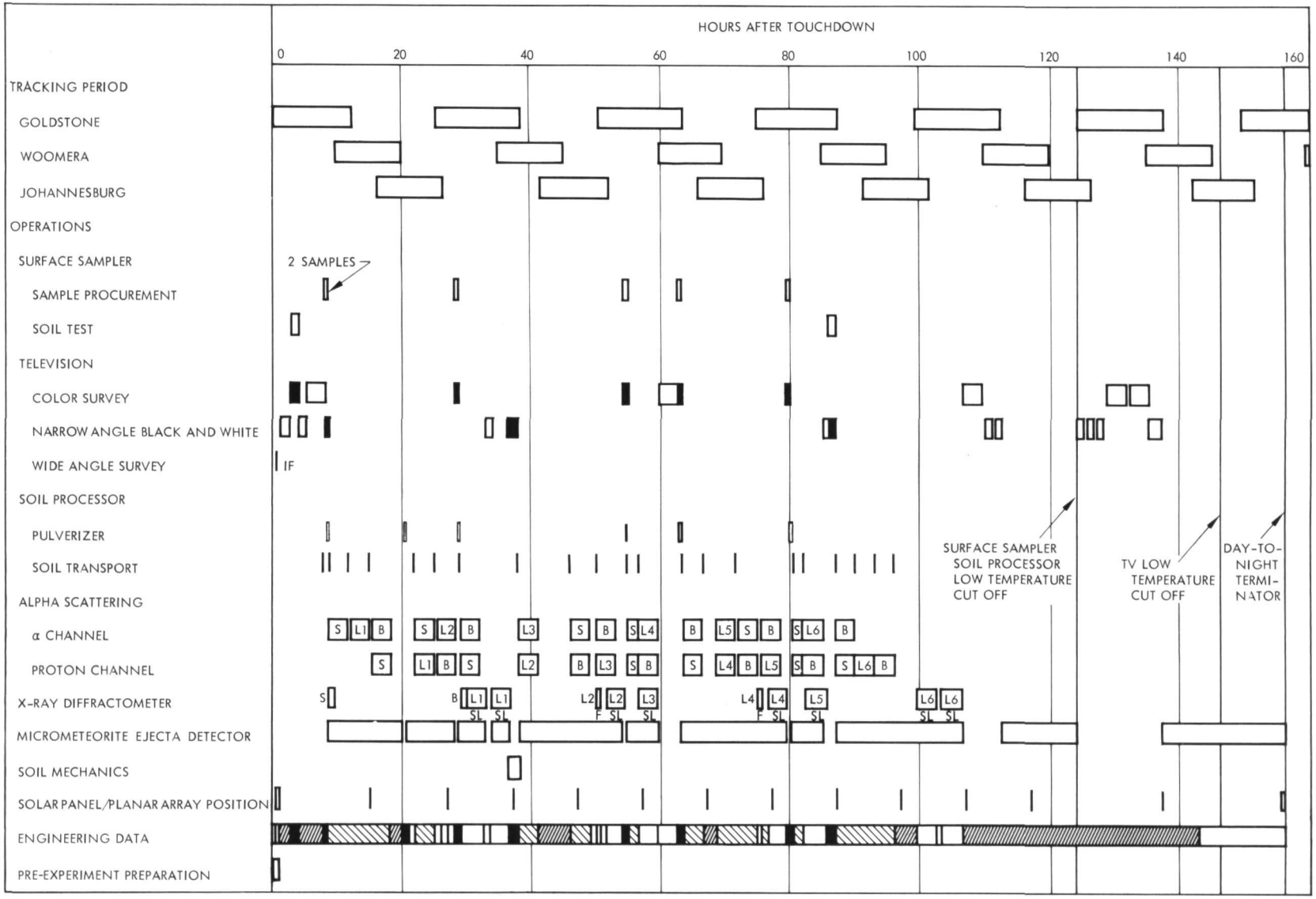


**Fig. 42. Design mission sequence**

CONFIDENTIAL

tions require real-time TV coverage of the area to be sampled and real-time control of the instrument, they must be conducted only during Goldstone tracking periods. Except for the operation shown during the first Goldstone period when two lunar samples will be selected, each block indicates 1/2 hr of operating time for the selection of one lunar sample.

*Soil test:* During the first and fourth Goldstone tracking periods, the texture of the lunar soil will be measured by scraping the surface with the surface sampler. TV coverage will be provided for these measurements.

***b. Television***

*Color survey.* Color TV surveys consist of programmed 3300-frame, narrow-angle scans and require about 3 hr of operating time. In addition to the programmed surveys, color TV coverage of the surface sampler will be provided to aid in the selection of samples as a function of possible mineralogical color of the lunar surface.

*Narrow-angle black and white survey.* The narrow-angle black and white survey consists of 1-hr 1100-frame programmed narrow-angle scans.

*Wide-angle survey.* The wide-angle survey requires about 7.4 min of operating time. Normally, the wide-angle survey is used only for focusing, and as such it is shown only once in the mission during the initial focus survey immediately after touchdown.

***c. Soil processor.*** The pulverizer grinds the lunar soil, selected by the surface sampler, into the fine mesh required by the soil analysis experiments. Approximately 2 min operating time is required to process each sample.

The soil transport mechanism, during this operation, is used to provide lunar material to the pulverizer and to position the lunar and standard samples for the appropriate instrument. The functional capability of this mechanism has not been defined due to the preliminary design status.

***d. Alpha scattering.*** The maximum operating temperature of the alpha scattering instrument results in a severe operating constraint under lunar noon conditions. It is assumed in this sequence that the thermal control-operating temperature restrictions will be resolved and are therefore not considered at present.

*Alpha channel.* The alpha channel portion of the alpha scattering instrument performs an analysis of the minerals contained in the lunar soil by determining the energy distribution of alpha particles scattered from the soil sample by a Cm 242 radioactive source. An Earth soil standard sample analysis and a background count are provided within 6 hr of the lunar sample analysis. Normally, 3 hr operating time is provided for each analysis or background count; however, during the third and fourth Goldstone tracking periods, the time allotted for the standard sample analysis has been reduced to 1.5 hr to allow analysis of two diffractometer samples.

*Proton channel.* The operation of the proton channel is the same as the alpha channel except that the constituents of the lunar sample are determined by a measurement of the proton energy distribution caused by $\alpha$,P reactions in the sample. The delay shown before the first standard sample analysis results from the sequential positioning of the sample cups by the soil transport mechanism. Operation of both alpha and proton channels from overseas DSIF stations is scheduled.

***e. X-ray diffractometer.*** The operating profile as shown in Figure 42 will consist of an Earth standard sample analysis, a background count (performed first), two goniometer slow scans of Lunar Samples 1 and 6, a goniometer fast scan and a slow scan of Lunar Samples 2 and 4, and a single goniometer slow scan of Lunar Samples 3 and 5. The fast scan of Samples 3 and 5 were omitted to provide a capability for two lunar sample analyses during the Goldstone tracking periods affected. Real-time operational control and analysis of the data is provided by scheduling operation during Goldstone tracking periods.

***f. Micrometeorite ejecta detector.*** This detector measures the distribution of meteoric ejecta impacts on the spacecraft and surrounding environment. Operation is continuous except during TV operation.

***g. Soil mechanics.*** The soil mechanics experiment is operated under conditions of Goldstone tracking to provide real-time control.

***h. Solar panel/planar array position.*** The solar panel and planar array will be positioned to acquire the Earth and Sun immediately after touchdown. They will be repositioned periodically to correct for changes in Sun angle and to null out errors due to Earth-Moon geometrical librations.

***i. Engineering data.*** Spacecraft engineering data such as critical voltages, temperatures, and mechanism positions such as appear on Mode 4 of the engineering commutator are transmitted at various times. The sampling frequency which will be required during the first lunar day is scheduled to evaluate the performance of basic bus and scientific payload equipment and to provide the data required to conduct the power and thermal management functions.

# D. Flight Control

## 1. Introduction

The flight control subsystem consists of the spacecraft units which provide velocity and attitude control during the transit and landing phase of the *Surveyor* mission. These units, which include optical sensors, inertial instruments, attitude controls, and flight control electronics, are discussed in this section. Functionally, the lunar radar and propulsion are also included, although these items are covered in other sections.

## 2. System Status

***a. Summary.*** Design of an all-spur-gear train for the roll actuator was begun to replace the final stage worm gear which caused unacceptable thrust phase roll control system limit cycling. Layouts of the new design were completed and final drawings will be completed in January. This change is not expected to affect scheduled delivery of the upgraded T-21 roll actuator.

Thermal vacuum tests were completed on the thermal model of the flight control sensor group using the SERF (Space Environment Research Facility) C-1 thermal vacuum chamber. Initial evaluation of test results indicates the basic thermal design of the sensor group is valid although minor changes in the structure thermal coating may be required to achieve a design goal of sensor group bulk base temperature of 70° F.

Evaluation of the total error in sensor group roll axis orientation during the main retro phase was completed. Results indicated that the $3\sigma$ error will be less than 0.3 deg for the worst possible combination of contributing spacecraft characteristics, which include vernier engine misalignment, main retro offset and misalignment, downgraded roll actuator performance, marginal vernier engine thrust characteristics, and errors associated with the pre-retro maneuver.

The gyro temperature controller module in the inertial reference unit was redesigned to provide adequate performance in the presence of noise and to prevent intermittent operation caused by stray gyro capacitance. The new design also eliminates the need to match controller components to individual gyros. Final drawings were completed and parts procurement initiated.

Subsystem tests of the T-2 spare electronics unit, inertial reference unit, and roll actuator were completed.

***b. Vernier descent phase.*** The analysis of roll axis pointing accuracy during the main retro phase was completed. It was determined that the sensor group roll axis error will not exceed 0.3 deg for the worst-case conditions of vernier engine misalignment, main retro offset and misalignment, marginal roll actuator performance, and imperfect integration in the pitch and yaw control channels. The following spacecraft characteristics were used:

(1) Maximum roll actuator torque: 52 in-lb.

(2) Vernier engine static characteristics: see Figure 43.

(3) Pitch and yaw shaping: $\dfrac{(0.5+1)\,(S+1)}{(S+0.05)\,(0.05\,S+1)}$

(4) Main retro thrust vector offset: 0.18 in.

(5) Main retro thrust vector misalignment: 0.2 deg.

(6) Vernier engine thrust vector misalignment: 0.5 deg.

The maximum pointing error contributed by the effect of noncommutable spacecraft angular rotations and combined disturbance moments was 0.2 deg. The maximum $3\sigma$ pre-retro maneuver contribution was 0.22 deg. The root sum square of these contributors is 0.297 deg and represents a conservative calculation in that each of the spacecraft characteristics was considered to have a $3\sigma$ value.

Additional analog computer runs were made to define the complete envelope of acceptable thrust axis to lunar vertical angles as a function of thrust axis velocity (Figure 44). This envelope depicts the acceptable vehicle attitude, range, and velocity at main retro burnout based on the criterion that the thrust axis is aligned to the lunar vertical within 1 deg at the cutoff altitude of 13 ft.

***c. Thrust phase roll control.*** Detailed analysis of the thrust phase roll control system was completed. Incorporation of the all-spur-gear roll actuator in the position control loop provided the additional system performance required to ensure adequate control in the presence of larger vernier engine fuel line spring loads, combined with a possible reduction in roll actuator motor torque

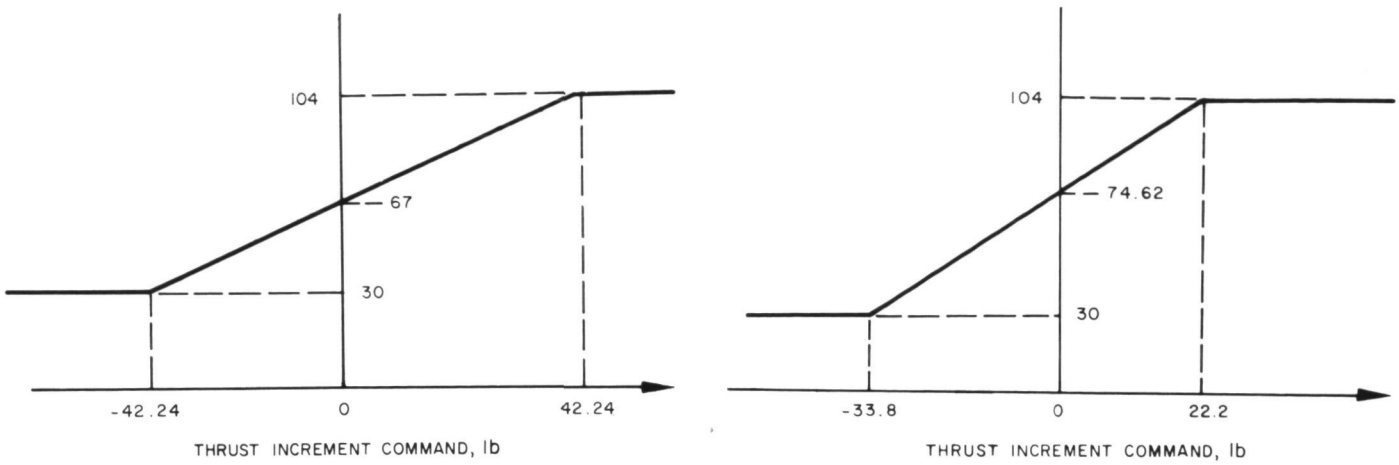


**(a) Engines 2 and 3 (lowest permissible scope)** **(b) Engine 1 (highest permissible scope)**

**Fig. 43. Vernier engine static characteristics**

capability in a high temperature environment. The final design of the thrust phase roll control system is shown in Figure 45.

The control electronics transfer function includes a decrease in the electronic gain which was required to ensure adequate system performance for large variations in vernier engine thrust during main retro operation. The all-spur-gear roll actuator design was required for several reasons. Mixed analog computer simulations indicated the presence of a low frequency (0.1 to 0.2 cps) steady-state limit cycle with a spring-loaded worm-gear actuator. The computer runs (Figure 46) present a comparison of typical transient responses for an actuator with a worm-gear final stage and the all-spur-gear design. The large steady-state roll angle of 1.3 deg is due to the large disturbance torque of 6.0 ft-lb (the sum of $3\sigma$ disturbance torques) and the lower electronic gain. For a root sum square disturbance torque of 4.0 ft-lb and an electronic gain as indicated in Figure 45, the steady-state roll angle would be 0.69 deg.

The limit cycle was caused by the tendency of the worm gear to lock with a spring-loaded output as the servomotor voltage approached zero. The locking caused an error signal to build up servomotor voltage and eventually break the actuator free. However, at this instant, the worm gear friction level would drop from static to dynamic, causing actuator acceleration and overshoot of the steady-state position; this led to a repetition of the locking in the opposite direction, causing a limit cycle of very low frequency. Because of the low frequency, the double integration between vernier engine angle and spacecraft roll angle fails to filter the oscillation. In addition to its tendency to cause a spacecraft limit cycle, the low torque efficiency of the worm gear actuator (about 35%) compared to that of an all-spur-gear actuator (about 70%) caused marginal roll system performance when the servomotor output torque was reduced at high temperatures. The final roll system design, shown in Figure 45,

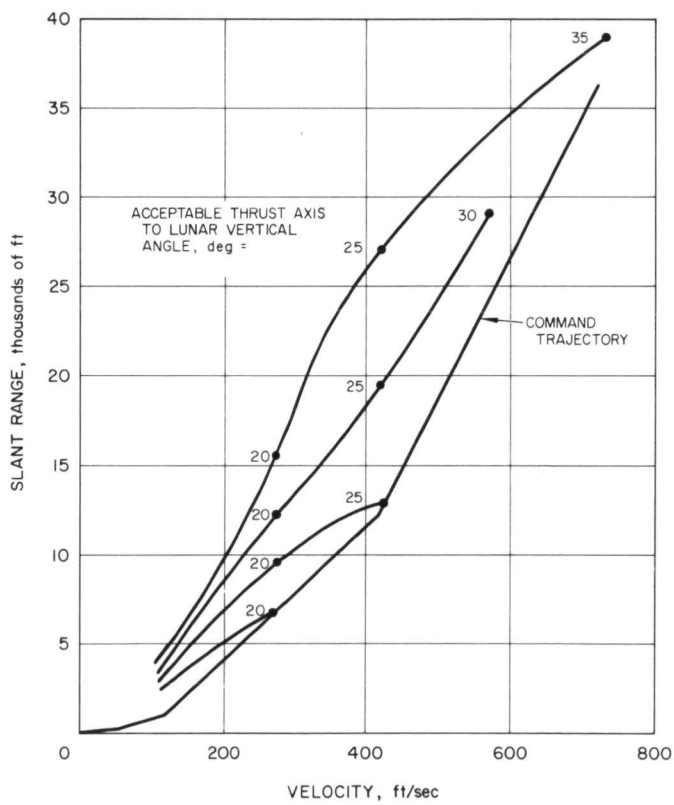


**Fig. 44. Acceptable thrust axis misalignment**

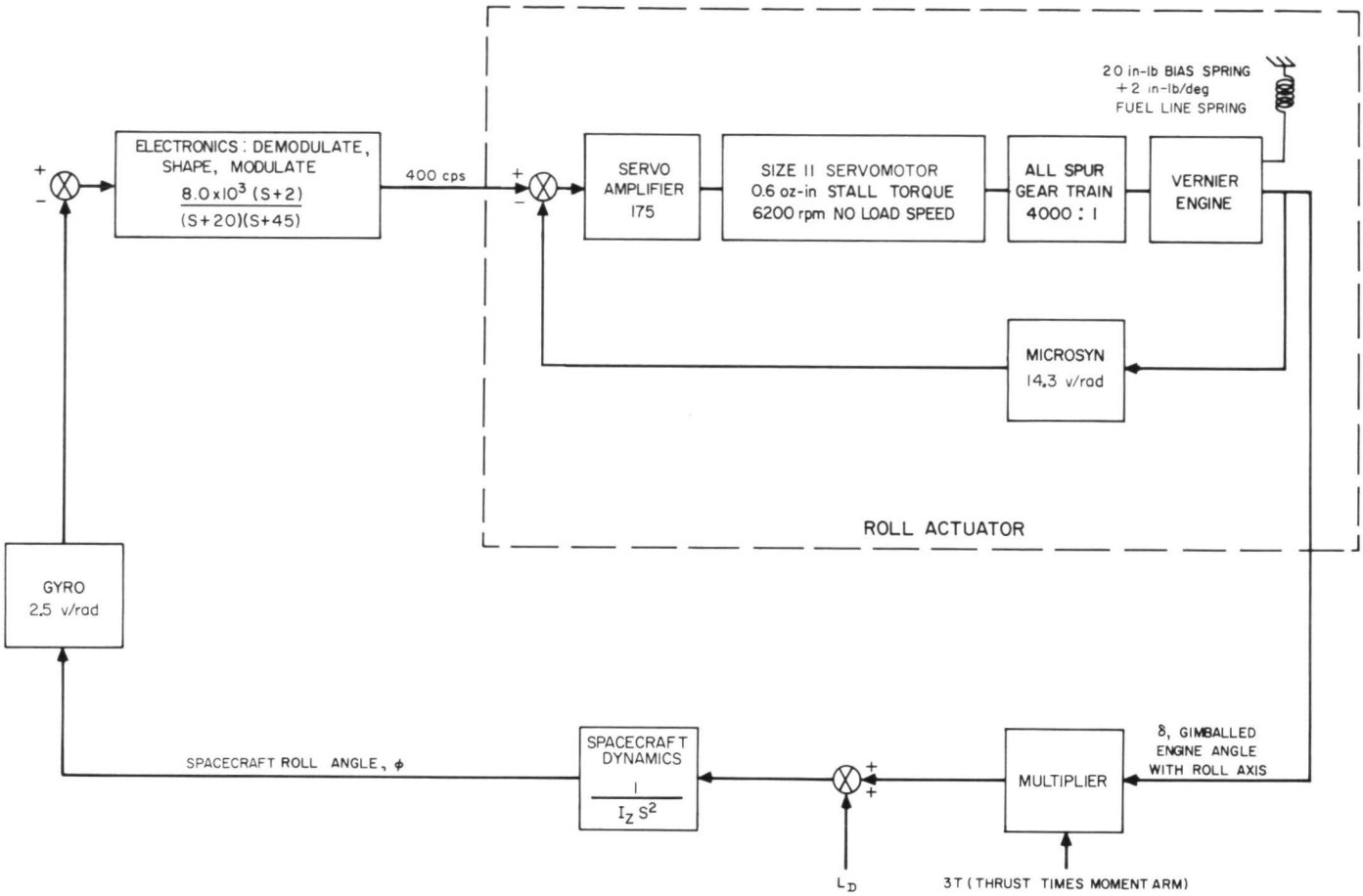


**Fig. 45. Thrust phase roll control system**

provides adequate system performance for the entire spacecraft mission.

### 3. Subsystem Tests

*a. T-2 test program.* The T-2 spare flight control units, which include the flight control electronics, inertial reference unit, and roll actuator, were delivered for system integration.

*b. Air-bearing table tests.* Additional tests were performed on the air-bearing table in the star acquisition mode to determine the effect of a reduced Canopus sensor field of view on system performance. The measured data are presented in Figure 47. With a roll rate of 0.5 deg/sec at the initiation of the star lockon mode, acquisition was possible in every instance, for a Canopus sensor field of view down to ±2 deg, both at nominal gas jet thrust and at 90% of nominal.

*c. Flight acceptance tests.* The flight acceptance test console for the flight control sensor group (Figure 48) was completed and will be used to check out the T-21 flight control sensor group.

### 4. Sensor Group Integration

Thermal-vacuum tests were completed on the thermal model of the flight control sensor group using the SERF C-1 vacuum coldwall chamber at Hughes Space Environmental Laboratory. Although evaluation of test results is incomplete pending reduction of test data, preliminary analysis indicates that the basic thermal design of the sensor group is valid even though sensor group temperatures stabilized at values 18° below those predicted by computer studies during transit tests. If required, the sensor group bulk base temperature can be increased to the design goal value of 70° F by removal of paint from the sensor group structure. No changes are planned in the thermal design until completion of Sector 2 tests. Some peeling of thermal paint occurred on the electronics unit and sensor group structure prior to and during the tests, although none occurred on the Canopus sensor.

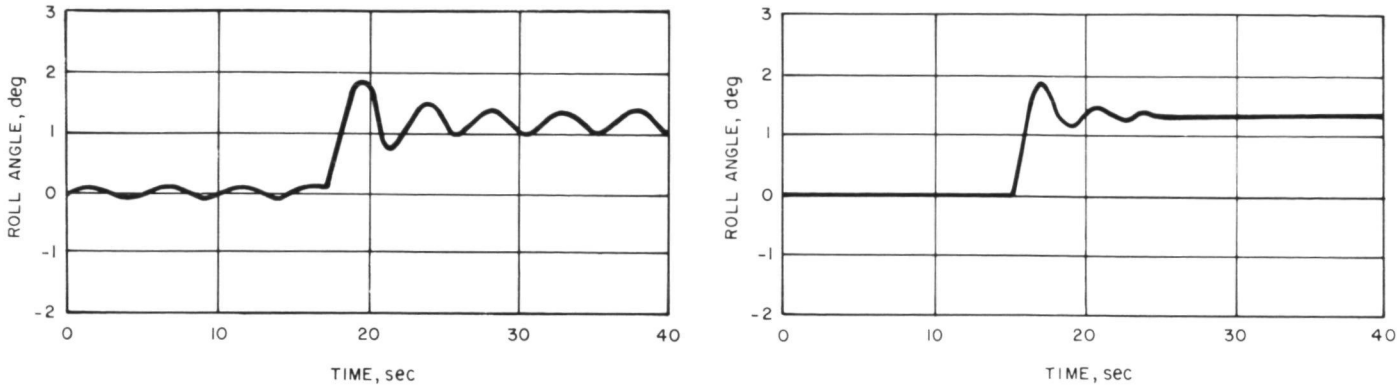


**(a) Worm-gear actuator** **(b) All-spur-gear actuator**

**Fig. 46. Actuator transient response**

6 ft-lb roll disturbance step torque at t = 17

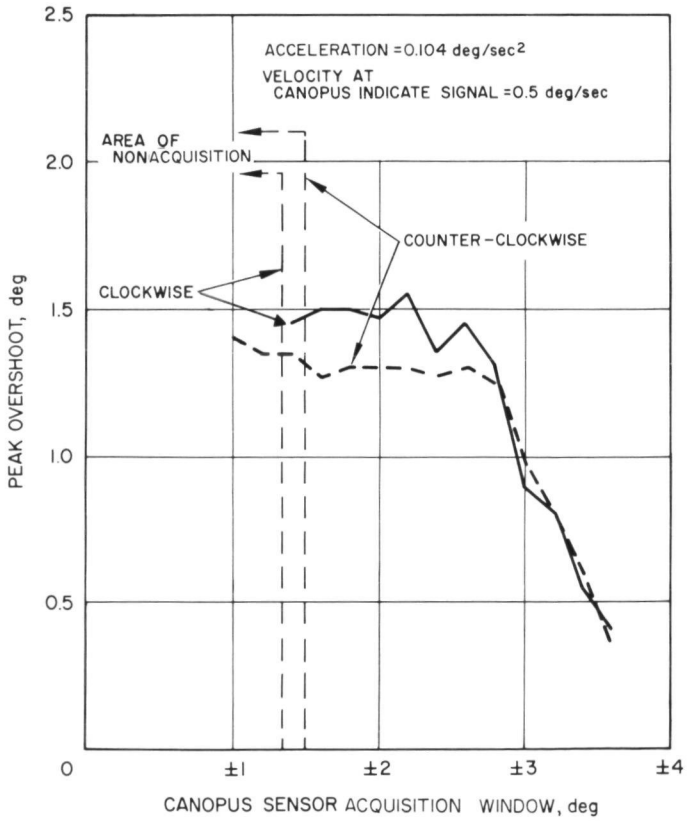


**Fig. 47. Star acquisition peak overshoot**

Thermal finishes used on the various units were described in the preceding bimonthly report. Thermocouples were used to monitor internal and external temperatures of the units, cold wall, simulated spaceframe, and wire bundle blocking temperatures. Heaters were used to simulate solar radiation on the inertial reference unit thermal radiator, the Canopus sensor Sun shade, and the sensor group base structure. Multilayered aluminized mylar radiation shielding was used between the base heaters and the control electronics unit to prevent artificial heat loading of that unit. Wires coming off the thermal models were grouped into two bundles. One group of wires was used only by the inertial reference unit because of associated higher temperaturse. A heater on this bundle provided a blocking temperature of approximately 100° F to prevent artificial heat loss through the wires. The second group of wires used by the remaining units had a heater to provide a blocking temperature of approximately 50° F.

The sensor group thermal model was supported by an angle aluminum fixture with 3-in. teflon standoffs to provide thermal isolation (Figure 49). Fixed aluminum bus bars were connected between the nitrogen-cooled wall of the chamber and the three mounting legs on the sensor group base structure. Heaters were located on each bar so that the conductance from the heater location to the sensor group mounting lug was representative of that expected on the actual spacecraft. By controlling power to the heaters on the three bars, a simulated spacecraft temperature range from —85 to —15° F could be achieved. These conductance bars were wrapped with multilayered aluminized mylar to reduce radiation and permit more accurate calculations of heat flow from the sensor group.

Normal transit tests with coast phase power applied were run with a chamber pressure of $10^{-8}$ mm Hg, a cold-wall temperature of —200° F and a simulated spaceframe temperature of —70° F. The sensor group base temperature stabilized at approximately 18° below the 63° F value which was expected based on computer studies. Unit temperatures were low by this amount also.

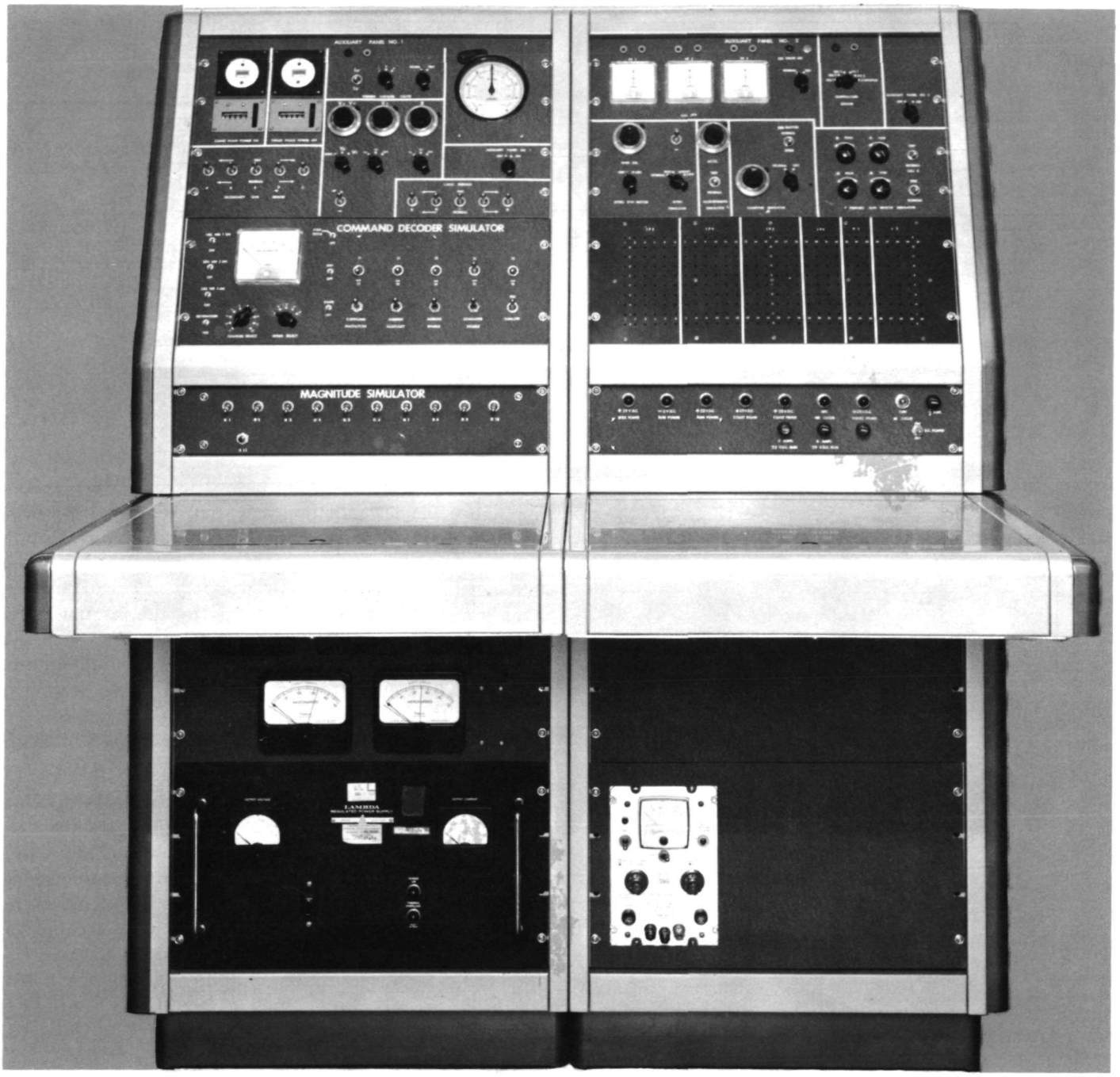


**Fig. 48. Flight acceptance test console for sensor group**

Although the reason for these lower temperatures is not known at this time, they have been tentatively attributed to questionable thermal characteristics of chem-milled surfaces. Before continuing the tests, the sensor group base temperature was increased to 63° F by using the heaters located in the base. The 63° F is equivalent to the design goal value of 70° F which was used in computer studies. The 7° difference is a correction applied due to the fact that an actual spaceframe was not used in the tests. After stabilization at 63° F, thrust phase power was applied to the electronics unit and all temperatures were monitored continuously. Thrust phase power was applied until the design maximum electronics unit radiator temperature of 140° F was reached, at which

time thrust phase power was shut off. It required approximately 1 hr to reach this temperature, whereas computer studies had predicted that this temperature would be reached in approximately 15 min.

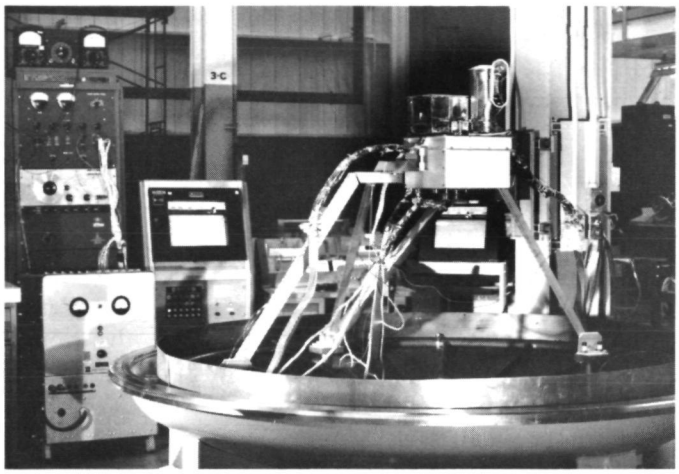

**Fig. 49. Thermal-vacuum test of sensor group**

After the base temperature had again stabilized at 63° F, tests were run with simulated spaceframe temperatures of −85, −65, −30, and −15° F. Although test data are still being processed, preliminary analysis indicates that changes in spaceframe temperatures do not cause large variations in sensor group temperatures.

The final tests consisted of stabilizing at normal transit temperatures and simulating flight in complete shade for 2 hr by removing power from the heaters used to simulate solar radiation. Test data on this phase are still being reduced.

The mechanical model of the new configuration of the flight control sensor group was completed and is being vibration tested. The Canopus sensor and electronics unit in this configuration are recessed into the support structure, as described in a previous bimonthly report.

## 5. Optical Sensors

*a. Canopus sensor.* Acceptance testing of the upgraded T-21 Canopus sensor was completed on November 21,

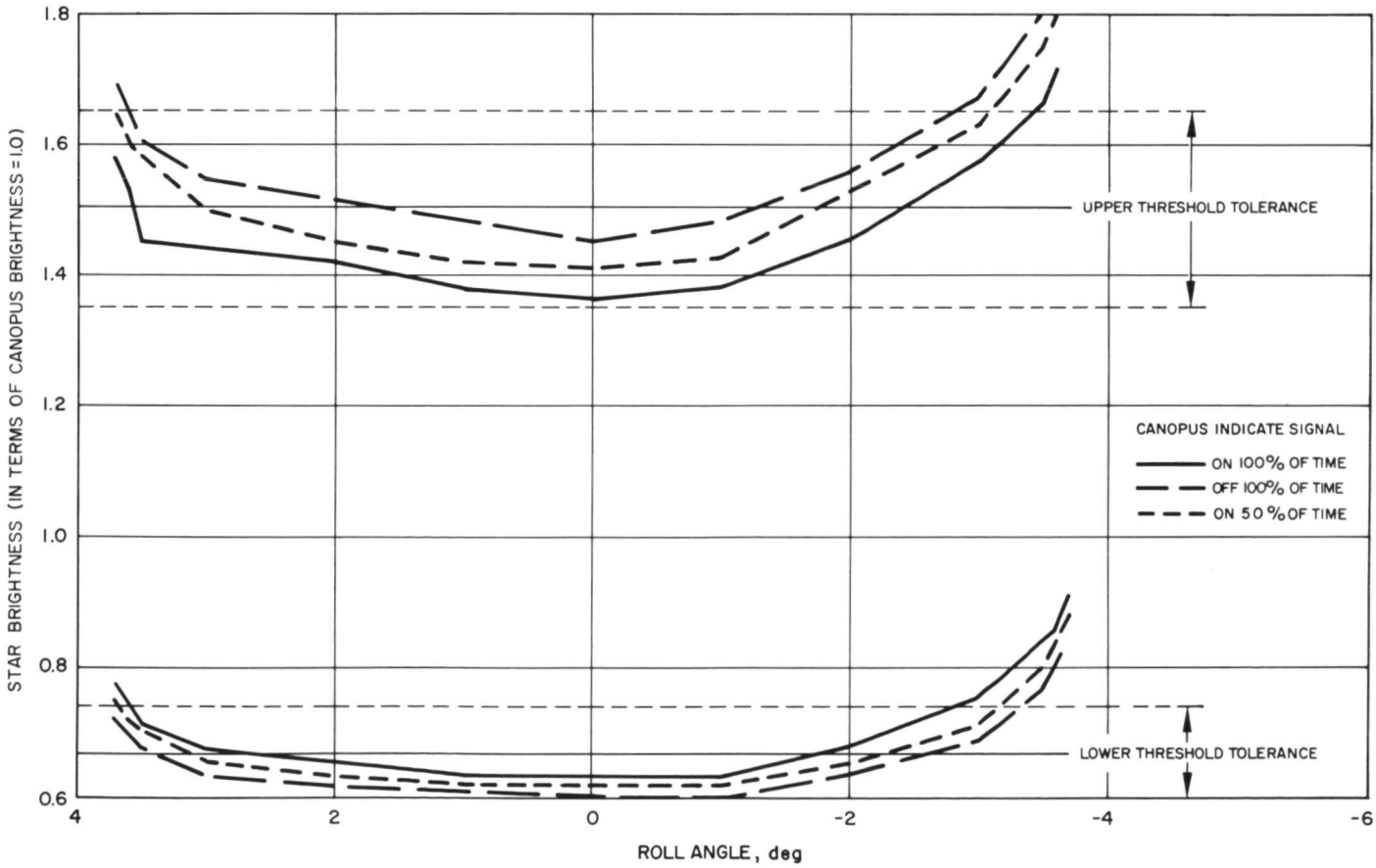


**Fig. 50. Indicate signal operation of breadboard Canopus sensor**

1962. The electrical performance was acceptable. The field-of-view window dimension along the roll axis was determined to be ±3.0 deg at a simulated star magnitude 0.66 times that of Canopus. The window dimension along the roll axis at nominal Canopus magnitude was ±3.6 deg and at 1.5 times that of Canopus the dimension was slightly less than ±3.0 deg. Mechanically the unit performed satisfactorily except for the acquisition mirror locking mechanism; the mirror had rotated approximately 2 deg after having been adjusted for a nominal star acquisition angle setting prior to vibration testing. The unit was considered unacceptable pending resolution of this problem, which was attributed to two causes: (1) the friction lock was not set tight enough, and (2) after setting, the adjusting shaft was not turned back far enough into the backlash area to relieve direct contact between the mirror and cover, which moves considerably during vibration testing. Testing will be conducted on the X-1 sensor to substantiate a fix prior to further testing and final acceptance of the upgraded T-21 unit.

A study was conducted to determine the repeatability of the field-of-view window along the roll axis, especially at lower threshold intensity levels. Data relating effective star brightness required to operate the "Canopus-indicate" circuit as a function of roll angle were obtained from three different sensors: (1) X-1, (2) X-2, and (3) the breadboard model. The data are presented in Figures 50, 51, and 52. Only the lower threshold curves are discussed here since the field of view around the roll axis is severely diminished only at lower star intensities.

For all tests the star acquisition angle setting was set at zero. The Canopus-indicate time delay was 0.2 sec. Variations in acquisition angles were made at various roll angle settings but were determined to have negligible effect on the curves shown. The probability of the Canopus-indicate signal being on is defined by the upper curve labeled 100% ON. Any time a star of selected intensity appears inside this curve, the Canopus-indicate signal will be on 100% of the time. The ⅔ Canopus intensity condition is shown as a solid horizontal line. The

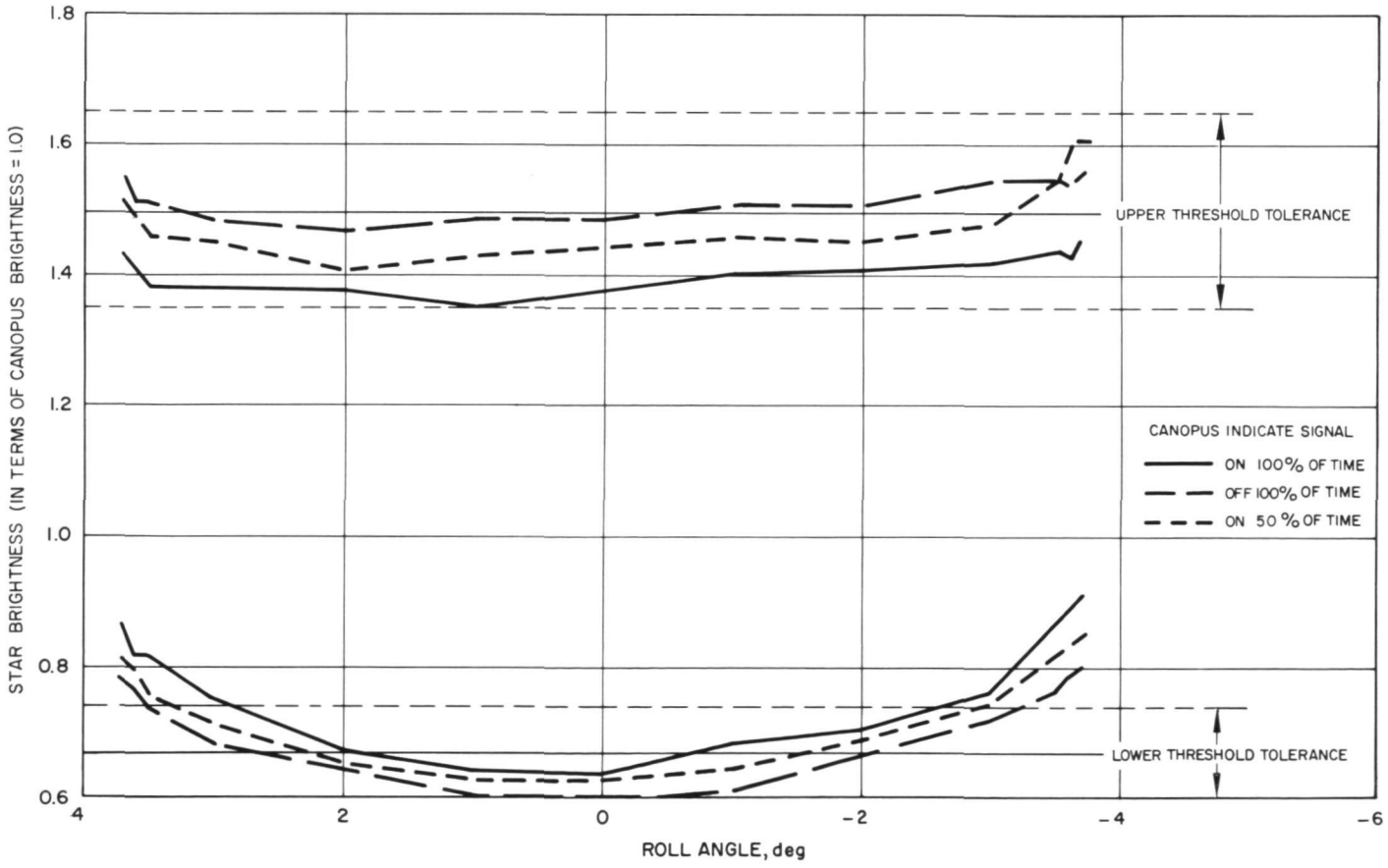


**Fig. 51. *Indicate signal operation of X-1 Canopus sensor***

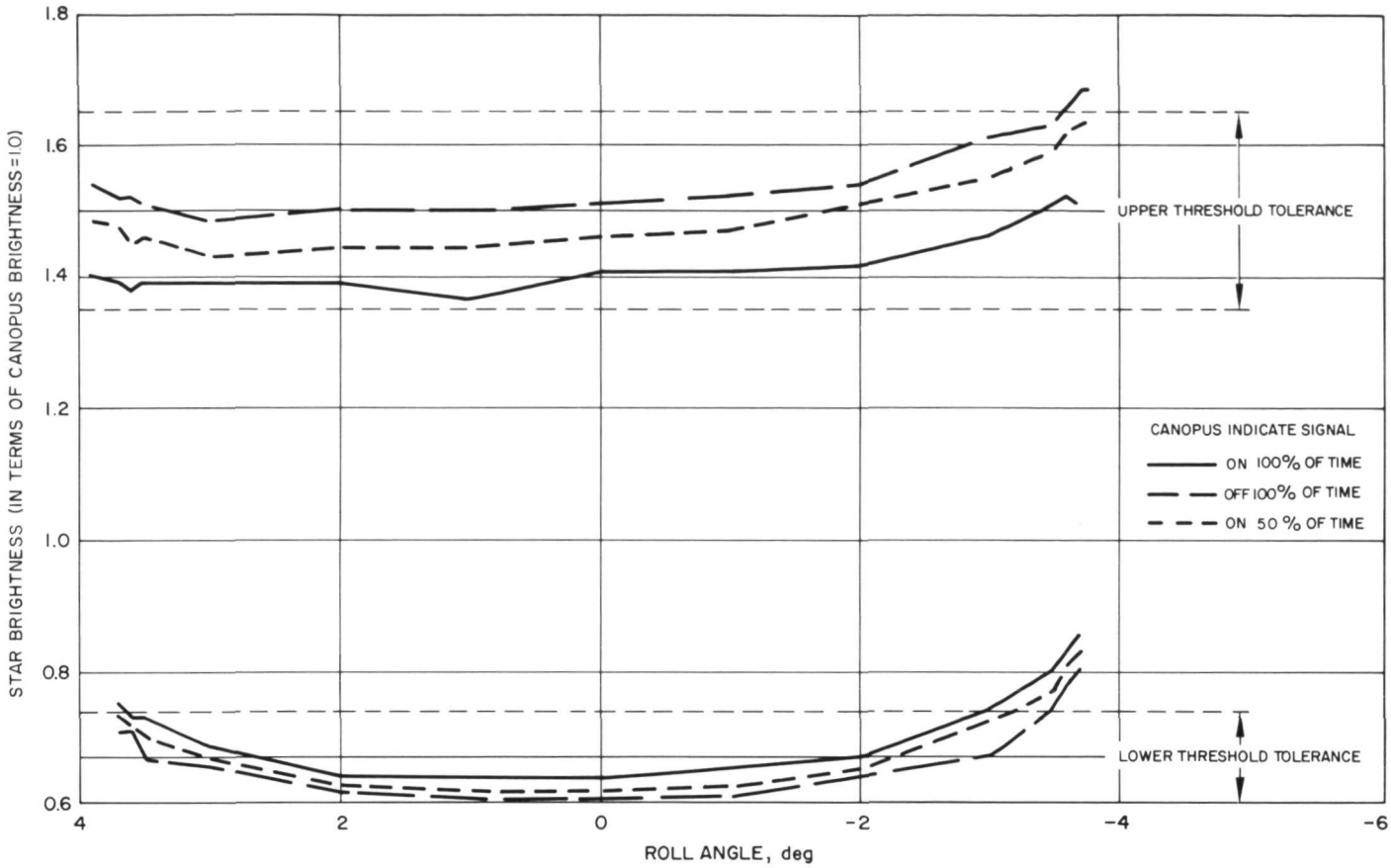


**Fig. 52. Indicate signal operation of X-2 Canopus sensor**

specification requires a discrimination capability equivalent to an intensity band of ±10% and is defined by the broken horizontal lines. The lower edge of the band must not contact the 100% OFF curve at any roll angle position. Therefore, the upper edge of the band determines the reliable field-of-view window parameters.

As can be seen, an increase in star intensity will increase the field-of-view roll angle which will maximize at 3.6 deg as Canopus approaches nominal intensity. The reason for the lack of symmetry across the field of view has not yet been determined, but data from the upgraded T-21 unit acceptance tests indicate the existence of symmetry along the roll axis field of view. There is reasonable evidence to conclude that a window roll dimension of ±2.5 deg can be assured at a magnitude 0.66 times that of Canopus. Recent tests on the air-bearing table revealed that a 2.0 deg window would be acceptable provided lockon was not required when Canopus first appears. It is intended to relax the present specification requirement to provide ±2.5 deg along the roll axis at 0.66 Canopus and ±3.6 deg at nominal Canopus.

Vibration testing of the development model (X-1) was conducted according to type approval requirements which require the unit to withstand 18 *g* input between 2.5 and 400 cps, and 4 *g* between 400 and 1500 cps, about the orthogonal axes. Tests were run shaking the unit in the lateral axis to determine a method for shifting the critical resonances, which occured at approximately 300 cps, to above 400 cps where the input of 4 *g* can be tolerated. Figure 53 shows the shift in the critical resonant frequency from 300 to 385 cps gained when the phototube mount was stiffened by welding half-cylinders into the mounting screw cutouts. Acceleration in these tests was measured at the top of the motor with the input along the axis of the photomultiplier tube. A further improvement to 400 cps was achieved with the cover in place. New sidewise restraints are being designed that should provide additional improvement.

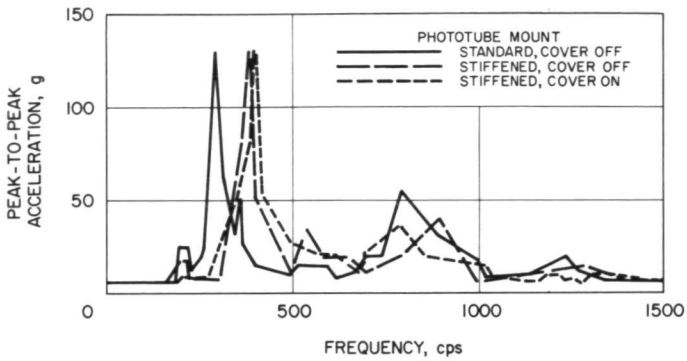


**Fig. 53. Vibration results for X-1 Canopus sensor**

It has been determined that sunlight reflected from one spacecraft leg near the sensor can enter the sunshade obliquely. Tests were conducted to determine the effect on sensor operation and compare the effectiveness of three sunshade configurations for minimizing the effect of stray light. The original shade, which has two inner baffles and two shades innerlined with open-faced honeycomb, was used with a simulated spacecraft leg of approximately 1.5 times the expected brightness. Noise on the roll error output signal remained within acceptable limits with each of the three shades when a simulated star was in the field of view. The honeycomb innerlining proved effective in reducing the stray light level. Additional tests will be conducted to determine the noise level with no star in the field of view.

Viewing of the sunlit Earth by the Canopus sensor is possible when launching early in the launch window. The possibility of sensor damage resulting from Earth reflections is under investigation. Calculations show that the light input could be as much as $10^6$ times greater than Canopus intensity. While it appears that the sensor circuitry has been designed with inherent limitations on the current of the photomultiplier tube which will protect against damage from bright sources, a test will be conducted using white clouds as a reflection source to verify that no damage results.

*b. Sun sensors.* Assembly and alignment of the primary Sun sensor for the T-21 spacecraft was completed. The sensor will be available for assembly as part of the sensor group wiring harness following completion of flight acceptance tests in December. Fabrication and assembly of the primary and secondary Sun sensor type approval units, as well as the upgraded secondary Sun sensor for T-21, will be completed in December.

### 6. Inertial Reference Unit

*a. Instruments.* Seven gyros are currently undergoing acceptance tests; two are being subjected to ten-cycle drift tests while the remaining five have started dynamic tests. One gryo (S/N-24) failed to pass the ten-cycle drift tests and was returned to the vendor. Another gyro (S/N-20) has successfully passed all tests and is available for installation in the upgraded T-21 inertial reference unit.

A coordination meeting was held with Kearfott to discuss the acceptance-rejection problems of gyros delivered to date. Of the total of 24 gyros received, 11 have been accepted by Hughes while the remainder are in various stages of testing or rework. There have been three rejections for internal short-circuit problems, four rejections for excessive drift, and three rejections for torquer scale factor discrepancies. The cause of the short-circuit failures has been determined and corrective action taken. The nature of each failure has not been repeated in any other gyros to date. It was agreed that the drift failures would all have been detected prior to delivery if a "burn-in" test of reasonable duration such as ten cycles and 50 hr operation had been performed on each gyro before shipping.

Test setups, test techniques, and data were discussed in an effort to isolate the cause of gyro torquer scale factor discrepancies. It was found that Kearfott has been using the 50-w warm-up heater to maintain gyro operating temperature with the gyro case exposed to the laboratory environment. In tests made at Hughes, only the 10-w operate heater is used and the gyro is shielded from convection currents in the room to maintain proper temperature. It was then considered that a variation in temperature of the gyro case, and consequently the trimming networks, could be realized between these two techniques of thermal control. Any such temperature difference would certainly affect the torquer scale factor calibration. Tests were run both at Kearfott and Hughes to confirm this variable as a source of error. Results were essentially identical, proving that the scale factor is approximately 0.05% lower when the gyro is testing using only its operate heater. The gyro procurement specification is being changed to make this a requirement for future procurements. It was also decided that all future calibrations of torquer scale factor by Kearfott, including reworks, should include the observed nominal value shift after potting of the padding resistor and after run-in.

*b. Unit design.* A decision was made to incorporate a new gyro temperature controller design into the inertial reference unit because of operational problems encountered during unit and subsystem tests. The old design which utilized an ac bridge circuit required precise matching of components in order to achieve the desired performance with a given gyro. In addition, the circuit

was extremely sensitive to noise and stray gyro capacitance which biased the operating temperature level. The new design uses a dc bridge circuit requiring approximately half as many components operating from a single voltage source instead of three, as was the case with the old design. Final drawings of the new controller have been completed and parts procurement initiated. Although the gyro temperature controller change will cause assembly of the upgraded T-21 inertial reference unit to be moved back to January, no delay of scheduled sensor group deliveries is anticipated.

A test specimen of the second surface thermal control mirror was bonded with the same epoxy bonding technique that is used on the inertial reference unit fiberglass structure and was successfully thermal-cycled from room temperature to 200° F with no resulting cracking of the mirror. Additional tests will be made to determine the effect, if any, of creep over long periods of time. Tests using a silver-filled epoxy for mirror bonding were unsuccessful because the high viscosity of the epoxy resulted in voids along the bond line which could produce mirror cracking under certain conditions. A smaller mosaic pattern mirror was tested also, but appeared to offer no advantages over the existing 4-section mirror design.

The initial results of inertial reference unit thermal-vacuum tests indicated that temperatures were running 15 to 20° lower than expected based on thermal analysis computer studies. It appears that the inertial reference unit thermal model may not be valid with respect to thermal characteristics of the simulated gyros. Measurement of operating temperatures on the spare T-2 unit indicate that the overall unit temperature is higher than that achieved on the thermal model. Depending on an evaluation of the sensor group thermal-vacuum test results, it may be necessary to perform additional unit tests with an actual inertial reference unit in order to verify the validity of the thermal design.

### 7. Attitude Controls

*a. Gas jet system.* A total of four gas tanks have been received from the vendor. Additional tank deliveries will be delayed pending completion of the tank qualification test program and a demonstration of tank reliability to be determined by comprehensive inspection and tests. One tank failure occurred during the ninth cycle of a ten-cycle acceptance proof pressure test at a pressure of 7750 psig. Engineering laboratory analysis of the ruptured vessel failed to reveal any physical or metallurgical cause for this failure. An investigation is being made of manufacturing processes and handling procedures in an effort to determine the cause and remedial action necessary to prevent similar failures in the future.

Initial results indicate that a contributing factor in the failure may have been the presence of oxidation on the surface of the pressure vessel. A cleaning process has been discovered which appears to prevent the oxidation. A tank has been subjected to this cleaning process and is presently undergoing formal qualification tests.

During static tests on the pressure regulator at ambient temperature with variable pressures and loads, damage occurred to the solenoid shutoff valve seat due to misalignment between the ball valve and seat. Minor changes in the regulator to eliminate this misalignment are being tested. This condition, which apparently is not serious under normal regulation, prevented positive solenoid valve shutoff and produced a small valve leak.

The jet valve ball seat was changed to improve life and reduce leakage. The new jet valve step seat is shown in Figure 54. The step seat design permits seat forming without throat deformation and provides a smaller seat with increased ball valve guide and support in the open position to improve resistance to vibration. Jet valve leakage tests after vibration and 50,000 cycles of operation indicate that the step seat design will meet the specification requirements of 0.6 $in^3/hr$. Acceptable correlation of flow and thrust measurements at sea level and vacuum conditions was obtained.

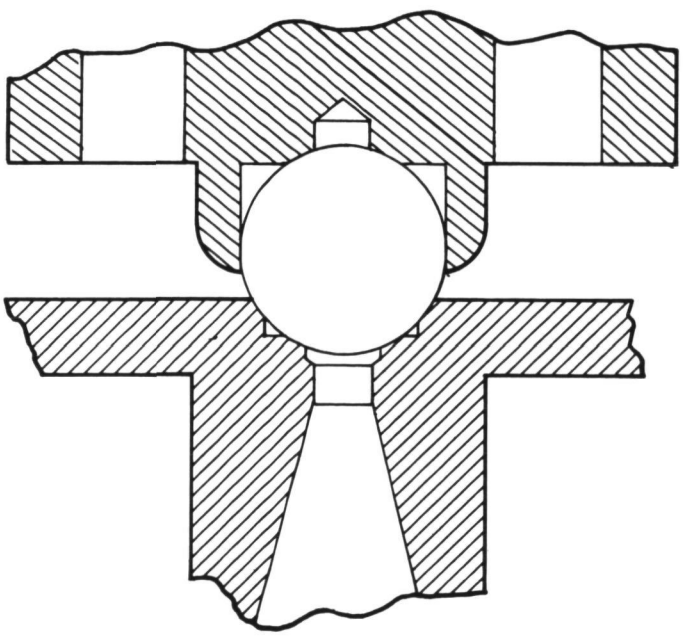

**Fig. 54. Jet valve step seat**

Thermal analysis of the gas jet system indicated that reduced gas temperatures at the jet valves due to expansion and lack of heat recovery from the lines could reduce the total impulse by as much as 10%. Consequently, it is planned to provide thermal insulation between the manifold supports on the spacecraft legs and the jet valve mountings to increase gas temperature and maintain the desired total impulse. Although thermal control of the gas tank itself is not required during normal transit operation, the gas supply will be thermally coated to prevent excessively high tank temperatures during injection and while on the lunar surface. The most desirable thermal finish appears to consist of vacuum-deposited aluminum on the bottom half of the tank as viewed normal to the lunar surface with the top half covered by a high emittance black paint.

The squib valve electrical requirements have been changed to 1-amp, 1-w, no-fire. The reliability demonstration program has been approved and the procurement specification is being changed to permit leakage after operation of the dump valve and to prevent a possible requirement for two different squibs. Ten production type units are in fabrication. Two will be used for qualification tests by Hughes. The remaining eight will be given a destruction test as part of the reliability demonstration program.

Engineering models of the gas jets and gas supply were supplied for the T-21 vehicle for initial system tests. Upgraded versions of the gas jets and gas supply will be available for the T-21 in February.

***b. Roll actuator.*** Acceptance tests on the T-2 spare roll actuator were completed and the actuator was delivered for system tests on the T-2 spare vehicle. This actuator experienced an electrical null shift during vibration testing which was traced to a failure internal to the potentiometer. The failure resulted because the engineering model potentiometer used a three-piece armature: two stub shafts epoxy-cemented to the rotor laminations. The cantilever-mounted gear on the shaft, when vibration loaded, broke the epoxy bond and permitted the rotor to creep at certain frequencies. The malfunction was corrected by replacing the potentiometer and reducing the gear weight by about 60%.

Potentiometers being obtained for flight hardware will have a one-piece shaft in the rotor and will be coupled directly to the actuator shaft instead of being gear driven. Both the T-2 and T-2 spare roll actuators are essentially engineering development models which use an all-spur-gear train. Test results on these actuators provided the basis for specifications for flight quality hardware. Motors and induction potentiometers procured to these specifications were received and are undergoing acceptance tests prior to assembly of the upgraded T-21 roll actuator, which is expected to be completed in February.

Because of problems caused by excessive wear in the final stage worm-gear design which resulted in an unacceptable roll control system limit cycle during mixed simulation tests, an all-spur-gear design was initiated. Layouts of the new design were completed and final drawings are expected to be released in January. The all-spur-gear design will require a slightly larger housing than the worm-gear design, but weight and envelope requirements are not exceeded.

This design is a four-stage gear train of approximately 4000 to 1 reduction. For reasons of reliability and weight, the three sets of gears between the motor and output shaft will be fabricated integral with their respective shafts. Lubrication on gears and bearings will be of the dry lubricant type. Mechanical stops that limit the output shaft travel will be on the next-to-last gear shaft to reduce loading and permit greater tolerance in positioning. In addition, the inertia loading of the motor as seen by the stops will be reduced by a factor of 47 at that position. The essentially rolling contact of the spur gears is the characteristic which alleviates the excessive friction and hence the limit cycle problem peculiar to the worm gear design. The spur gear also provides an increase in gear train efficiency to compensate for the potentially marginal torque characteristic of the motor, which was described in a previous report. The present motor and induction potentiometers will be used with the new design.

Evaluation of an improved worm-gear final stage is continuing in order to provide a backup design for the roll actuator in the event that the all-spur-gear design presents a schedule problem. Drawings of a redesigned set of worm gears were completed and fabrication is in process. The design improvements consist of an enlarged tooth size to reduce tooth surface loadings, as described in the previous bimonthly report, and an increased lead angle to provide greater efficiency. The additional gear reduction caused by the increased lead angle was compensated by a minor change in the spur gear section so that the overall gear reduction remains unchanged. It is felt that the possible advantage to be gained by completing the evaluation of the worm gear design to provide a backup for the all-spur-gear design warrants the expenditure of the minimum effort involved.

The basic design approach for the roll actuator requires the pressure inside the housing to be no less than 10 Torr. A glass-filled teflon gasket is used for the static seal. The shaft seal, through which the actuator drives

the vernier engine, is a face seal type in the configuration of an all-teflon diaphragm. It will have a flat, smooth face lightly preloaded against a polished face on the actuator driving arm.

Initial development evaluation tests of this design were successfully completed. A simulated actuator with the rotating seal was placed in a bell jar which was then evacuated to less than $10^{-4}$ Torr. The pressure inside the simulated actuator was monitored, with the results shown in Figure 55. The seal was oscillated in a manner simulating actuator operation for two 5-min periods. The pressure in the bell jar was held at less than $10^{-4}$ Torr for 250 hr, and the actuator internal pressure did not go below 360 Torr. During the next 175 hr, a pump leak occurred and the bell jar pressure gradually increased to 39 Torr, at which time the test was terminated. The actuator pressure at this time was only 330 Torr. Since pressure differential across the seal is the primary criterion of sealing efficacy, it is expected that subsequent hard vacuum tests will result in acceptable performance.

### 8. *Electronics Unit*

The T-21 electronics unit will be subjected to unit functional tests in the flight acceptance test console and delivered to the system test area in December. This console (Figure 56) permits integrated testing of the programmer and decoder, the electrical conversion unit circuits, and the control circuitry. The T-21 unit will function essentially the same as the upgraded T-21 unit and type approval test unit and differs only in the partial use of nonqualified components.

Two chassis from the unit are shown in Figures 57 and 58. Chassis 1 (Figure 57) contains the optical signal amplifier circuits and gas jet circuits. Chassis 3 (Figure 58) contains three modules of coast phase logic circuitry, the doppler modulator circuitry, and thrust phase pitch and yaw shaping amplifiers.

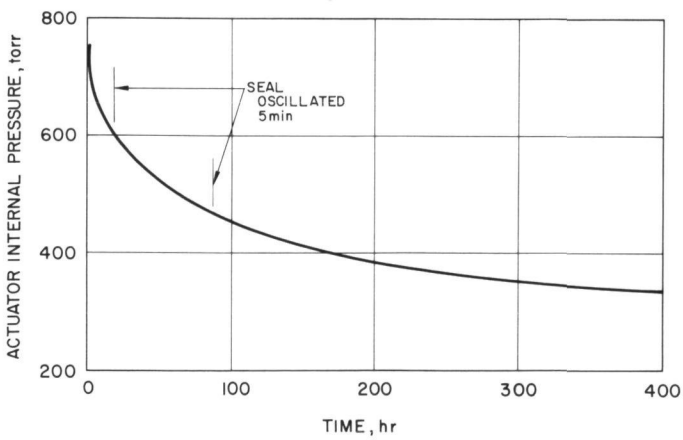


**Fig. 55. Pressure within simulated actuator**

The T-21 flight control programmer circuit boards (Figure 59) were delivered for assembly as part of the control electronics unit. The four boards are shown in test (Figure 60) using the programmer test console.

After an evaluation of the results of the weight reduction study described in the previous bimonthly report, it was decided to implement replacement of the transformers used in the bilateral switches with a smaller type, which would affect 24 transformers and save about ½ lb. This change will be incorporated in the upgraded T-21 and type approval units. The remaining proposals were ruled out after careful consideration, primarily because the weight reduction achieved did not warrant the effort involved, as well as the possibility of schedule slippages.

Based on experience gained with system testing of the T-2 electronics unit, the following changes will be incorporated in the upgraded T-21 unit:

(1) Addition of a regulator to the 29-v and −29-v coast phase power supplies.

(2) Utilization of decoupling techniques on the 29-v and −29-v thrust phase power supplies.

(3) Separation of the battery power leads to the various electrical conversion units within the electronics unit to minimize conducted interference.

(4) Installation of spike suppressors in the electrical conversion unit circuits.

(5) Use of heavier gauge wire between the electronics unit and the central power source.

(6) Use of desensitizing circuits in critical control circuits.

It is estimated that the time required to productize the changes will delay delivery of the upgraded T-21 unit to system test until February.

During T-2 subsystem tests, the interface between the roll-shaping amplifiers and the roll modulator exhibited a breakdown phenomenon in which a point of bistable operation was reached accompanied by a hysteretic variation of signal beyond this point. The point at which the breakdown occurs was a function of signal amplitude. The exact cause of this problem, which decreases the dynamic range of the roll actuator, has not yet been

established. Although this problem was not experienced on the early breadboard circuits, the T-2 electronics units and present breadboard circuits exhibit this characteristic. Investigations are continuing, with initial results indicating the possibility of a breakdown in the modulator transistors due to the presence of large transients caused by the lead-lag shaping network in the shaping amplifier.

Fig. 56. Test console for flight control electronics unit

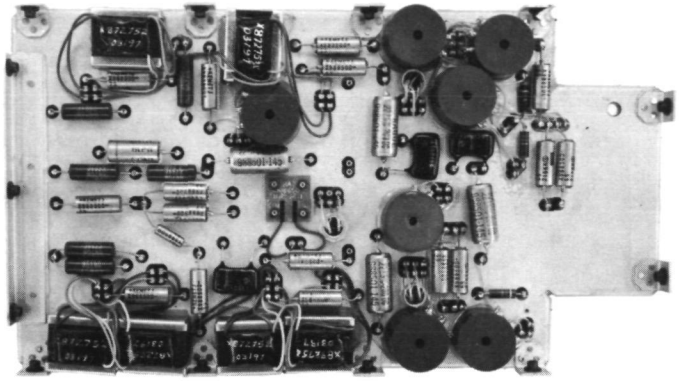

(a) Top view

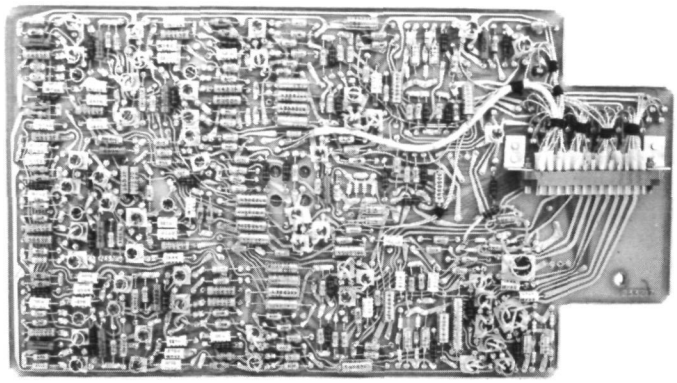

(b) Bottom view

Fig. 57. Chassis 1 for T-21 electronics unit

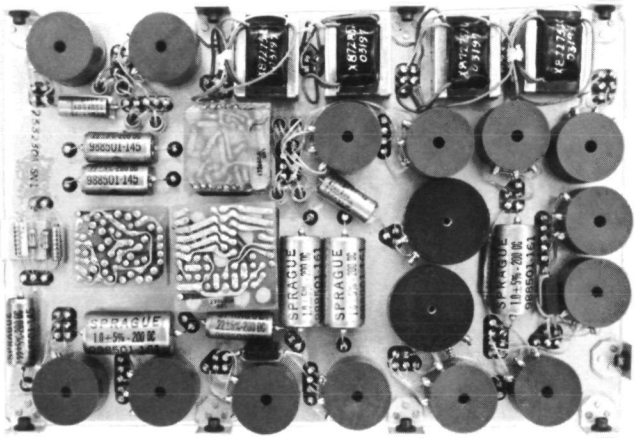

(a) Top view

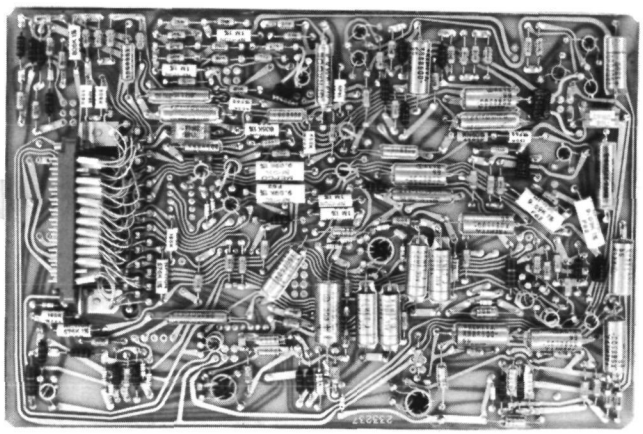

(b) Bottom view

Fig. 58. Chassis 3 for T-21 electronics unit

Fig. 59. Circuit boards for T-21 flight control programmer

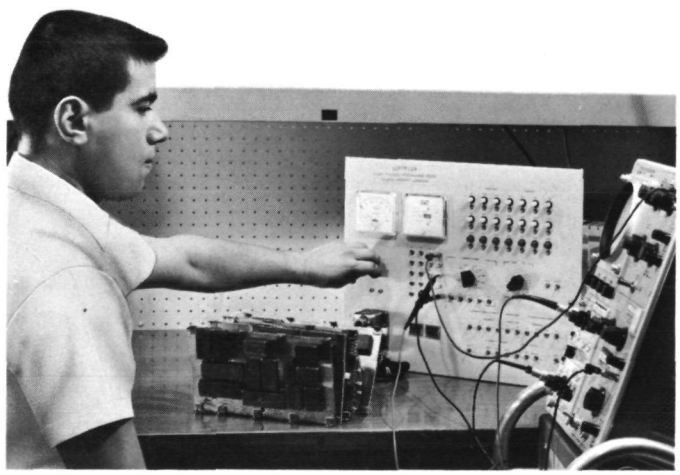

Fig. 60. Testing of circuit boards for T-21 flight control programmer

A mechanical model of the electronics unit was fabricated for combined sensor group vibration tests. This unit has been modified to reflect the addition of the eleventh chassis.

# E. Electronics

## 1. Introduction

The various systems of the spacecraft used for receiving and processing Earth-originated commands and transmitting data to Earth are covered in this section. Included are (1) the radio frequency components consisting of two identical receivers and transmitters which assure reliability through redundancy, transponder interconnection circuits for operating the receivers and transmitters in the transponder mode, and the planar array (high-gain) and two omnidirectional antennas; (2) command decoding circuitry which receives Earth commands from the receiver and provides output signals to command all spacecraft functions; (3) signal processing circuitry for processing data from individual scientific experiments, processing basic spacecraft data through the engineering signal processor, and final processing and multiplexing of data which modulates the transmitter. Also included are the radar systems associated with flight control functions of the spacecraft. The television system, spacecraft flight control electronics, and power management are discussed in Sections B, D, and F, respectively.

## 2. Planar Array (High-Gain) Antenna

The primary function of the planar array antenna is to concentrate the energy of the wide-band television channel in the direction of the Earth. It is located high on the central mast of the spacecraft and will be used for transmitting some of the telemetry data.

The high-gain antenna is a slotted waveguide planar array which is circularly polarized. This polarization is accomplished by utilizing crossed slots and pairs of linearly polarized planer arrays in a given aperture. These two interlaced arrays are fed in time quadrature. Higher order beams, characteristic of large slot spacing, are eliminated through the special placement of slots. In addition, corrugations in the waveguide produce the small amount of wave slowing which completes the suppression of higher order beams. This antenna has the following characteristics: gain of $27 \pm 0.5$ db, 3-db beam width of approximately 6.5 deg, and polarization which is elliptical with an axial ratio under 2 db.

Fabrication of the initial antenna, an engineering model, for T-21 has been completed. The antenna weight was below the allowed amount. The only electrical requirement was to present an impedance match to the transmission line, which was done quite satisfactorily. The other electrical parameters were measured to check on the fabrication technique. On this particular model some tolerances were not held within close range. Nevertheless, electrical performance was encouraging. The gain was only 1.8 db below the specified 27.0 db, and the axial ratio at 2.3 db was only 0.3 db above the maximum allowed.

Efforts are continuing on the fabrication of the aluminum-clad fiberglass aperture plate with "corrected" slot lengths as described in the last bimonthly report. In addition, as an alternate approach an aperture plate has been fabricated using 10-mil copper-clad circuit-board type fiberglass laminate. It has the same "corrected" slot lengths and will be tested on the planar array test bed.

Drawings have been completed and checked for the antenna configuration which consists of aluminum-clad fiberglass corrugations and aperture plate. However, high-temperature tests indicate some redesign will be necessary. The amount of redesign will be determined after two development models, now under construction, have been tested. The redesign will consist of changing materials to match linear coefficients of thermal expansion, thereby minimizing thermally induced loads in the expected temperature environment.

Following design selection–based on weight, electrical performance, cost, reliability, and productivity–fabrication will proceed on a T-21 upgrade unit. The development models are expected to prove manufacturing processes and aid in selection of an optimum design for flight hardware. The developmental models will be expended in environmental test. Fabrication of the first one of these development antennas has been completed. It is primarily an all aluminum unit, with the aperture plate consisting of 10-mil aluminum with a 2-mil teflon cover. This antenna has a short on the load end. Electrical testing has been completed with the following results: gain, 27.0 db; axial ratio, 1.0 db; and beamtilt, 7.2 deg. This unit is now scheduled for vibration tests.

A reworked structural model has been delivered for vibration test.

### 3. Omnidirectional Antenna

The omnidirectional antenna system is designed to provide essentially spherical antenna pattern coverage about the *Surveyor* spacecraft. It is to be used in conjunction with the spacecraft command system, doppler velocity tracking loop, telemetry and television link, and transmitter used for initial acquisition by the tracking station.

The antenna system consists of two circularly polarized low-gain antennas oriented with respect to each other and to the spacecraft in such a manner that optimum coverage is provided. Each of the two antennas is designed to provide broad pattern coverage (approximately 270 deg) in all directions except for a small cone behind the antenna within which the main bulk of the spacecraft lies.

Preliminary radiation patterns of the omnidirectional antennas on the full-scale *Surveyor* spacecraft model, MA-2, at the 3000-ft antenna pattern range have been completed. Before starting the radiation pattern work, a study was made of the antenna locations. The decision was made from this data that the first antenna would remain as is, but the other antenna would be turned down by an angle of approximately 30 deg, relative to the end of the boom.

**Table 15. Omnidirectional antenna coverage on Surveyor spacecraft Model MA-2**

| Pattern | Minimum coverage, db (isotropic) | |
|---|---|---|
| | MA-2 mounted at retro-rocket | MA-2 mounted at planar array mast |
| Right circular polarization | | |
| 2215 mc | −7.5 | −10.0 |
| 2295 mc | −4.5 | − 5.5 |
| Right and left circular polarization | | |
| 2115 mc | −5.0 | − 6.0 |
| 2295 mc | −5.5 | − 5.0 |

Radiation patterns were taken with the spacecraft mounted at the retro-rocket engine and at the planar array mast for right and left circular polarization at 2115 and 2295 mc. The minimum coverage in terms of gain relative to isotropic is shown in Table 15.

Several typical patterns are shown in Figures 61 and 62. All four patterns are right circular polarization. Three Class IV antennas have been fabricated. Two have been flight acceptance tested and delivered for T-21. The third has been delivered for type approval testing.

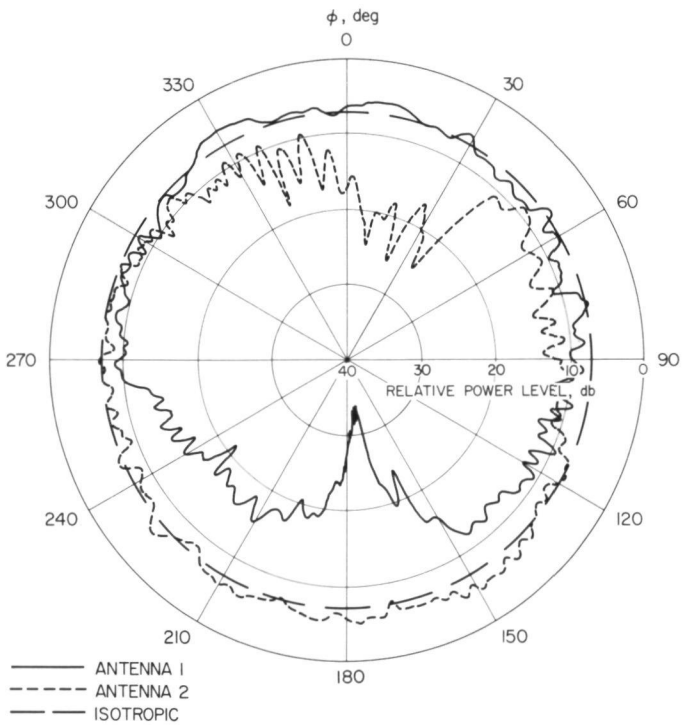


(a) Frequency = 2295 mc; $\theta$ = 60 deg

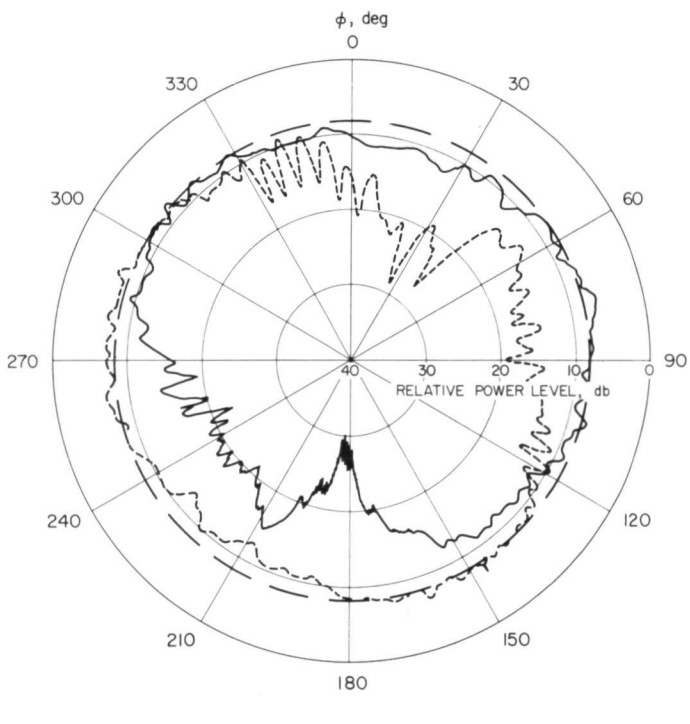


(b) Frequency = 2115 mc; $\theta$ = 60 deg

**Fig. 61. Antenna patterns with MA-2 mounted at retro-rocket engine**

**Table 16. Operational data for traveling-wave tube 349 H-104**

| | Voltage, v | Current, ma |
|---|---|---|
| Filament | 5.2 | 285.0 |
| Anode[a] | 60.0 | 0.048 |
| Cathode[a] | −1250.0 | 6.3 |
| Collector[a] | −400.0 | 50.0 |
| Power out | 12 w | |
| Power in (total) | 51.8 w | |

[a]Voltages with respect to grounded helix.

## 4. Transmitter

Two identical transmitters are included in each spacecraft to assure reliability through redundancy. Each transmitter consists of exciter circuitry that receives video signals and generates a modulated voltage at 19.125 mc The modulated power is then amplified and multiplied to 100 mw at 2295 mc by means of solid-state circuitry. This output can be radiated directly or a traveling-wave tube amplifier may be switched into the path to provide 10 w of transmitter power. High or low power from either transmitter may be directed into any of the three antennas by means of RF latching switches.

The solid-state circuitry from the exciter up to 382.5 mc utilizes lumped constant circuit elements and is packaged in four modules. Multiplication from 382.5 to 2295 mc is accomplished with distributed constant circuitry, and the circuitry is housed in a separate package mounted adjacent to the four companion modules. An electrical conversion unit, RF switch, traveling-wave tube, diplexer, and RF power monitor complete the transmitter unit.

*a. Traveling-wave tube.* A third amplifier has been delivered. This tube has successfully met the flight acceptance test specifications and will be used in the type approval transmitter. Its RF and dc characteristics are summarized in Table 16.

*b. Product design and fabrication.* Two X6 stripline frequency multipliers have been assembled for use in T-21. These units have been successfully subjected to temperature and vibration flight acceptance tests per subassembly test specifications. Maximum output power deviation from the nominal (70°F) over the temperature range of −10 to 160° F was ±0.4 db; at no temperature did the output power fall below the required 100 mw. Vibration input to the X6 was 4 *g* rms over the frequency range 40 to 1500 cps. Final tuning and functional testing of the multipliers is accomplished in a system which

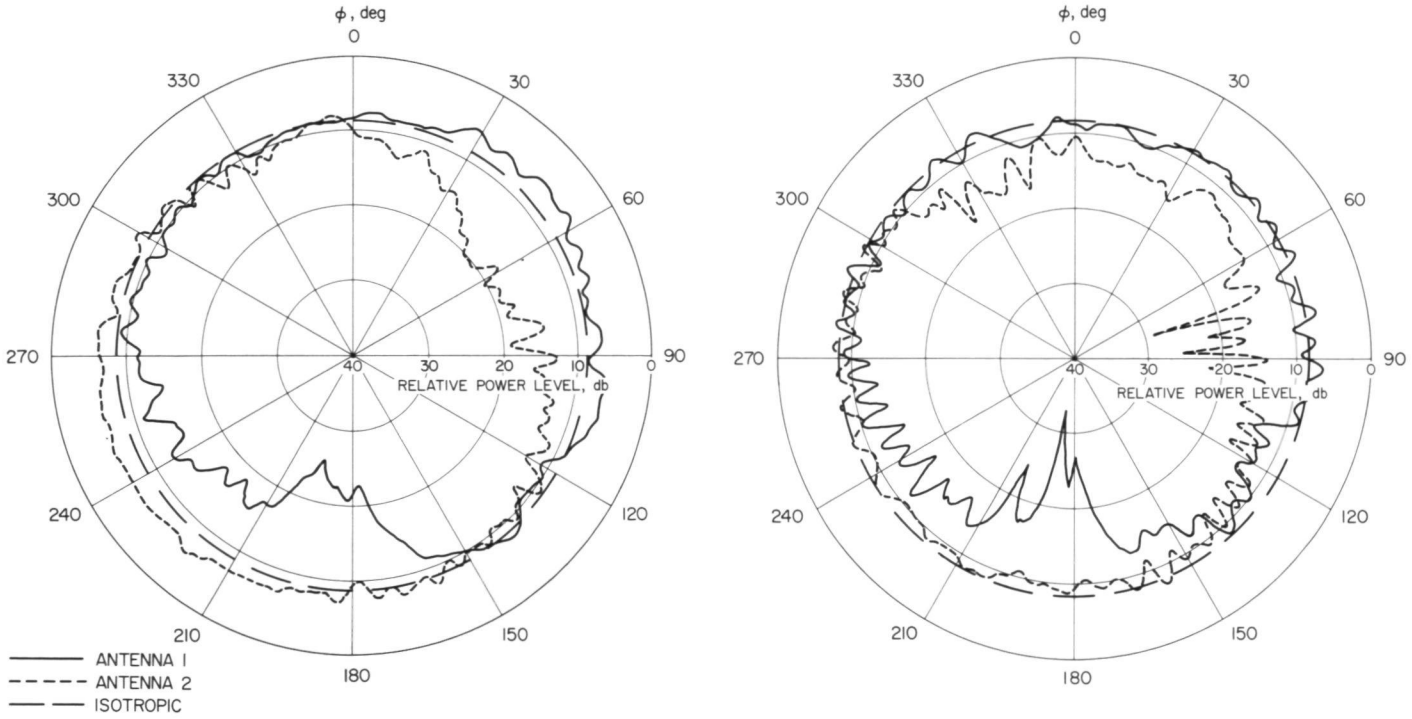


(a) Frequency = 2295 mc; $\theta$ = 140 deg

(b) Frequency = 2115 mc; $\theta$ = 140 deg

**Fig. 62. Antenna patterns with MA-2 mounted at planar array mast**

includes the diplexer, transfer switch, coaxial attenuator, traveling-wave tube, associated RF cables, and low-frequency driver.

The four lumped parameter assemblies have been fabricated and tested. During the initial test of Module IV, difficulty was experienced in obtaining the required output of 550 mw. This difficulty was traced to a defective transistor, Q2, in the second stage amplifier.

The electrical conversion unit circuit board assemblies and the conversion unit and high-frequency structures have been assembled. Final unit test will be completed and the units delivered for T-21 in December. This hardware will not be foamed until initial system tests have been completed and units are removed from the spacecraft for upgrade.

Figure 63a shows T-bar Assemblies A1 and A2 in final stages of assembly. Figure 63b shows Assembly A1 in its complete stage just prior to final bonding.

### 5. Command Receiver-Transponder Interconnections

The command link of the spacecraft telecommunications system contains two identical, independent command receivers. Both receivers operate continuously throughout the life of the spacecraft and provide continued operation of the command link in the event of a failure in one of the receivers. The command receiver operates normally as a crystal-controlled double-conversion FM receiver. Commands are frequency-modulated on a subcarrier which in turn phase-modulates the main carrier of the Earth-to-spacecraft transmissions. The digitized command signals are detected and fed to the central command decoder.

Transponder interconnection circuits are associated with each receiver so that each receiver may be connected to a transmitter for transponder operation, with the transmitted signal in phase coherence with the received signal. When these circuits are activated by command signals, the receiver operates in a phase-lock mode. The receiver local oscillator signal is fed to the transmitter exciter and transmitted back to Earth after the proper frequency multiplications have been applied to it.

The two command receivers for T-21 were delivered to bonded stores (Figure 64). Although these units were neither foamed nor environmentally flight acceptance tested, they had been electrically tested and had accumulated approximately 90 hr running time including satisfactory operation in a breadboard RF-link subsystem test position. The performance of the receivers was satisfactory over the required input signal power levels. The noise figures for both receivers were below the specified 13-db maximum. Phase lock and FM-FM thresholds were about 10 db better than the requirements.

A third command receiver unit is presently being fabricated and is to be completed in January, except for

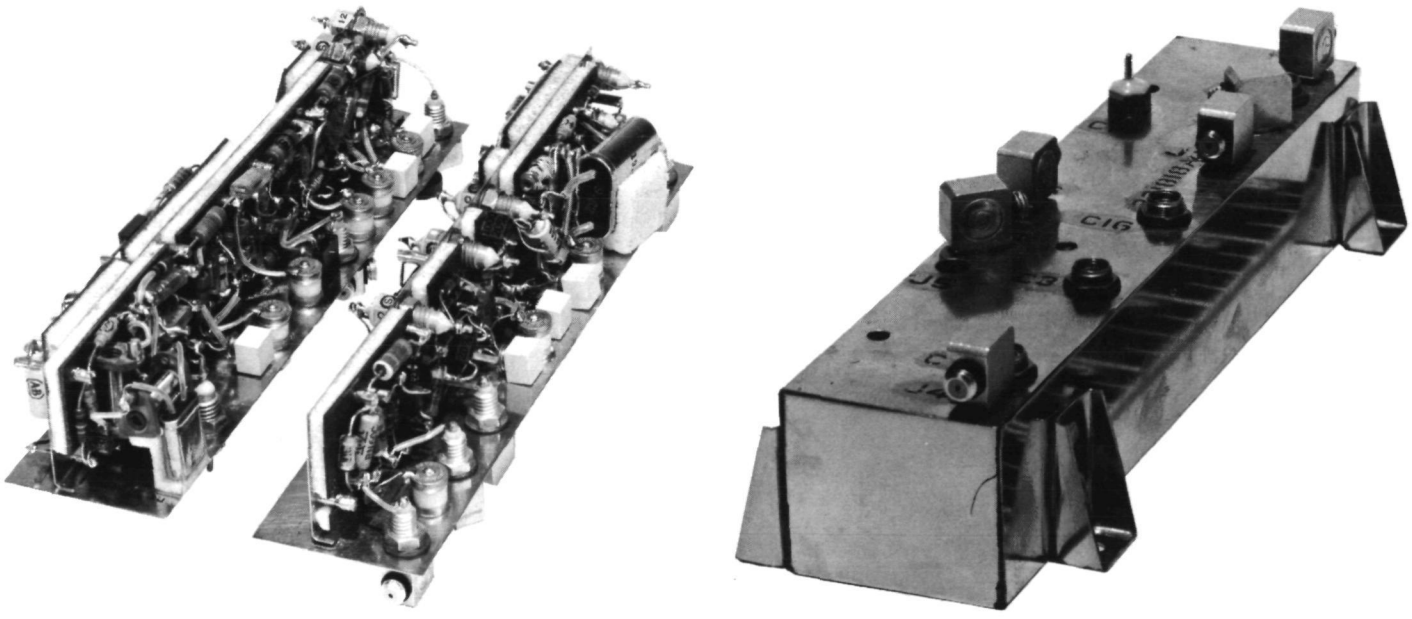

(a) A1 and A2 (b) A1

Fig. 63. T-bar assemblies

foaming. In February, after initial *Surveyor* spacecraft systems tests have been completed, one receiver will be removed and any necessary upgrading and foaming of the two receivers will be completed. The other receiver will be removed from the spacecraft in mid-March at the time of general upgrading of hardware. After upgrading and foaming, two receivers will be subjected to flight acceptance tests and returned to the spacecraft. The third will be subjected to the type approval test program.

## 6. Signal Processing

The signal processing system processes the variety of signals from the scientific instruments and the many channels of engineering information into a form suitable for modulating the transmitter. The spacecraft-to-Earth telemetry link, of which the signal processing circuits are a part, uses an FM-FM and FM-PM subcarrier system. FM-FM is used after landing and FM-PM is used during transit. Wide-band FM is used for television transmission.

The signal processing system may be divided into three main categories: (1) engineering signal processor, (2) central signal processor, and (3) the scientific signal processor.

Individual processing circuits are designed for each particular scientific instrument auxiliary. The output of the individual circuits are either subcarrier signals or signals suitable for analog-to-digital conversion.

Most of the engineering information from the spacecraft is transmitted in a pulse-code-modulation format. The engineering signal processor contains circuits for commutating the data into a single channel such that it may be converted to a digital form. Circuitry is also included to handle a few signals that require special processing.

The central signal processor is the common link in the processing system. The various subcarrier signals from the scientific signal processor are combined and fed to the proper transmitter modulator. The analog-to-digital conversion process also is provided in the central signal processor.

***a. Product design and fabrication.*** The central signal processor unit has been completed and is in final functional test. The engineering signal processor unit is now in its final assembly stages.

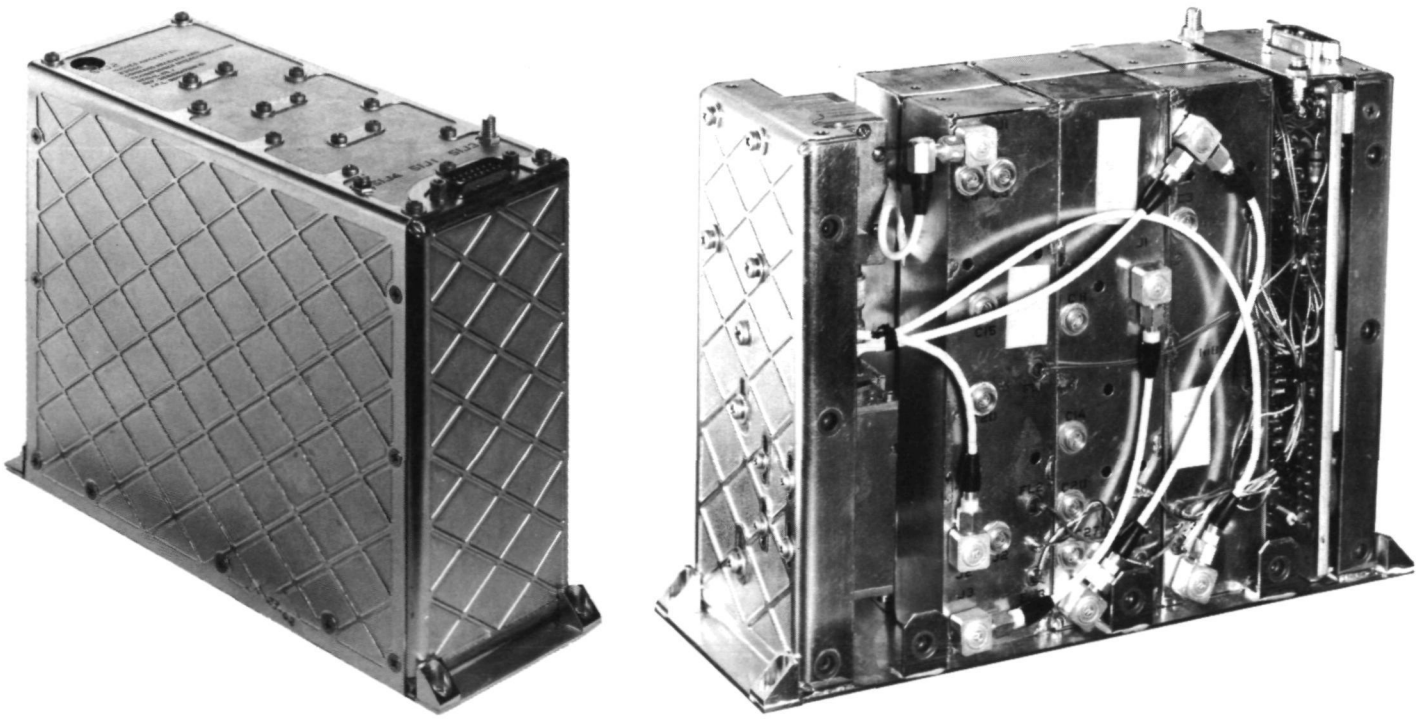

**Fig. 64. Command receiver-transponder interconnections unit for T-21**

*b. Integration and test.* A possible problem was detected while testing certain modules. There were indications that the foaming process used in encapsulating these modules tended to lower the effective resistance values of certain carbon composition resistors. The experimental modules on which this occurred had not been freeze-coated prior to encapsulation. Further investigation into this problem is being performed to ensure a complete solution.

## 7. Command Decoding

The command decoding system for the *Surveyor* spacecraft decodes Earth-transmitted command messages from the spacecraft receivers and provides output signals to command the addressed subsystems. It can handle up to 960 ordinary commands, which control on-off operations, and magnitude commands, which control time-interval operations. The system consists of two redundant central command decoders, a receiver-decoder selector, and up to 30 subsystem command decoders.

The receiver-decoder selector turns on an electrical conversion unit in one central command decoders when a message is initially received from either or both receivers. The output of one of the two receivers is selected for decoding processing. The selected receiver and the selected central decoder are determined by the states of two receiver-decoder selector flip-flops that form a two-stage binary counter having four possible states which correspond to one combination of one receiver and one central decoder. The counter is indexed to its next state every time messages stop coming out of either receiver.

To synchronize the entire operation of the command decoding system, the central decoder unit derives synchronization and timing information from the incoming commands. The central command decoder compares the address and command bits of each message to their respective complements. If this comparison fails to check, the message is rejected. One additional command interlock is incorporated in the command structure. A two-command sequence is required to execute certain irreversible or otherwise critical commands. The address bits select and turn on one of the subsystem command decoders. The command bits are decoded in a diode decoding matrix in this decoder to select one of the outputs.

*a. Product design and fabrication.* The central command decoder has completed fabrication. Figure 65 shows the basic components prior to final assembly. Figure 66 shows the complete unit during test.

*b. Integration and test.* Prior to final assembly, the modules in the central command decoder had been tested according to individual test procedures. Final unit testing prior to delivery of the unit for system integration was limited to a thorough functional test. Environmental testing will be performed on this unit during the upgrade period. This testing will follow the environmental testing of the type approval unit.

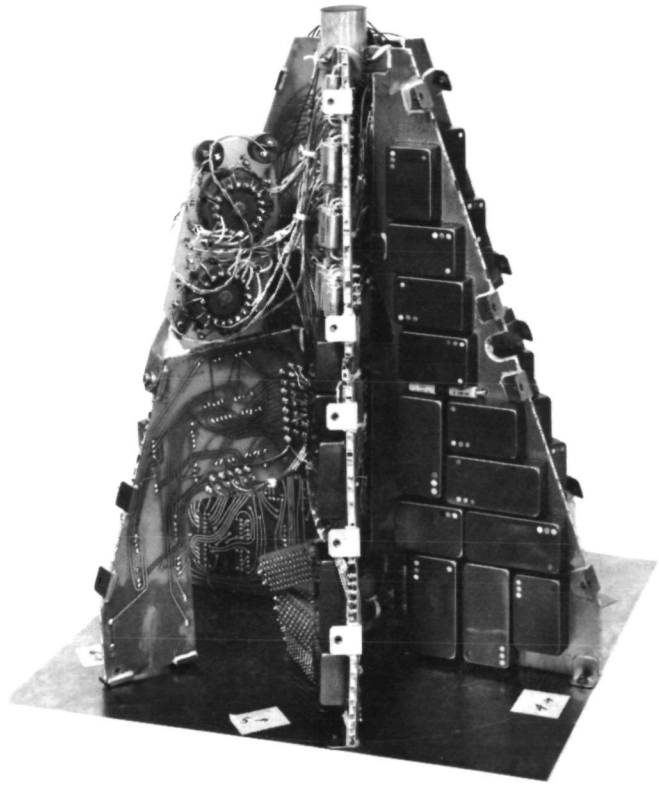

**Fig. 65. Central command decoder**

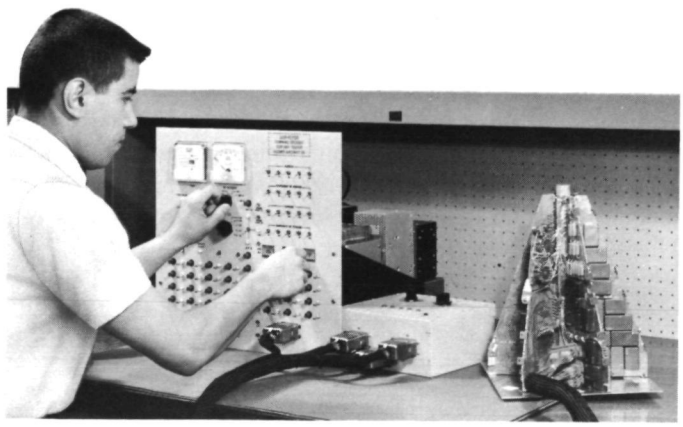

**Fig. 66. Central command decoder undergoing test**

## 8. Subsystem Testing

An integration laboratory has been established for the purpose of testing *Surveyor* electronic components as a subsystem. The laboratory will operate through two phases: (1) testing breadboard hardware received from the circuit engineering department and (2) testing prototype hardware to be received after type approval testing.

During recent tests, the video output of the TV camera modulated the transmitter for the first time and was received via the RF link and displayed on a monitor. In the test the spacecraft central decoder decoded the spacecraft receiver output and controlled the TV camera with commands transmitted via the RF link. The TV video transmitted through the RF link produced a 600-line picture.

The *Surveyor* electronics subsystem laboratory is being used to investigate various types of interactions between units. One principal area of such interactions is that of commands. The main requirements for each circuit are that it always trigger on the standard command pulse and that it not trigger on spurious energy. Measurements are being made to determine the command triggering thresholds, both in amplitude and rise time, at which the various circuits trigger. These levels will then be compared to energy levels existing on the command leads, both when a command is present and when it is not.

A simulated DSIF receiver and transmitter was delivered to the *Surveyor* electronics subsystem laboratory. A command and data handling console FM demodulator completed the test equipment required to perform quantitative RF measurements. Several problems were encountered in all three pieces of test equipment, and the necessary modifications were made during the integration.

Although the subsystem laboratory is not scheduled to check T-21 hardware, the two T-21 receivers were available and have been used instead of the breadboard receiver for quantitative evaluation. In general, it has been found that the receivers meet or exceed the design specifications on a unit basis in tests performed to date. The tests include the following:

(1) Phase-lock threshold.
(2) Phase-lock tracking range.
(3) Automatic gain control dynamic range.
(4) FM-FM threshold.
(5) Automatic frequency control pull-in range and tracking range.

One design problem was found in the receiver during integration tests of the spacecraft transponder mode and the simulated DSIF receiver and transmitter. Here, the spacecraft receiver voltage-controlled crystal oscillator was being modulated by the incoming command subcarrier (2.3 kc). This unwanted modulation appeared at the output of the spacecraft transmitter in the transponder mode; in this mode, the receiver voltage-controlled crystal oscillator is used as the local oscillator for the transmitter. The amount of extraneous phase modulation caused by the command subcarrier was 75 deg peak-to-peak. This unwanted modulation was caused by the output from the first discriminator feeding through the decoupling circuit into the local oscillator control loop. Changes are being made to correct this problem.

Quantitative testing is in progress on the breadboard spacecraft transmitter. The tests already completed include the following: (1) residual FM, (2) residual PM, and (3) data frequency response. The traveling-wave tube was successfully integrated into the breadboard subsystems with the associated electrical conversion units and power switches.

A successful operation of the breadboard TV camera with the complete RF link provided excellent qualitative results. Quantitative evaluation is now under way. The first step, writing a test plan, has been completed. A number of special fixtures, including test patterns of various line densities, are being fabricated, and the actual tests are now beginning. These tests will include quantitative evaluation of certain parameters of the TV camera that were not measured in the circuit laboratory as well as quantitative evaluation of the TV camera in conjunction with the RF link.

Evaluation of the breadboard configuration of the command decoder is complete. However, the plan is to write a new test outline to cover the evaluation of the prototype-configuration command decoder.

A test plan for the quantitative evaluation of the central signal processor has been written. The tests are now in progress.

## 9. Radars

***a. Altitude marking radar.*** The purpose of the altitude marking radar (AMR) is to indicate the proper *Surveyor* spacecraft to lunar surface slant range to fire the retro-rocket. The firing signal is generated at approximately 56 mi. The altitude marking radar employs pulse modulation of transmitted microwave energy in which the transit time of the return signal is compared to a

predetermined delay (corresponding to slant range). At the appropriate range, the presence of microwave energy in the delayed gate is detected and integrated. If a preset threshold is exceeded in two channels, a marking signal is generated as required by the *Surveyor* system.

Drawings required to add thermal insulation to the antenna dish and for the cable assembly have been completed and are in the release cycle. All other drawings have been released.

Fabrication of a video processor chassis, synchronizer chassis, and regulator-electrical conversion unit has been completed for T-21. Additional subassemblies for the type approval test unit are in process. The video processor and synchronizer chassis are shown in Figures 67 and 68. Two antenna feeds have been completed, one for T-21 and one for the type approval test unit. Fabrication of an IF amplifier and a local oscillator is in process.

Fabrication of a prototype antenna dish has been completed at Hughes, to be used on T-21 until a Class IV dish is completed. Fabrication difficulties have been experienced by the antenna dish vendor causing a delay in the delivery of a satisfactory product. The dishes developed a warp along one axis after several months of shelf life. This problem has been under study by Hughes personnel and is believed solved. A new dish is being fabricated and will be delivered in the near future.

Tests have been made of the two feeds and of the prototype antenna dish using a brass development feed. The focal length of the dish was longer than desired, which prevented adjustment of the dish to fit the template in all planes. The antenna patterns were made with the dish adjusted to fit the template in the E-plane, and therefore the dish was out of tolerance in the H-plane. The antenna pattern in the E-plane was very good, with a first sidelobe level of —30.3 db. However, the pattern in the H-plane was asymmetrical, with first sidelobe levels of —28.0 and —29.8 db.

During tests of the two feeds at temperatures around 60°F, the teflon dipole support blocks became loose and slipped out of place. One feed was allowed to warm up until the teflon block was just snug. Then the dipoles were positioned for best match by sliding the teflon block within the waveguide. This feed had the following voltage standing wave ratios: 1.04 at 9300 mc, 1.30 at

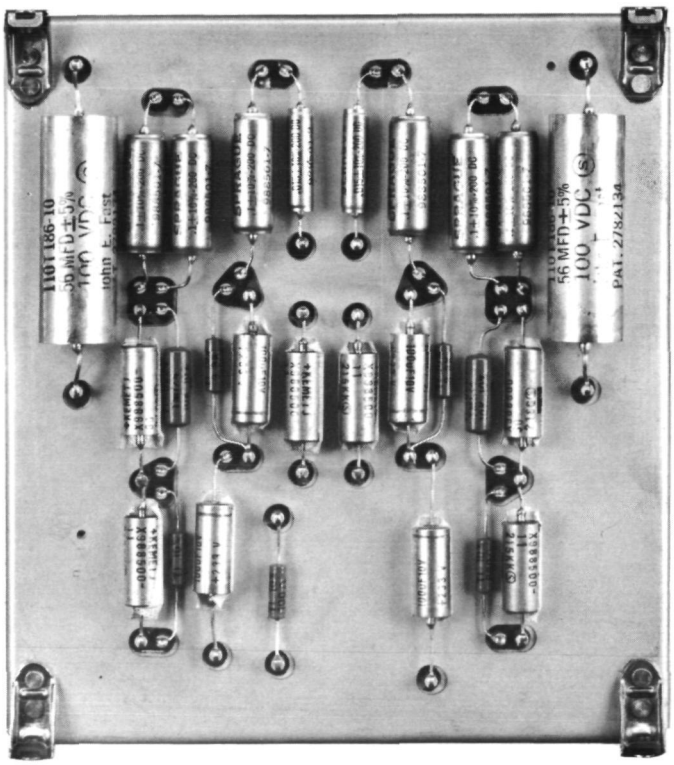

(a) Plate side

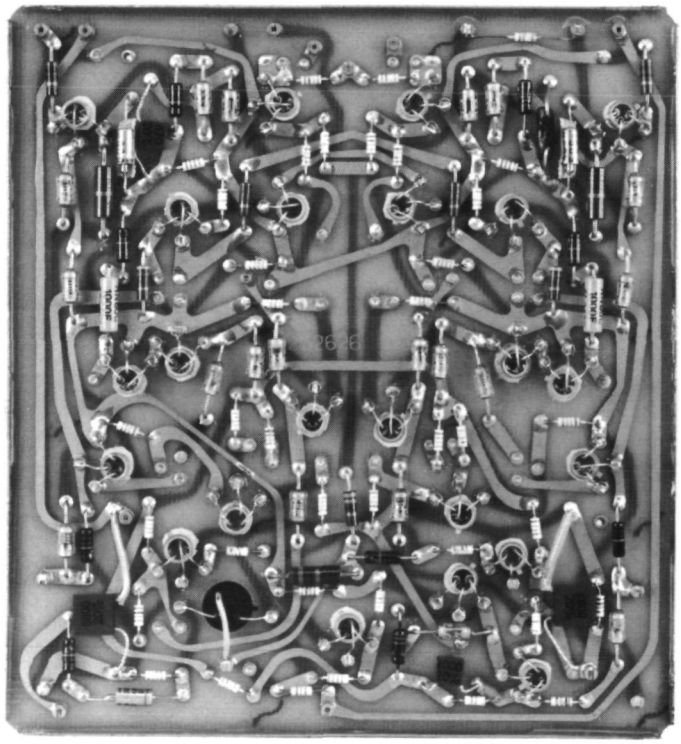

(b) Board side

Fig. 67. Video processor

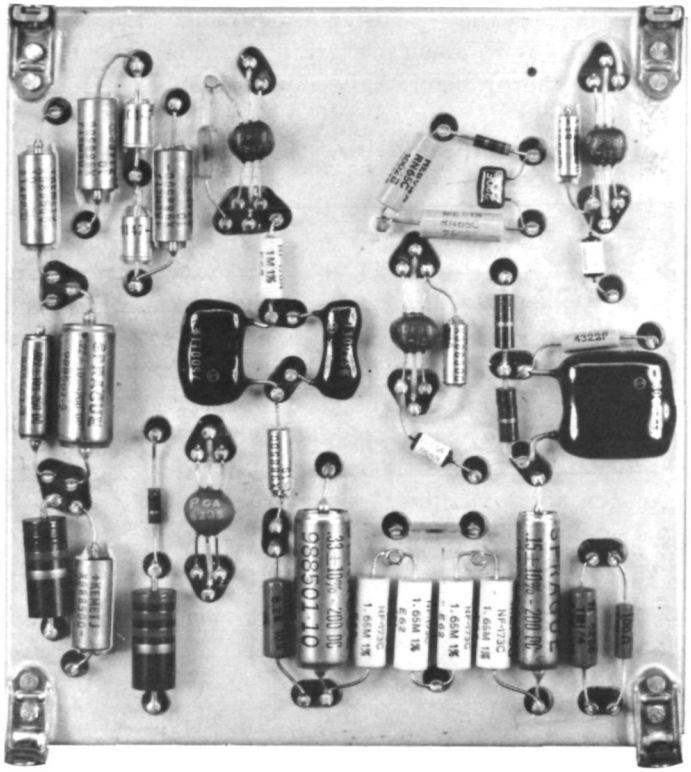

(a) Plate side

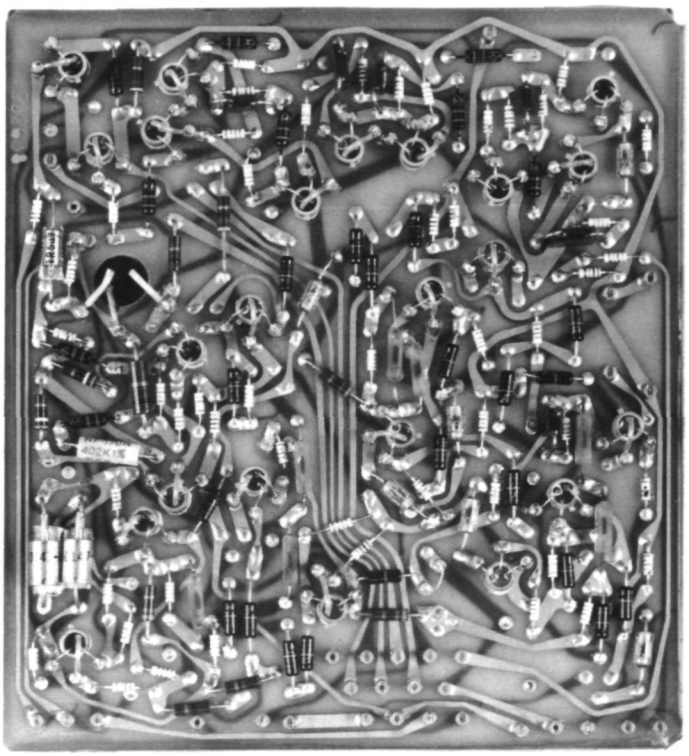

(b) Board side

Fig. 68. Synchronizer

9250 mc, and 1.26 at 9350 mc. No antenna patterns were made of these two feeds.

The subcontracted items (mixer, magnetic modulator, and RF assembly) required for T-21 have been received. A new thermal analysis of the AMR unit has been started based on the antenna dish design and nozzle configuration.

A breadboard model of the AMR antenna coupler has been designed and fabricated. This model consists of (1) a two-piece circular collar that fits over the antenna feed near the parabolic reflector surface (Figure 69), (2) a 2.5-in diameter tube 12 in long, and (3) a 3 in section of waveguide with a circular plate on one end and a waveguide choke flange on the other end. There are three tuning screws in the waveguide. The 12-in tube is threaded inside each end. The two-piece circular collar and the circular plate on the waveguide section are both threaded. When the coupler is assembled, it forms a cavity about the antenna feed.

The coupler is presently undergoing test in the laboratory. The breadboard model provides means for adjusting cavity length, position of the antenna feed in the cavity, and impedance matching by means of the tuning screws. Dimensions for an engineering model will be determined by the results of the laboratory tests in progress. Tests to date indicate that (1) close tolerance must be held in the fabrication and assembly of this coupler in order to obtain repeatability, (2) the coupler exhibits an insertion loss of approximately 4 db and (3) it will be difficult to obtain repeatable voltage standing wave ratios of less than 1.5 to 1 over the required bandwidth. A mounting fixture that supports the coupler on the parabolic reflector has been designed and is being fabricated.

*b. Radar altimeter and doppler velocity sensor.* The purpose of the radar altimeter and doppler velocity

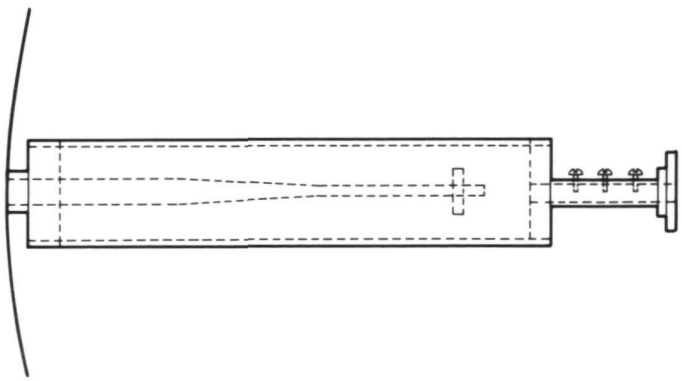

Fig. 69. Altitude marking radar coupler over antenna feed

sensor, being developed by Ryan Electronics, is to provide spacecraft altitude, attitude, and velocity information to the spacecraft flight control system during the final portion of the lunar landing phase of the mission. The doppler velocity sensor utilizes three continuous-wave radar beams to obtain three orthogonal velocity components which are referenced to the spacecraft roll axis. The radar altimeter utilizes a single frequency-modulated beam directed along the spacecraft roll axis to obtain slant range to the lunar surface.

The radar altimeter and doppler velocity sensor consists of four major units. The klystron/power supply/modulator unit includes the altimeter klystron transmitter tube and the doppler velocity sensor tube, the high-voltage power supply for the klystrons, and the FM modulator. The velocity sensor receiver-transmitter consists of an antenna which produces two of the three doppler velocity beams and also contains microwave filters and isolators, microwave-to-audio detectors, and gain-controlled preamplifiers. The altitude-velocity sensor receiver-transmitter is similar to the velocity sensor receiver-transmitter except that its function is to produce the third velocity sensor beam and the altitude beam.

The fourth unit is the signal data converter. This unit performs the search and tracking functions for all four channels and processes the signals to produce the velocity, altitude, altitude mark (1000 and 13 ft), and reliable operation signals.

The X-1 radar altimeter and doppler velocity sensor was delivered to Hughes in early December as well as associated test equipment for initial system testing. Extensive delays have been caused primarily by problems such as power supply ripple, arcing, and component and wiring failures within the klystron/power supply/modulator. It has been determined that packaging of that unit was too tight, creating the above problems and causing maintenance to be extremely difficult. To resolve this difficulty, the unit has been converted to a breadboard configuration (Figures 70 and 71), which is being used in system test. For flight use, the unit is being completely redesigned. The signal data converter is assembled in a test assembly that permits expeditious installation and removal of circuit boards. The system test equipment assembly used in testing the radar altimeter and doppler velocity sensor is shown in Figure 72.

Fabrication on the RADVS sytem Serial No. 1 has been stopped. It is being redesigned to meet the requirements of the revised procurement specification.

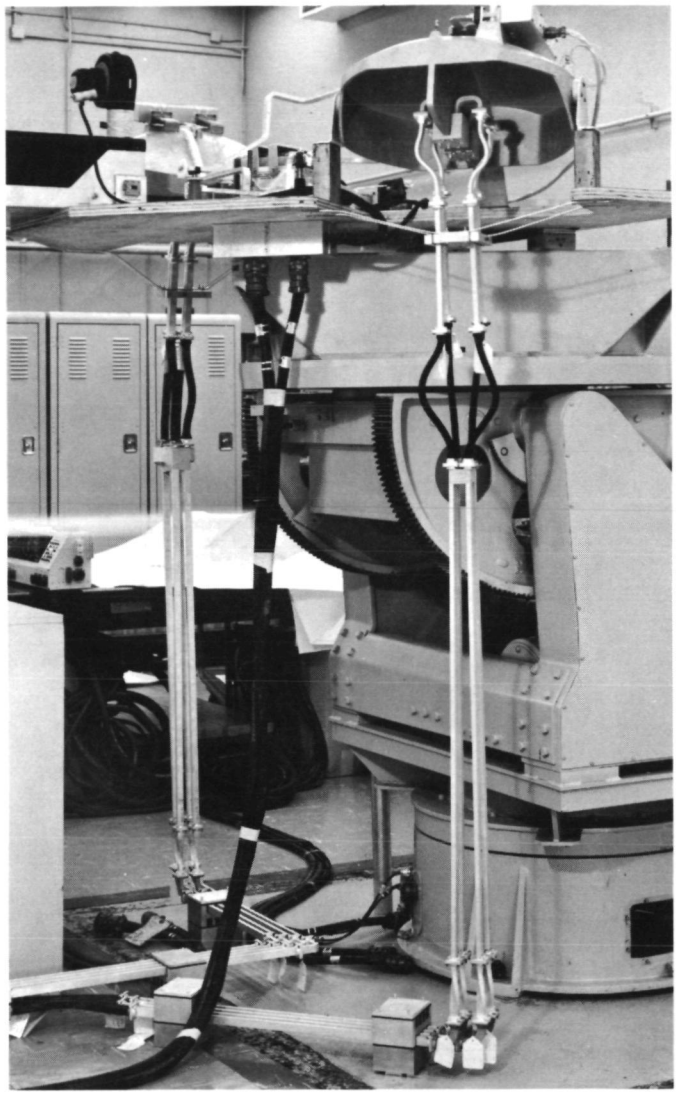

**Figure 70. Radar altimeter and doppler velocity sensor in system test**

The X-2 radar altimeter and doppler velocity sensor is in fabrication. The antennas are complete; preamplifiers, attached to the antennas, are receiving minor structural improvements. The signal data converter is complete and in test; it will require some circuit changes which are being determined by X-1 system testing. The klystron/power supply/modulator is being rebuilt to the redesigned circuit configuration with packaging suitable for use on the T-2 vehicle.

Because receipt of the development model systems X-1 and X-2 (for use on the T-2 and T-2S test vehicles) is behind schedule, a supplementary plan has been established for receiving the X-1 and X-2 systems in order to reduce delays of T-2 tests.

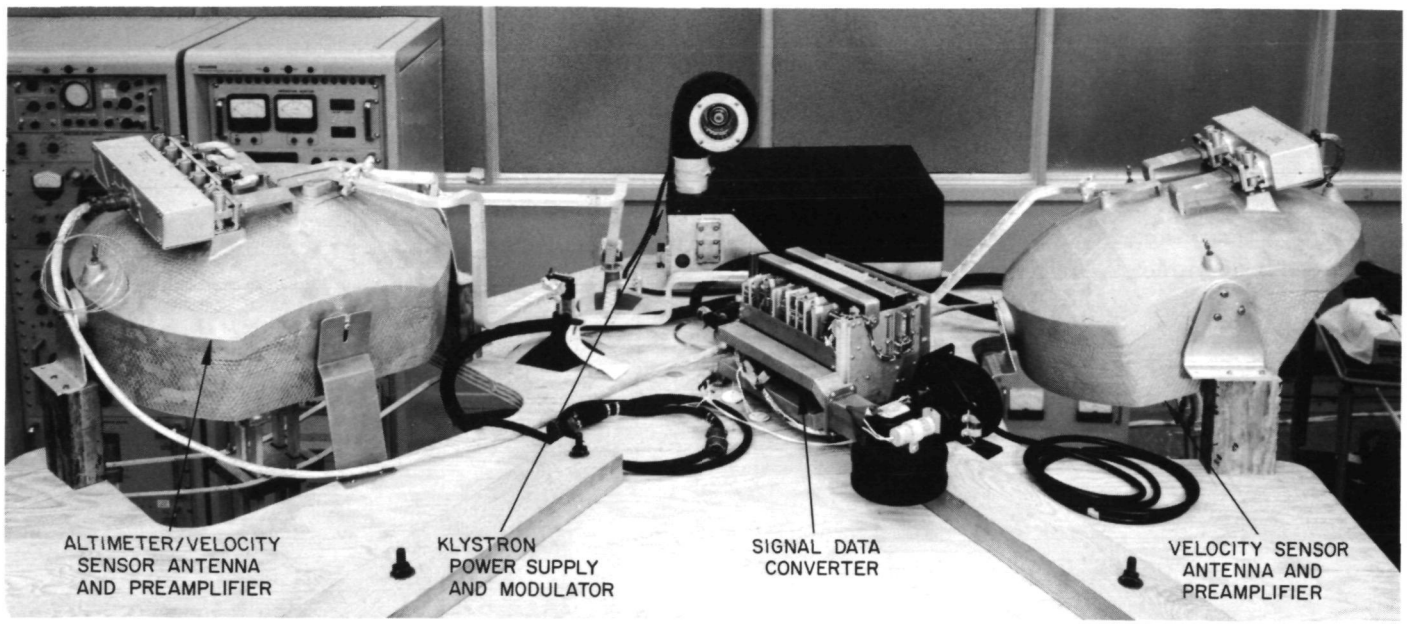


**Fig. 71. Radar altimeter and doppler velocity sensor X-1**

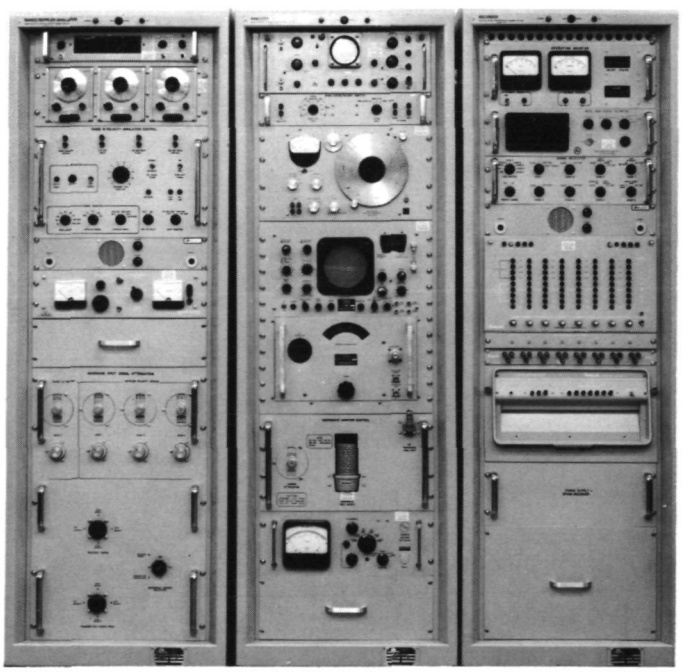

**Fig. 72. System test equipment assembly for radar altimeter and doppler velocity sensor**

System X-1 was received in an interim configuration consisting of a breadboard klystron/power supply/modulator and a test assembly signal data converter, both suitable only for preliminary T-2 system integration tests (not for T-2 drop tests). System X-2 will also be delivered with a breadboard klystron/power supply/modulator. Performance and electrical design may vary from the final design to the extent permitted by the T-2 test objectives. System X-2 will replace X-1 on the T-2 vehicle. System X-1 will then be returned to Ryan Electronics where it will be upgraded to the X-2 configuration for use on the spare test vehicle, T-2S. Hughes will fabricate klystron/power supply/modulator units for both X-1 and X-2 which are suitable for T-2 drop tests.

Studies of the current tracker design are continuing. The necessity of replacing the "bang-bang" discriminator with a linear discriminator has been established. Breadboard circuitry of a linear discriminator is in test. It has been found that the use of the linear discriminator results in a reduced level of noise on the output signal.

One set of interconnecting waveguides (Figure 73) with a configuration suitable for use on the T-2 test vehicle, has been received. Prior to chemical-milling of the external surfaces (to reduce weight), this waveguide was installed on the T-2 vehicle to verify compatibility (configuration and interference) with the T-2 application. Flanges which will mate with the antennas have not been installed at the ends of the waveguide, allowing a final fit and adjustment to the boresighted antennas by

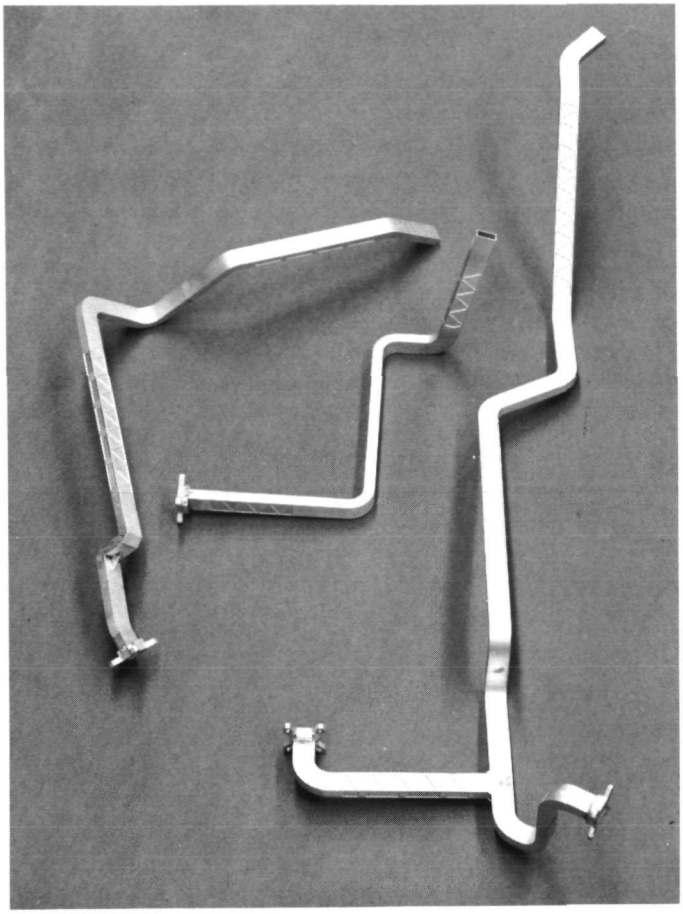

**Fig. 73. Radar altimeter and doppler velocity sensor interconnecting waveguide for T-2 vehicle**

cutting the waveguide and installing the flanges to fit as required.

The interconnecting waveguide (Figure 74) for the radar altimeter and doppler velocity sensor to be used on the T-21 test vehicle has been received and used to make an approximate check of waveguide compatibility with the T-21 vehicle. A complete check of waveguide compatibility will be made when the antennas and klystron/power supply/modulator are available.

A final configuration of the waveguide to interconnect the test equipment with the radar altimeter and doppler velocity sensor in *Surveyor* system testing has been established. This configuration utilizes a minimum number of flanges in the waveguide runs to reduce RF leakage problems.

Construction has been started on a framework to be used for investigating the effects of microphonics on the radar altimeter and doppler velocity sensor interconnecting waveguide. Since the waveguide is designed for minimum weight, it may be susceptible to audio noise and to vibration.

The shock mounts to support the waveguide have been redesigned to eliminate the use of silicone rubber, which is no longer approved for *Surveyor* applications. The new shock mount utilizes a block of wire mesh to absorb the shocks.

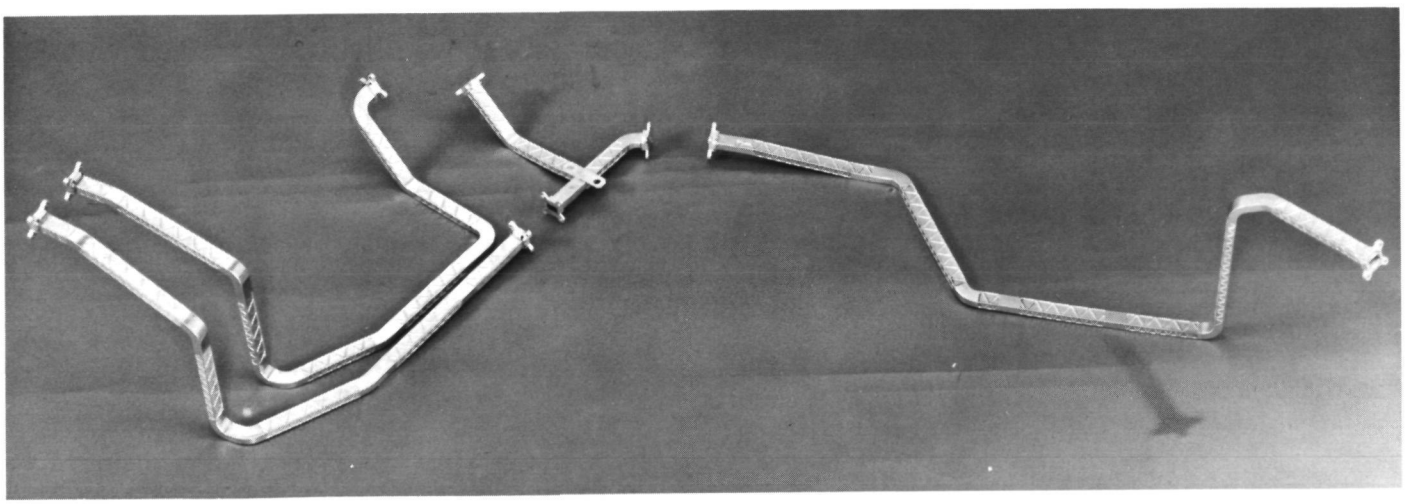

**Fig. 74. Radar altimeter and doppler velocity sensor interconnecting waveguide for T-21 vehicle**

# F. Electrical Power Supply

Electrical power for *Surveyor* spacecraft is supplied by a Sun-tracking planar solar panel and a sealed secondary silver-zinc battery. The solar panel is the prime source of power during transit and the lunar day, and the battery provides the electrical energy for operation during the lunar night.

The power management system is composed of a central power control unit and a variety of voltage converters, regulators, and power switches located in other units that provide power management for the various instruments and subsystems. The central power control unit provides power conversion from the solar panel, main bus regulation, overload sensing, battery charge control, and several switching functions. The optimum-charge regulator circuit provides the most efficient conversion of solar panel power to battery charging current. The battery output voltage from the unregulated bus is converted to the main regulated bus voltage by a boost regulator. A main overload trip circuit using tunnel-diode sensing removes all nonessential spacecraft loads when an overload condition is detected. The battery charge logic system controls the charging current to the spacecraft batteries. Normally, the system operates in the automatic mode and the batteries are charged until their voltages reach a predetermined level. A command mode is available whereby the battery may be commanded to be charged.

## 1. Progress Summary

Two thermal-vacuum tests to simulate lunar-night conditions have been completed on the second developmental solar panel. A maximum power reduction of approximately 14% in the series-parallel subgroup was incurred as the result of two open solar cell failures at $-265°$ F and vacuum of $10^{-6}$ Torr. Vibration tests at type approval test levels are 70% complete.

The T-21 dummy solar panel has been fabricated and delivered for T-21 systems test. The Norair Division of Northrop Corporation was awarded the subcontract for fabrication of the solar panel substrates. Delivery of the first three substrates is scheduled for mid-December. Fabrication of the prototype solar panel will begin late in December with completion scheduled for mid-February.

Tests and calibration of the Optical Coating Laboratories, Inc. (OCLI) solar simulator have been completed by Hughes Aircraft Company and OCLI. Spectral distribution and intensity are now within specification requirements and the simulator can be used for solar cell performance evaluation.

Development battery X-10 has satisfactorily completed fourteen 100% charge-discharge cycles, well in excess of the specification requirement of approximately five cycles. Cycle tests were stopped during the fifteenth charge period as a result of low battery voltage and reduction in capacity. Design of the prototype batteries has been changed from an individually sealed cell to a vented-cell manifolded sealed battery. This design change has resulted from tests and performance data on the experimental and development batteries which showed potential problem areas due to on-charge pressure and voltage characteristics of the battery. The new design provides an increase of 25 times in volume and will allow battery capacity to be maximized at all times during the lunar day. Delivery of the first six prototype batteries from Electric Storage Battery Company will be made on February 1, 1963.

## 2. Solar Panel

*a. Second development panel.* During the report period the second development solar panel has been subjected to low temperature–high vacuum and vibration tests. After each test, the panel was taken to Table Mountain, California for sunlight electrical performance tests. The first low temperature–vacuum test resulted in a simulated lunar night temperature of $-265°$ F. A vacuum of $2 \times 10^{-6}$ Torr was attained. At the conclusion of the test one solar cell was partially cracked and resulted in current-limiting of the series-parallel subgroup of 88 modules. The loss in maximum power for this subgroup was 1.4%.

A second thermal-vacuum test was performed in an attempt to attain a solar panel equilibrium temperature of $-300°$F. The test resulted in a temperature of $-265°$F and vacuum of $5 \times 10^{-8}$ Torr. Upon completion of the test, another solar cell was cracked. Subsequent electrical tests at Table Mountain showed the panel maximum power output reduced an additional 4.5%. This indicated

that further damage was done to the cell broken during the first thermal-vacuum test, causing it to fail completely open.

Vibration tests are now under way and tests have been completed in two planes with no failures attributed to vibration. The solar cells damaged during thermal-vacuum testing, however, did separate from the undamaged portion of the shingled module. The tests were performed at type-approval test levels from 20 to 1500 cps. The solar panel assembly and vibration test equipment is shown in Figure 75.

*b. T-21 dummy panel.* A dummy solar panel assembly simulating weight, dimensions, and center of gravity has been fabricated and delivered for use on the T-21 spacecraft. Delivery of a flight-quality solar panel is scheduled for delivery in first quarter 1963 for system environmental testing.

*c. Panel substrate procurement.* The solar panel substrate subcontract was awarded to the Norair Division of Northrop Corporation on November 9, 1962. Three substrates will be delivered by December 15 and will be utilized for type-approval testing, fabrication of the prototype solar panel, and fabrication of the T-21 solar panel.

*d. Fabrication procedures and tooling.* The solar panel fabrication procedures document and definition of assembly processes are 80% complete. All fabrication tooling drawings have been released and tooling delivery is scheduled for mid-December for initial use in fabrication of the prototype solar panel. The tooling provides for drilling, bonding, solar cell placement, and alignment of all solar panel components.

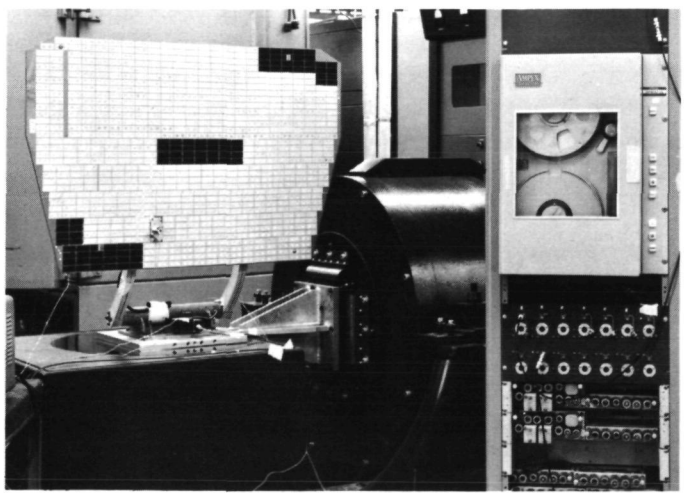

**Fig. 75. Vibration test of solar panel**

*e. Solar simulator.* The solar simulator has been returned to Hughes from OCLI, where correlation measurements were performed jointly by Hughes and OCLI. The correct xenon-tungsten lamp balance was achieved in laboratory test and a spectral distribution measurement was made. Figure 76 illustrates the most recent spectral energy distribution of the solar simulator. Although there is an excessive energy spike at 0.465$\mu$, the solar simulator is now ready for use in acceptance testing of the incoming solar cell module lots. The excess solar simulator spectral energy at this wavelength will not cause any significant error in solar cell performance evaluations since the solar cell has a very low response at 0.465$\mu$.

OCLI and Hughes pyrheliometer measurements were compared with those of several other companies at Table Mountain. Table 17 summarizes the results. As noted in the last bimonthly report, Hughes and OCLI 180-deg pyrheliometers differed by 5% in solar simulator intensity measurements performed at OCLI. Both instruments, however, provided equal measurements in sunlight. Table 17 also shows that Hughes and OCLI 180-deg pyrheliometers read 5% higher than the average of the other companies. This discrepancy can be offset by a change in correction factors, which are somewhat arbitrary. On the basis of the tests to date, Hughes and OCLI have correlated solar simulator acceptance test data and agreed upon evaluation of solar simulator performance.

*f. Solar cell modules.* There were no solar cell module deliveries during the report period. Lot 6 is expected in late December 1962.

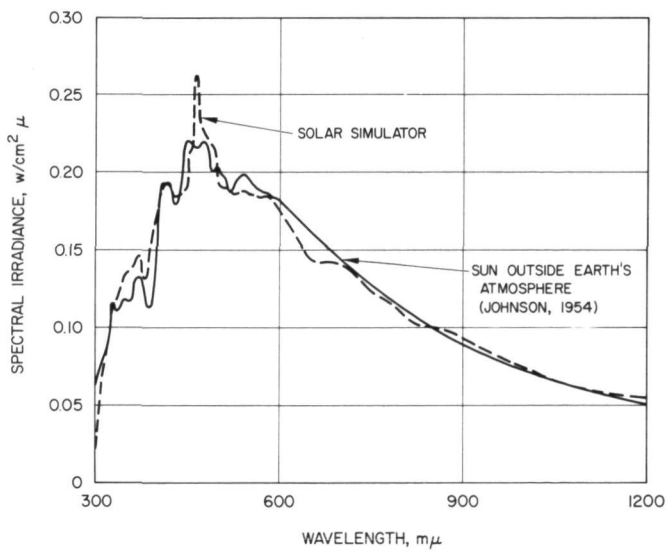


**Fig. 76. Solar simulator spectral energy**

**Table 17. Comparison of pyrheliometer measurements at Table Mountain on September 19, 1962**

Intensity in mw/cm²

| Time | Normal incident with water jacket | | 180-deg with collimating tube | | | | Temperature-compensated normal incident |
|---|---|---|---|---|---|---|---|
| | Hughes | Heliotek | Hughes | OCLI | STL | JPL | IRC |
| 1314 | | 99.8 | | | | 99.9 | |
| 1316 | | 99.9 | | | | | |
| 1319 | 102.4 | | 105.4 | | 97.9 | 99.9 | |
| 1320 | | 100.7 | | | | 100.5 | |
| 1321 | 102.9 | | 104.9 | | 98.2 | 99.9 | |
| 1322 | 102.6 | 100.4 | 105.6 | | 97.6 | 99.8 | |
| 1323 | 102.4 | | 105.4 | | 97.9 | 99.8 | |
| 1327 | | 100.6 | | | | | |
| 1330 | | 100.3 | | | | | |
| 1335 | 102.3 | | | 105.4 | 97.2 | | 100.6 |
| 1336 | 102.4 | | | 106.0 | 97.2 | | 101.7 |
| 1337 | 102.7 | | | 106.3 | 97.6 | | 101.8 |
| 1338 | 102.6 | | | 105.2 | 97.2 | | 101.4 |
| 1339 | 102.3 | | | 104.6 | 97.2 | | 102.8 |
| 1341 | | 99.6 | | | | | |

Because of module negative tab breakage, all delivered module lots were reinspected. Fifty modules out of 2000 received to date were found to have defective tabs and have been returned to Heliotek for replacement.

### 3. Battery

*a. Development battery program.* Development model battery X-10, which was employed on the life-cycle test, completed 14 100% charge-discharge cycles prior to failure. Failure of the battery was induced by malfunction of test equipment used to limit end-of-discharge voltage, causing the battery to discharge excessively. The life-cycle test was performed at 70°F and consisted of a 2.0 amp constant-current charge to 27.3 v, followed by a 5.0 amp constant-current discharge to 18.0 v. The normal discharge voltage cutoff of 17.5 v was increased to 18.0 v after the third cycle to protect one low-capacity cell, with a potential approaching 0 v at discharge cutoff. This test has demonstrated a battery cycle life well in excess of the specification requirement of approximately five cycles.

The investigation of non-uniformity of separator materials has been completed. Quantitative results were not obtained but inconsistent quality of both the Synpor and Polypor materials has resulted in elimination of these materials from the separator system. The prototype battery separator system is composed of one layer of nylon cloth and seven layers of cellophane. Both of these materials are produced in large production quantities to assure consistent quality and their use has been successful.

Cycolac cell case development has been abandoned due to molding difficulties and schedule considerations.

The test program to chemically inhibit the dynamic voltage surge characteristic has been concluded. Lead oxide was the most promising additive to the positive plate. This additive appreciably subdued the voltage surge characteristic under most test conditions but was not 100% effective for all conditions. This approach is considered promising as an eventual solution, but extensive testing of secondary effects must be evaluated before incorporating it into a flight battery. Present schedule requirements do not permit a complete evaluation of this solution, and further testing is not contemplated at this time.

*b. Prototype battery program.* A detailed evaluation of the experimental model battery program, the development model battery program, and systems compatibility tests with the breadboard central power control unit has resulted in a change in the design concept of the *Surveyor* battery. The experimental and development model batteries consisted of individually sealed cells of the type successfully used on both the *Ranger* and *Mariner* spacecraft.

Battery charge on the *Surveyor* is accomplished utilizing a constant power charge with full-charge cutoff at a battery voltage of 27.3 v. Pressure and charge voltage characteristics of the sealed cell battery have caused charging and power system control difficulties which are reflected in overall system performance. Characteristics of the present battery design are summarized and briefly discussed below.

(1) The dynamic voltage surge characteristics of the sealed silver-zinc battery is primarily a function of battery history or conditioning and cannot be adequately defined in terms of temperature, capacity, and charge rate.

(2) End-of-charge voltage limiting utilizing constant power, and the battery dynamic voltage surge characteristic, can result in premature charge termination at battery capacities as low as 30% and up to 100% of full charge.

(3) Manufacturing or forming charge methods employed for the experimental and development batteries produced good capacity balance between cells at the end of discharge, but resulted in cell unbalance at full-charge termination. This cell unbalance results in gassing of low-capacity cells near full-charge termination.

(4) Good capacity balance between cells can be achieved only by culling individual cells, which results in a high rejection rate. This method of cell selection also requires additional battery weight and size, since cells cannot be manufactured in monoblocks.

On the basis of these conclusions, an alternate design approach has been defined and will incorporate the following: (1) use of a manifolded cell, sealed battery with a manifold pressure transducer, (2) constant power battery charge with potential limiting to 27.3 v, (3) manifold pressure transducer to provide failure mode battery charge operation up to a battery pressure equivalent to cell case proof pressure, and (4) implementation of a cell forming charge technique during manufacture to balance voltages at the full-charge condition instead of the full-discharge condition.

A typical battery charge cycle utilizing the new design is shown in Figure 77. Advantages gained by implementation of the new design are as follows:

(1) Free volume available for gas containment will be increased from 75 per cell to approximately 2100 cc overall.

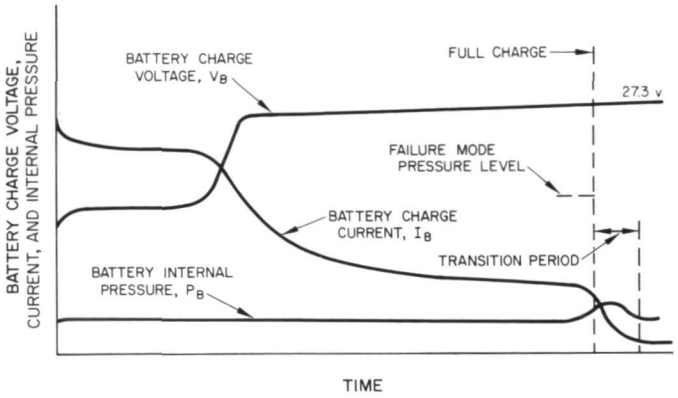


**Fig. 77. Battery charge characteristics**

(2) Excessive pressure conditions will be detected by the pressure transducer. The pressure transducer signal will terminate charging if pressure level equals battery case proof pressure.

(3) Capability to continue charge during the transition period at the full-capacity state without creating excessive pressure can be determined during acceptance testing of each battery.

(4) Balancing the cells at the end of charge during the manufacturing cycle will diminish the probability of excessive gassing near the full-charge state.

(5) Battery charge current at a given temperature will assist in determination of battery state-of-charge.

(6) Battery charging will be highly efficient and float conditions at the end of charge will increase battery capacity.

(7) The battery dynamic voltage surge characteristic no longer influences power system operation.

Design of the prototype manifolded cell, sealed battery is 95% complete. The first six prototype batteries are scheduled to be delivered to Hughes on February 1, 1963.

### 4. Central Power Control

During the checkout of T-2 breadboards, excess noise was present on the unregulated bus input to the boost regulator. The noise resulted from large current transients which occurred on alternate half-cycles of the boost regulator dc-dc converter.

Investigation revealed that the square-loop characteristic of the current feedback transformer was causing

premature saturation of that transformer, preventing proper resetting of the main transformer which in turn caused the transients. Also involved was the main transformer, which used two dissimilar cores for the purpose of reducing current transients in the dc-dc converter. It was determined that the second (or hold-off) core must be of a non-square-loop material with a poor squareness ratio and must have a higher coercive force than the saturable main core. A second core of Q-1 ferrite, manufactured by General Ceramics, was used and effected the desired results. Modification of the converter transformers has minimized the noise feedback on the unregulated bus. New transformers have been made and interchanged with those in the T-21 boost regulator.

Activity has centered on the assembly and testing phases of manufacture. In-process tests completed thus far on the T-21 central power control indicate satisfactory results. Effort is continuing to complete the functional test, and delivery of the unit is scheduled for mid-December.

### *5. Compartment Heater Assembly*

The compartment heater assembly provides a heater element, sensor element, and control circuitry for the purpose of maintaining and controlling the temperature of the thermal tray in Compartments A and B. The lunar night temperature of the thermal tray of Compartment A is controlled between 35 to 40°F and of Compartment B from 0 to 5°F. The assembly can be commanded from the earth to operate in either of two modes – automatic or manual. In the automatic mode, the sensor element controls operation of the heater element within the designed temperature limits. The manual mode is employed shortly after nightfall for determination of compartment thermal characteristics.

A flight-type model has been tested extensively, and the resulting circuit modifications have been incorporated in the heater assembly. Two assemblies for compartments A and B on the T-21 spacecraft have been assembled and are ready for final tests.

# G. Thermal Control

## 1. Compartment Group

The thermal response of Compartment A to a lunar day mission sequence has been examined using the IBM nodal model. The sequence chosen to obtain maximum information for the steady-state and transient thermal characteristics of the compartments includes:

(1) A continuous low power mode simulating the combined dissipation in the command receivers and transmitter (6.1 w).

(2) Two high power modes simulating high power transmission corresponding to planar array lock operation after touchdown, followed by a continuous TV scan for the remainder of the lunar day. The thermal forcing function of these two high power modes consists of 68 w for 1 hr on a 100% duty-cycle basis followed by 30 w for the remainder of the day.

Figure 78 illustrates the temperature response of the thermal tray to the sequence. Thermal tray temperatures range from 85 to 50°F in response to the low power profile. The temperatures are representative of the lowest temperature levels and ranges expected in Compartment A during the lunar day, since the average dissipation in the compartment will always be in excess of the assumed 6.1 w. An upper limit on Compartment A temperatures is provided by the thermal tray response to the conservative high power profile shown by the dashed curves in Figure 78. For this situation thermal tray temperatures range from 60 to 133°F, the extremes occurring at different times of the day.

Because of the relatively short duration and intermittence of the peak power dissipation levels, the actual mission sequence power profile will be between the two assumed power profiles. For example, the present mission sequence requires 1 hr of continuous high power

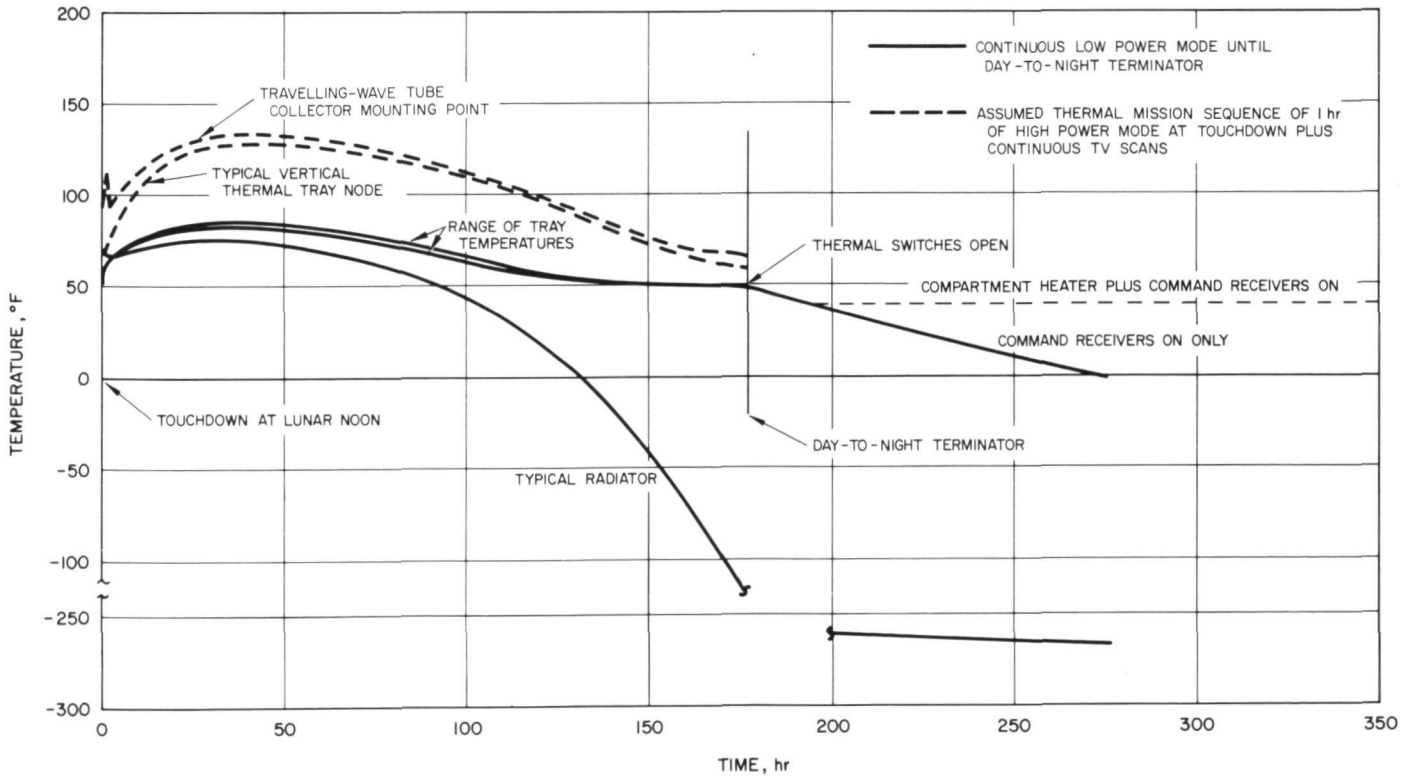


**Fig. 78. Thermal tray temperature response in Compartment A**

transmission to complete planar array lock; however, the TV scans that follow vary from 1 to 3 hr in duration and are intermittent. This sequence prevents sustained temperature increases resulting in thermal tray temperatures in excess of 125°F and also allows the compartment to cool between periods of repeated peak power operation. When an actual mission sequence power profile is incorporated in the compartment thermal study, it is expected that thermal tray temperatures can be controlled easily to less than 125°F.

The response of the thermal tray to the assumed power profiles results in a gradual rise in compartment temperature which peaks 3 to 4 days past lunar noon. This trend is a characteristic unique to both a lunar noon touch-down and the first lunar day since compartment temperatures at the end of terminal descent are lower than the minimal temperatures that prevail during steady-state lunar noon operation, even at the lowest compartment dissipating level. This illustrates the significant increase in the intensity of the thermal environment on the lunar surface as compared with the environment of free space.

Figure 79 illustrates the steady-state temperature distributions within the thermal tray resulting from 6.1- and 23-w dissipation levels. For the 6.1-w case, tray temperatures range from 81 to 86°F; the division of power is approximately 4.3 w on the inboard side of the top tray and 1.8 w on the bottom of the vertical tray. For the 23-w case, tray temperatures range from 114 to 123°F; the division of power is 18 w on the inboard

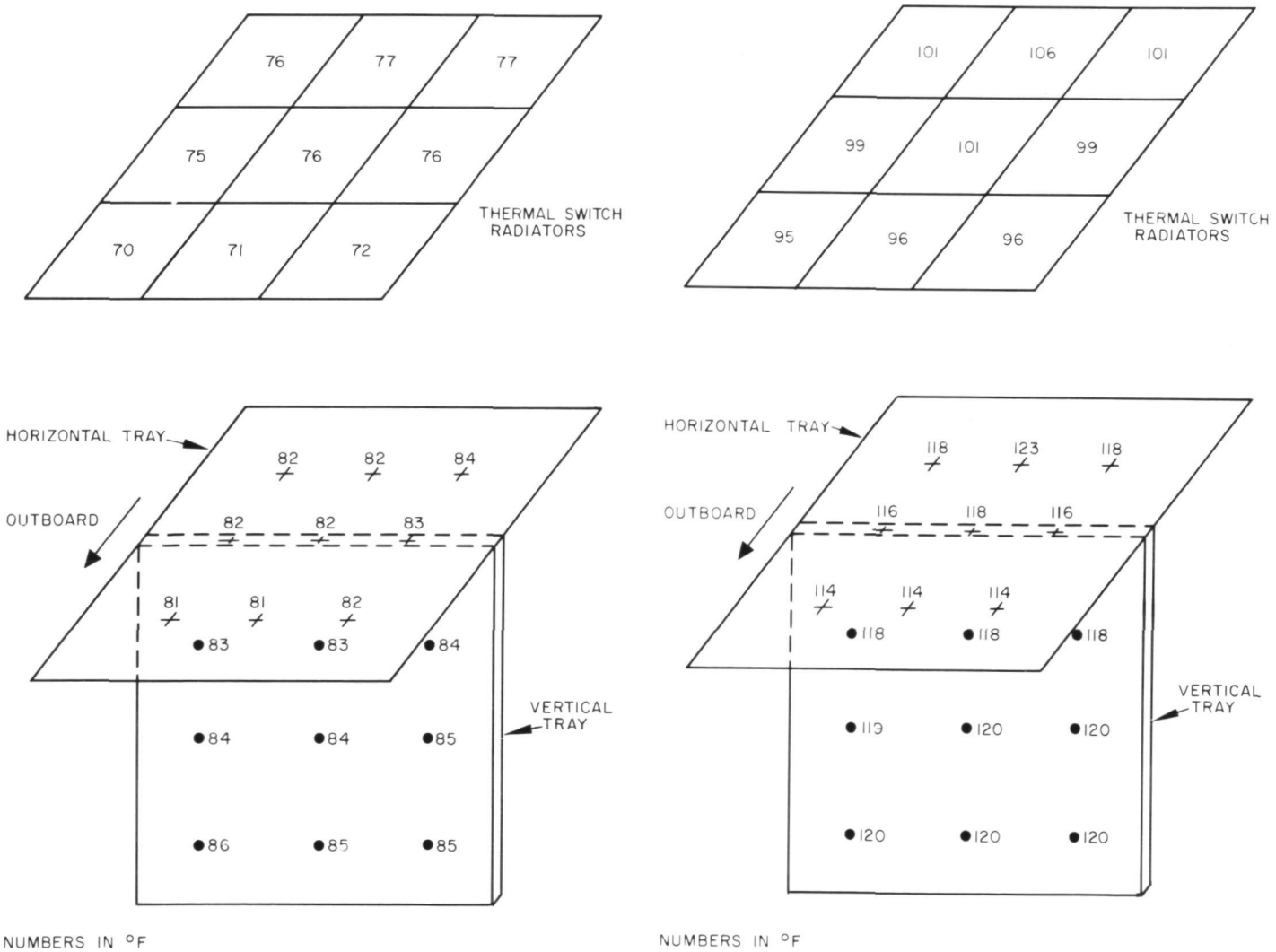


**(a) Equipment heat dissipation of 6.1 w**

**(b) Equipment heat dissipation of 23 w**

**Fig. 79. Compartment A lunar noon steady-state temperatures**

side of the top thermal tray and 5 w on the vertical tray. The distributions indicate that the thermal tray is nearly isothermal and that local hot spots should not exist.

The detailed thermal model of Compartment B has been completed. The thermal response of the compartment to a preliminary transit and partial lunar day mission sequence has been obtained. Figure 80 presents these results in the form of maximum and minimum thermal tray temperature histories within the compartment. The power profile appearing on each figure describes the mission sequence. The thermal tray temperatures used as initial conditions for the transit profile range from 106 to 125°F and correspond to current estimates of compartment temperatures prior to launch.

As seen in Figure 80a, the maximum thermal tray temperature of 127°F occurs at the end of the 60-min acquisition-star lock operation and is caused by high initial temperatures at launch and compartment peak power dissipation during the acquisition operation. The 127°F thermal tray temperature exists at the central power control system attach points, where 35 w of the 40-w compartment total are rejected into the tray and the local equipment. In general, thermal tray temperatures will decrease to a range of 80 to 90°F during the remainder of the transit phase. The peak power loads existing during a typical 28-min midcourse maneuver and a 43-min terminal descent maneuver will cause temperature increases in the thermal tray to a maximum of 103°F, allowing some margin for additional operation if it becomes necessary.

In general, Compartment B transit thermal performance is adequate with the possible exception of the launch through acquisition-star lock period, where tem-

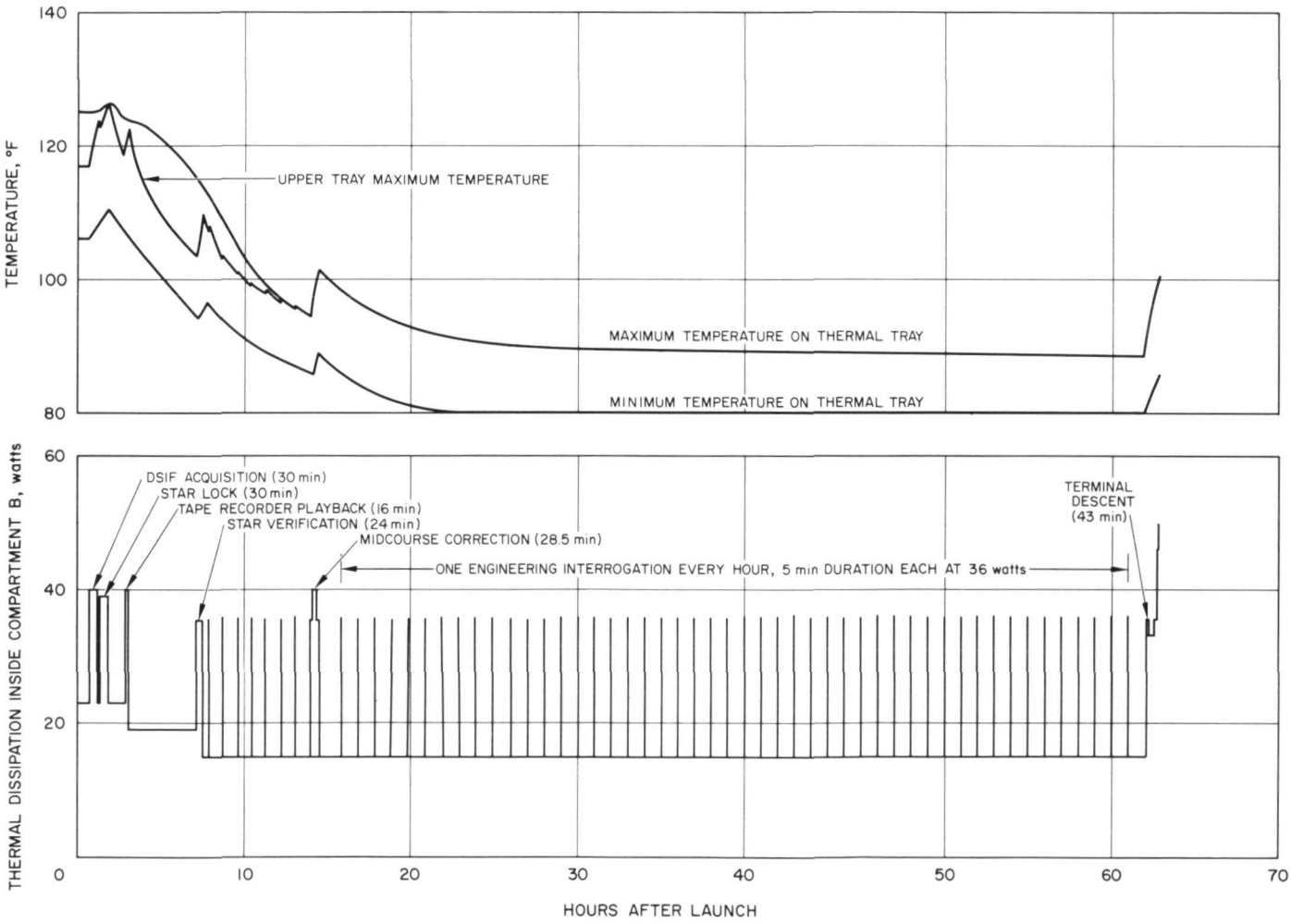


**(a) Transit phase**

**Fig. 80. Compartment B thermal performance**

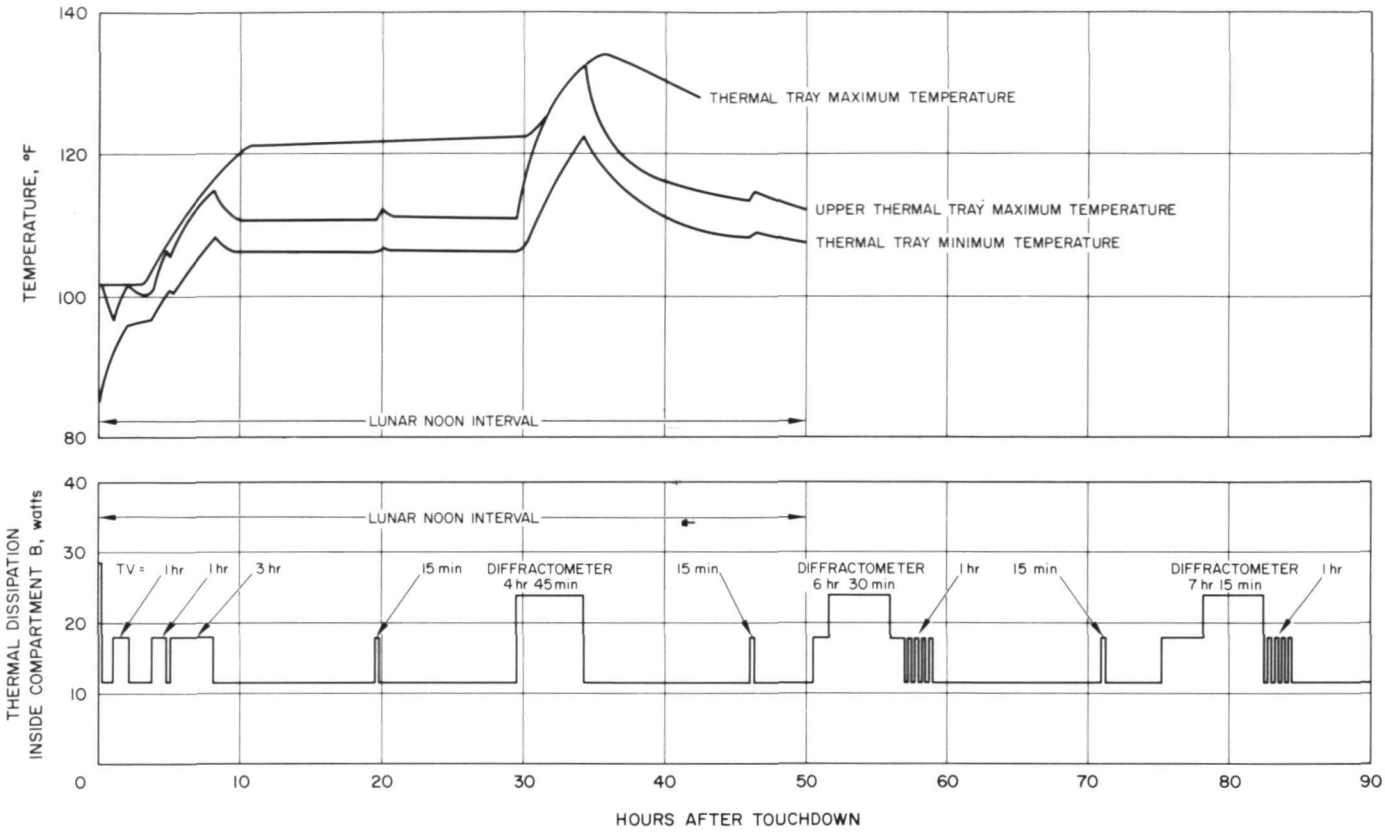


**(b) Lunar noon**

**Fig. 80. Compartment B thermal performance (continued)**

peratures are now slightly in excess of the 125°F upper temperature limit. The assumed 60-min combined acquisition-star lock operation is in excess of the 45-min maximum operating time recommended for this particular peak power event. Further study on this critical area is planned.

A preliminary definition of the thermal performance of Compartment B during the lunar day is presented in Figure 80b. The three temperature profiles represent the general compartment thermal performance. All equipment mounting surfaces are within the temperature envelope formed by the maximum and minimum temperature profiles. During the 11.5-w minimum power dissipation mode, thermal tray temperatures at equilibrium range from 106 to 123°F. The upper thermal tray to which the central power control system is attached experiences the most rapid temperature rise during peak power dissipation levels, such as during TV scans and diffractometer operation, and will serve as the prime indicator of remaining compartment transient capability. In general, thermal tray temperatures of less than 125°F will prevail for the particular mission sequence selected with the sole exception of a 4.75-hr diffractometer mode. These results indicate that a maximum of approximately 1.5 hr of diffractometer operation is allowable before 125°F temperatures are exceeded. The results are conservative because a normal solar load was assumed to exist for the entire lunar day to induce thermal equilibrium by removing variations in the influential external environment.

The ability of the spacecraft to survive lunar night depends on: (1) heat losses of Compartments A and B and the thermal tunnel, (2) recoverable battery capacity, and (3) magnitude of power dissipation in the central power control system located in Compartment B. Table 18 is a compartment heat loss summary for 0 and 50°F compartment temperatures. The 7.2- and 9.5-w heat loss values at 0 and 50°F, respectively, are based on the present compartment design assuming a wiring harness at the compartment wall interface as defined in Table 19. The thermal switches are assumed open with closure initiated at 50 ± 5°F.

Figure 81 presents the spacecraft electrical energy requirements to achieve lunar night survival and the available battery capacity as a function of Compartment A temperature (based on a 350-hr lunar night). The Compartment A temperature range extends from operation at or near 0°F, (minimum operational temperature limit) to 45°F (minimum switch closure temperature). The figure shows that the achievable battery capacity is approximately 2310 w-hr at 0°F and 3200 w-hr at 40°F based on a discharge rate of ½ amp. The lunar night electrical energy requirements for the system, comprised of Compartments A and B and the thermal tunnel, were examined assuming that the power dissipation of the central power control system is 2.5 w at no load, plus approximately 10% of the regulated power demand for the command receivers and heater assembly in Compartment A. The solid curve (Figure 81) depicts the resulting situation; the available battery capacity exceeds the system energy demands by a margin of approximately 200 w-hr occurring at the Compartment A control point of 40°F. Compartment B temperatures resulting from the dissipation level of the power control system and the thermal tunnel conduction coupling effect are also indicated.

To illustrate the significance of the power control system dissipation, Figure 81 also presents a performance curve for a power control system dissipation of 5.0 w.

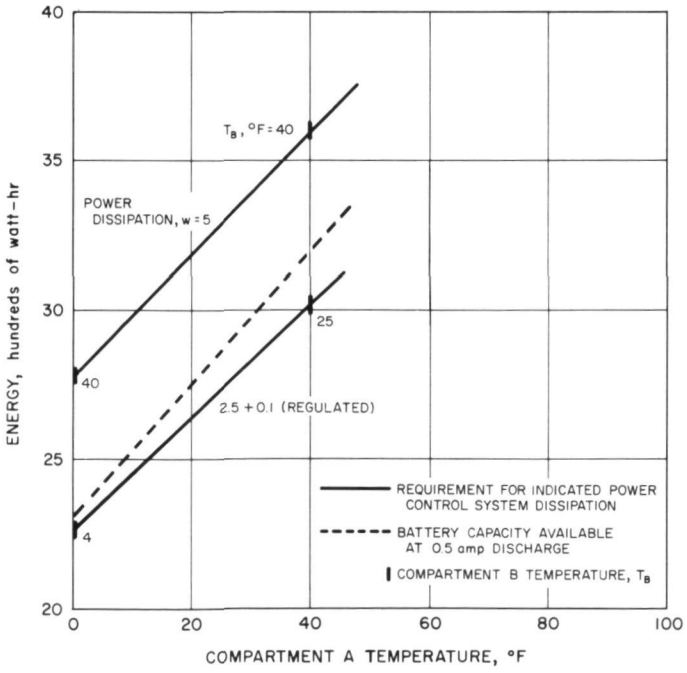


**Figure 81. Compartment A and B energy requirements for lunar night survival**

**Table 18. Lunar night heat loss summary for Compartments A and B**

| Thermal path | Heat loss at 0°F, w | | Heat loss at 50°F, w | |
|---|---|---|---|---|
| | A | B | A | B |
| Supports | 0.22 | 0.17 | 0.26 | 0.20 |
| Thermal switches | 0.87 | 0.57 | 1.03 | 0.67 |
| Superinsulation ($F_\epsilon$ = 0.005) | 1.51 | 1.28 | 2.3 | 1.95 |
| Wiring harness | 1.46 | 0.50 | 1.7 | 0.59 |
| Subtotal | 4.06 | 2.52 | 5.29 | 3.41 |
| Subtotal (Compartments A and B) | 6.58 | | 8.70 | |
| Thermal tunnel | 0.50 | | 0.79 | |
| Total (Compartments A and B) | 7.2 | | 9.5 | |

**Table 19. Wiring harness at compartment interfaces**

| Location | Harness |
|---|---|
| Compartment A | 170 No. 28, 3-in. nichrome sections<br>3600 circular mils of copper (RADVS system)<br>3 RG 115 A/U coaxial cables |
| Compartment B | 285 No. 28, 3-in. nichrome sections |

Under this condition, the surplus of existing electrical energy would result in an unnecessarily high equilibrium condition in Compartment B of 40 to 50°F, causing an unwanted thermal switch closure. The system electrical energy requirements in this case vary from 2770 w-hr at 0°F to 3600 w-hr at 40°F for Compartment A temperatures and exceed the available electrical energy by approximately 400 w-hr. Lunar night survival is not possible under these circumstances, showing the necessity of minimizing lunar night power dissipation in the power control system.

Recent problems involving excessive voltage drops in many leads presently containing a nichrome insert may require removal of the affected nichrome sections. Present estimates are that 42 affected leads would require approximately 1500 w-hr additional energy for lunar night survival.

## 2. *Remote Subsystem Group*

*a. Main retro-engine.* Thermal analysis of the main retro-engine is continuing. Recent progress includes (1)

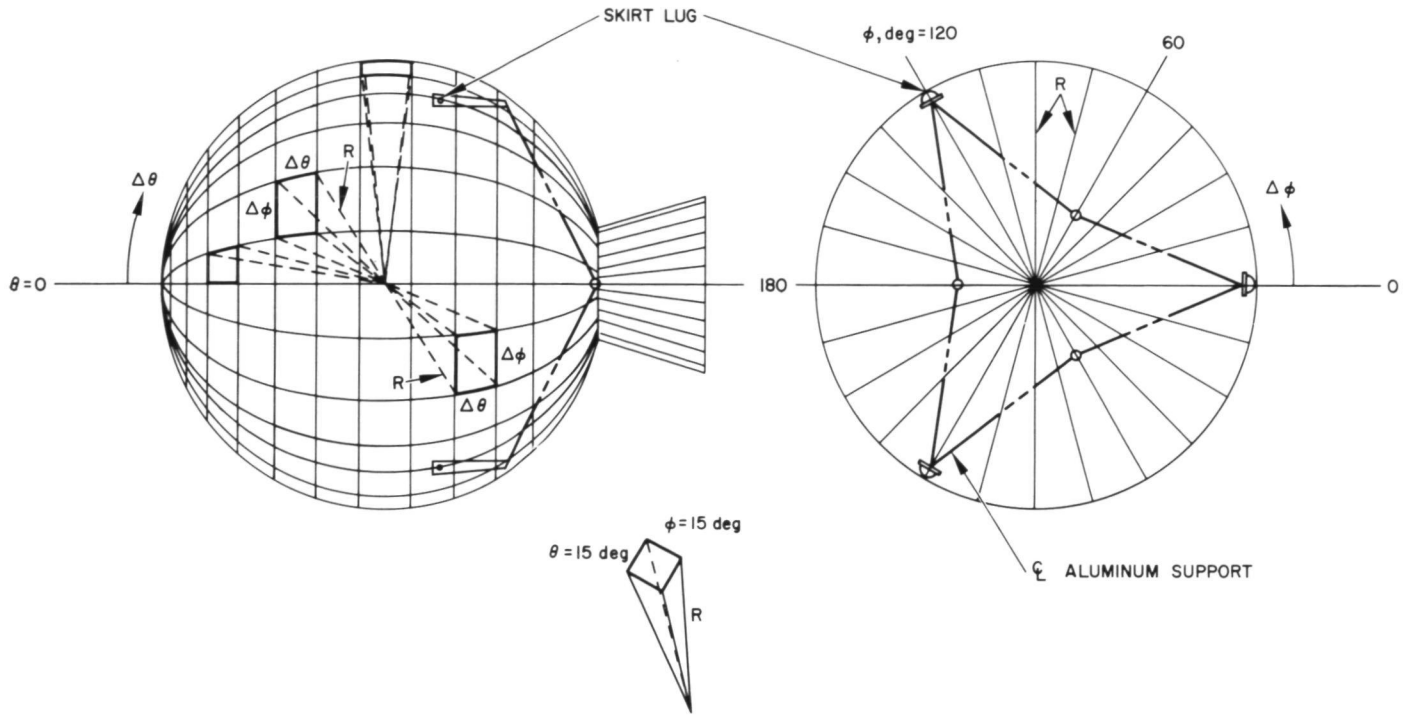


**Fig. 82. Coordinate system for heat transfer analysis of main retro-engine**

completion of a three-dimensional analysis based on the revised assumed outer case effective emittance of $F_\epsilon = 0.020$ and (2) modification of the two-dimensional thermal model to be consistent with the current physical design for use in various tradeoff studies to improve minimum propellant temperatures and reduce thermal control weight.

Figure 82 shows the coordinate system for the three-dimensional study related to the retro support skirt and strut attach locations on the case. Figure 83 presents the maximum and minimum propellant temperature profiles during transit obtained for a 60 deg line segment from the three-dimensional thermal analysis. Geometric and thermal environmental symmetry assure this division to be representative of the entire engine. The temperature profiles form an envelope which includes all remaining propellant nodal elements. For a 66-hr transit, propellant temperatures at ignition range from −3 to 65°F; the minimum temperature occurs along a $\theta = 45$ deg radial line, 2.5 in. from the cavity. Examination of the data reveals that the minimum temperatures occur on the propellant aft face and not along the case as previously reported. Radiation coupling between the propellant aft face and the cold steel case caused the shift in the minimal temperature location.

A study of the propellant temperature distribution shows that 94% of the grain elements remained above

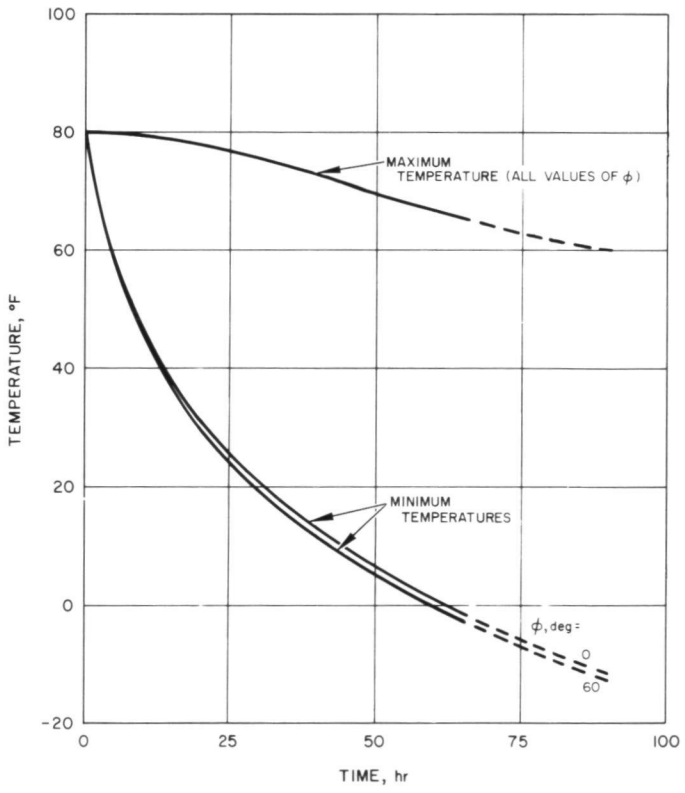


**Fig. 83. Main retro-engine propellant temperature range vs time**

20°F. The results presented are based on a grain thermal conductivity of $K = 0.126$ Btu/hr ft °F. Since completion of this study, Thiokol informed Hughes that propellant thermal conductivity measurements have revised this value to $K = 0.20$ Btu/hr ft °F. This is expected to increase the minimum propellant temperatures.

The main retro thermal blanket (M-12 model) performance test data indicate an effective emittance factor of $F_\epsilon = 0.021$. The design goal value is $F_\epsilon = 0.020$; therefore, the blanket can be considered as flight quality. A slight modification in the blanket fabrication technique should yield improved blanket performance; further tests are planned before a final flight blanket fabrication technique is selected.

***b. Vernier propulsion system.*** The current status of vernier system thermal control is summarized in Table 20 with references to additional curves containing detailed analytical results for specific subsystems. The indicators of thermal performance are: (1) the steady-state temperature of the particular subsystem during normal transit attitude when the spacecraft roll axis is aligned to the Sun; and (2) the cooling times from steady-state conditions to 0°F during the acquisition, midcourse and terminal descent maneuvers. These indicators are the primary criteria used to judge the applicability of the various passive thermal control techniques considered for the vernier system.

Passive thermal control techniques are employed on the three vernier thrust chamber assemblies. The presence or absence of direct solar irradiation on the thrust chamber requires the use of either of two distinct forms of passive measures. Thrust Chambers 1 and 3 receive direct solar irradiation during normal transit attitude, and Thrust Chamber 2 is shaded from the Sun by the solar panel. The mechanism used to transport the solar energy to the thrust chamber was selected on the basis of feasibility, weight, and system reliability.

Thrust Chambers 1 and 3 rely on high solar energy absorbent black paint on the top illuminated surfaces to establish the desired temperature. Figures 84 and 85 show that the steady-state temperatures on the thrust chamber and valve assembly range from 40 to 85°F when solar irradiation is present. When solar energy is absent, the time to cool to 0°F is 1 hr. The previously

**Table 20. Vernier system thermal control summary**

| Subsystem | Temperature requirements, °F | Temperature control technique | Steady-state temperature in transit, °F | Cooling time to 0°F from steady-state, hr |
|---|---|---|---|---|
| Vernier thrust chamber and Valves | | | | |
| Chambers 1 and 3 | 0 to 100 | *Passive.* selective surface treatment and conduction isolation | 40 to 85 (See Figure 84) | 1.0 (See Figure 85) |
| Chamber 2 | 0 to 100 | *Passive.* solar collector and selective surface treatment plus conduction isolation | 40 to 72 (See Figures 86 and 87) | 1.0 (See Figure 88) |
| Vernier tanks | | | | |
| Fuel tanks 1 and 3 Oxidizer tank 1 | 0 to 100 | *Passive.* selective surface treatment and conduction isolation | 50 to 75 | 4.0 |
| Fuel tank 3 Oxidizer tanks 2 and 3 | 0 to 100 | *Passive.* extreme thermal isolation and controlled depletion of propellant internal energy | Requires 80°F propellant temperature at launch | (See Figure 89) |
| Fuel and oxidizer in lines | 0 to 100 | *Active.* Auxiliary heating with low emissivity wrap and low conductance bracketry | 20 (See Figure 90) | *Active.* Thermally controlled |
| Helium gas supply | 0 to 100 | *Passive:* selective surface treatment and conduction isolation | 70 | 1.0 |
| Helium lines and enclosed gas | Minimizes heat losses from vernier tanks | *Passive.* selective surface treatment and partial conduction isolation (proposed) | −115 along space-frame routing | — |

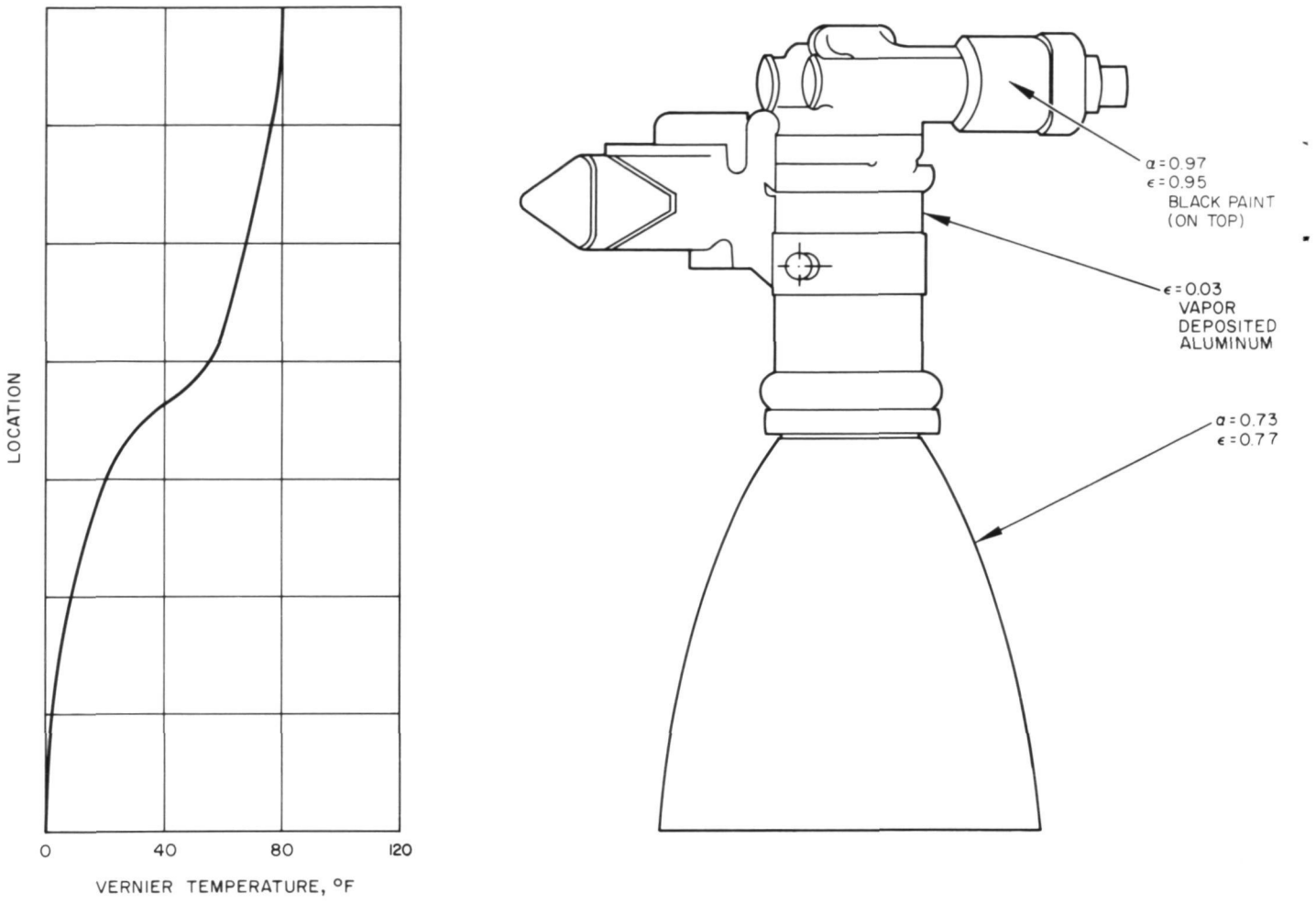


**Fig. 84. Steady-state transit temperatures for Vernier Engines 1 and 3**

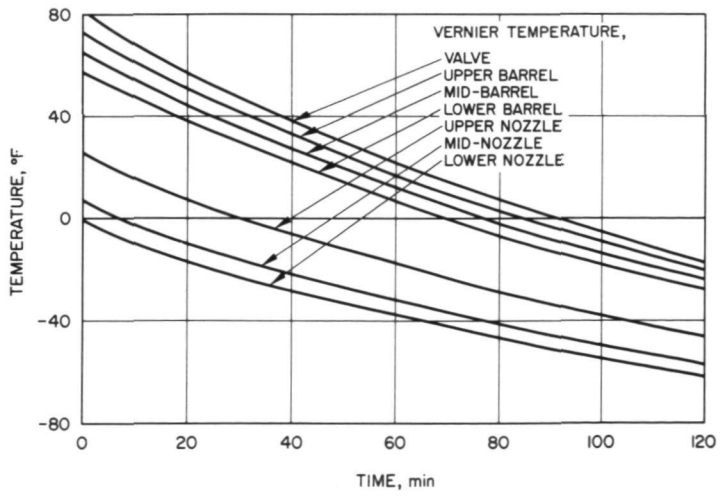


**Fig. 85. Transient temperature profiles for Vernier Engines 1 and 3**

reported incompatibility between required radiation property values and a single surface treatment is not a factor in the present thermal design. At this time the surface treatment for vernier thrust chamber and Valve Assemblies 1 and 3 is a combination of vapor-deposited aluminum over epoxy and a commercially available black paint (Black Velvet) manufactured by the Minnesota Mining and Manufacturing Company.

Thrust Chamber 2 employs a solar collector extending beyond the outer edge of the solar panel to intercept and absorb solar energy which is conducted to the vernier engine. Figure 86 is a sketch of the solar collector attached to the vernier thrust chamber mount. The temperature distribution for the normal transit attitude is superimposed on the sketch. The solar collector results in a temperature range of 40 to 72°F in Thrust Chamber 2 and the valve assembly as shown in Figure

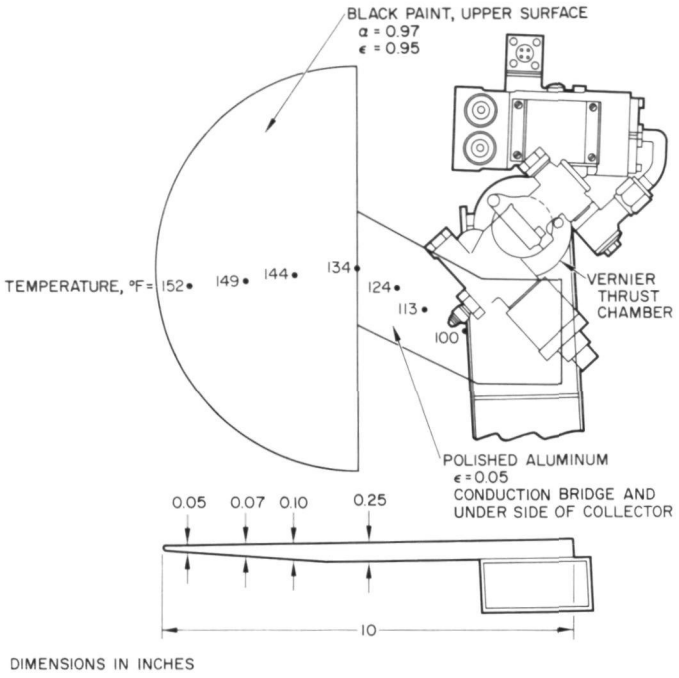


**Fig. 86. Solar collector attached to vernier thrust chamber mount**

87. The cooling time from equilibrium to 0°F of the thrust chamber assembly is 1 hr as shown in Figure 88.

The recommended chamber and valve assembly surface treatment is vapor-deposited aluminum over epoxy. The solar collector is fabricated from aluminum 1100, H-18 alloy for maximum conduction. The surface treatment is polished aluminum and black paint. The solar collector is attached to the vernier thrust chamber bracket, thereby avoiding direct contact with the thrust chamber. The present analysis indicates that satisfactory thermal performance of the three vernier thrust chambers may be expected throughout transit. Furthermore, the assumed radiation property values are achievable with commercially available surface treatments.

The vernier propellant tanks are thermally controlled by two methods: (1) conventional surface treatment for tanks receiving sufficient solar illumination and (2) thermal isolation to reduce the internal energy dissipation for tanks that do not receive sufficient solar illumination (Table 20).

Thermal control of the tanks by the first method is achieved by a surface treatment of vapor-deposited aluminum over epoxy painted black to allow high absorption of solar energy. This method results in equilibrium temperatures between 50 and 75°F depending upon the degree of shading the particular tank receives. During the midcourse correction maneuver, it would take approximately 4 hr to reach 0°F if no further solar illumination occurred.

Figure 89 shows temperature profiles of the three tanks controlled by the second method described above. The graphical data presents tank temperature at touchdown as a function of the average heat losses in the tank. Parameters considered include transit times of 66 and 90 hr and a fuel expenditure of 21.5 and 43 lb during the midcourse maneuver 18 hr after liftoff.

If several helium line brackets in the vicinity of the tank are modified to a low conductance material the average heat losses from the tank range from 2.75 to 3.25 w. The 0.5-w range is a prediction envelope accounting for spaceframe and helium line conduction uncertainties. Based upon a 66-hr transit and a 21.5-lb total midcourse expenditure and the uncertainty envelope described, tank temperatures at lunar touchdown range from 5 to 16°F. For the midcourse expenditure of 43 lb (66 hr), tank temperatures could fall below the 0°F minimum allowable; tank temperatures for a 90-hr transit period would also undoubtedly fall below the 0°F minimum allowable. If compensating action is indicated, electrical heating is recommended.

The thermal requirements for tanks requiring extreme isolation from thermal conduction and radiation are a spaceframe attachment conductance of $8.8 \times 10^{-3}$ w/°F and an outer tank surface effective emittance of $F_\epsilon = 0.005$. The MT-1 Sector 1 and 2 lunar night tests verified the design of the low conductance mount. A series of vernier-tank thermal-blanket tests were conducted to evaluate fabrication techniques. A variety of fabrication techniques were tested to determine effective emittance value. The results in Table 21 indicate that a superior fabrication technique has been developed. Effective emittance values of the blanket as low as $F_\epsilon = 0.0026$ were obtained for uncrushed tank/blanket systems. Furthermore, a special test conducted on an installed tank during the Sector 2 lunar night tests indicates that the blanket exhibited an effective emittance factor of $F_\epsilon = 0.0044$ including the crushing effects from installation. On the basis of tests conducted to date, the thermal parameters of the extreme isolation design are being attained.

Several improvements were incorporated into the vernier fuel and oxidizer line thermal control system, including a design improvement on the attachment bracketry and a reduction in the heater thermostatic control temperature from 80 to 20°F. Figure 90 presents the fuel and oxidizer line heating requirements in transit; only 7.2 w of power are required to maintain 20°F line tem-

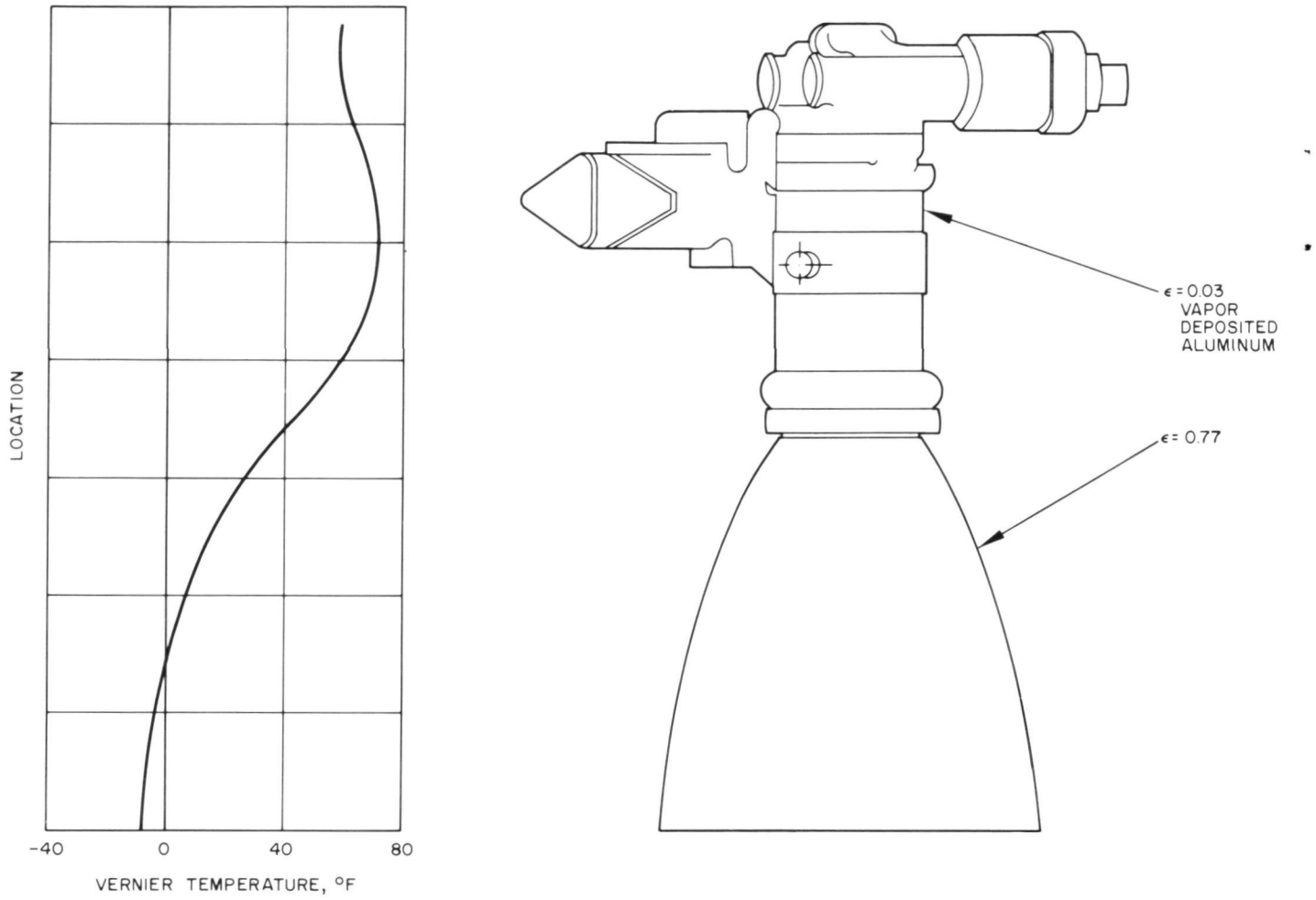


**Fig. 87. Steady-state transit temperatures for Vernier Engine 2**

peratures throughout transit, a decrease of 9 w in heating power.

As previously reported, the helium gas supply tank is surface treated with vapor-deposited aluminum over epoxy on the lower hemisphere and an alternately white and black painted gore-shaped pattern on the upper hemisphere. The equilibrium temperature in transit will be 70°F; the tank cooling time to 0°F is 1 hr.

The helium lines do not require thermal control; the objective has been to minimize thermal interaction effects with other spacecraft subsystems, particularly the three insulated vernier tanks. Analysis indicates that the vernier tank heat losses caused by the attached cold helium line can be reduced by approximately 1 w if minor bracketry modifications are made. The additional 1-w heat loss represents approximately 30% of the total vernier heat losses and therefore justifies corrective action.

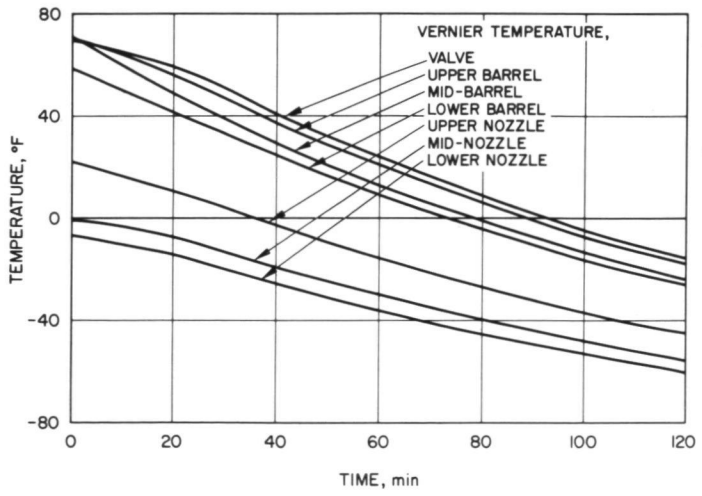


**Fig. 88. Transient temperature profiles for Vernier Engine 2**

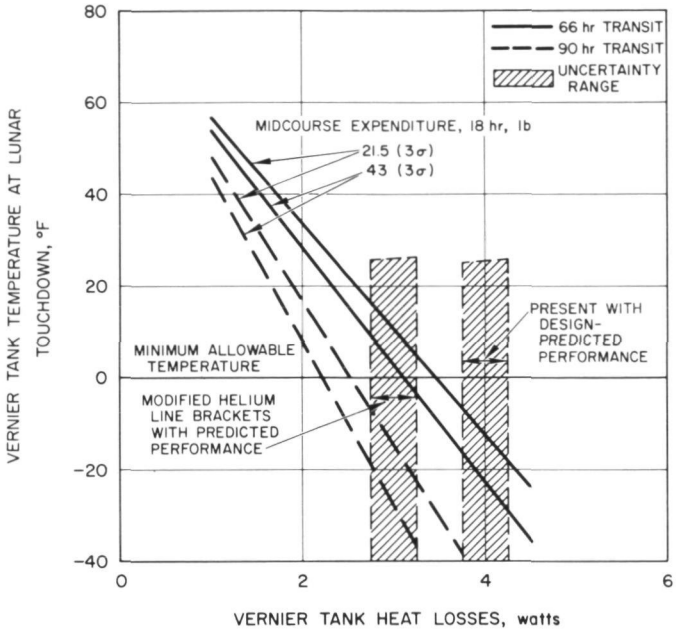


**Fig. 89. Vernier oxidizer tank terminal descent temperatures**

149 lb propellant; 80°F at launch

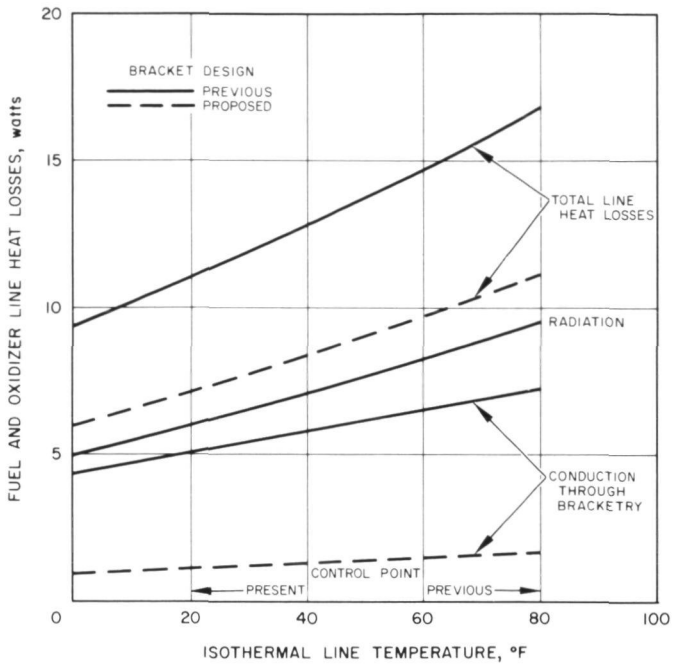


**Fig. 90. Predicted fuel and oxidizer line heating requirements in transit**

*c. Shock absorber.* The surface treatment selected for the shock absorber assembly is a combination of white paint and gold-surfaced paper applied to the exterior surface. The pattern is a variable-width white strip extending along the top of the shock tube; the remaining surfaces are covered with gold paper. This surface treatment was chosen because: (1) it allows adjustment of the effective radiation property values and (2) it is applied easily following the hydraulic fluid filling operation.

The surface treatment materials are a commercially available gold coating on Kraft paper and Ditzler white paint (DMA-311) which have undergone tests and exhibit the desired properties. Tests to show stability under ultra-violet radiation are in progress.

*d. Attitude control system.* Thermal analysis of the nitrogen tank has continued to maximize temperatures during transit while minimizing the tank temperatures under near-lunar noon conditions. Although the tank is used only during transit, it is undesirable for overall spacecraft thermal control to allow local hot spots on the spacecraft during lunar noon operation. Some of the results of the study are shown in Table 22 which shows that if the surface yielding the best transit results is used (Case 3) the tank would remain above the −70°F minimum allowable transit temperature, but would become too warm at lunar noon. For this consideration, the most desirable surface finish is the dual surface finish of Case 4 with the bottom hemisphere, normal to the lunar surface, covered with vacuum-deposited aluminum and the upper hemisphere painted with black paint. The assumed surface thermal properties are $\alpha = 0.11$, $\epsilon = 0.04$ for the vacuum deposited aluminum; and $\alpha = 0.95$, $\epsilon = 0.90$ for the black paint.

*e. Television system.* Thermal analysis of the TV camera has indicated satisfactory, but marginal, operation. Electronic equipment inside the camera has been shown to rise in temperature from about 95°F under lunar noon nonoperating conditions to about 180°F after 5 hr of camera operation. These temperatures are within the specified temperature tolerances but in most cases are close to the upper limit. In addition, the narrow operating temperature limits of the vidicon face, operation between 73 and 99°F, leaves little room for tolerances to be applied to the final computed temperature. Therefore, the television camera thermal design is to be re-examined to gain further data on expected camera operating temperatures.

The minimum operating temperature limits of the camera, and the requirement that the cameras operate up to within 5 deg of solar angle before the day/night terminator, has prompted further analysis. Although the electronics within the camera are supplied with electrical

**Table 21. Vernier-tank thermal-blanket development test summary**

| Facility | Aluminized mylar blanket fabrication techniques | Number of aluminized mylar sheets | Experimental emittance factor, $F_\epsilon$ | Test blanket equivalent heat losses at 80°F inner wall, w | Average outer sheet temperature, °F |
|---|---|---|---|---|---|
| HiVac 4, Hughes building 21 $P < 10^{-5}$ Torr | Orange peel pattern with laced seams | 100 | 0.015 | 2.34 | —260 |
| SERF[a] C-1, Hughes building 365 $P < 10^{-6}$ Torr | Spiral wrap — continuous wrap for ten revolutions | 60 | 0.0068 | 1.06 | —175 |
| | Individually overlapped sheets | 50 | 0.0082 | 1.28 | —160 |
| SERF C-1, Hughes building 365 $P < 10^{-6}$ Torr | Tight spiral wrap — continuous wrap for ten revolutions | 50 | 0.0103 | 1.65 | —200 |
| | | 100 | 0.0079 | 1.27 | —200 |
| SERF C-1, Hughes building 365 $P < 10^{-6}$ Torr | Loose spiral wrap — continuous wrap for ten revolutions | 100 | 0.0027 | 0.43 | —171 |
| | | 100 | 0.0026 | 0.42 | —172 |

[a]Space Environment Research Facility.

**Table 22. Nitrogen tank temperature analysis**

| Nitrogen tank surface finish | | Lunar noon maximum temperature, °F | Transit minimum temperature, °F |
|---|---|---|---|
| Case | Configuration | | |
| 1 | Tank covered completely with black paint ($\alpha = 0.95, \epsilon = 0.90$) | 300 | —114 |
| 2 | Tank covered completely with white paint ($\alpha = 0.24, \epsilon = 0.95$) | 283 | —161 |
| 3 | Tank covered completely with vacuum-deposited aluminum ($\alpha = 0.11, \epsilon = 0.04$) | 330 | — 62 |
| 4[a] | Black paint on top half and vacuum-deposited aluminum on bottom half | 240 | — 70 |

[a]Recommended surface finish.

heaters for warmup during late lunar day operation, the TV mirror assembly on top of the camera does not include this provision. Analyses have been performed on typical vertical cylinders mounted on the spaceframe for both an equatorial and a 65° latitude landing site. Results are shown in Figures 91 and 92 for both an illuminated and a nonilluminated situation. For the nonilluminated configuration when the cylinder is shaded from the Sun by other spacecraft components during the complete lunar afternoon, the cylinder temperature drops to approximately —200°F at a Sun angle of 5 deg before terminator at a lunar latitude of 65°. A cylinder on the equator drops to —160°F. For the illuminated configuration, the cylinder is maintained at —30°F at the equator and —50°F at the 65° latitude for the 5 deg solar angle.

For the reasonable assumption that the TV cameras will always be illuminated, the cameras will be required to be operational at approximately —50°F. The electronics heaters can be utilized to bring the electronics up to operational temperatures (approximately —20°F) but the TV mirror and hood assembly unless equipped with heating equipment must be operational at temperatures as low as —50°F.

Since the temperatures of spacecraft components, as typified by the vertical cylinder discussed above, are functions of the Moon and solar heat loads on the package, and since the lunar surface temperatures at near-terminator conditions are difficult to establish accurately because of the relatively rapid lunar surface cooling rate, calculations have been performed to establish the package sensitivity to the Moon surface temperature. If at near-terminator conditions, the lunar surface temperature is actually 15°F warmer than assumed, the illuminated package temperature will increase approximately 1.5% from —50 to —44°F. If the lunar surface temperature is 15°F cooler than assumed, the package temperature will decrease about 1.4% from —50 to —55°F. The illuminated package temperature is a stronger function of the solar heat input, i.e., the solar absorptance of the surface, than of the lunar heat input at near-terminator conditions.

### 3. *Scientific Payload Integration*

The thermal integration function has been resumed, with redefinition of the payload. The X-ray diffractometer

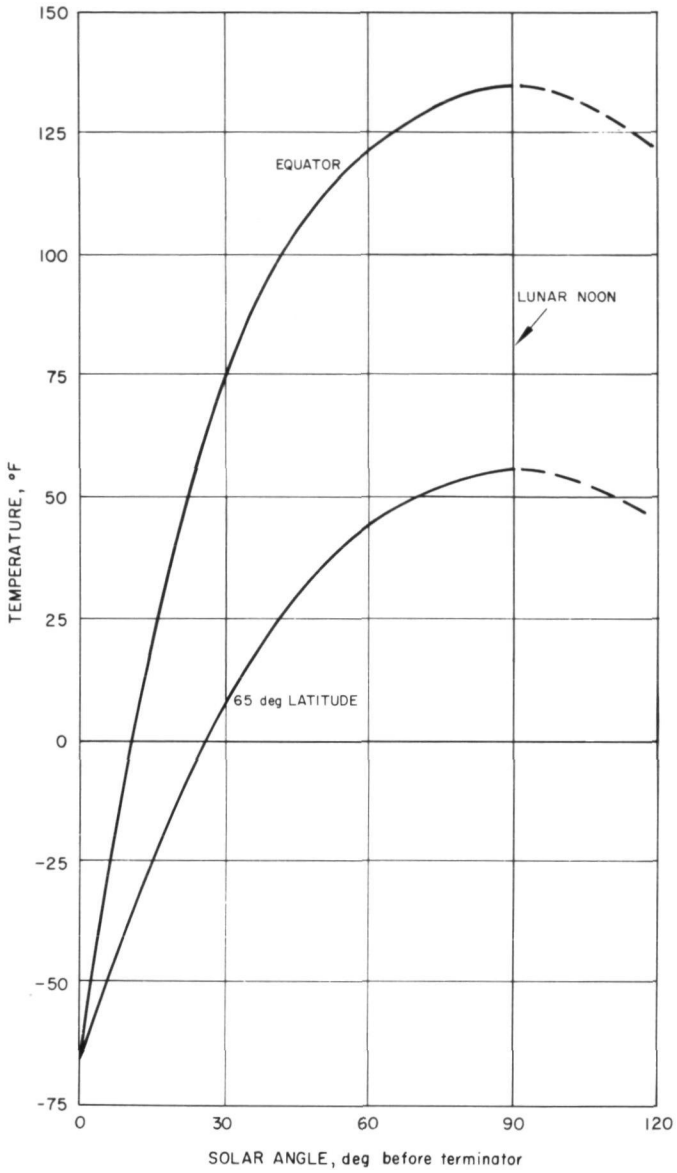


**Fig. 91. Temperature vs solar angle for illuminated vertical cylinder**
**white paint surface treatment**

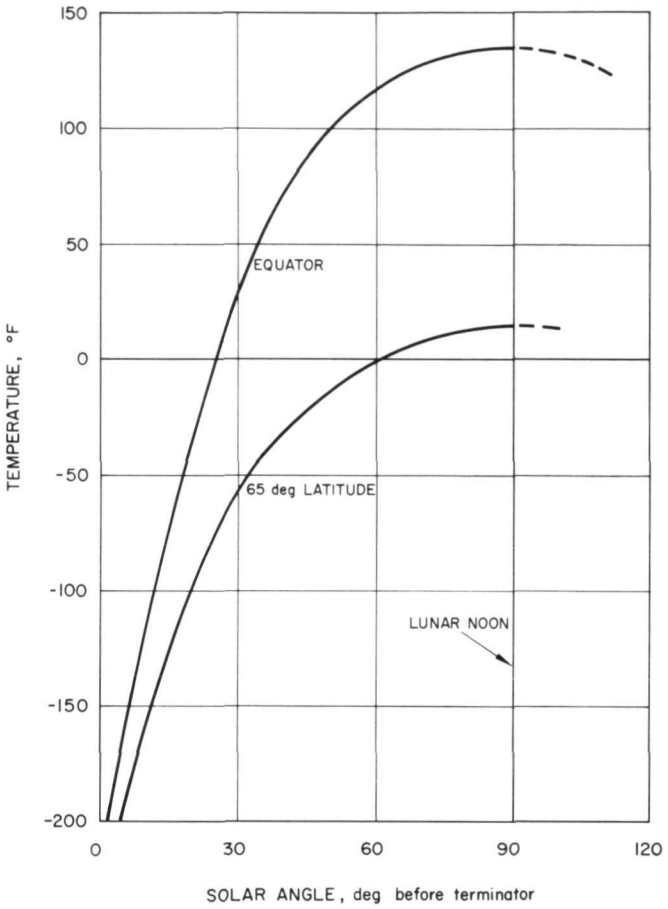


**Fig. 92. Temperature vs solar angle for non-illuminated vertical cylinder ($\epsilon = 0.95$)**

experiment, originally included in the 2500-lb *Surveyor* payload, has been re-examined. The diffractometer head is expected to perform approximately the same as predicted for the 2500-lb spacecraft, i.e., the X-ray tube radiator maximum temperature will be 325 °F. As shown in the spacecraft general arrangement (Figure 1) the X-ray tube radiator radiates inboard, but because of the high allowable X-ray tube temperature (450°F), this inefficient manner of heat rejection to space can be tolerated. The high voltage power supply (HVPS) package has been located adjacent to the diffractometer with the radiator facing inboard on the spacecraft. Thermal anlysis of the HVPS requires a radiation view factor to space of approximately 50% for lunar noon radiator operation at 190°F. In the former configuration, the view factor to space was approximately 30%; consequently, the radiator would have exceeded the allowable temperature of 210°F. Relocating the HVPS to a more favorable position at the outboard end of the X-ray diffractometer head allows operation within the current thermal specification.

Preliminary thermal study of the micrometeorite ejecta detector experiment has been made. The instrument, which basically consists of a vertical flate plate on which a sensor is centrally located, appears to have acceptable temperature limits. The sensor will survive the lunar night and can operate at temperatures between —75 and 260°F. A sensor heater will be included if night operation is required. The experiment electronics, located in a thermal compartment, receive adequate thermal control.

The soil mechanics experiment will operate at approximately 160°F at lunar noon within the allowable temperature limits of 0 to 261°F. However, late in the lunar afternoon, the temperature of this device will drop below 0°F if the spacecraft is oriented to shade the instrument from direct solar illumination. The condition could occur approximately 50 hr before the day/night terminator at the equator or 120 hr before the terminator at 65° latitude. To establish a reasonable allowable operating time on the lunar surface, critical components of the instrument may require electrical heaters. The device is designed to survive the extreme cold temperatures during lunar night without heating.

The surface sampler will operate at a temperature of approximately 160°F maximum, with the exception of the drive motors, which will rise to higher temperatures during periods of operation.

A special thermal analysis of the alpha scattering experiment was requested by JPL to establish the feasibility of inclusion of this experiment into the *Surveyor* payload. The results of this analysis are shown in Figure 93. For the proposed location the radiator temperature is a function of the view factor to space and is affected by the X-ray diffractometer head and HVPS location. The maximum allowable sensor temperature is specified at 122°F. This requires a view factor to space of more than 60%. If the alpha scattering package radiator were raised to the same level as the diffractometer head top surface, the view factor to space would be increased from 55 to 68%. Thus, for successful operation, further configuration changes will be required.

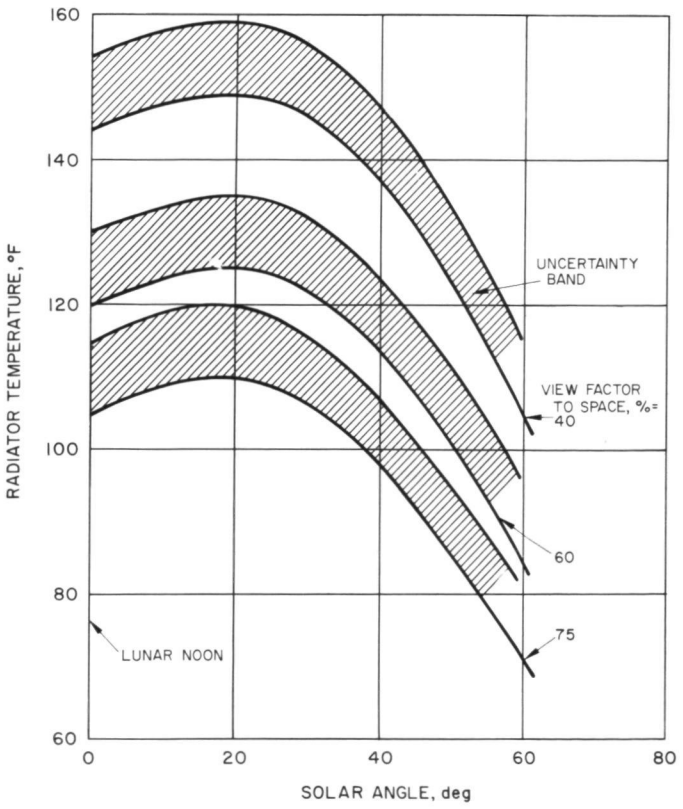


**Fig. 93. Alpha scattering experiment radiator temperature**

### 4. Thermal Switch

The drawing package of the thermal switch has been released for units for T-21 and type approval testing. Fabrication of the basic switch parts is approximately 50% complete.

A complete set of MT-1 Compartment A switch units are in final assembly and test. These units were built with the latest T-21 configuration design modifications as discussed in the previous bimonthly report.

Preliminary vibration testing of the thermal switch will be completed during December using one of the new MT-1 units. Thermal performance will be checked before and after the vibration test.

Effort toward obtaining the best possible bonding technique for the Vycor radiators is continuing. Several units have been bonded using indium solder and temperature cycled between +100 and −200°F. These bonded assemblies withstand the temperature cycling without cracking the glass; however, as previously reported, the process is both complicated and difficult to implement. The use of RTV-60 (silicon rubber) as an alternate bond material is promising. One radiator, bonded with RTV-60, has

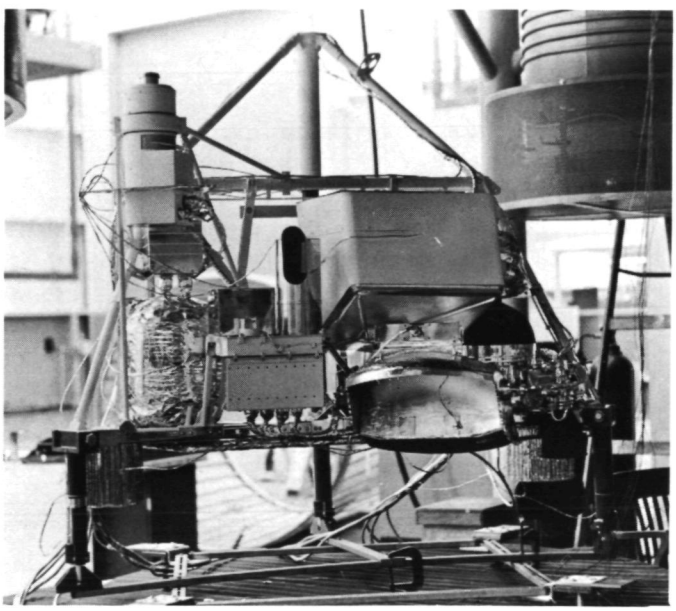

**Fig. 94. MT-1 Sector 2 after lunar night test**

been temperature cycled successfully. Development of the RTV-60 process will continue concurrently with the use of indium solder technique for the T-21 thermal switch units.

## 5. Thermal Testing

*a. MT-1 test.* The lunar night test of MT-1, Sector 2 was completed on October 19, 1962 after 168 hr of continuous testing. The test was conducted in the SERF C-3 chamber at the Hughes Space Environment Laboratory. Figure 94 shows the sector at the completion of the test. The chamber pressure was held below $10^{-6}$ Torr and the chamber shroud temperature below —300°F.

During the test thermal equilibrium was closely approximated at four Compartment B power levels and at two vernier tank heater settings. Table 23 lists the average steady-state conditions, and Figures 95 and 96 are plots of the test temperature and power histories.

The Compartment B insulation consisted of 75 sheets with a single overlap at the main closure seam, whereas

**Table 23. Sector 2 average steady-state data**

| Compartment B | | | Vernier tank | | |
|---|---|---|---|---|---|
| Time, hr | Temperature, °F | Applied power, w | Time, hr | Temperature, °F | Applied power, w |
| 43.2-63.2 | +31 | 2.31 | 112.2-123.2 | —102 | 1.47 |
| 75-110 | — 2 | 2.05 | 140.7-154.2 | + 52 | 3.38 |
| 125-141 | —27 | 1.69 | | | |
| 141-162 | —33 | 1.64 | | | |

Sector 1 Compartment A test insulation consisted of 100 sheets of individually interleaved mylar. Since the Compartment B emittance factor ($F_\epsilon$) was found to be approximately 0.005, all future compartments will utilize 75 sheets with a single overlap. Figure 97 shows the proximity of the experimental data to the analytical performance for an effective emittance factor $F_\epsilon$ of 0.005 with 100 interleaved sheets. A correction for temperature drift from nonsteady-state conditions is also shown. The

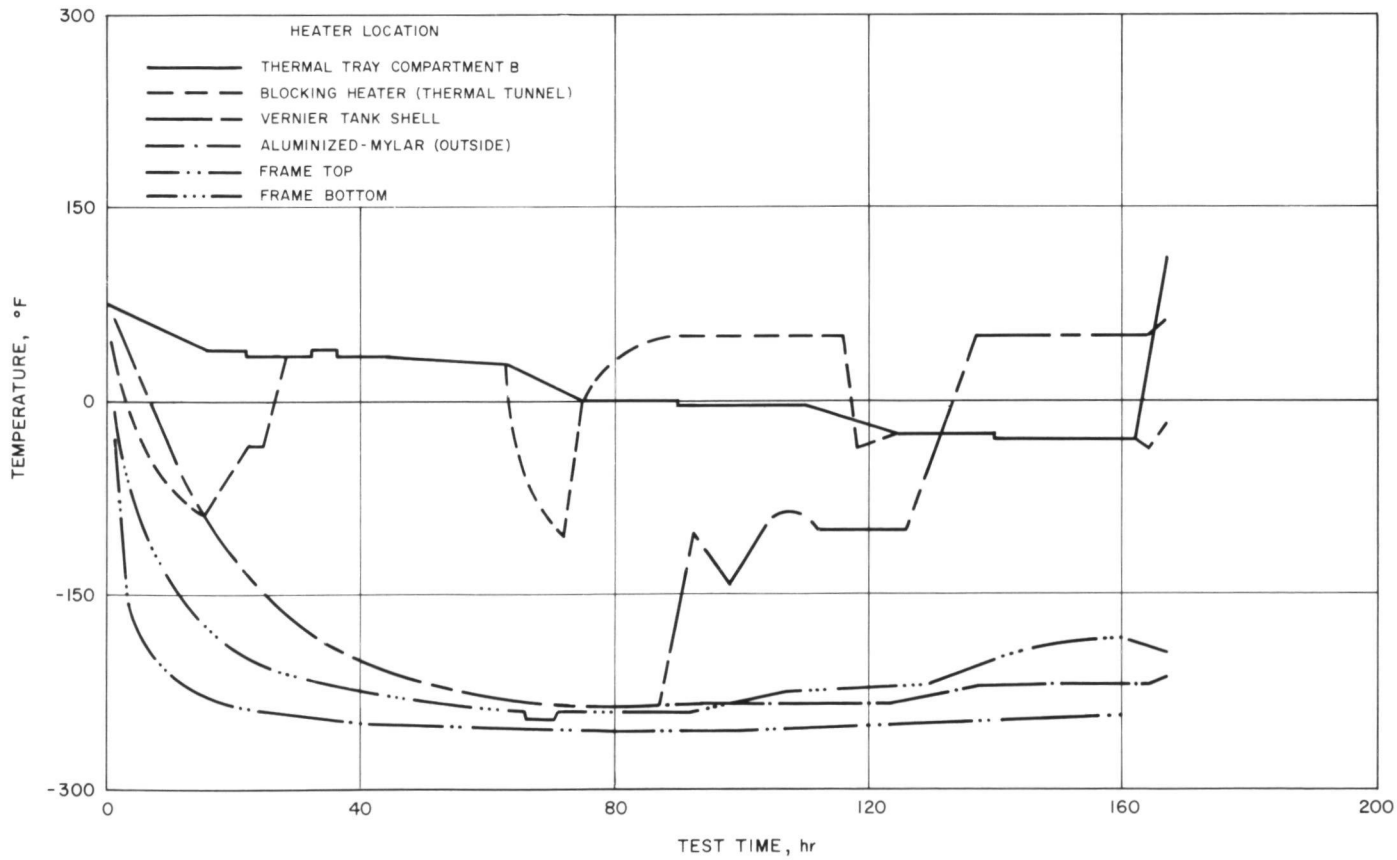


**Fig. 95. MT-1 Sector 2 lunar night test temperature histories**

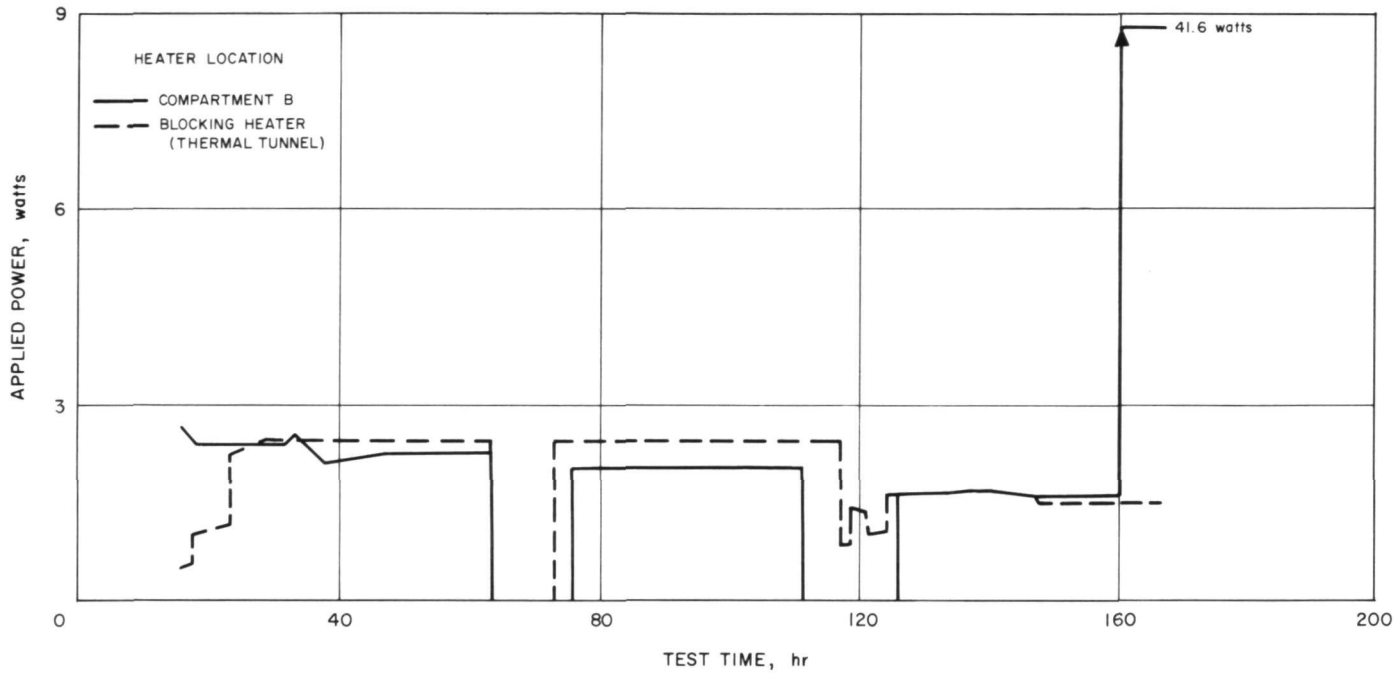


**(a) Compartment B blocking heater**

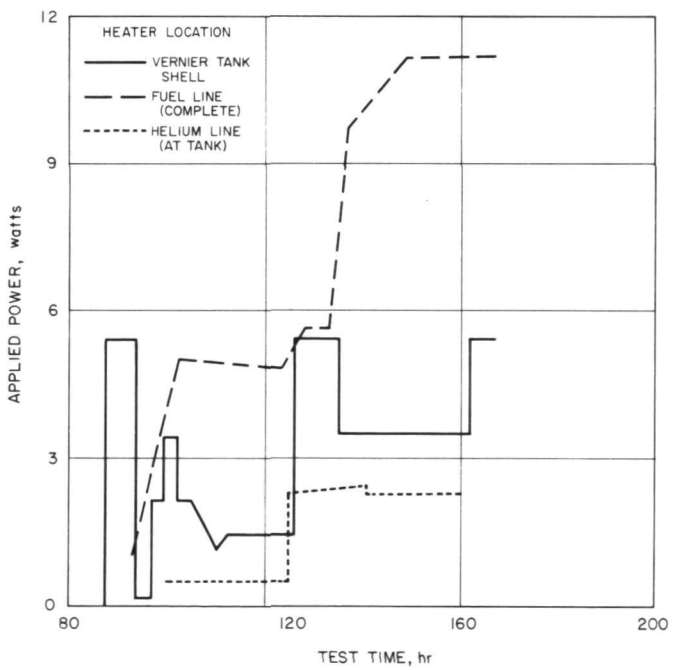


**(b) Vernier tank shell, fuel line and helium tank**

**Fig. 96. MT-1 Sector 2 lunar night test power history**

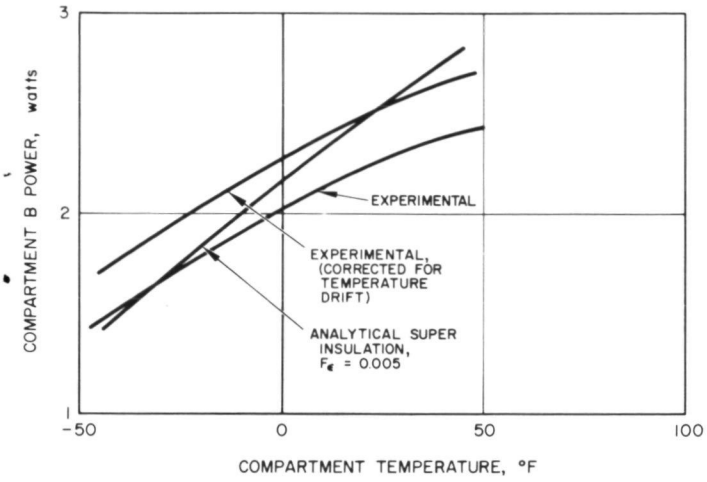


**Fig. 97. Compartment B power temperature characteristic**

**MT-1 Sector 2 lunar night test**

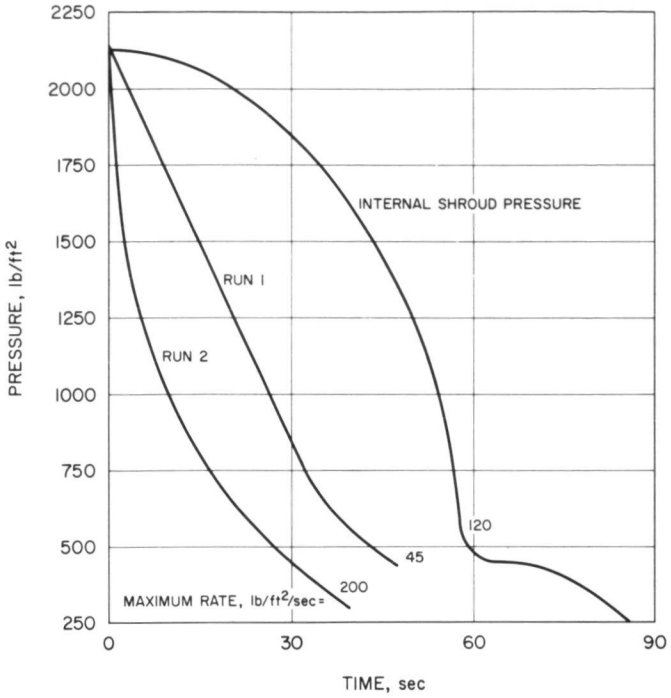


**Fig. 98. Vernier tank mylar blanket depressurization tests**

corrected curve indicates the theoretical actual power dissipation when compartment tray reaches true steady state.

The adherence paint to Sector 2 surfaces was good. No material degradation was observed as the result of vacuum and cold wall environment.

Sector 2 is being modified to include an upgraded flight control system, and a segment of the main retro-engine is in preparation for the transit and lunar noon thermal tests. The transit test will not begin until late January 1963 because of carbon-arc solar simulation installation difficulties.

***b. Vernier tank insulation depressurization test.*** A vernier tank with a 100-layer spiral-wrapped aluminized-mylar insulation blanket was subjected to a depressurization rate comparable to launch depressurization. The blanket was observed to depressurize without a harmful ballooning effect. The pressure history of the test is given in Figure 98. Run 1 is representative of the maximum unrestricted time-altitude depressurization rate; Run 2 is in excess of the depressurization rates within the *Centaur* shroud.

***c. Vernier tank tests.*** Seven vernier tank insulation tests have been conducted. The test data and wrapping procedures are summarized in Table 21. As indicated in the table the last test, using a spiral-wrapped 100-layer blanket, resulted in the best thermal performance. This final wrap technique reduced the heat loss to about one-sixth of the originally proposed "orange peel" wrap.

The original "orange peel" approach was developed for ease of assembly as the prime consideration. However, the several stitched seams joining the orange peel segments resulted in a significant degradation in thermal performance since the seams represent radiant short circuits through the blanket. The spiral wrap, while more difficult to fabricate, minimizes cracks and openings through the blanket.

## 6. *Thermal Coatings*

Work has progressed on the investigation of additives to improve the adhesion of the Hughes inorganic white paint. Typical of the additives investigated are: (1) zinc chloride, (2) sodium sulfate, (3) silicone formulations, (4) polyethylene-imine, and (5) formaldehyde. The inorganic salts were not successful. The zinc salt immediately coagulated the paint, and the 2% sodium sulfate caused thickening. The polyethylene-imine material caused visible yellowing of the paint. Formaldehyde and the silicone formulations had no apparent effect.

Tests have been designed and conducted to determine the bond strength between the inorganic paint and aluminum substrates. The test utilizes the paint as an adhesive between two shear plates as shown in Figure 99. An average shear stress of 170 psi has been obtained from ten specimens. As shown in the figure, failure is occurring at the paint interface and within the paint itself.

Figure 100 shows specimens prepared for ultraviolet irradiation tests. Spectral measurements will be made as

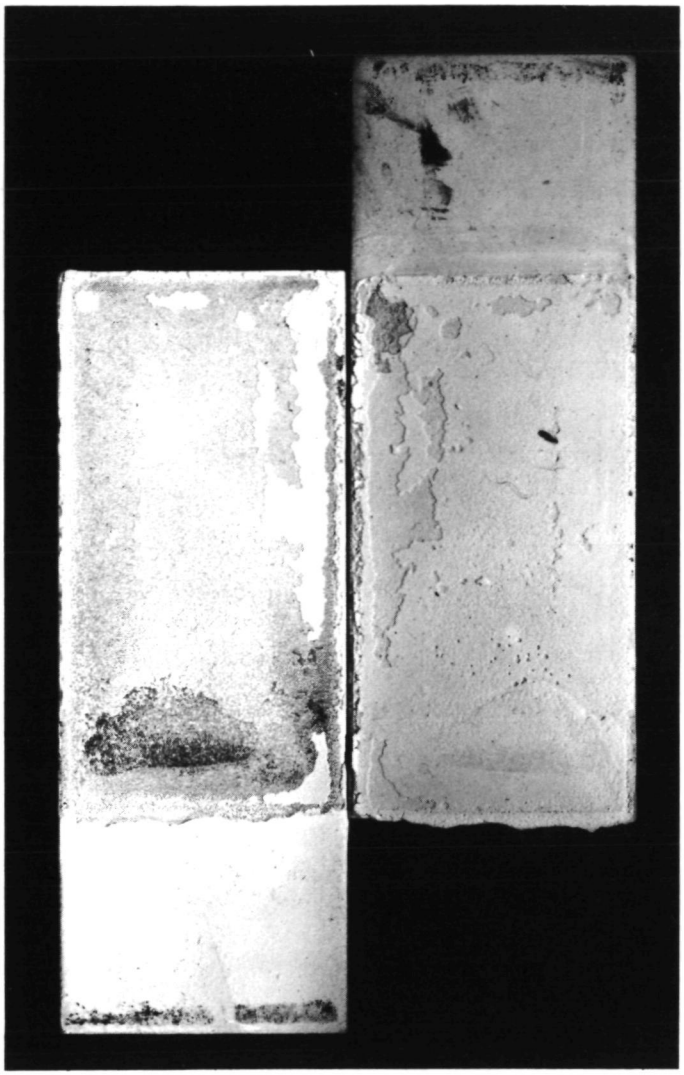

**Fig. 99. Paint adhesion test specimens**

a function of exposure time and solar intensity. The effect of atmospheric aging will also be examined.

The stability of the prime thermal coatings to the vernier fuels and oxidizer is being investigated. Samples have been prepared for placement around fuel and oxidizer tanks at Reaction Motors Division to determine if spectral properties are affected. The tests are to be conducted in early January.

**Fig. 100. Paint specimens for ultraviolet irradiation tests**

Because of the increase in solar flare activity during the *Surveyor* mission period the effect of electron impingement on the inorganic paint is being investigated. Arrangements have been made for samples to be irradiated in vacuum with 1-mev and 3-kev electrons. These tests will aid materially in understanding the effects of energy spectrum on the aging of white paint.

Hughes has joined in a cooperative program to correlate laboratory ultraviolet degradation studies with actual space tests. The program will involve thermal paint samples placed on the Orbiting Solar Observatory satellite with duplicates being sent to 20 laboratories for independent evaluation. The satellite will also carry degradable paint samples which change noticeably under ultraviolet radiation, for determination of the environment.

# H. Engineering Mechanics

## 1. Touchdown Dynamics

Further investigation has been made into the stability characteristics of the A-21 configuration. The results of previous studies on the effect of friction on stability (Figure 120 in *SPS 37-17*, Vol. I) have been expanded to include the effects of lower values of friction coefficient as shown in Figure 101.

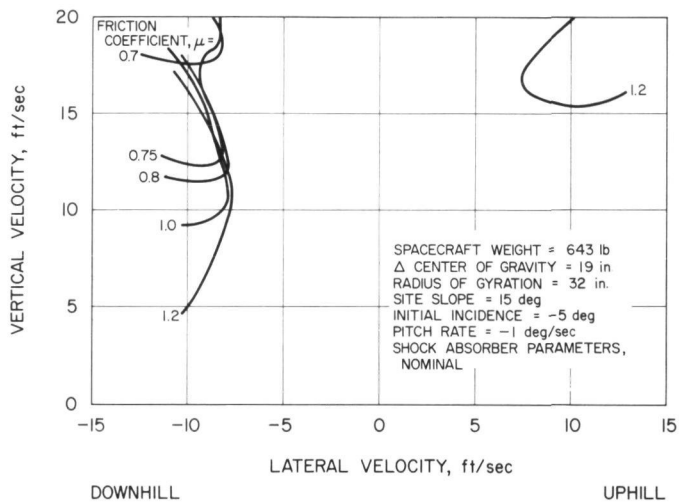


**Fig. 101. Effect of friction on landing stability**

The effect of variation in the landed weight of *Surveyor* on stability has been examined. The landing gear parameters are constant with respect to landed weight. As the weight decreases, the relative stiffness of the landing system increases. The result is a variation in the maximum allowable lateral velocity for a given center of gravity height, as illustrated in Figure 102.

From this investigation, the center of gravity height, which gives no instability inside the $10\sigma$ dispersion ellipse for the various landed weights, can be determined as shown in Figure 103. For the present payload configuration, the expected center of gravity height at minimum and maximum landed weights is well below this limit.

## 2. Full-Scale Drop Tests (T-1)

The second series of drop tests using a reduced-weight version of the T-1 vehicle will begin in December. Since the first group of earlier tests investigated the effect of site slope and friction coefficient quite extensively, the new program will be limited to drops on a 15-degree site slope. Twenty-five drops, half on the hard "rocky" surface and half on the soft surface similar to that defined in JPL Specification 30240, are planned. The hard surface drops with high friction will demonstrate the improved stability of the A-21 configuration compared with the A-25; the soft surface tests will investigate landings on a surface with energy absorption capability. The first test program demonstrated the correlation between analytical and test results; the second program will demonstrate acceptability of the A-21 design. Landing gear force and deflection data, as well as acceleration information, will be collected during this new drop test program. Flight weight shock absorbers and an alternate foot pad design (see Section J) will be tested under representative loading conditions.

The material to be used for the soft surface is being determined. Because of the problems with dynamic loading of the wood shavings used during the first test pro-

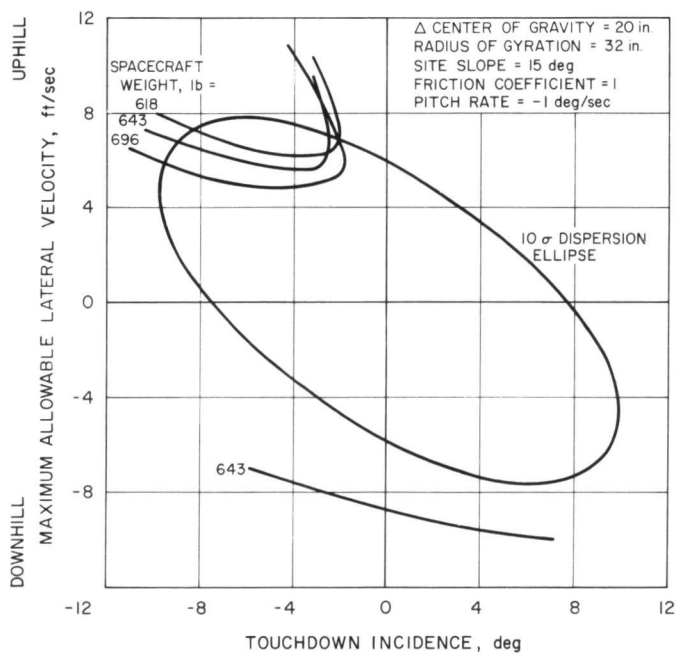


**Fig. 102. Effect of weight on maximum allowable lateral velocity**

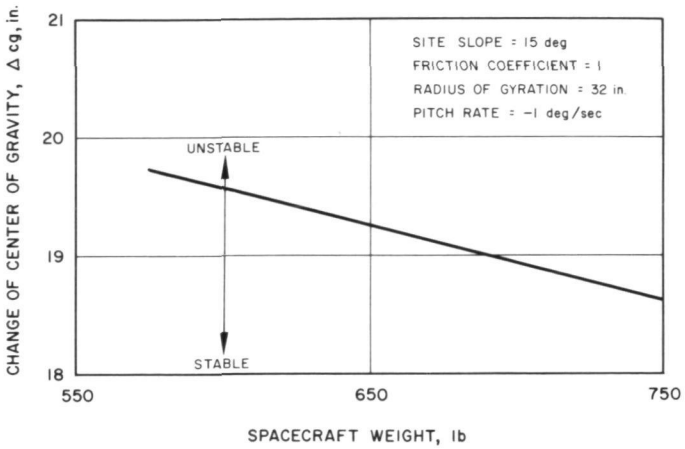


**Fig. 103. Effect of weight on allowable center of gravity height**

gram, the dynamic load stroke characteristics of various materials are being investigated. The requirement for a non-springy surface is of primary importance.

### 3. Shock Absorber Development

The shock absorber used to determine the new damper orifice size for the lighter-weight version of T-1 is being tested. Fabrication of all the parts for the prototype units has been completed and assembly has begun. The units for the T-1 vehicle will be delivered during the early part of December.

The National Water Lift Company has been notified that the thermal coating for the shock absorber is a white paint stripe on the top side; the remainder of the unit is covered with a gold foil paper. When testing of the development unit is completed, it will be covered in the specified manner to determine if any application problems exist.

### 4. Analytical Dynamic Studies

The revised structural design criteria and loads document has been completed. The loads described in the document do not reflect the recent redefinition of the spacecraft payload. This short-coming will be remedied in the near future by an addendum.

An investigation has been undertaken to establish a method for determining the rigid-body accelerations of the T-1 vehicle during test drop. This problem arose because the accelerometer traces obtained during the first series of T-1 drops were obscured by the presence of high frequency acceleration components caused by elastic-deformations of the structure. Data from these first tests were passed through various low-pass filters to determine the filter which would remove the high-frequency acceleration components most effectively. It was discovered that if the acceleration traces were passed through a 6-cps filter, the resulting data compared well with calculated rigid-body accelerations.

Design criteria for the shipping container for the T-2 vehicle were defined. This task was accomplished as part of the continuing effort to establish design loads and criteria for all shipping containers required in the *Surveyor* program.

### 5. Dynamic Testing

The program to determine the magnitude of retro-engine vibration levels imparted to the spacecraft during burning is proceeding satisfactorily, although the orignal schedule has slipped considerably. The present schedule for test firings is as follows: one in March, two in April, and one in May. These firings will be made with complete flight-weight A-21 assemblies.

Vibration levels will be measured by a group of three mutually perpendicular accelerometers mounted at each of the three retro-to-stand attach points and will be recorded on magnetic tape for future data reduction and interpretation. An attempt will also be made to measure the sound pressure levels during the first firing to ascertain whether acoustic insulation will be required. Most pre-test preparations including the establishment of a test plan, preparation of equipment, and solution of interface problems between Thiokol and Hughes have been completed. Calibrations of the accelerometer systems have yet to be completed.

Tests are being planned to determine the transportation loads that will be imposed on spacecraft T-21 and SC-1 during towing at Atlantic Missile Range. Accelerations will be measured aboard loaded ground transport vehicles GTV-1 and GTV-2 while being towed over simulated AMR roads. The results will be compared with the fragility levels previously derived for these spacecraft.

The feasibility of performing development-type vibration tests on prototype Compartments A and B is being investigated. Strain gage and accelerometer data would provide loads information for the design of equipments mounted in the compartments.

The recent payload redefinition has required an extension in the S-2 test schedule. The S-2 vehicle will be upgraded to reflect the payload changes before the commencement of testing, expected to begin about mid-April,

1963. The test plan document is being modified for the payload and schedule changes.

The design of test hardware, including vehicle suspension and shaker positioners and support, is in progress. The modal shakers to be used in the S-2 tests have been received from Stephens, Inc. The shaker control system and associated equipment deliveries are expected in January 1963.

### 6. Flight Vehicle Instrumentation

Satisfactory progress has been made by Endevco Corporation on their subcontract to provide the *Surveyor* flight vehicle accelerometers and associated amplifiers. Endevco has requested waivers on certain contractual requirements involving test procedures and performance specifications. These requests are being evaluated and will be discussed in the next bimonthly progress summary.

It appears likely that the tape recorder will be excluded from all spacecraft payloads. Touchdown loads will therefore be unobtainable except by real-time data transmission during the touchdown event. The feasibility of such transmission will be investigated in the near future. A scheme being considered requires the addition of a rigid stub antenna and provisions for high-speed switching and commutation between the four accelerometer outputs.

### 7. Static Test of Model S-2

The first static tests of the structural type approval model, S-2, were completed on November 19. Although the original test plan called for a single static-load application, two separate loadings were performed to obtain greater reliability in test results and to correct error-producing deficiencies observed during the first test.

During both tests, dead weights simulating a maximum retro-engine deceleration of 11.72 $g$ were applied to the vehicle parallel to the roll axis. Section H-7 of the preceding bimonthly report describes the method of loading. In the first test, loads were applied in 25% increments. The readings of balance scales, dial gages, and strain gages were recorded at each 25% point from 0 to 100% during loading and during unloading. The size of the increments was reduced to 10% in Test No. 2 to reduce the amount of roll and pitch observed in the vehicle during Test No. 1.

During both tests, static loads were applied by means of dead weights to 29 of the major dummy components which are mounted on S-2. Test No. 1 was performed without a retro-engine; a frame was designed to simulate the stiffness of an actual engine and was installed during Test No. 2. Retro-engine stiffness characteristics were determined from data contained in Thiokol's preliminary stress analysis report.

Because of the lag in upgrading the S-2 test vehicle to reflect the latest A-21 spacecraft design changes, there are currently significant differences between several dummy component installations on the S-2 vehicle and the actual counterparts on the spacecraft. In addition, the recently defined payload configuration is not yet reflected in S-2. However, static tests of the types described above are of value in discovering any large deviation from the allowable spacecraft center of gravity shift set by functional requirements, as well as demonstrating the feasibility of determining a shift of this magnitude (0.10 in.) by means of static testing. Test results are being evaluated and will be available in the near future.

### 8. Stress Analysis of T-2 Support Fixture

An extension boom has been added to the Aerobee launch tower to support the T-2 vehicle during checkout tests. T-2 will be tethered to the boom during operational tests of the vernier system and release mechanism prior to actual drop tests from a balloon. The boom was analyzed for loads caused by a 2-in. free drop of the T-2 vehicle. To satisfy the requirement that T-2 be subjected to an acceleration of no more than 10 $g$ during the test, the tether line should have a spring constant of less than 3800 lb/in. and an allowable maximum deflection greater than 0.5 in. Analysis indicated that a nylon rope 0.5-in. in diameter and 4 in. or more in length would satisfy all requirements. Drop tests were performed on a 13.5-in. long section of 0.5-in. nylon cord using a dummy weight of 187 lb. The results are shown in Figure 104.

### 9. Stiffness Characteristics of Super-Insulation

To provide thermal protection, compartments A and B are enclosed in a multilayer blanket of super insulation comprised of 75 sheets of aluminized mylar. The outer supports for the blankets are 0.016-in. beaded aluminum alloy sheets. The design criteria for these outer supporting shells include acoustic noise, vibration during the boost phase, and stiffness requirements needed to adequately support the mylar blanket.

To evaluate the effect of compressing the mylar blanket from its free shape to the final 1-in. thickness on the outer supporting shell, a static load-deflection test was performed. The results of a compression test of a section of mylar 12 in. square and 100 sheets thick are

shown in Figure 105. (At the time the test was performed, 100 sheets were to be used in spacecraft compartments.) As a result of the test, stiffeners were added to the edges of the outer shells and the configuration of beading in the shells was modified.

### 10. Structural Tests of Substructure to Spaceframe Joints

A series of static and fatigue tests are being performed to evaluate strength of a typical substructure to spaceframe attachment. The majority of unit-mounting substructure tubes are attached to the basic frame by yokes or "saddle fittings." A typical unit support tube is riveted to a fitting which is pinned to a yoke. The yoke is attached to a basic spaceframe tube by blind rivets as shown in Figure 106.

Figure 107 shows early static tests of a typical yoke joint. Figure 108 shows that failure occurred at the external radius of the yoke. As a result of these tests, the external radius was increased. Additional static load tests have been made in which failure occurred in the rivet that attach the yoke to the spaceframe. The rivets

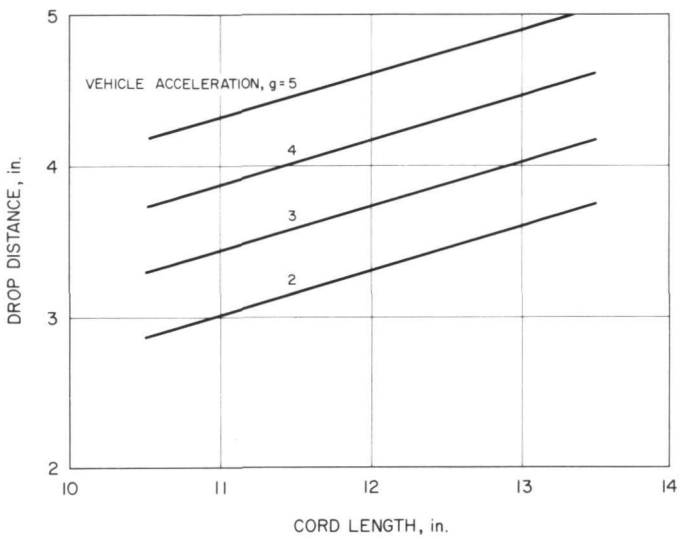


Fig. 104. Results of nylon cord tests

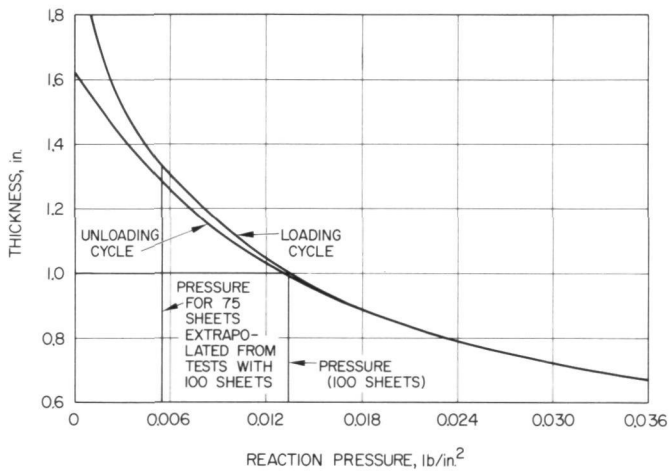


Fig. 105. Compression tests of superinsulation

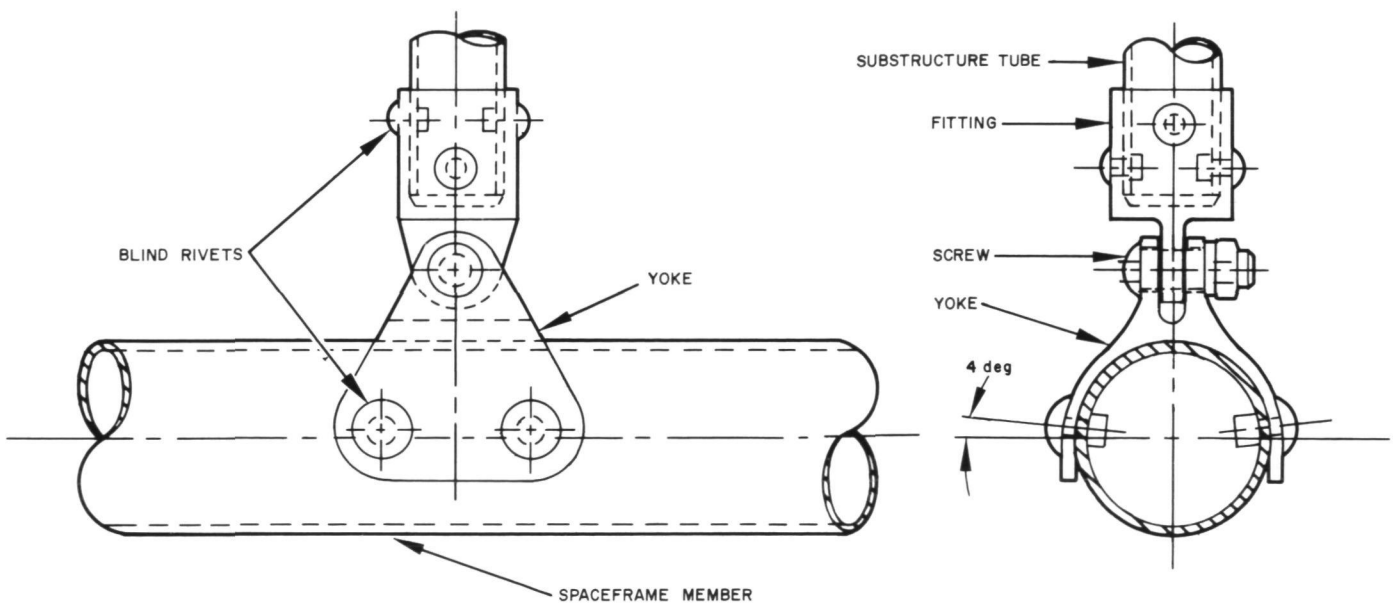


Fig. 106. Typical substructure to spaceframe joint

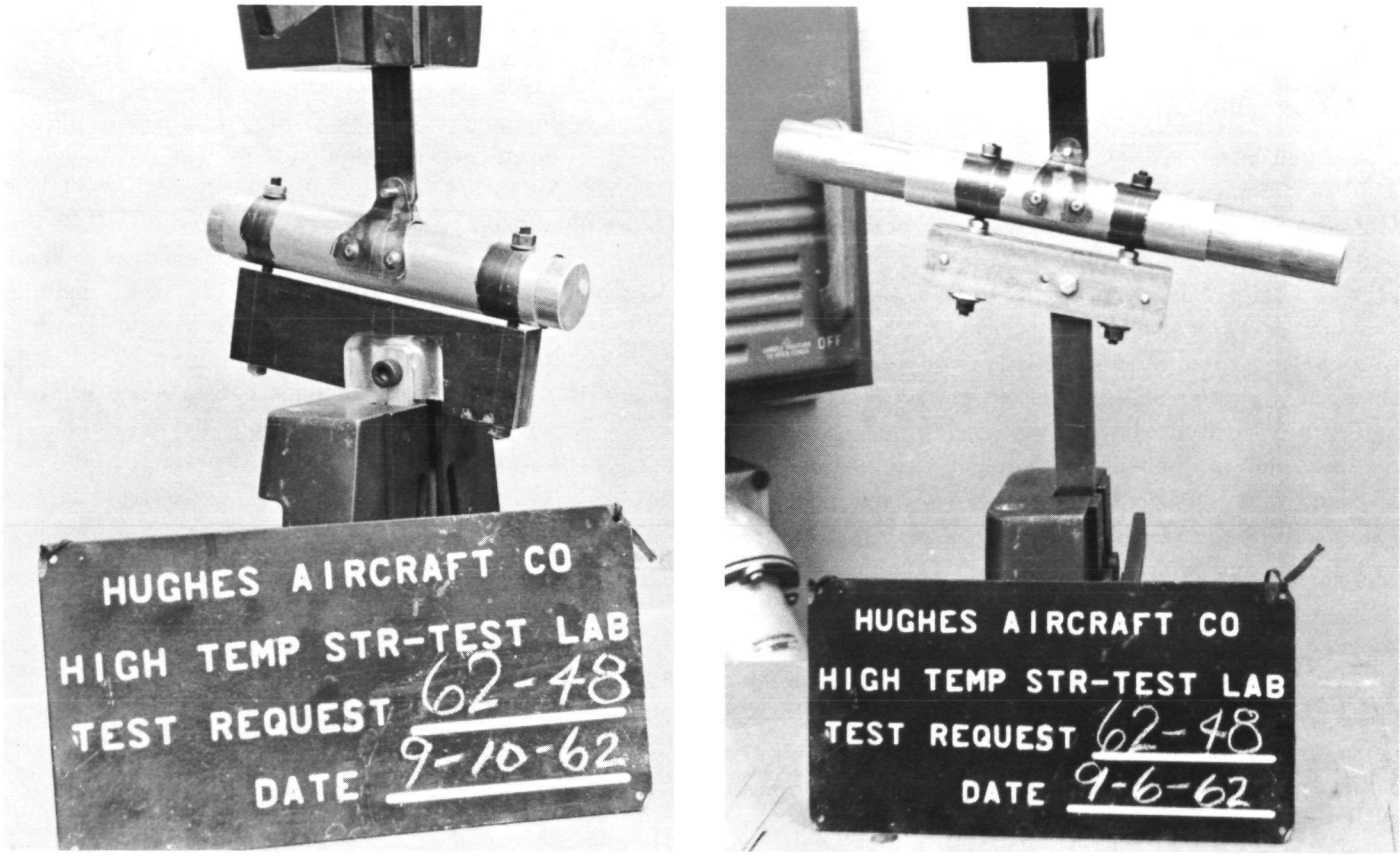


**Fig. 107. Static test of yoke to spaceframe joint**

which failed in shear were 3/16 Cherrylock blind rivets having 2017-T4 aluminum sleeves and 7075-T6 stems. Static test results which conform to data published by the Cherry Rivet Division are:

| Shear Load per Rivet at Failure, lb | Allowable Shear Load (7075-T6 sheet, 0.050 in. thick), lb |
|---|---|
| 1061 | 695 |
| 1130 | |
| 1080 | |
| Average: 1090 | |

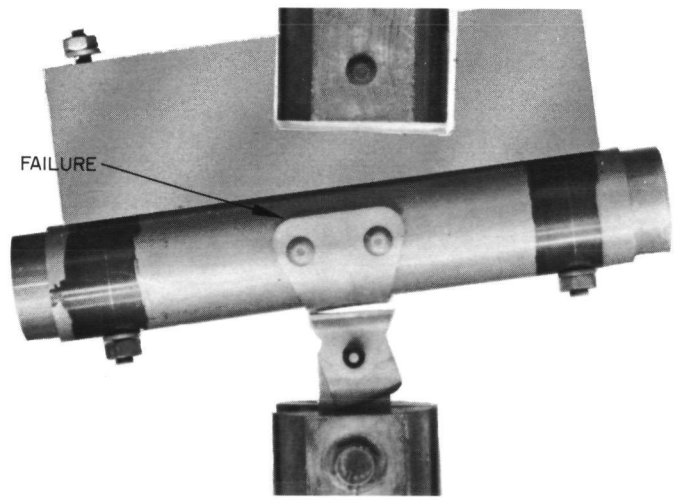


**Fig. 108. Failure of yoke due to static loading**

# I. Propulsion

## 1. Introduction

The spacecraft has two propulsion systems, a spherical solid propellant retro-rocket engine and a liquid propellant vernier engine system. The retro-rocket engine decelerates the spacecraft preparatory to landing; development of this engine has been subcontracted to the Elkton Division of Thiokol Chemical Corporation. The vernier propulsion system performs incremental velocity corrections for the midcourse maneuver and terminal descent and controls attitude during operation of the retro-rocket engine. One of the three vernier thrust chambers is swiveled to supply a roll-control thrust component. Development of the vernier system has been subcontracted to the Reaction Motors Division (RMD) of Thiokol.

## 2. Progress Summary

*a. Main retro-engine.* The design changes reflecting the new nozzle and other refinements to the A-21 retro-rocket engine were completed. Detailed engineering analysis of test results from two engines fired with improved nozzle contour confirms satisfactory performance. Procurement was initiated for a safe-and-arm assembly compatible with the safety requirements at Atlantic Missile Range. The structural adequacy of the engine case was demonstrated in an additional hydrostatic burst test.

The altitude test facility which is located at the Elkton Division of the Thiokol Chemical Corporation is operational and the initial test with engine A-25-11 is scheduled for mid-December, 1962.

*b. Vernier engine system.* During this report period, the T-21 vernier propulsion system was delivered to Hughes Aircraft Company. Previously delivered T-2 thrust chamber assemblies were returned to RMD for rework after an injector clogging problem was defined. After successful rework, the T-2 and T-2S thrust chamber assemblies were delivered to Air Force Missile Development Center to support the T-2 test program. Four flight design thrust chamber assemblies have been fabricated and will be fired during the next report period to confirm performance and dynamic response characteristics.

## 3. Main Retro-Rocket Engine

*a. Engine tests.* Two firings at Arnold Engineering Development Center (AEDC) indicate that redesign of the nozzle was successful in achieving the design specific impulse, as indicated from preliminary data reported in the preceding bimonthly progress summary. The thrust curves for the two engines are given in Figure 109. Engine A-25-7 operated abnormally because the nozzle inlet fractured after 5 sec of operation. Performance data for the two engines are given in Table 24, together with data corrected to vacuum operation and projections of what A-25-7 performance would have been if the nozzle had not fractured. The test setup at AEDC is shown in Figure 110.

Engine A-25-11 will be tested in the Elkton Division altitude test facility in mid-December, 1962, to substantiate the test results obtained at AEDC.

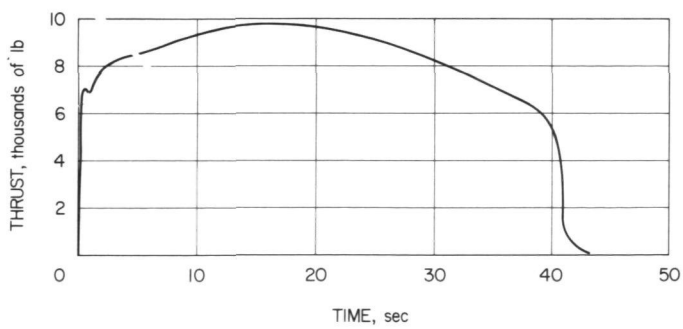


(a) A-21-3

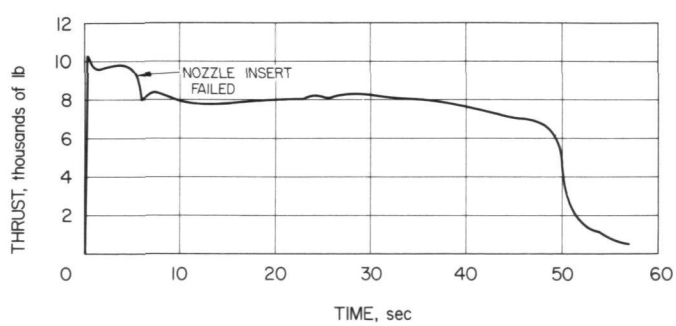


(b) A-25-7

Fig. 109. Vacuum thrust of retro-rocket engine

**Table 24. Data from engine tests at AEDC**

| Parameter | A-21-3 Engine | A-25-7 Engine |
|---|---|---|
| Total impulse, lb-sec | | |
| Measured | 344,630 | 404,030 (416,510)[a] |
| Vacuum corrected | 345,464 | (417,500)[a] |
| Specific impulse, sec | | |
| Measured | 289.3 | 283.5 (291)[a] |
| Vacuum corrected | 290.0 | (292)[a] |
| $W_p$ loaded, lb | 1191.39 | 1424.75 |
| Thrust, lb | | |
| Maximum (during $t_b$) | 9790 | 10,300 |
| Minimum | 7900 | [b] |
| Average | 8540 | [b] |
| Pressure (maximum), psia | 570 | 550 |
| Burn time ($t_b$), sec | 39.6 | 49.4 |
| Action time ($t_a$), sec | 41.5 | 51.9 |
| Time to 40-lb thrust, sec | 43.5 | [b] |
| Initial expansion ratio ($A_e/A_t$) | 50.3:1 | 46:1 |

[a]Calculated value if nozzle insert had not failed.
[b]No meaningful data because of nozzle insert failure.

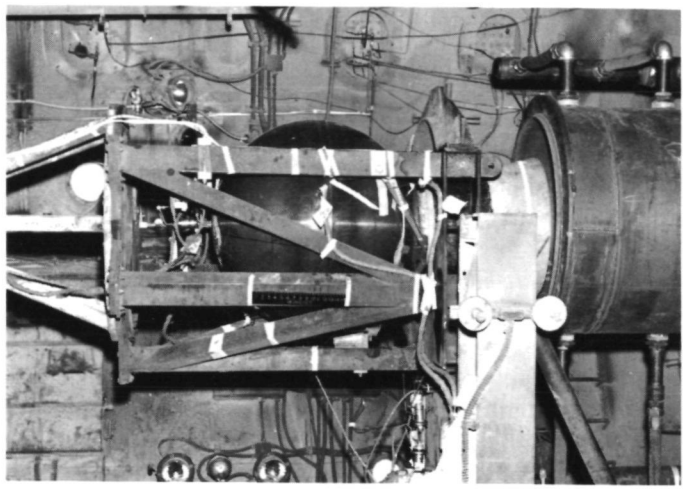

**Fig. 110. Engine A-21-3 in test mount at AEDC**

*b. Design changes.* The design changes to optimize the A-21 engine configuration were completed. The changes include: (1) modification of the case insulation, (2) revision of propellant geometry to neutralize the pressure-time profile, (3) removal of excess case material for weight reduction, and (4) increase in expansion ratio by reduction of the nozzle throat area.

Procurement of a safe-and-arm assembly for the retro-rocket engine was initiated. The requirements will include: (1) 1-amp, 1-w, no-fire squibs, (2) electrical shorting of the firing circuit in the safe position, (3) mechanized out-of-line provisions in the safe position, and (4) a mechanical safety mechanism for use during handling and storage. The retro-rocket engine will be armed just prior to launch to permit a final remote verification of safe-and-arm position and squib continuity.

*c. Flight-weight case.* The first flight-weight case fabricated by the Lycoming Division of AVCO was hydrostatically burst tested. The case burst at a pressure of 976 psig; this represents a substantial margin of safety over the minimum design burst pressure of 770 psig. Final welding and machining operations have been resumed and fabrication of cases is on schedule.

*d. Flight-weight nozzles.* The H. I. Thompson Co. was selected on the basis of competitive bidding to fabricate the flight-weight nozzle. Delivery of the first sea-level configuration nozzle in early February, 1963, is expected. Delivery of the flight-weight nozzle is the pacing item in the development program.

*e. Altitude test facility.* Incorporation of a hydrogen peroxide thrust augmentation system into the Elkton Division altitude test facility was completed. This system has a capacity of 70 lb of steam per second and enables testing of the A-21 rocket engines at a simulated altitude of 70,000 ft from ignition to burnout.

*f. Thermal control.* The results of the initial three-dimensional thermal analysis are being evaluated. A complete program for prediction of critical performance parameters (thrust-time and pressure-time) of the retro-engine for various thermal gradient conditions is being generated. The scheduled completion date of the evaluation is March 2, 1963.

### 4. Vernier Engine System

The vernier propulsion system is comprised of three thrust chambers, six propellant tanks (three each for oxidizer and fuel), and a single helium tank for pressurization. Each thrust chamber is regeneratively cooled by the fuel (monomethyl hydrazine) and is capable of being throttled from 104 to 30 lb vacuum thrust. The oxidizer is a mixture of 10% nitric oxide and 90% nitrogen tetroxide by weight. Nitric oxide acts as a freezing point depressant. The entire vernier propulsion system is capable of producing approximately 50,000 lb-sec of impulse.

*a. Delivery phase.* The vernier propulsion system for the T-21 spacecraft was fabricated and delivered to Hughes on October 22, 1962. It was the first system built to flight quality standards.

During system acceptance tests of the system for the T-2S spacecraft, two of the three thrust chamber assemblies did not operate satisfactorily. Particles from a Viton-A O-ring lodged in the oxidizer injector. The vacuum flushing procedure, at first suspected of causing O-ring deterioration, has been eliminated as the source of the difficulty. It has been concluded that the problem

is caused by mechanical deformation of the O-ring and cutting from installation and swelling. The Viton-A O-ring compound was originally chosen over teflon because of the heat sterilization requirement. Since the T-2 spacecraft does not require sterilization, teflon O-rings were substituted in the critical areas of the T-2 and T-2S thrust chamber assemblies, and all assemblies were delivered to Hughes.

*b. Complete system development.* Static expulsion and unbalance tests are in progress on the S-4 development system. Data are being accumulated to define the most suitable propellant loading technique to minimize any unbalance conditions. Firing of the system to define the propellant unbalance caused by asymmetric thrusting is scheduled for the early part of the next report period. Thermal gradient and low and high temperature tests on the second development system will follow the expulsion and balance tests.

*c. Component development.* The fabrication of four flight-type thrust chamber assemblies was completed during this report period. These assemblies will be used to determine the performance characteristics, including dynamic response, of the flight design over a temperature range of 0 to 100°F.

O-ring problems and the throttle valve improvement program currently being conducted have delayed the throttle valve approval tests until the next report period. The improvement program includes changes to the valve to improve fabrication reproducibility and to reduce hand rework and adjustment.

The helium regulator approval tests were successfully completed.

# J. Spacecraft Vehicle and Mechanisms for Basic Bus

## 1. Spacecraft Vehicle

***a. Configuration.*** Preliminary layouts and detail studies were made to integrate the redefined scientific payload as listed in Section B. Mechanical provisions for this new payload will be incorporated during the early upgrade period for T-21. To achieve this deadline the payload configuration, as well as the outline and mounting drawings of the individual components, were frozen early in December, 1962.

***b. Vehicle status.***

*T-21–system type approval prototype.* The T-21 vehicle was returned from the Reaction Motors Division after vernier engine installation, and mounting of component attach bracketry and components is under way. New substructure to incorporate the new payload is being developed as unit locations are determined. Assembly of this vehicle within a protective canopy is shown in Figure 111.

*T-2–terminal descent dynamics vehicle.* The T-2 vehicle and its spare (T-2S) were completed and delivered for checkout and test operations at Air Force Missile Development Center.

*S–2 structure test vehicle.* The S-2 vehicle has completed initial static tests. It was returned for upgrading to T-21 type support structure for Compartment A and B, the flight control sensor, doppler antennas, and vernier engines (Figure 112).

*MT-1–thermal test A-21 type spacecraft.* The MT-1 vehicle is constructed in three sectors. Sector 2, containing Compartment B and flight control units, is being prepared for transit and lunar day tests. These tests are planned for the latter part of January when the solar simulator will first be available in the Space Environment Laboratory. Sector 3, which contains the bulk of the new payload will be prepared for testing upon final integration of these units.

Thermal finish adherence problems which first became apparent on the vehicle are the subject of continued

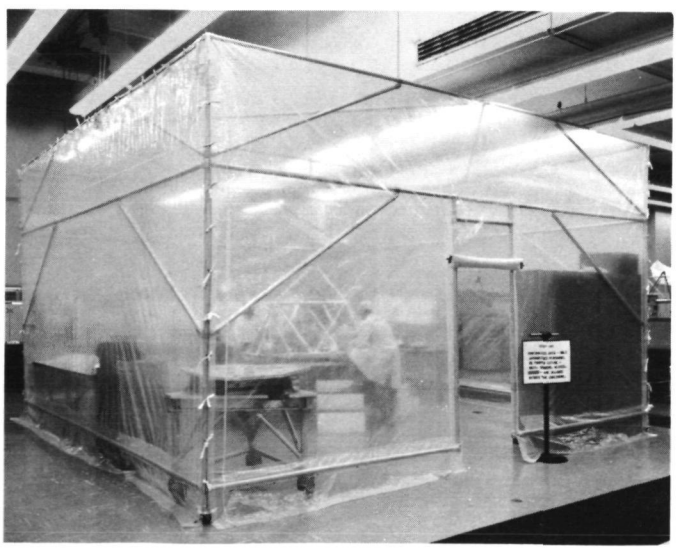

Fig. 111. Assembly of T-21 vehicle

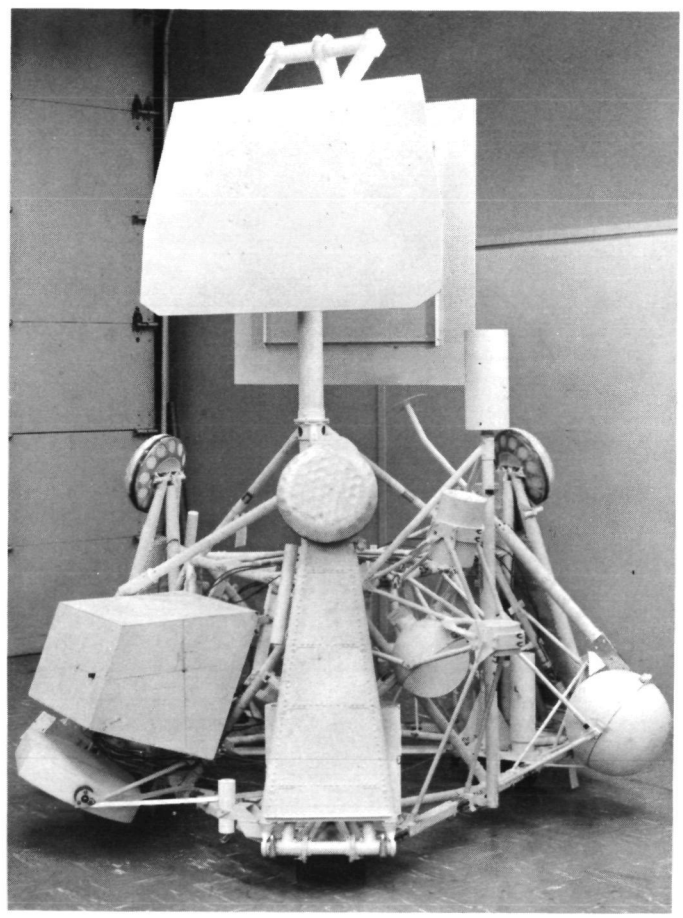

Fig. 112. S-2 structural test vehicle

study. A new paint laboratory is being set up and personnel are being given special training in the finishing of spacecraft surfaces. In addition, studies are being performed to select alternate methods of lubricating blind rivets prior to pulling. Earlier studies indicate that oily substances are escaping from these fasteners, causing surface contamination and local blistering of paint.

*S-6, S-7 — vernier propulsion test vehicles.* The S-6 and S-7 vehicles have been rescheduled for completion in 1963.

***c. Wiring harness.*** The harness design was modified to permit minimum restraint to retro-engine separation during lunar terminal descent. The ejection force on the altitude marking radar dish from retro-engine ignition is also used to separate the igniter and radar leads.

In the present design, the igniter leads follow the upper hemisphere of the retro-engine to the disconnect. The cable is attached to a flexible aluminum strap to prevent puncture of the thermal insulation blanket. The strap is attached at the upper end to the igniter receptacle and held in tension by a helical spring attached to the lower retro-engine mounting bracket. However, this flexible strap tends to compress the insulation and therefore is being replaced by a rigid fiberglass plastic support as shown in Figure 113.

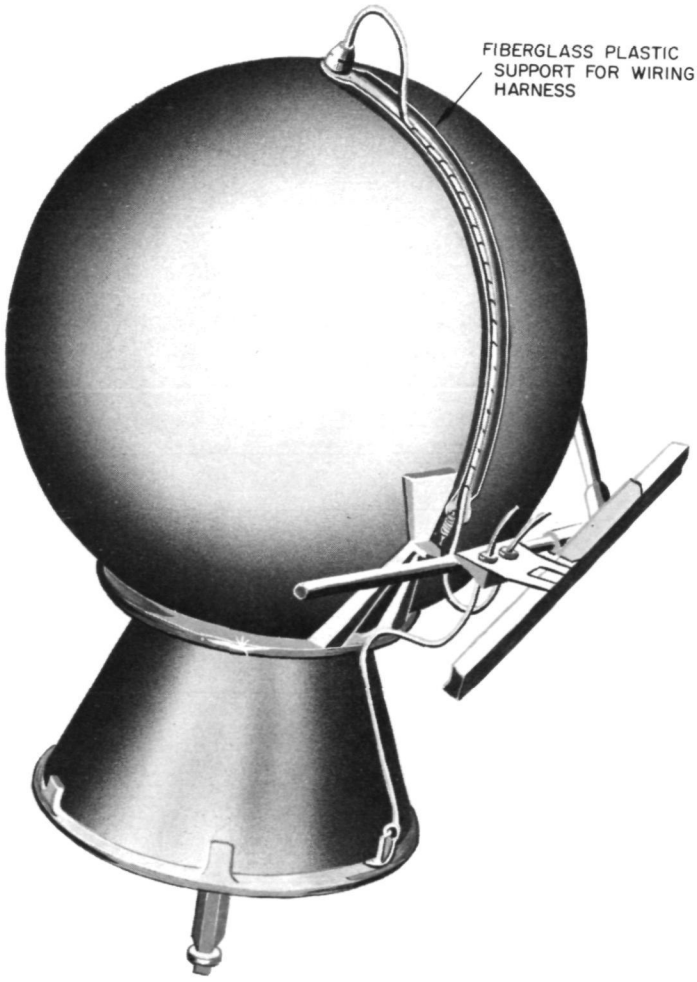


**Fig. 113. S-3 wiring harness support**

***d. Landing gear footpad.*** In an earlier bimonthly report (SS-108), June/August 62 period landing gear foot modifications and tests results were described. The most satisfactory design tested was a low-density stafoam pad having holes in the sides and bottom. The pad was supported by an aluminum cap and enclosed in a fiberglass bag. Results were satisfactory except that puncture of the bag allowed crushed stafoam pieces to spread over the landing area.

A new aluminum honeycomb pad has been designed to minimize spreading of material over the landing area. A prototype model (Figure 114) will be tested during the latter part of the next series of T-1 drop tests. The yoke is the connection between the foot and landing gear structure. A support plate provides an efficient pad support which will crush laterally at safe loads. The honeycomb provides progressively lower crushing strengths to minimize vertical loads. The separator acts as a bearing surface between the honeycomb layers. The bottom cover provides bearing to limit the foot penetration in very soft surfaces.

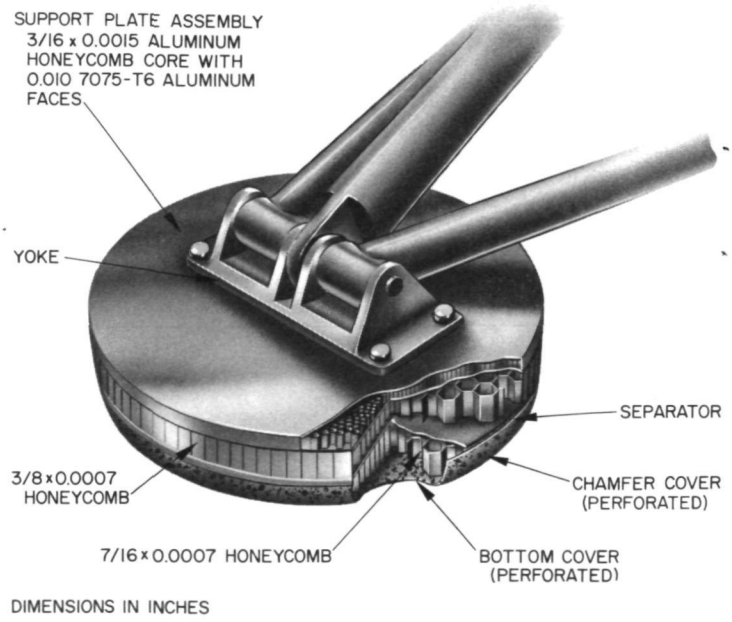


**Fig. 114. Prototype footpad design**

*e. Retro-engine separation tests.* After the first separation test, the firing control and instrumentation circuits were rebuilt to include extra safety features. Necessary components to obtain more accurate results on the remaining tests were added. In addition, the simulated retro-engine was reworked to allow it to be supported at the cg with a thin cable. The cable is attached to the spacecraft drop-test anti-gravity device, which was used to control the separation acceleration of the simulated retro-engine from the test fixture. (During the first separation test, the simulated retro-engine was allowed to free-fall after the explosive nuts were fired.)

The second separation test was performed on November 9 using only two explosive nuts. For this test the anti-gravity device was adjusted to simulate a separation acceleration under the conditions where the verniers are each producing 30 lb thrust. The oscillograph recording showed that both squibs received current and fired simultaneously. Because of power failure, the cameras never reached full speed, and the films could not be used for analysis. However, the simulated retro-engine appeared to drop straight down without any radial or axial tipping.

**Fig. 115. Simulated retro-engine in separation test fixture**

The third separation test was performed on November 15 using only one explosive nut. The anti-gravity device was adjusted for a separation acceleration simulating the condition where the vernier engines are each producing 30 lb thrust. The squib fired satisfactorily, but an error in reading the calibration of the load cell from the anti-gravity device caused an excess of 100 lb lifting force to be applied to the simulated retro-engine. As a result, the simulated engine did not separate from the fixture when the nut fired. The fourth separation test was performed on November 20 using two explosive nuts. During this test the anti-gravity device was adjusted for a separation acceleration simulating the situation where the vernier engines are each producing 104 lb thrust. The simulated retro-engine again appeared to drop without any tipping.

In general, the oscillograph recordings of the tests indicate that the bridge wires in the squibs are burning through in 0.00131 to 0.00187 sec after they receive current. In addition, accelerometers located on the fixture are registering shock spikes of 560 to 875 $g$ from the firing of the explosive nuts. Figure 115 indicates the test setup.

## 2. Basic Bus Mechanisms

*a. Omnidirectional antenna mechanisms.* The antenna mechanisms (A and B), consisting of tapered fiberglass tubes bonded to aluminum hinge brackets, deploy the two omnidirectional antennas and coaxial cabling prior to separation of the spacecraft from the *Centaur*.

During this report period the redesigned pin puller bracket for Mechanism B was fabricated and attached to the mechanism; it successfully passed three-axis vibration tests in both the stowed and extended positions. In addition, both engineering model mechanisms passed the tests of landing shock along the thrust axis and both lateral axes. The models have been delivered for assembly and additional testing on the S-2 vehicle.

Initial deliveries for the T-21 test spacecraft have been made. Improved hardware fabrication and assembly have begun.

*b. Antenna/solar panel positioner.* Assembly of the prototype and type approval units is continuing. The initial four-axis engineering model was painted to check the paint pattern and masking callouts. This unit has been delivered to the spacecraft assembly area to confirm the mounting provisions and clearances on the T-21 test spaceframe.

The second prototype engineering model underwent a second thermal-vacuum test at $-200°F$ and $7 \times 10^{-7}$ Torr pressure prior to vibration testing. The spacecraft logic circuitry was used to drive the gimbal assembly

(Figure 116). During the test the motor response rates, current, voltage, and potentiometer continuity were monitored. The unit functioned satisfactorily, using spacecraft logic circuitry, with the exception of erratic potentiometer and polar axis drive operation. The potentiometer wiper is being redesigned to increase the wiper tension and the wiper carrier material has been changed from teflon to a thermally stable, glass-filled teflon. The polar axis worm gear drive is being tested separately in a fixture to monitor friction levels (Figure 117). The efficiency of the drive has been considerably improved by the addition of "DU" journal and thrust bearings at the worm. Great difficulty has occurred in obtaining proper alignment of the worm and gear sector at assembly; these misalignments have contributed to erratic performance of the polar axis drive in the thermal-vacuum tests.

The material for the gas restrictor which controls the rate of mast extension has been changed from a sintered metal restrictor to a fixed orifice with a sintered metal filter. Fabrication problems with the sintered restrictor resulted in inconsistent operation.

*c. Motors and mechanisms drive units.* One Curtiss-Wright and one Ledex rotary solenoid motor are currently undergoing long-term high temperature-vacuum testing.

The four-axis drive assembly of the antenna/solar panel positioner, mounted on a stub mast, was subjected to an ambient-pressure, low-temperature test under simulated lunar loads (Figure 118). The objective of the test was to reveal any temperature-induced malfunction of the drive mechanism components at temperatures as low as −300°F. The drive motor currents were limited to simulate the current limiting characteristics of the spacecraft motor drive logic. The only malfunction detected was erratic potentiometer function, confirming the information obtained from the antenna/solar panel positioner thermal-vacuum operation.

*d. Separation sensing and arming devices.* Three prototype models of the separation sensing and arming devices which provide interruption of some portions of the spacecraft explosive circuitry, have been delivered to the T-21 test vehicle. The type approval test model has been assembled, and the test specification is being prepared.

*e. Anchoring device.* All effort ceased on this task and the explosive anchor subcontract was terminated upon receipt of the firm redefinition of the scientific payload.

*f. Pyrotechnic actuated devices.* The specifications, statement of work, and associated documents for the

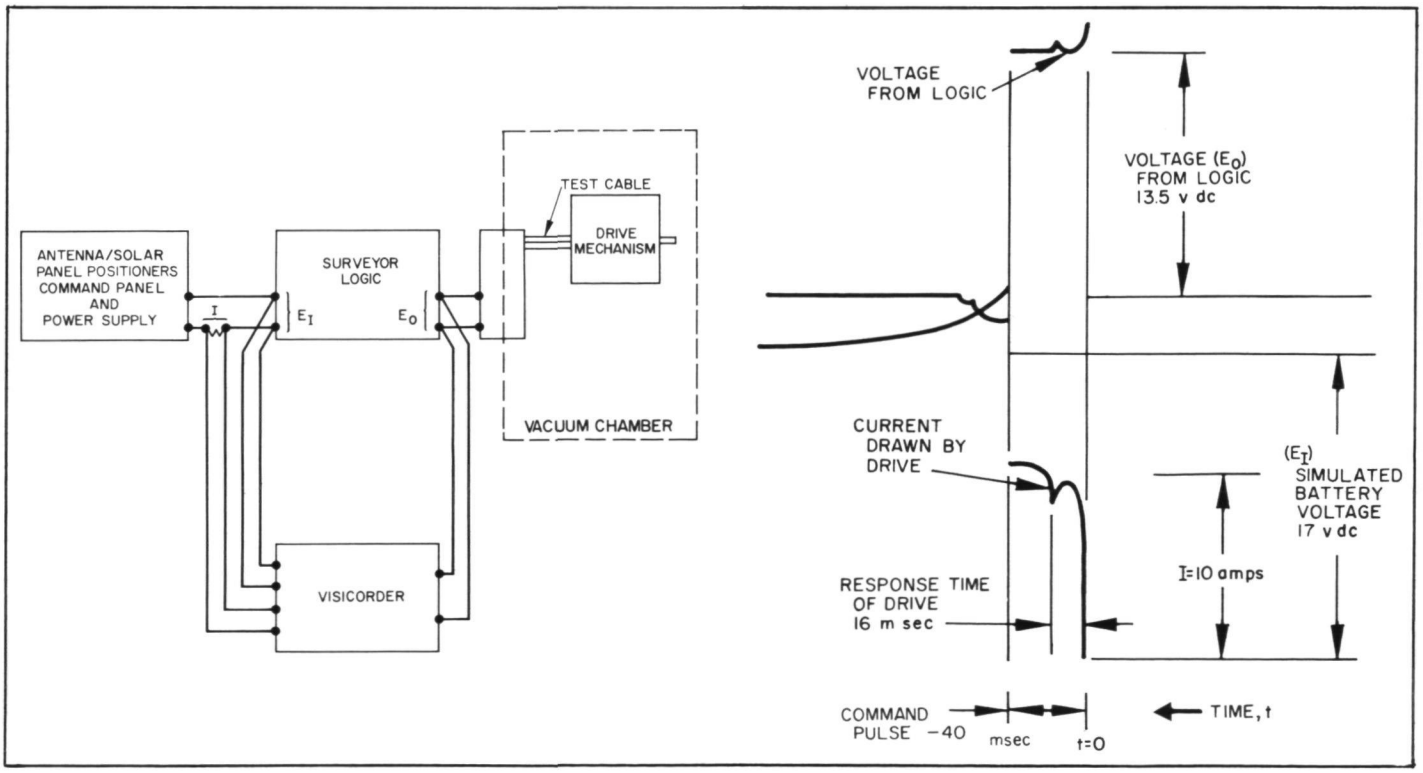


**Fig. 116. Test set-up for antenna-solar panel positioner with typical recorder**

electric squib have been revised to reflect the requirement for a 1-amp, 1-w, 5-min, no-fire characteristic. Pending submission of formal cost and schedule proposals, the vendor has started preliminary development work on the new squib bridge wire configuration.

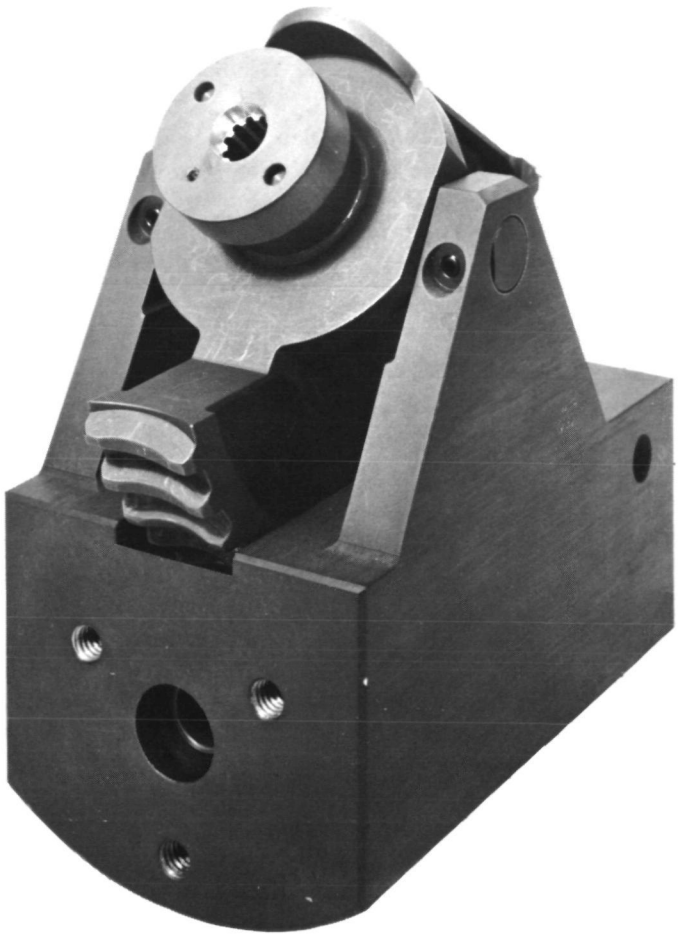

**Fig. 117. Polar axis worm gear test fixture**

Prior to stopping work on the 1-amp, 60-sec, no-fire squib, a minimal quantity of each dash number was obtained for engineering testing of the squib-actuated devices. Since the squib output will remain unchanged in the new squib, such operational tests are valid for the new firing characteristics. A successful firing test was conducted on an explosive valve assembly utilizing a squib of the 1-amp, 60-sec no-fire type to evaluate the squib output and functional capability in the device at −180°F. Complete shearing of the valve diaphragm by the squib propelled ram was accomplished.

**Fig. 118. Low temperature test of gimbal system**

# K. Reliability and System Test

## 1. System Test

*a. STEA checkout and integration.* The checkout and integration of the T-21 system test equipment is progressing on schedule. All of the major items required during the initial T-21 testing phase have been delivered. Final checkout is scheduled for completion by December 15. The following major integration tasks have been accomplished to date:

(1) Installation and alignment of the system test stand.

(2) Unit checkout of all STEA equipment racks.

(3) Verification of the STEA intercommunications system.

(4) Verification of the primary standard NASA time code distribution system. This system supplies a time reference to the tape recorder, the digital printers, and the strip chart recorders.

(5) Verification of the 115/208 v 60-cycle power distribution system.

(6) Verification of the 22 and 29 v dc auxiliary power distribution circuits.

(7) Verification of the telemetry data distribution system. The 16 analog, 40 parallel binary and 7 discriminator output channels from the command and data handling console have been tested through the command decoding and signal processing test rack distribution circuits and to their destinations in the power, RF and flight control racks.

(8) Verification of all signal and power wiring from the flight control, power, and RF test racks to the Sector I junction box. This constitutes 95% of the Sector I junction box interconnections.

(9) Verification of all signal and power wiring from the flight control test rack to the Sector II junction box. This constitutes 35% of the Section II junction box.

(10) Verification of the system test stand interface with the flight control rack control circuit.

*b. System test procedures.* Preparation of detailed system test procedures to be used during the initial group test phase of system functional tests is nearly complete. The procedures include those necessary for group quantitative tests of the transmitter and receiver, command decoding and signal processing, television, flight control, altitude marking radar, radar altimeter and doppler velocity sensor, vernier engine, basic bus mechanisms, and spacecraft power control. Initial power and grounding procedures are also being written.

The procedures are being converted to use automatic data processing technique. A general format has been adopted that allows the capabilities of an IBM 1401 computer to be used for printing, storing, changing, and sorting the procedure information. A rapid method of changing the procedures to keep them up to date at all times has been a major objective.

Rapid access is one of the advantages to be gained by using data processing to prepare procedures. Once the fundamental procedue steps are stored on magnetic tape with a library reference numbering system, the new set of procedures can be written by selecting the proper references in the required order and sequence.

A complete book of procedures will be written for each of the various tests to be performed, such as thermal-vacuum, RFI, and launch pad tests. Data processing allows necessary changes discovered in one test to be incorporated rapidly in all other tests that may be affected.

An operator code letter will be used to indicate the STEA operator responsible for a particular step. The code letter will specify the operator who will initiate an action, observe the results, and record the observations on the test data sheets.

The log and data sheets for test operations will also use the data processing facilities. A book of these sheets will accompany each set of procedures and summarize the required observations and necessary tolerances for a particular step. The operator will make his notations in the spaces following the typewritten requirements. Changes in the procedures will also affect the log and data sheets, since they are both printed from the same computer information.

A standard operating procedure for acquisition and reduction of the data recorded by the FR600 magnetic tape recorder during system tests have been established. This procedure ensures rapid, accurate, and objective requests for data reduction by use of a convenient and easily compiled form. The procedure outlines the type of data format available for the various types of data. The output forms are either analog or tabular, depending on the needs of the data analyst.

For telemetered data, a magnetic tape is utilized. The data can be transmitted either via a radio frequency link or via hard line, bypassing the transmitter. Also recorded on the magnetic tape are commands generated by the CDC command generator, power profile voltages and current data, NASA time code, and voice. The voice channel can be conveniently utilized for entering variations in test procedures, speed changes, procedure number, etc., on the magnetic tape, aiding in effective and timely reduction of the data.

It is planned to utilize punched paper tape during group integration and mission sequence tests to record commands generated from the CDC and the time of occurrence. During group tests, timers and on-off counters perform this function. This method allows collection of data on the length of time each item of spacecraft equipment was on and the number of times it was turned on and off during tests. The data will be used for reliability failure analysis.

*c. Scientific instrument system test.* After the recent payload definition, block diagrams were prepared for group and system testing of the scientific experiments. The diagrams are expected to change somewhat as the instruments are better defined. A tentative list of test equipment has been prepared and will be added to the STEA master index. This list includes both off-the-shelf and special test equipment, including stimuli. Where practical, stimuli identical to those at JPL will be used. To implement this objective it is planned that Hughes will write stimuli procurement specifications that will be submitted to JPL for approval.

Work is under way to coordinate the efforts of the system test area with the experiment compatibility evaluation area at Hughes. It is intended to use identical stimuli in both areas. It is also planned to use the same test equipment in both areas to avoid duplicating engineering design effort.

*d. Descent dynamics test vehicles.* Testing of the spacecraft soft landing capability is presently under way at the Air Force Missile Development Center (AFMDC) utilizing the T-2 vehicle. In preparation, vehicle recovery characteristics were investigated and a parachute recovery system was devised with a modified vehicle, T-2R. Subsequently, a simulated T-2R vehicle was employed in a ten-drop test to establish minimum safe recovery altitudes for the T-2 program. Results of that test were summarized in the last bimonthly report.

Initial system testing of the T-2 vehicle was performed during the period October 4 to November 9, 1962, at Culver City. Primary objectives were to integrate the vehicle subsystems and resolve incompatibilities before delivery to AFMDC. The vehicle consisted of frame, wiring harness, recovery system control electronics, telemetry unit, power subsystem, flight control subsystem, and balloon gondola. The vernier engines were installed at AFMDC.

Prior to system integration tests, each unit and subsystem was subjected to a functional check and the few minor discrepancies revealed were corrected. During system integration tests involving the recovery system control electronics, telemetry, balloon gondola, and power subsystem, minor interface problems necessitated installation of diodes to eliminate sneak switching paths. Integration of the flight control subsystem revealed RF interface problems with the recovery system command receiver and with the power subsystem boost regulator. Both interference problems were corrected through filtering techniques and impedance changes. During tests to determine system susceptibility to an externally applied RF environment, no problems were evident.

System checkout of the T-2 vehicle at AFMDC has been completed and two dry runs performed in preparation for actual engine firing in tethered tests. Weather and range operations permitting, this phase of testing should conclude in December when the vehicle will be returned to Culver City for installation and checkout of the radar altimeter and doppler velocity sensor.

*e. T-21 Test planning status.* In a joint JPL-Hughes spacecraft system test meeting on October 16, 1962, the T-21 testing program and master test specification for type approval testing were reviewed. Revisions resulting from this review have been incorporated and the revised specification transmitted to JPL for approval. A significant addition to the specification is the establishment of a requirement for a radio frequency interference test phase. The objectives will be to verify compatibility of the spacecraft with the RF interference environment generated by the launch vehicle and its ground support equipment, and with the RF interference environment to be encountered during prelaunch check-

out operations at Atlantic Missile Range. A preliminary version of the system functional test phase specification has been completed and will be reviewed at the next joint spacecraft system test meeting in December. Regular meetings of this type are expected to afford several advantages: (1) maximize test effectiveness by continuous review of the current system test plan, (2) maintain communication of pertinent JPL spacecraft experience to the *Surveyor* program, and (3) provide JPL project staff participation in top level system test planning.

***f. Environmental test facilities.*** The thermal vacuum chambers of the Space Environment Laboratory have been redesignated as follows:

| Present designation | Former designation |
|---|---|
| Space Environment Research Facility C-1 | Hi-Vac V |
| Space Environment Research Facility C-2 | Hi-Vac VI |
| Space Environment Research Facility C-3 | Hi-Vac VII |
| Space Environment Research Facility C-4 | Hi-Vac VIII |
| Space Environment Research Facility C-5 | (none) |

*Space Environment Research Facility C-1.* The C-1 facility was used to perform three subsystem thermal-vacuum tests during the past 2 mo. Two Vernier tanks, the flight control sensor group, and the antenna and solar panel positioner were subjected to thermal-vacuum conditions in development model tests.

*Space Environment Research Facility C-2.* Two deficiencies were revealed in initial operation of the C-2 facility: excessive thermal gradient over the cold shroud and backstreaming of diffusion pump oil. A new shroud made of stainless steel panels has been designed and will be installed in December. To alleviate oil backstreaming, the oil-condensing baffle is being relocated and an improved oil trap used.

*Space Environment Research Facility C-3.* The C-3 facility has been used for subsystem, MT-1 Sector II lunar night, and solar panel tests. The chamber is now in the final stages of the acceptance testing and is scheduled to be used for acceptance test of the 5-ft diameter solar simulator in the near future. The combined chamber and solar simulator facility, SERF SC-3, is scheduled for operational availability in mid-January, 1963, for subsystem transit and lunar day tests. Figure 119 shows the solar simulator being assembled onto SERF C-3.

*Space Environment Research Facility C-4.* Installation of the large system test chamber is progressing satisfactorily, and the facility is scheduled for operation without solar simulation during late February, 1963. Figure 120 shows the chamber during assembly and leak testing. The chamber has been evacuated to $1 \times 10^{-6}$ Torr using only one of the six diffusion pumps. The liquid nitrogen plumbing is now being installed; the solar simulator is scheduled for installation during May, 1963. It is anticipated that the complete system test facility, with solar simulation, will be available for operational use in late June, 1963.

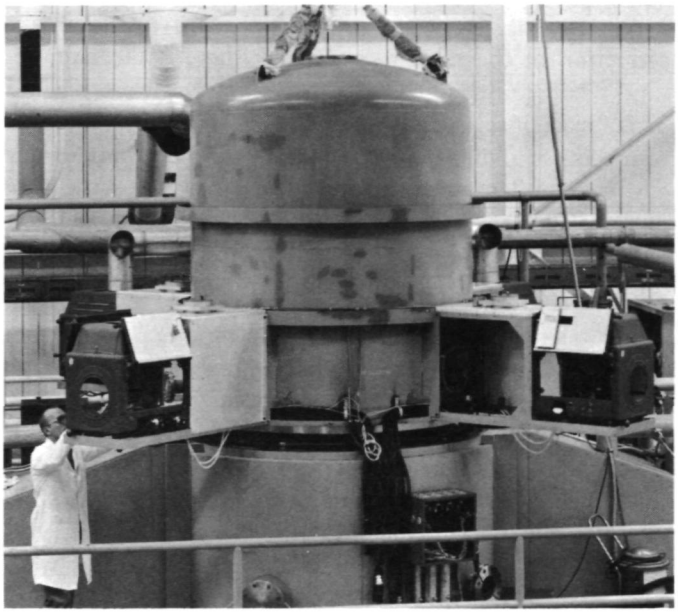

**Fig. 119. Solar simulator installation on SERF C-3**

*Space Environment Research Facility C-5.* The C-5 facility is a new thermal vacuum testing system consisting of three test chambers with one central pumping system and individual chamber shutoff valves. The three stainless steel chambers are each 2 ft in diameter and 3 ft long. The nominal test space in each chamber is 12 by 12 by 15 in. They are temperature-controlled by internal thermal shrouds using liquid or gaseous nitrogen. Fabricated by the Guardite Division of Martin-Marietta Co., the facility is scheduled to be installed during December, 1962. Evaluation testing and modification to improve thermal capability, vacuum performance, and flexibility will be initiated.

*Vibration System V-1.* The V-1 vibration system was used to perform two sinusoidal vibration tests of development model subsystems, the omnidirectional antenna mechanisms, and the planar array antenna and solar panel positioner. The vibration system is currently being evaluated under increased loading conditions. A manual equalization system has been installed and checked out for random vibration testing. The automatic equalization system is scheduled for installation in late January, 1963.

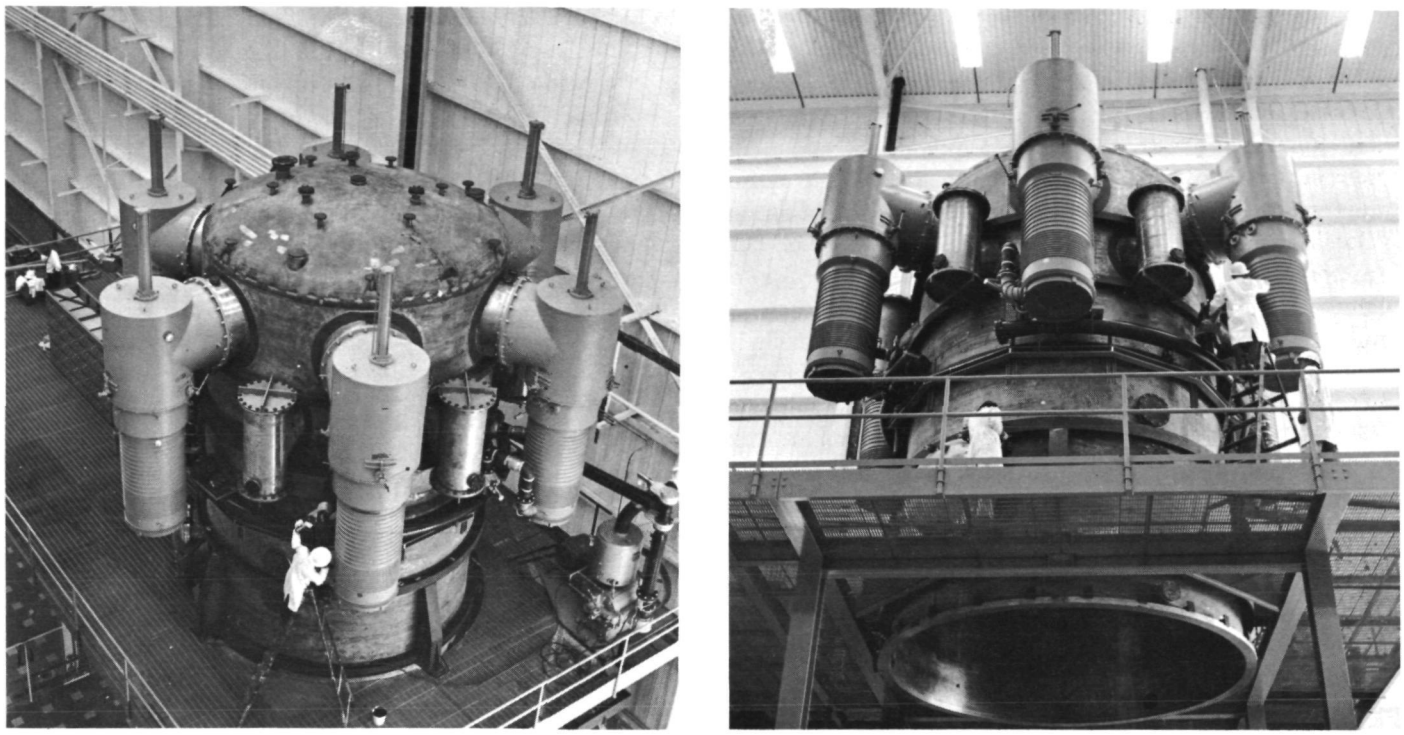

**Fig. 120. Facility C-4**

*600-channel temperature recording system.* The temperature recording system is being modified to permit the use of grounded thermocouples. The original design of the Kin-Tel temperature recording system required the use of insulated (electrically floating) thermocouples to prevent errors induced by ground loops. The modifications involve switching both legs of the thermocouple lead instead of one, adding compensating junctions, and replacing the amplifiers with floating differential dc amplifiers. Preliminary tests on five channels of the modified system using a Leeds Northrop potentiometer and a Honeywell-Brown recorder for comparison have indicated the feasibility and accuracy of the modification. The modified system is scheduled for operational availability in mid-January, 1963, for use during the transit and lunar day tests of the MT-1 sectors.

## 2. Sterilization

Evaluation of aseptic methods of sterilization has been the main effort during the report period. The methods include approaches for retouching damaged painted surfaces, evaluation of the stability of liquid sterilants, and evaluation of the self-sterilizing properties of the epoxy material utilized in the inertial reference unit gyroscopes.

A recent change in sterilization requirements is deletion of aseptic assembly and heat and radiation sterilization. Studies associated with these requirements will therefore be brought to a logical conclusion and the results formally reported. The future sterilization program will consist of clean handling techniques and sterilization of the spacecraft within the missile nose fairing using the ethylene oxide-Freon 12 process.

Since retouching of thermal control paint coatings may be necessary, a method of aseptic application is required. Two methods were evaluated: (1) diffusion of ethylene oxide gas through the coating and (2) use of formaldehyde in the coating formulation. Aluminum coupons were inoculated with spores, painted with the coating, and exposed to ETO-Freon 12 gas for 11 hr. Results indicate that the thermal coating is not permeable enough to ETO gas for sterilization of the coating and the surfaces covered by it. Aluminum coupons inoculated with spores were then painted with the thermal coating mixed with 3.7% formalin. The coupons were allowed to dry at 37° C for 24 hr with the petri dishes slightly opened. The plates were incubated for 48 hr at 37° C after the thermal coating was removed by ultrasonic cleaning. Plate counts on the coupons indicated negative viability. Hence the results indicate that thermal coating touchup could be accomplished following heat sterilization by incorporating 3.7% formaldehyde in the coating formulation. Shelf life tests on the formulation showed that its effectiveness will be maintained for at least 4 wk.

Because of the potential cost of using formaldehyde-methanol solutions in liquid sterilant applications related to stability (shelf life), a study was initiated to establish the efficiency of 5% formaldehyde in methanol as a sterilant, compared to 5% formaldehyde in water. To compare their initial sterilizing effects, smooth and rough aluminum coupons and steel screws inoculated with $10^6$ spores (Bacillus subtilis) were sprayed with each sterilant formulation. After 1- or 4-hr sterilant exposures, the spores were recovered and checked for viability. Between 60 and 2130 spores remained viable on the test specimens exposed to formaldehyde-methanol for 1 hr, and approximately 16 spores remained viable after 4-hr exposure. Less than 10 spores remained viable on the specimens exposed to formaldehyde-water for 1 hr, and no viable spores remained after 4-hr exposure.

To compare their effects after storage, a test study was begun in which rough and smooth aluminum coupons and steel screws are inoculated with $10^4$, $10^5$, or $10^6$ spores and exposed for 4, 6 or 24 hr to liquid sterilant samples that had been stored from 2 wk to 2 mo. After 4 wk storage, the formaldehyde-water solution is still effective in sterilizing all test specimens. No data is available yet on the formaldehyde-methanol storage tests.

As part of the aseptic assembly procedures on the inertial reference unit, the self-sterilizing properties of a candidate compound, Eccofoam PT syntatic foam, have been studied for encapsulating the external gyroscope electronics. The microorganisms used to test the sterilizing properties of the resin were spores of Bacillus subtilis, absorbed on diatomaceous earth, having a viable count of $10^{12}$ spores/gm. After seeding resin samples with $2.6 \times 10^7$ organisms and setting them aside for 2½ hr, a recovery analysis indicated no significant change in spore population, hence the resin is considered nonbactericidal. It is possible that if the resin were allowed to cure before recovering the spores, the resin might have some effect on their viability. However, little change in the bactericidal properties is anticipated from the uncured to the cured stage.

## 3. Reliability

### a. Reliability analysis and estimates.

*System reliability estimates.* The estimated reliability for the flight and landing phase has changed from 0.818 to 0.819. First lunar month reliability has decreased from 0.57 to 0.54 as a result of further refinement of mission time cycles. The estimate for the first 80 hr of lunar operation remains unchanged. A comparison of system reliability estimates by mission phase is shown in Table 25.

*Subsystem reliability estimates.* Updated *a priori* reliability estimates for the A-21 spacecraft subsystems are presented in Table 26. Although estimated subsystem reliability has not changed appreciably, the following changes are of interest. For the flight controls set, failure modes analyses resulted in increased reliability for electronics and decreased reliability for the Canopus sensor and attitude jets. The increase was greater than the decrease for this set. For the mechanisms set, there were revisions in the retro-rocket release estimate which decreased set reliability. For the electric power set, more realistic estimates for the central power control resulted in decreased set reliability.

**Table 25. Estimated system reliability**

| Mission phase | Current value | | Value in preceding report | |
|---|---|---|---|---|
| | Estimate | 80% confidence interval | Estimate | 80% confidence interval |
| Flight and landing | 0.82 | 0.580 to 0.887 | 0.81 | 0.579 to 0.886 |
| First 80 hr of lunar operation | 0.93[a] | Not calculated | 0.93[a] | Not calculated |
| First lunar month | 0.54[a] | Not calculated | 0.57[a] | Not calculated |

[a]Estimate does not include scientific instruments.

**Table 26. Subsystem reliability estimates**

| Item | Flight and landing phase | | Lunar phase[a] | |
|---|---|---|---|---|
| | Current | Previous | First 80 hr | Lunar month |
| Command data and decoding | 0.986 | 0.986 | 0.999 | 0.992 |
| Data processing | 0.992 | 0.992 | 0.988 | 0.911 |
| Structures (includes harness and interconnections) | 0.973 | 0.973 | 0.968 | 0.773 |
| Thermal controls | 0.998 | 0.998 | 0.999 | 0.998 |
| Telecommunications | 0.997 | 0.997 | 0.999 | 0.999 |
| Flight controls | 0.953 | 0.945 | | |
| Propulsion | 0.959 | 0.959 | | |
| Electrical power | 0.958 | 0.960 | 0.973 | 0.780 |
| Mechanisms | 0.988 | 0.993 | | |
| System estimate | 0.819 | 0.818 | 0.931 | 0.543 |
| Minimum system requirement per JPL Specification 30240B | 0.75 | 0.75 | 0.95 | 0.75 |

[a]Excludes scientific instruments.

*Reliability growth curves.* Estimated reliability growth based on test data is shown in Figure 121. It will be noted that a slight decrease has occurred. Primary causes were a decrease in retro-rocket reliability from 0.750 to 0.69 and in vernier propulsion reliability from 0.47 to 0.46. However, the gyroscope reliability increased from 0.77 to 0.81.

***b. Reliability assurance test program.*** The basic objective of the reliability assurance test program is to provide necessary confidence, by test, on the probability of the spacecraft successfully completing its mission. Selection of items requiring assurance testing is based on three criteria: (1) low reliability ranking based on *a priori* predictions, (2) failure history indicating marginal reliability, and (3) necessity of functioning for success in the flight and landing phases of the mission.

*Approach.* Economical attainment of the basic objective is achieved by analytical conversion of data from all system, subsystem, or unit tests (developmental, type approval, T-2 vehicle, qualification, flight acceptance, etc.) into "equivalent mission cycles" (EMC). The EMCs are then utilized as a basic input to a reliability distribution $f(EMC) = R$, which has been calculated from accumulated data as the best representation of expected behavior of the *Surveyor* spacecraft. Adoption of the EMC concept will permit reliability statements to be made at various confidence levels.

Figure 122 shows a plot of EMC per subsystem vs confidence level for various numbers of failures. For example, an accumulation of 11 EMCs on the 9 major subsystems with only one failure would indicate that

**Table 27. Potential equivalent mission**

Cycle data units

| Type of test | Expected equivalent mission cycles | Remarks |
|---|---|---|
| Developmental tests | 1 | Data must be carefully examined regarding (1) degree of configuration that will apply to flight spacecraft and (2) environmental condition and running time correlation with expected mission |
| Subsystem and unit type approval | 2 | High probability that data will be applicable |
| System type approval (T-21) | 2 | Applicable data |
| Flight acceptance | ½ | Applicable data |
| T-2 | ¼ | Tests are on limited number of components |
| Reliability assurance | 5¼ | Applicable data |

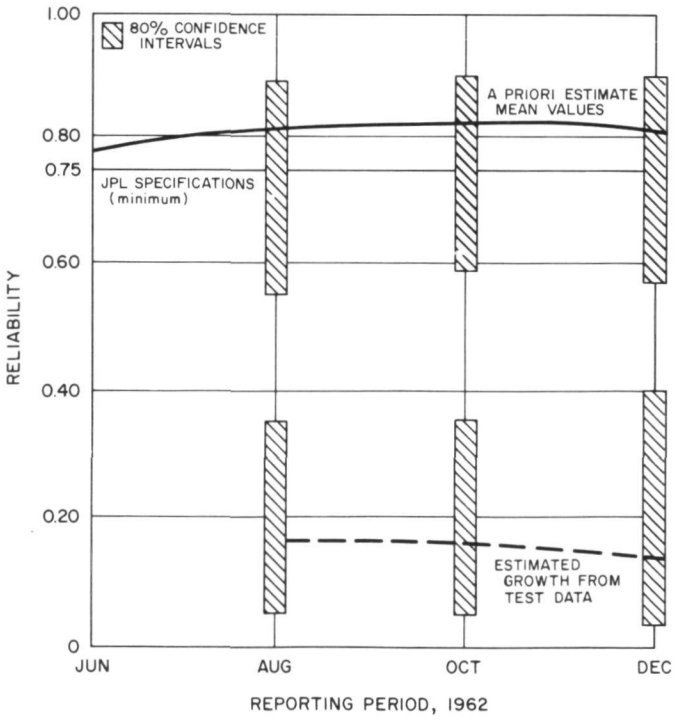


**Fig. 121. A-21 spacecraft reliability growth — flight and handling**

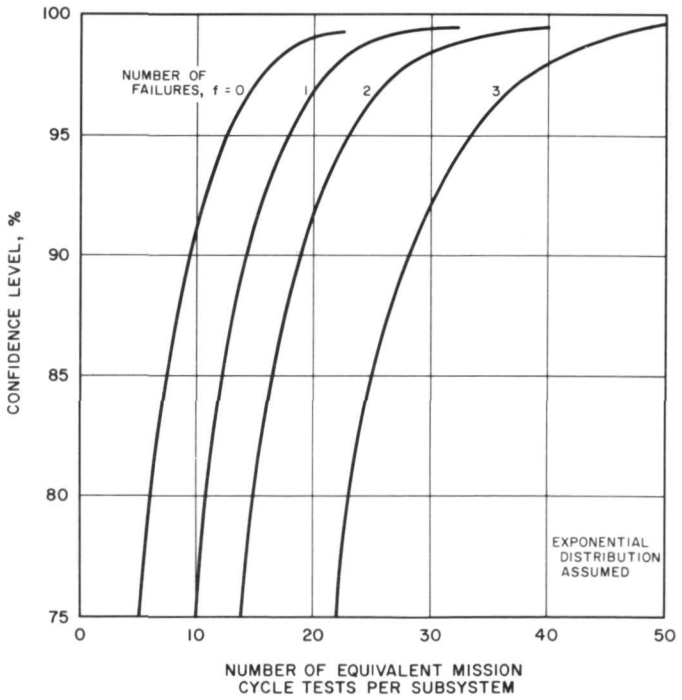


**Fig. 122. Confidence level for reliability of 0.75**

the required reliability of 0.75 has been met at the 80% confidence level. If only 10 EMCs were completed, the confidence level would be 75% for a reliability of 0.75. Table 27 shows potential yields of equivalent mission cycles from various test phases. Analysis of this chart shows that a yield of 5¾ EMCs may be expected from developmental through flight acceptance and T-2 test categories. Comparison of this yield with Figure 122 indicates that insufficient EMCs will have accrued during these phases to make a 0.75 reliability estimate with 80% confidence. Thus, items selected for reliability assurance testing will be utilized primarily to gain confidence in those units which have had a marginal reliability in their developmental history. A detailed schedule of the test plan for selected control items has been formulated.

In summary, the present reliability test plan utilizes to maximum advantage all test data so that sufficient confidence, by test, may be provided regarding *Surveyor* reliability requirements. Versatility for greater or lesser testing commensurate with required reliability is also provided by the equivalent mission cycle concept. Use of the EMC system also significantly reduces test and sample-size costs that would be required by rigorous statistical methods without compromising confidence.

# L. Mission Operations

## 1. Spacecraft Launch Pad Countdown

One of the most critical periods in the operational sequence of the *Surveyor* mission occurs during spacecraft countdown. Some of the more important operations performed on the spacecraft during this period include mating of the spacecraft to the *Atlas-Centaur* launch vehicle, spacecraft readiness tests conducted during the countdown period, final flight preparations, and spacecraft monitoring occurring immediately prior to launch. During the same general time period, the *Atlas-Centaur* will be undergoing final preparations, such as propellant loading, gas pressurization, and electrical operations.

In addition to the items that directly concern the spacecraft or the *Atlas-Centaur*, a number of support functions occur during the countdown period. The support functions include establishing and maintaining the missile operational paging system, the Deep Space Instrumentation Facility link check, and launch status reporting to the DSIF. These operations illustrate the need for:

(1) Defining operations occurring during the spacecraft launch pad countdown.

(2) Establishing the time sequence for these operations during countdown.

(3) Determining elapsed time for each item.

As part of an analysis of these requirements, a spacecraft launch pad countdown sequence chart has been developed (Figure 123). This chart illustrates the spacecraft launch pad countdown and integrates the most recent information concerning the *Atlas-Centaur* countdown, mating operations, and the launch operations. Exact details defining the specific execution of these operations are not available at the present time but will be defined as the program evolves. However, an analysis of basic operations occurring during the spacecraft countdown, with respect to the time span required by each operation and the integrated sequencing of these operations, is represented.

## 2. Handling of Main Retro-Rocket Engine

Because of its lightweight spherical construction, the rocket engine requires special handling procedures and specially designed equipment. This equipment includes:

| | |
|---|---|
| Roll-over equipment | To rotate the engine 180 deg (thrust chamber in down position) in preparation for installation in the spacecraft |
| Support stand | To support engine prior to installation |
| Weighing fitting | Used as temporary extension to engine to mount load cells of weight, balance, and optical alignment equipment |
| Lifting tool | Used in lifting rocket engine from shipping container |

The retro-rocket engine will be installed in the spacecraft when preparations have been completed in the weight, balance, and alignment dock. Handling procedures are illustrated in Figure 124.

## 3. Detailed Test Procedures

***a. Data processing system.*** A system of organizing detailed test procedures through use of data processing techniques has been developed. This method will be applied to all phases of spacecraft checkout prior to launch, with particular emphasis on acceptance testing, explosive safe area operations, and launch countdown. These techniques will improve the efficiency of operational testing and permit rapid correlation of test results by:

(1) Increasing change flexibility for all test procedures.

(2) Implementing changes within a procedure rapidly, without causing additional delay in reissuance of the procedure. (This will be particularly valuable during preliminary periods of spacecraft testing and will facilitate rapid test procedure revision as required by unique portions of particular spacecraft.)

(3) Identifying basic spacecraft test parameters by an assigned code number.

The use of data processing techniques in the development of a comprehensive test procedure format will result in a flexible and coherent system which will help eliminate confusion and wasted effort. The governing factor concerning application of data processing techniques to test procedures is called the test requirement

CONFIDENTIAL

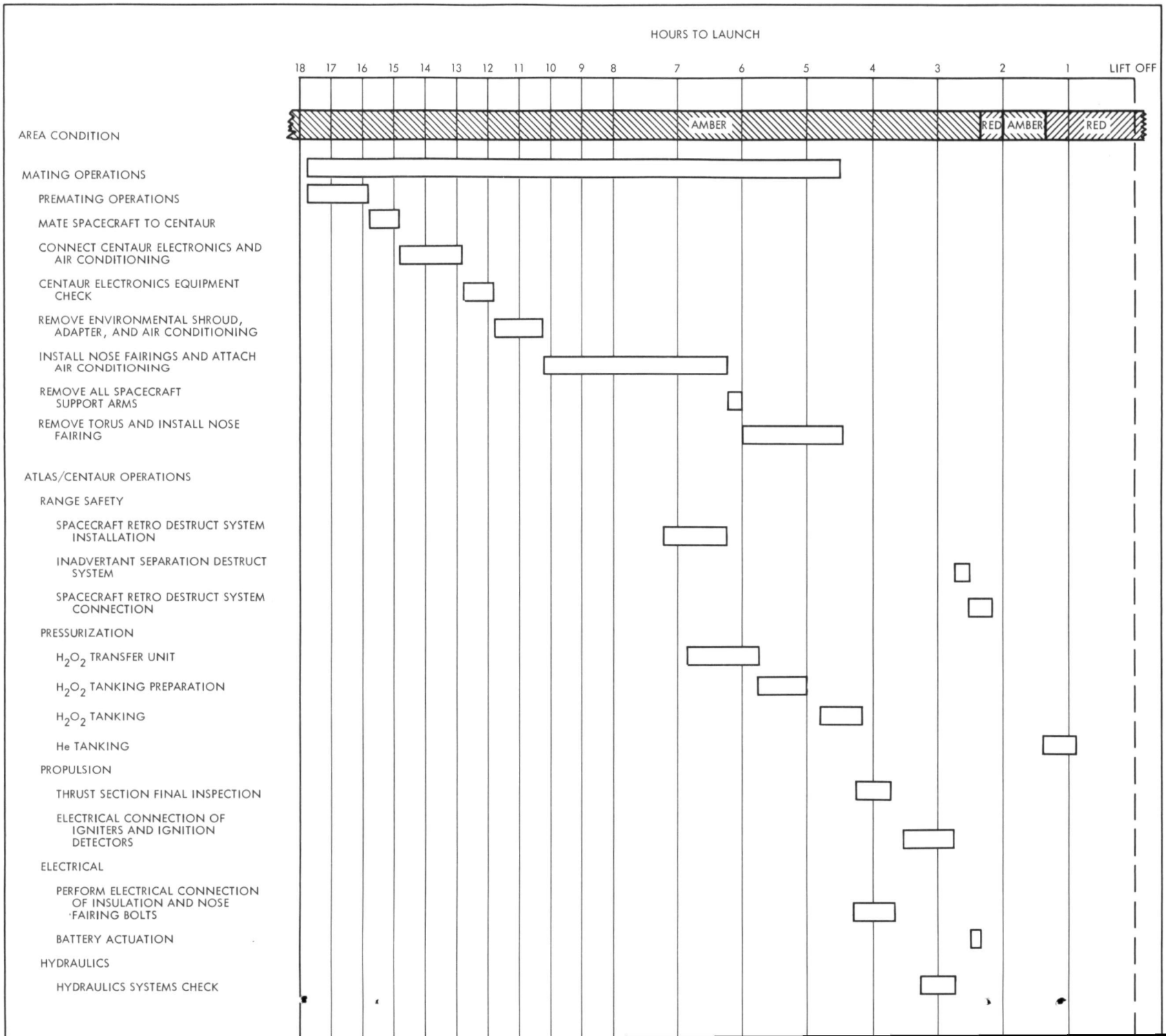


CONFIDENTIAL

GANTRY REMOVAL

PROPELLANT LOADING

$LO_2$ TANKING PREPARATION

CENTAUR $LO_2$ TANKING

CENTAUR $LH_2$ TANKING

ATLAS $LO_2$ TANKING

SPACECRAFT OPERATIONS

INTERCOMMUNICATIONS

ESTABLISH AND MAINTAIN MISSILE OPERATIONAL PAGING SYSTEM

POWER

CONNECT AND MAINTAIN GROUND POWER TO SPACECRAFT

RF LINK

ESTABLISH AND MAINTAIN RF LINK FROM SURVEYOR LAUNCH OPERATIONS TRAILER TO GANTRY/ SURVEYOR RF RELAY SYSTEM

ESTABLISH AND MAINTAIN RF LINK, SURVEYOR LAUNCH OPERATIONS TRAILER TO SPACECRAFT

SPACECRAFT READINESS TESTING

POWER

RF

FLIGHT CONTROL

COMMAND DECODING AND SIGNAL PROCESSING

SCIENTIFIC INSTRUMENTS

MECHANISMS

FLIGHT PREPARATIONS AND MONITORING

FLIGHT PREPARATIONS AND MONITORING OF SPACECRAFT SYSTEMS

GYRO TURN ON TEMPERATURE AND SPEED MONITORING

CONTINUOUS DATA CHANNEL MONITORING

MONITOR TRANSMITTER POWER, TEMPERATURE, AND FREQUENCY; TRANSMIT TO SPACE FLIGHT OPERATIONS FACILITY

TRANSMITTER FILAMENT POWER TURN ON

VERNIER LINES THERMAL POWER ON

SPACECRAFT COMMIT SWITCH TO "GO"

DSIF LINK CHECK AND STATUS REPORTING

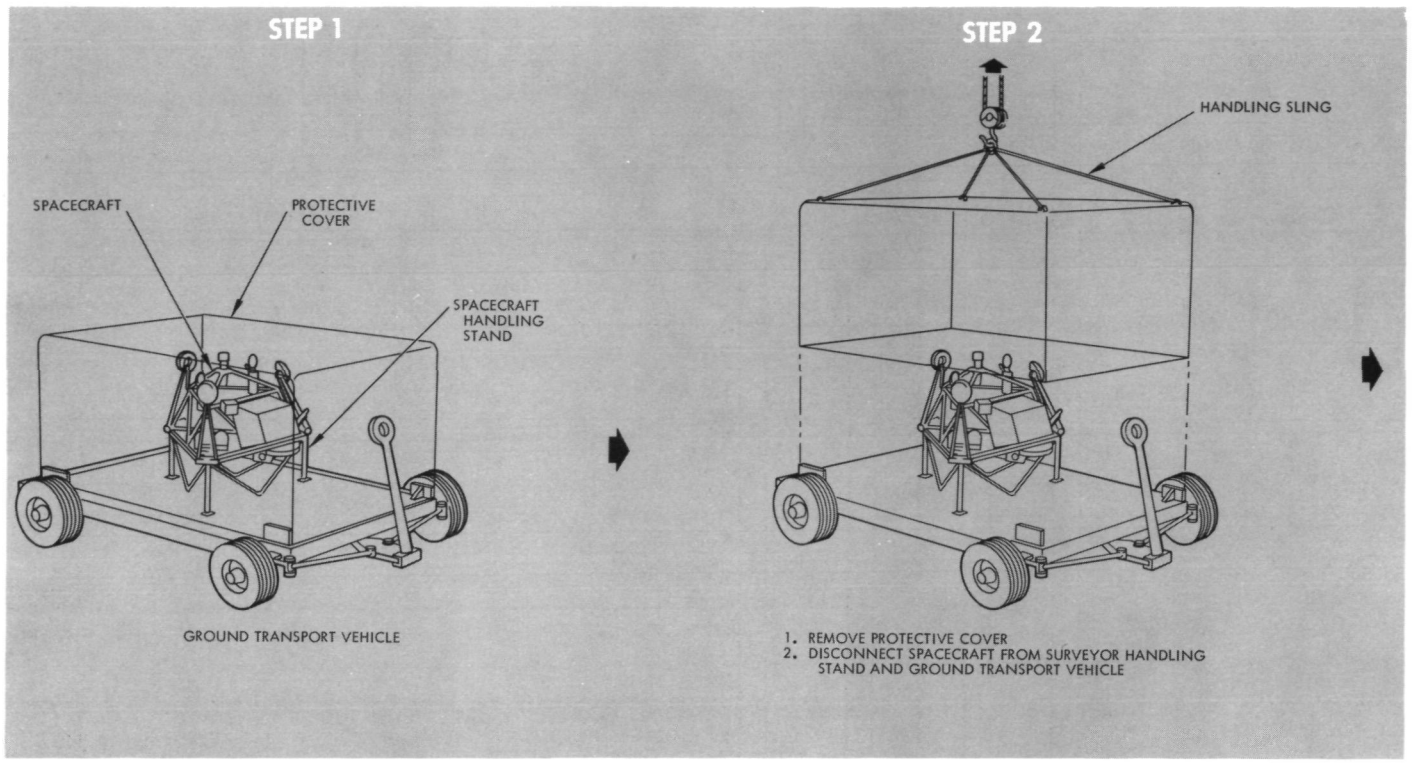


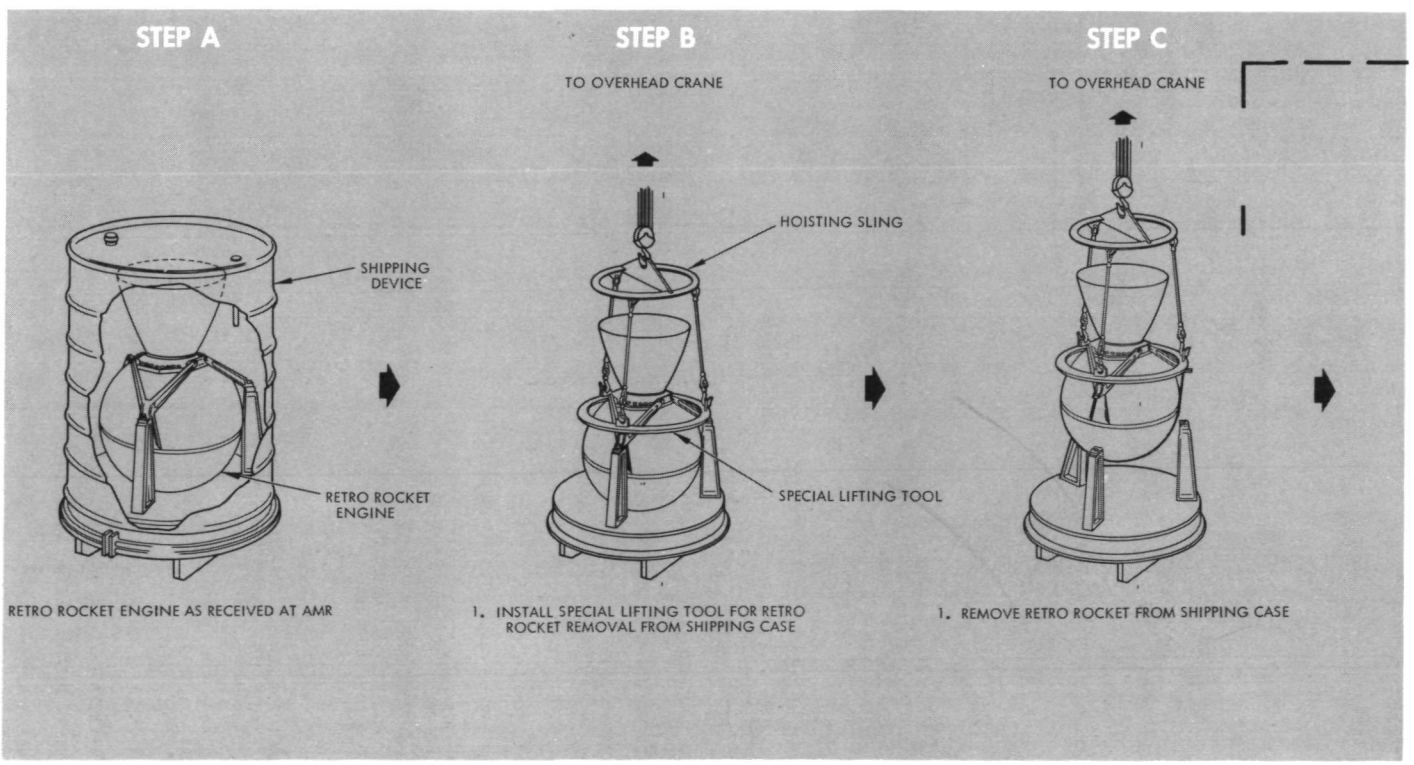


STEPS 1 THROUGH 5 PERFORMED IN SPACECRAFT ASSEMBLY AND CHECKOUT FACILITY.
ALL OTHER STEPS PERFORMED IN EXPLOSIVE SAFE AREA

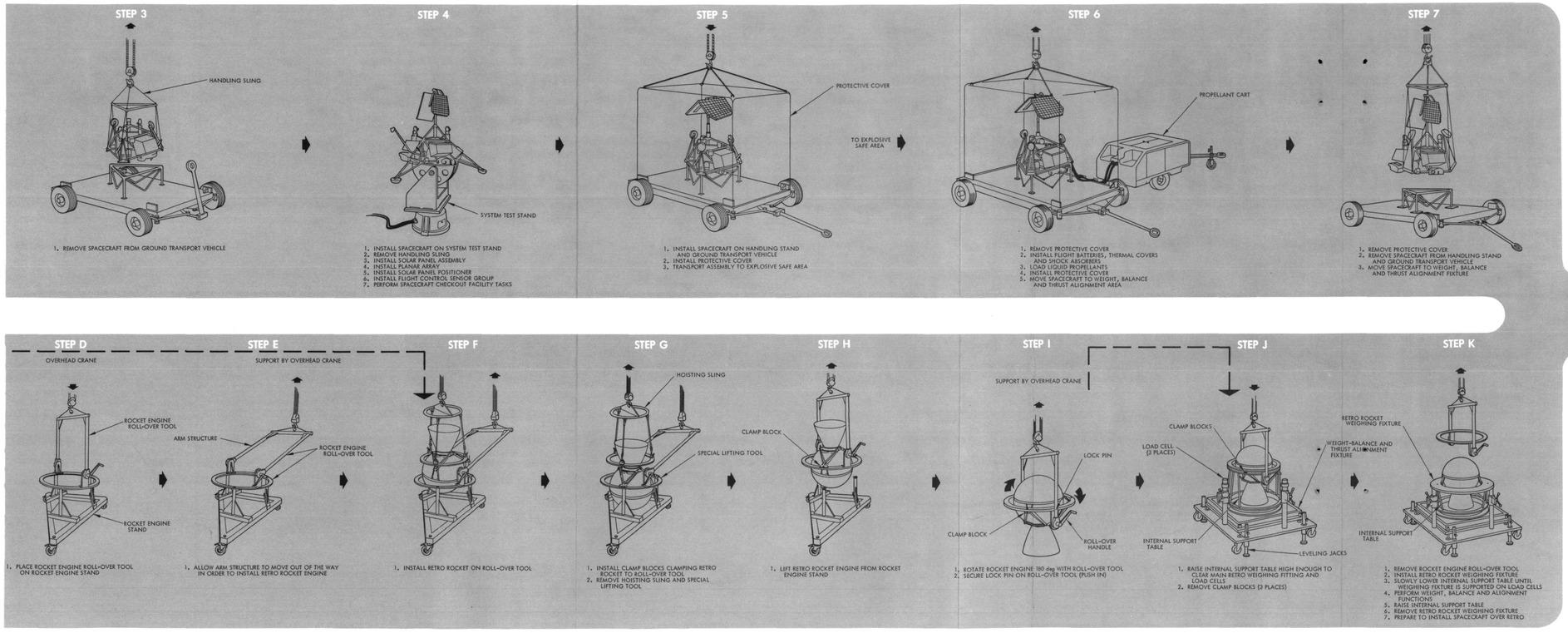


**Fig. 124. Surveyor spacecraft operations and installation of retro-rocket engine**

identification system. It consists of eight information positions which identify individual test phases, the subsystem undergoing test, the specific subsystem test parameter under consideration, and the actual technique employed in evaluating this parameter.

*b. Nomenclature.* The following nomenclature is used in the test requirement identification system. New nomenclature may be added as required.

*Column 1 machine format language.* The following list explains the meaning of the machine language in Column 1 of the IBM card. Machine language refers to the code that indicates the type of information contained by a particular card and subsequently designates the columns to be printed out.

| Machine language letter | | Machine language | | Begin typing at space number |
|---|---|---|---|---|
| A | Space | Skip one line | | |
| B | Titles | Print only columns: | | |
| | | 2-9 | Test requirement number | 1 |
| | | 12-13 | Test technique step number | 11 |
| | | 14-16 | Step reference number | 16 |
| | | 19 | Operator code | 22 |
| | | 20-80 | Detailed procedure information | 26 |
| C | Command numbers only | Print only columns to present command numbers: | | |
| | | 12-13 | Test technique step number | 11 |
| | | 14-16 | Step reference number | 16 |
| | | 19 | Operator code | 22 |
| | | 20-70 | Detailed procedure information | 30 |
| | | 71-80 | Detailed procedure information | 96 |
| G | Commands, not numbers | Print only columns: | | |
| | | 12-13 | Test technique step number | 11 |
| | | 14-16 | Step reference number | 16 |
| | | 19 | Operator code | 22 |
| | | 20-80 | Detailed procedure information | 30 |
| D | Command language | Print only columns: | | |
| | | 20-80 | Detailed procedure information | 30 |
| E | Observations | Print only columns: | | |
| | | 12-13 | Test technique step number | 11 |
| | | 14-16 | Step reference number | 16 |
| | | 19 | Operator code | 22 |
| | | 20-80 | Detailed procedure information | 39 |
| F | Observation language | Print only columns: | | |
| | | 20-80 | Detailed procedure information | 39 |

The mode and command numbers on a "C" card will be printed at two places on a line. The first will be at the indented command headings, and the second will be at the edge of the page. Summarizing the command numbers at the edge of the page will give a quick reference for a test operator.

*Column 2, 3 testing phase information*

| | |
|---|---|
| I1 | Initial gross error tests in Culver City and El Segundo |
| I2 | Initial group quantitative tests in Culver City and El Segundo |
| I3 | Initial integration tests in Culver City and El Segundo |
| I4 | Initial mission sequence tests in Culver City and El Segundo |
| V1 | Vibration tests in Culver City and El Segundo |
| R1 | RFI tests in Culver City and El Segundo |
| T1 | Thermal-vacuum tests in Culver City and El Segundo |
| T2 | Thermal-vacuum mission sequence tests |
| B1 | Buzz tests at AFMDC, New Mexico |
| D1 | Drop tests |
| F1 | Field tests, other than AMR tests |
| G1 | Combined system tests conducted at GD/A |
| C1 | Calibration procedures, spacecraft checkout facility |
| M1 | Mission sequence tests, spacecraft checkout facility |
| S1 | Simulated countdown, spacecraft checkout facility |
| E1 | System confidence tests, explosive safe area |
| L1 | Launch pad tests, launch pad |

Additional test phase designations will be added as required.

*Columns 4, 5 spacecraft equipment identification*

| | |
|---|---|
| AM | Altitude marking radar |
| PR | Propulsion |
| RA | Radar altimeter – doppler velocity sensor |
| TV | Television |
| CD | Command decoding |
| SP | Signal processing |
| RF | Radio frequency |
| PO | Power |
| MV | Mechanisms vehicle |
| SM | Soil mechanics |
| SS | Soil sampler |
| XD | X-ray diffractometer |
| AS | Alpha scattering |
| MD | Micrometeorite detection |
| ST | Sample transport and processor |
| EI | Engineering instrumentation |
| WH | Wiring harness |
| FC | Flight control |

*Columns 6, 7, 8 test requirement number.* The numbers in Columns 6, 7, and 8 refer to the test requirements established by the phase specifications. Each parameter for each group will have its own reference number. For example, one reference number will identify transmitter low-power output A and B. In the case of TV, the camera number will be the first digit. For example:

Resolution normal mode Camera 2.....TV201
Resolution normal mode Camera 3.....TV301
Resolution normal mode Camera 4.....TV401

*Column 9 test technique suffix letter.* The letter appearing in Column 9 will define a specific testing technique employed to satisfy a basic test requirement. Column 9 letters used on a basic test requirement will differentiate the various testing methods developed to accomplish the same end. For example, RF001 could represent the requirement to measure RF power generated by Transmitter A. RF001A could further specify that the power measurement would be accomplished by using a directional coupler, and RF001B would satisfy the same requirement by using a calibrated antenna and a power meter. Different testing techniques used to satisfy the same test requirement would be dictated by the environment in which the test is being conducted, the test equipment being employed, and the status of the spacecraft during test.

When a change is required in a testing technique, the title card will identify that the change has been incorporated by using a Revision A in Column 77 to 80. The exact procedure for identifying, controlling, and releasing procedural changes will be defined in a separate document which will be released at a later date.

The preceding discussion involved the elements that form the test requirement identification system, which is the nucleus of the test procedure reference numbering system. The remaining columns (10 to 80) on the IBM cards are used to describe the actual tests, required observations, operation involved, and commands being employed. The following list includes a general description of column use and is followed by a brief description of the test sequence number, test technique step number, step reference number, and operator code.

| *Column Number* | *Description of Card Information* |
|---|---|
| 1 | Machine language |
| 2 -3 | Test phase information |
| 4 -5 } | Equipment group and |
| 6 -8 } | test requirement number |
| 9 | Test technique suffix |
| 10-11 | Test sequence number |
| 12-13 | Test technique step number |
| 14-16 | Step reference number |
| 17-18 | Technique step line number |
| 19 | Operator code |
| 20-80 | Detailed procedure information |
| 71-80 | Octal commands used for command card only |
| 76-80 | Revision letter for title line, title card only |

*Column 10, 11 test sequence number.* Columns 10 and 11 designate the particular order of testing techniques in a specific test procedure. The sequence will be unique for each procedure.

*Column 12, 13 test technique step number.* The test technique step number is used by the engineer writing a specific test technique to denote definite steps in that technique.

*Column 14-16 step reference number.* Columns 14 to 16 are used to identify statements that form part of a testing technique description. Whenever a particular statement is used to describe tests for TV, RF, or any of the items in the group identification columns, a reference number will be assigned to this statement. Coordinated dictionaries will be established so that magnetic tape can be used for storage and access.

*Column 17, 18 technique step line number.* Columns 17 and 18 identify the lines necessary to explain the details in any step reference.

*Column 19 operator code.* The operator code indicates the STEA operator responsible for this particular step. The lack of a letter in this column indicates an operation other than the STEA. The code identifying specific operators will have the following designation:

| | |
|---|---|
| T | Television station |
| C | Command station |
| D | Data station |
| R | Rack station |
| P | Power station |
| F | Flight control station |
| M | RF station |
| S | Command decoding and signal processing station |
| I | Scientific instruments station |
| A | Mechanisms station |

## 4. Command and Data Handling Console

***a. Status report.*** Subsystem and system testing of the command and data handling console for STEA 1 was completed during the report period and system testing of the prototype CDC is in its final stages. No serious problems have been encountered, although several minor design deficiencies have been isolated and corrected. Among these was a problem with the decommutator which allowed it to indicate frame synchronization and shift out data as though frame synchronization were completed when, under certain conditions, the decommutator was actually out of synchronization by one bit. This condition has been corrected by a minor design change.

*b. Command subsystem.* Prior to completing subsystem tests on the first production unit, a number of changes were incorporated in the command subsystem to increase reliability and ease of operation. Several product improvements were incorporated in the tape reader-spooler, and the following two improvements are under investigation in the command subcarrier oscillator:

(1) Addition of a rate-limiter in the input circuitry of the oscillator to prevent the fast reverse and fall times of the command generator from causing distortion in the transmitted signal.

(2) Modification of the signal simulator circuit in the subcarrier oscillator so that it more closely duplicates the dynamic input from the command generator for ease and accuracy of subcarrier oscillator frequency adjustments.

*c. System test oscillator.* A test unit designed for use in CDC system testing and also applicable for demodulator unit tests has been completed. The unit incorporates the necessary features required to simulate the various types of complex signals generated by the spacecraft which appear as inputs to the CDC. The test unit incorporates the following subunits:

(1) A 60-mc FM oscillator which can be deviated plus and minus 1.5 mc by modulation frequencies from dc to 220 kc. Linearity of this unit is approximately 1%.

(2) A 60-mc pulse-modulated oscillator which can be modulated to greater than 2.0 radians by frequencies from 20 cps to 200 kc.

(3) A 2.4-mc FM oscillator which can be deviated plus and minus 16 kc by modulation frequencies from dc to 10 kc. Linearity is better than 0.5%.

(4) A noise source and 60-mc IF strip which generates noise in the 60-mc region. This noise source is used in making system threshold tests when operating in the video-band FM or wide-band PM modes.

(5) A bank of subcarrier oscillators which can be selected singly or in any combination for modulation of the RF oscillators mentioned above. These subcarrier oscillators will be used for simulating typical spacecraft subcarrier frequency combinations. The CDC-PCM simulator is used to modulate selected subcarrier oscillators in order to simulate PCM-FM data.

(6) A television-PCM telemetry gating circuit, a special gating circuit which accepts inputs from the graybar generator and PCM simulator in the CDC and generates composite signals simulating the spacecraft TV-PCM formats. The outputs of this circuit are used to modulate either the 60-mc FM oscillator for wide-band TV simulation or the 2.4-mc FM oscillator for emergency TV simulation.

CONFIDENTIAL

This document contains information affecting the national defense of the United States, within the meaning of the Espionage Laws, Title 18, U.S.C., Sections 793 and 794, the transmission or revelation of which in any manner to an unauthorized person is prohibited by law.

CONFIDENTIAL